http://shpenkov.com/pdf/Vol.5.Shell-NodalAtomicStructure.pdf

DIALECTICAL VIEW OF THE WORLD

The Wave Model
(Selected Lectures)

George P. Shpenkov

Vol. 5

Shell-Nodal Structure of the Atoms

2015

Volume 5

Shell-Nodal Structure of the Atoms

Contents

General Introduction

We have finished consideration of the Dynamic Model (DM) of elementary particles characterized by its pioneer *discoveries*, which uncovered the *origin of mass* and the *nature of charges*. The latter led (as in the domino effect) to a series of the subsequent resultant discoveries. Among them it should be noted, first of all, the discovery of *fundamental frequencies* of subatomic, atomic and gravitational levels, ω_e and ω_g, which were made as a direct consequence of the aforementioned pioneer discoveries

In this series of Lectures, we turn to the description of the next key problem resolved in the framework of dialectical physics thanks to the Wave Model – to the problem of atoms. What atoms represent by themselves as *physical* formations and how they are formed? We focus our attention on elucidating the *wave structure of atoms* and *molecules*, which are material formations consisting of elementary *atoms*, the *hydrogen atoms*, to which we refer *protons*, *neutrons* and, directly, *atoms of hydrogen*.

It is not surprising that the modern atomic model raises for a long time the well-grounded doubts [1-3]. With all the responsibility we can be argued that the problem on the atom structure is unsolved in physics and, generally, is unsolvable presently in principle due to the weakness of mainstream theories. Apparently, everyone from the readers-physicists already understood the main reasons conditioning an appearance of such theories that led to the disadvantageous current state in physics noted by many. The matter is that the modern concept on atomic structure is based on the *abstract-mathematical* quantum-mechanical model (theory) of atoms, which inadequately reflects reality since it was/is developed in the framework of the dubious Standard Model (SM) dominating, unfortunately, still in physics [4].

In particular, the concept of the SM on the *quark structure* of constituents of atoms, nucleons, as is believed, is contrived. An existence of quarks is not confirmed directly by any experiment. Further, the *size of nucleons*, accepted to be comparable to the electron size, *i.e.*, of the order $10^{-13}\ cm$ in magnitude, is at variance with common sense. Really, the mass of the proton is by more than three orders of magnitude greater than the electron mass, $m_p = 1836.15267245\, m_e$. Mass is the amount of matter an object contains, while volume is how much space it takes. And mass and volume are related by the simple relation, $m = \rho V$. Hence, at such a relativity small size, the density ρ of nucleons must be much greater than the

density of electrons. As a result the unbelievably large magnitude of the order $10^{14}\ g\cdot cm^{-3}$ has been ascribed to their density. We have grounds to assert that the size of nucleons and electrons, one of the fundamental parameters of elementary particles, of the aforementioned order in magnitude accepted in the SM, is inadequate to reality. According to the DM, the size of the proton $r_p = 0.528421703\cdot 10^{-8}\ cm$ (L. 2, Vol. 2, Eq. (27)). Moreover, the comprehensive analysis shows that a single-site (monocentric) model of atoms is also questionable; see, for example, an analysis conducted in [5]; and *etc*. Accordingly, the *structure* of atoms and, hence, the specific *spatial disposition* of nucleons inside each of them, is unknown hitherto.

A lack of true knowledge about the structure of elementary particles and, hence, of atoms and molecules, has influenced on other branches of physics and, naturally, first of all on chemistry. Chemistry is chiefly concerned with atoms and molecules and their interactions and transformations. The modern theoretical models on the structure of individual molecules are based (in the framework of quantum chemistry) on quantum mechanical (QM) *nuclear* atomic model and on the key role that plays the so-called *electron configuration* of atoms in the formation of molecular structures.

This is taken for granted in the WM theory based on the wave concepts on the structure of matter, the spatial structure of molecules (the strictly ordered disposition of atoms in them) is *encoded* in the spatial disposition of atomic constituents of the molecules. Namely, the geometry of the disposition of interatomic bonds in space of molecules is defined by coordinates of a spatial position of neighboring nucleons in individual bonding atoms, but not due to the mystic "electron configuration". According to the WM, electrons define only the strength of chemical bonds [6], but not their directions as it is commonly believed.

Actually, in the last years, it was convincingly shown [7-9] that the simplest particular solutions of the ordinary wave equation,

$$\frac{\partial^2\hat{\Psi}}{\partial x^2}+\frac{\partial^2\hat{\Psi}}{\partial y^2}+\frac{\partial^2\hat{\Psi}}{\partial z^2}-\frac{1}{c^2}\frac{\partial^2\hat{\Psi}}{\partial t^2}=0\,,$$

contain information about the internal (spatial) nucleon structure of individual atoms and symmetry of crystals. These solutions reveal the structure of isotopes and the nature of Mendeleev's periodic law. An ordered equilibrium disposition of nucleons inside of individual atoms *predetermines* the disposition of "atomic nodes" in molecules and crystals. In the light of this discovery, elementary material microformations commonly called *atoms* are, in essence, the *nucleon molecules*. $\hat{\Psi}$ -Function represents in this case the *density of potential-kinetic phase probability* of occurrence of events in wave spaces [9] (we will talk about it in the second Lecture).

Since then as the aforesaid results were obtained, the internal structure of atoms and its reproducibility at the molecular level (in the short-range and long-range orders) got the first direct evidences.

The aforementioned revelations have become appeared for the first time immediately as a result of comparative analysis of the solutions of two equations: the ordinary ("classical") wave equation (1) and Schrödinger's wave equation [1-3]. This analysis has disclosed the conceptual flaws inherent in quantum mechanics and stimulated the search of an alternative theory to replace the inadequate QM. This search led to the WM that is the subject of consideration in these Lectures.

Developing the *Wave* (shell-nodal) *Atomic Model* (further shortly, the WM), we are based on an axiom about the *wave nature* of all objects and physical phenomena in the Universe and, hence, on the *Dynamic Model* of elementary particles [10], using its concepts and the resulting fundamental parameters unknown earlier, *i.e.*, inherent exceptionally in the DM. Remember, according to the DM, elementary particles are pulsating microobjects. *Interactions* between them and with an ambient space, or more correctly, *exchange* of matter-space and rest-motion (matter-space-time for brevity), are realized at the definite *fundamental frequency* ω_e characteristic for microobjects at the atomic and subatomic levels.

Waves of exchange form *standing waves* in *bound domains* of space. The nodal structure of the standing waves, as it turned out, defines the nucleonic structure of atoms. *Potential nodes* of the waves are natural places for the equilibrium disposition of the particles – constituents of atoms and molecules.

An obtainment of the unique results concerning the shell-nodal structure of atoms became possible also due to clarification of the nature of the imaginary number *i* in complex numbers [11 - 13] and, hence, thanks to emergence of a clear understanding of physical meaning of imaginary components in complex wave functions, which describe physical objects and phenomena.

The principal stages and all details related to particular solutions of the wave equation, which led to uncovering the wave (shell-nodal) structure of atoms, and considered in this set of Lectures, one can find in the indicated above References, to which we can add yet the following two reference papers published as selected Chapters in the books [14, 15].

References

[1] L. Kreidik and G. Shpenkov, "*Important Results of Analyzing Foundations of Quantum Mechanics*", Galilean Electrodynamics & QED-East, Special Issues 2, 13, 23-30, (2002); http://shpenkov.com/pdf/QM-Analysis.pdf

[2] G. Shpenkov and L. Kreidik, "*Schrodinger's Errors of Principle*", Galilean Electrodynamics, 3, 16, 51-56, (2005); http://shpenkov.com/pdf/blunders.pdf

[3] G. P. Shpenkov, *Conceptual Unfoundedness of Hybridization and the Nature of the Spherical Harmonics*, Hadronic Journal, Vol. 29. No. 4, p. 455, (2006); http://shpenkov.com/pdf/HybridizationShpenkov.pdf

[4] G. P. Shpenkov, *Some Words about Fundamental Problems of Physics*: *Constructive Analysis*, LAMBERT Academic Publishing, p.116 (2012); amazon.com/words-about-fundamental-problems-physics/dp/3659237507 http://shpenkov.com/pdf/Book-2011-Eng.pdf

[5] G. P. Shpenkov, *The Scattering of Particles and Waves on Nucleon Nodes of the Atom*, International Journal of Chemical Modelling, Vol. 2, No. 1, (2008).

[6] G. P. Shpenkov, *The Role of Electrons in Chemical Bonds Formations* (*In the Light of Shell-Nodal Atomic Model*), MOLECULAR PHYSICS REPORTS 41, 89-103, (2005).

[7]. L.G. Kreidik and G.P. Shpenkov, *Alternative Picture of the World*, Vol. 1-3, Bydgoszcz, 1996.

[8]. L.G. Kreidik and G.P. Shpenkov, *Foundations of Physics*; 13.644…*Collected Papers*, Bydgoszcz, 1998.

[9] L. G. Kreidik and G. P. Shpenkov, *Atomic Structure of Matter-Space*, Geo. S., Bydgoszcz, 2001, 584 p.; http://shpenkov.com/atom.html

[10] L. Kreidik and G. Shpenkov, *Dynamic Model of Elementary Particles and the Nature of Mass and 'Electric' Charge*, "Revista Ciencias Exatas e Naturais", Vol. 3, No 2, 157-170, (2001); http://shpenkov.com/pdf/masscharge.pdf

[11] L. Kreidik and G. Shpenkov, *Material-Ideal Numerical Field*, Proceedings of the General Scientific-Technological Session Contact'95, Vol. II (Bulgaria, Sofia, 1995), 34-39.

[12] L. Kreidik and G. Shpenkov, *Philosophy and the Language of Dialectics and the Algebra of Dialectical Judgments*, Proceedings of The Twentieth World Congress of Philosophy, Copley Place, Boston, Massachusetts, USA, 10-16 August, 1998; http://www.bu.edu/wcp/Papers/Logi/LogiShpe.htm

[13] G. Shpenkov and L. Kreidik, *Potential-Kinetic Parameters of Oscillations*, Hadronic Journal, Vol. 26, No 2, 217-230, (2003).

[14] G. P. Shpenkov, *An Elucidation of the Nature of the Periodic Law*, Chapter 7 in "*The Mathematics of the Periodic Table*", edited by Rouvray D. H. and King R. B., NOVA SCIENCE PUBLISHERS, NY, 119-160, 2006.

[15] G. P. Shpenkov, *Physics and Chemistry of Carbon in the Light of Shell-Nodal Atomic Model*, Chapter 12 in "*Quantum Frontiers of Atoms and Molecules*", edited by Putz M. V., NOVA SCIENCE PUBLISHERS, New York, 277-323, 2011.

George P. Shpenkov
Bielsko-Biala, 2015

Lecture 1

The Wave Equation

1. Introduction

At the beginning, in this Lecture, we present the very basics of mathematics concerning the general wave equation,

$$\frac{\partial^2\hat{\Psi}}{\partial x^2}+\frac{\partial^2\hat{\Psi}}{\partial y^2}+\frac{\partial^2\hat{\Psi}}{\partial z^2}-\frac{1}{c^2}\frac{\partial^2\hat{\Psi}}{\partial t^2}=0\,. \qquad (1)$$

As has been mentioned in General Introduction, particular solutions of this equation in the *spherical space* have promoted revealing the quasi-spherical *shell-nodal structure* of atoms. Therefore, an initial subject of the consideration on this issue is the familiarization with the origin of four main constituents-equations, to which the three-dimensional wave equation (1) comes to in the spherical system of coordinates. We mean the *radial*, *polar*, *azimuthal*, and *time* equations presented in the mathematical form well-known long ago in physics. Each of these four equations correspond to one of the four independent variables: r, θ, φ, and t .

2. Rectangular space

According to the definition, the potential-kinetic gradient $\vec{A}$ of the scalar field $\hat{\Phi}$ (of the field exchange potential) is defined by the expression,

$$\vec{A}=grad\hat{\Phi}=\nabla\hat{\Phi}=\left(\vec{e}_x\frac{\partial}{\partial x}+\vec{e}_y\frac{\partial}{\partial y}+\vec{e}_z\frac{\partial}{\partial z}\right)\hat{\Phi}. \qquad (2)$$

The qualitative operator vector,

$$\nabla=\left(\vec{e}_x\frac{\partial}{\partial x}+\vec{e}_y\frac{\partial}{\partial y}+\vec{e}_z\frac{\partial}{\partial z}\right), \qquad (3)$$

defines the actions that needs to perform on the scalar $\hat{\Phi}$; it is called in mathematics the *del operator* or the *operator nabla* (or ∇ *-operator*).

The gradient $\vec{A}$ defines the direction of the biggest spatial change of the potential $\hat{\Phi}$ of the scalar field of exchange.

The divergence or the flux density of the vector $\vec{A}$ of the field of exchange is represented by the expression,

$$div\vec{A} = \lim_{\Delta\Omega\to 0} \frac{1}{\Delta\Omega} \iint_S \vec{A}\cdot\vec{n}dS = \frac{\partial A_x}{\partial x} + \frac{\partial A_y}{\partial y} + \frac{\partial A_z}{\partial z} = \nabla\cdot\vec{A} \tag{4}$$

If the vector $\vec{A}$ is expressed through the potential $\hat{\Phi}$, then the divergence takes the form,

$$div(grad\hat{\Phi}) = \nabla\cdot\nabla\hat{\Phi} = \nabla^2\hat{\Phi} = \frac{\partial^2\hat{\Phi}}{\partial x^2} + \frac{\partial^2\hat{\Phi}}{\partial y^2} + \frac{\partial^2\hat{\Phi}}{\partial z^2} \tag{5}$$

or

$$div(grad\hat{\Phi}) = \nabla^2\hat{\Phi} = \Delta\hat{\Phi} = \frac{\partial^2\hat{\Phi}}{\partial x^2} + \frac{\partial^2\hat{\Phi}}{\partial y^2} + \frac{\partial^2\hat{\Phi}}{\partial z^2} \tag{6}$$

where

$$\Delta = \nabla^2 = \frac{\partial^2}{\partial x^2} + \frac{\partial^2}{\partial y^2} + \frac{\partial^2}{\partial z^2} \tag{7}$$

is the qualitative scalar of operations (a differential operator given by the divergence of the gradient of a function on Euclidean space), or the *Laplace operator* ("*Laplacian*").

The general wave equation,

$$\Delta\hat{\Phi} - \frac{1}{c^2}\frac{\partial^2\hat{\Phi}}{\partial t^2} = 0, \tag{8}$$

is the wave equation of exchange. It indicates that the flux density (4) of the vector $\vec{A}$ of the field of exchange is proportional to the scalar acceleration of the potential $\hat{\Phi}$.

Let us present the second term of the above equation in the following form,

$$\frac{1}{c^2}\frac{\partial^2\hat{\Phi}}{\partial t^2} = \frac{\omega^2}{c^2}\frac{\partial^2\hat{\Phi}}{\partial(\omega t)^2} = k^2\frac{\partial^2\hat{\Phi}}{\partial\tau^2}. \tag{9}$$

In this case the wave equation (8) takes the form,

$$\Delta\hat{\Phi} - k^2\frac{\partial^2\hat{\Phi}}{\partial\tau^2} = 0, \tag{10}$$

or

$$\Delta_k\hat{\Phi} - \frac{\partial^2\hat{\Phi}}{\partial\tau^2} = 0, \tag{11}$$

where

$$\Delta_k = \frac{\partial^2}{\partial(kx)^2} + \frac{\partial^2}{\partial(ky)^2} + \frac{\partial^2}{\partial(kz)^2} = \frac{1}{k^2}\Delta . \qquad (12)$$

For the sake of simplicity, the subscript *k* will be quite often omitted, and then the wave equation will have the form:

$$\Delta\hat{\Phi} - \frac{\partial^2\hat{\Phi}}{\partial\tau^2} = 0 . \qquad (13)$$

3. Curvilinear orthogonal space

Obviously, the formula (2) of the gradient $\vec{A}$ of the scalar potential $\hat{\Phi}$ for the rectangular reference space is also valid for a local volume of the reference *curvilinear space*. As regards of divergence, the formula in the curvilinear reference space takes a somewhat different form.

A flux of the vector $\vec{A}$ through the opposite facets, 1 and 2, (see Fig. 1) is equal to:

$$dN_1 = -A_1 dy_1 dz_1 + \left(A_1 dy_1 dz_1 + \frac{\partial(A_1 dy_1 dz_1)}{\partial x_1} dx_1 \right) = \frac{\partial(A_1 dy_1 dz_1)}{\partial x_1} dx_1 . \qquad (14)$$

The fluxes through the facets, 3 and 4, and 5 and 6, are defined analogously:

$$dN_2 = -A_2 dx_1 dz_1 + \left(A_2 dx_1 dz_1 + \frac{\partial(A_2 dx_1 dz_1)}{\partial y_1} dy_1 \right) = \frac{\partial(A_2 dx_1 dz_1)}{\partial y_1} dy_1 , \qquad (15)$$

$$dN_3 = -A_3 dx_1 dy_1 + \left(A_3 dx_1 dy_1 + \frac{\partial(A_3 dx_1 dy_1)}{\partial z_1} dz_1 \right) = \frac{\partial(A_3 dx_1 dy_1)}{\partial z_1} dz_1 . \qquad (16)$$

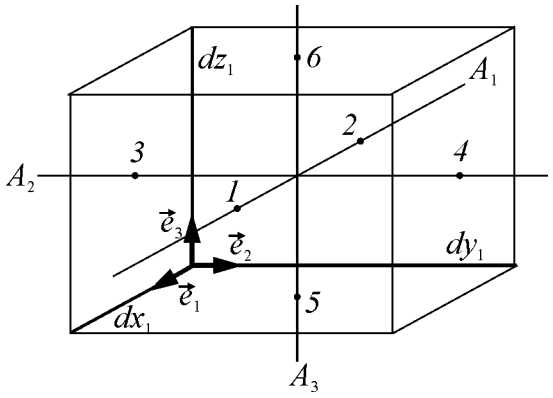

Fig. 1. An elementary volume of field-space with the reference orthogonal curvilinear space: $\vec{e}_1$, $\vec{e}_2$, $\vec{e}_3$ are local unit vectors; dx_1, dy_1, dz_1 are elementary volume edges; $d\Omega = dx_1 dy_1 dz_1$ is an elementary volume.

On the basis of (14) – (16), we obtain:

$$div\vec{A} = \frac{dN_1 + dN_2 + dN_3}{d\Omega}, \tag{17}$$

or

$$div\vec{A} = \frac{1}{d\Omega}\left(\frac{\partial(A_1 dy_1 dz_1)}{\partial x_1}dx_1 + \frac{\partial(A_2 dx_1 dz_1)}{\partial y_1}dy_1 + \frac{\partial(A_3 dx_1 dy_1)}{\partial z_1}dz_1\right). \tag{18}$$

4. Spherical orthogonal space

Let us consider the spherical wave field of exchange. Its coordinates are related with the reference rectilinear space by the following way (Fig. 2):

$$x = r\sin\theta\cos\varphi \qquad y = r\sin\theta\sin s\varphi \qquad z = r\cos\theta \tag{19}$$

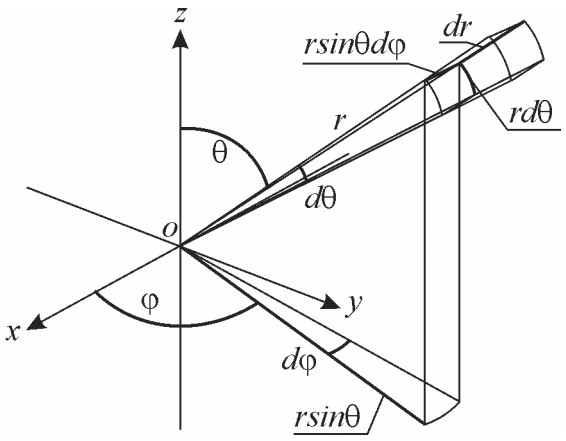

Fig. 2. The relation of rectilinear and spherical reference spaces.

In an elementary volume $d\Omega$ (Fig. 3), ∇ -operator takes the form,

$$\nabla = \left(\vec{e}_x\frac{\partial}{r\partial\theta} + \vec{e}_y\frac{\partial}{r\sin\theta\partial\varphi} + \vec{e}_z\frac{\partial}{\partial r}\right) \tag{20}$$

and

$$\vec{A} = grad\hat{\Phi} = \nabla\hat{\Phi} = \vec{e}_1\frac{\partial\hat{\Phi}}{r\partial\theta} + \vec{e}_2\frac{\partial\hat{\Phi}}{r\sin\theta\partial\varphi} + \vec{e}_3\frac{\partial\hat{\Phi}}{\partial r}, \tag{21}$$

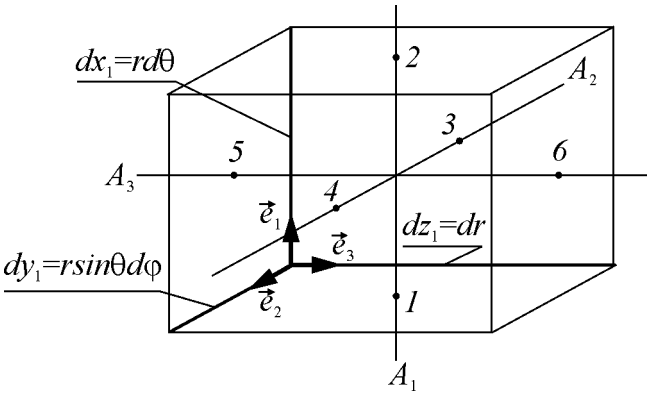

Fig. 3. An elementary volume of the reference spherical space: $\vec{e}_1$, $\vec{e}_2$, $\vec{e}_3$ are local unit vectors; $dz_1 = dr$, $dx_1 = rd\theta$, $dy_1 = r\sin\theta d\varphi$ are elementary volume edges; $d\Omega = dx_1 dy_1 dz_1 = r^2 \sin\theta d\varphi d\theta dr$ is an elementary volume.

where

$$A_1 = A_\theta = \frac{\partial\hat{\Phi}}{r\partial\theta} \tag{22}$$

is the polar constituent,

$$A_2 = A_\varphi = \frac{\partial\hat{\Phi}}{r\sin\theta\partial\varphi} \tag{23}$$

is the azimuthal constituent, and

$$A_3 = A_r = \frac{\partial\hat{\Phi}}{\partial r} \tag{24}$$

is the radial constituent of the gradient of the field of exchange.

Now we will consider the divergence of the vector $\vec{A}$. The flux of $\vec{A}$ through the opposite facets, 1 and 2, is equal to

$$-A_1 dy_1 dz_1 + \left(A_1 dy_1 dz_1 + \frac{\partial(A_1 dy_1 dz_1)}{\partial x_1} dx_1\right) = \frac{\partial(A_1 dy_1 dz_1)}{\partial x_1} dx_1 = \frac{\partial(A_1 r\sin\theta)}{rd\theta} rd\varphi d\theta dr,$$

or

$$dN_1 = \frac{\partial(A_1 r\sin\theta)}{r^2\sin\theta\partial\theta} d\Omega. \tag{25}$$

The fluxes through the facets, 3 and 4, and 5 and 6, are defined analogously:

$$-A_2 dx_1 dz_1 + \left(A_2 dx_1 dz_1 + \frac{\partial(A_2 dx_1 dz_1)}{\partial y_1} dy_1\right) = \frac{\partial(A_2 dx_1 dz_1)}{\partial y_1} dy_1 = \frac{\partial(A_2 r)}{r\sin\theta\partial\varphi} r\sin\theta d\varphi d\theta dr,$$

or

$$dN_2 = \frac{\partial(A_2 r)}{r^2 \sin\theta \partial\varphi} d\Omega \tag{26}$$

$$-A_3 dx_1 dy_1 + \left(A_3 dx_1 dy_1 + \frac{\partial(A_3 dx_1 dy_1)}{\partial z_1} dz_1 \right) = \frac{\partial(A_3 dx_1 dy_1)}{\partial z_1} dz_1 = \frac{d(A_s r^2 \sin\vartheta)}{\partial r} d\varphi d\theta dr .$$

or

$$dN_3 = \frac{\partial(A_3 r^2 \sin\theta)}{r^2 \sin\theta \partial r} d\Omega \tag{27}$$

On the basis of (25) – (27), we have:

$$div\vec{A} = \frac{1}{r^2 \sin\theta} \left(\frac{\partial(A_\vartheta r \sin\theta)}{\partial\theta} + \frac{\partial(A_\varphi rs)}{\partial\varphi} + \frac{\partial(A_r r^2 \sin\theta)}{\partial r} \right). \tag{28}$$

Taking into account (22), (23), and (24), we arrive at:

$$\Delta\hat{\Phi} = divgrad\hat{\Phi} = \frac{1}{r^2 \sin\theta} \left[\frac{\partial}{\partial\theta} \left(\sin\theta \frac{\partial\hat{\Phi}}{\partial\theta} \right) + \frac{\partial}{\partial\varphi} \left(\frac{1}{\sin\theta} \frac{\partial\hat{\Phi}}{\partial\varphi} \right) + \frac{\partial}{\partial r} \left(r^2 \sin\theta \frac{\partial\hat{\Phi}}{\partial r} \right) \right], \tag{29}$$

or

$$\Delta_k\hat{\Phi} = \frac{1}{(kr)^2 \sin\theta} \left[\frac{\partial}{\partial\theta} \left(\sin\theta \frac{\partial\hat{\Phi}}{\partial\theta} \right) + \frac{\partial}{\partial\varphi} \left(\frac{1}{\sin\theta} \frac{\partial\hat{\Phi}}{\partial\varphi} \right) + \frac{\partial}{\partial(kr)} \left((kr)^2 \sin\theta \frac{\partial\hat{\Phi}}{\partial(kr)} \right) \right], \tag{30}$$

Denoting the function $\hat{\Phi}$ as $\hat{\Psi}$ and assuming that

$$\hat{\Phi} = \hat{\Psi} = R(kr)\Theta(\theta)\Phi(\varphi)T(\tau) = \hat{\psi}(kr,\theta,\varphi)T(\tau), \tag{31}$$

we have:

$$\Delta_{k\theta}\hat{\Psi} = \frac{1}{(kr)^2 \sin\theta} \left[\frac{\partial}{\partial\theta} \left(\sin\theta \frac{\partial\hat{\Psi}}{\partial\theta} \right) \right] = \left(\frac{ctg}{(kr)^2} \frac{1}{\Theta} \frac{\partial\Theta}{\partial\theta} + \frac{1}{(kr)^2} \frac{1}{\Theta} \frac{\partial^2\Theta}{\partial\theta^2} \right) \hat{\Psi}, \tag{32}$$

$$\Delta_{k\varphi}\hat{\Psi} = \frac{1}{(kr)^2 \sin\theta} \left[\frac{\partial}{\partial\varphi} \left(\frac{1}{\sin\theta} \frac{\partial\hat{\Psi}}{\partial\varphi} \right) \right] = \left(\frac{1}{(kr)^2 \sin^2\theta} \frac{1}{\Phi} \frac{\partial^2\Phi}{\partial\varphi^2} \right) \hat{\Psi}, \tag{33}$$

$$\Delta_{kr}\hat{\Psi} = \frac{1}{(kr)^2 \sin\theta} \left[\frac{\partial}{\partial(kr)} \left((kr)^2 \sin\theta \frac{\partial\hat{\Psi}}{\partial(kr)} \right) \right] = \left(\frac{2}{(kr)} \frac{1}{R} \frac{\partial R}{\partial(kr)} + \frac{1}{R} \frac{\partial^2 R}{\partial(kr)^2} \right) \hat{\Psi} . \tag{34}$$

As a result we get

$$\Delta_k \hat{\Psi} = \left(\frac{ctg}{(kr)^2} \frac{1}{\Theta} \frac{\partial \Theta}{\partial \theta} + \frac{1}{(kr)^2} \frac{1}{\Theta} \frac{\partial^2 \Theta}{\partial \theta^2} + \frac{1}{(kr)^2 \sin^2 \theta} \frac{1}{\Phi} \frac{\partial^2 \Phi}{\partial \varphi^2} + \frac{2}{(kr)} \frac{1}{R} \frac{\partial R}{\partial (kr)} + \frac{1}{R} \frac{\partial^2 R}{\partial (kr)^2} \right) \hat{\Psi} \quad (35)$$

Considering (11), we can write now the following equality,

$$\frac{ctg\theta}{(kr)^2} \frac{1}{\Theta} \frac{\partial \Theta}{\partial \theta} + \frac{1}{(kr)^2} \frac{1}{\Theta} \frac{\partial^2 \Theta}{\partial \theta^2} + \frac{1}{(kr)^2 \sin^2 \theta} \frac{1}{\Phi} \frac{\partial^2 \Phi}{\partial \varphi^2} + \\ + \frac{2}{(kr)} \frac{1}{R} \frac{\partial R}{\partial (kr)} + \frac{1}{R} \frac{\partial^2 R}{\partial (kr)^2} = \frac{1}{\hat{\Psi}} \frac{\partial^2 \hat{\Psi}}{\partial \tau^2} = \frac{1}{T} \frac{d^2 T}{d\tau^2} \quad (36)$$

Assuming $\frac{1}{T} \frac{d^2 T}{d\tau^2} = -1$, we get

$$ctg\theta \frac{1}{\Theta} \frac{\partial \Theta}{\partial \theta} + \frac{1}{\Theta} \frac{\partial^2 \Theta}{\partial \theta^2} + \frac{1}{\sin^2 \theta} \frac{1}{\Phi} \frac{\partial^2 \Phi}{\partial \varphi^2} + 2(kr) \frac{1}{R} \frac{\partial R}{\partial (kr)} + \frac{(kr)^2}{R} \frac{\partial^2 R}{\partial (kr)^2} = -(kr)^2 \quad (37)$$

The further natural mathematical operation is grouping (37) by independent variables and equating the obtained groups to a *constant value*, for example, let us take $l(l+1)$, where $l = 0, 1, 2, 3, \ldots$:

$$\frac{(kr)^2}{R} \frac{\partial^2 R}{\partial (kr)^2} + 2(kr) \frac{1}{R} \frac{\partial R}{\partial (kr)} + (kr)^2 = \\ = -\left(ctg\theta \frac{1}{\Theta} \frac{\partial \Theta}{\partial \theta} + \frac{1}{\Theta} \frac{\partial^2 \Theta}{\partial \theta^2} + \frac{1}{\sin^2 \theta} \frac{1}{\Phi} \frac{\partial^2 \Phi}{\partial \varphi^2} \right) = l(l+1) \quad (38)$$

Thus, we have

$$(kr)^2 \frac{\partial^2 R}{\partial (kr)^2} + 2(kr) \frac{\partial R}{\partial (kr)} + \left((kr)^2 - l(l+1) \right) R = 0 . \quad (39)$$

Dividing the next variables (θ and φ) by the same way, we can write the following equality:

$$\left(ctg\theta \frac{1}{\Theta} \frac{\partial \Theta}{\partial \theta} + \frac{1}{\Theta} \frac{\partial^2 \Theta}{\partial \theta^2} + l(l+1) \right) \sin^2 \theta = -\frac{1}{\Phi} \frac{\partial^2 \Phi}{\partial \varphi^2} = m^2 \quad (40)$$

Hence, we have arrived at the following equation:

$$\frac{\partial^2 \Theta}{\partial \theta^2} + ctg\theta \frac{\partial \Theta}{\partial \theta} + \left(l(l+1) - \frac{m^2}{\sin^2 \theta} \right) \Theta = 0 \quad (41)$$

Eventually, the wave equation $\Delta_k \hat{\Psi} - \frac{\partial^2 \hat{\Psi}}{\partial \tau^2} = 0$ decomposes (for the case of the spherical orthogonal space) into

a) the *time* equation,

$$\frac{d^2 T}{d\tau^2} = -T\,, \tag{42}$$

and three equations of space:

b) the *radial* equation,

$$(kr)^2 \frac{d^2 R}{d(kr)^2} + 2(kr)\frac{dR}{d(kr)} + \left((kr)^2 - l(l+1)\right)R = 0\,, \tag{43}$$

c) the *polar* equation,

$$\frac{d^2\Theta}{d\theta^2} + ctg\theta \frac{d\Theta}{d\theta} + \left(l(l+1) - \frac{m^2}{\sin^2\theta} \right)\Theta = 0\,, \tag{44}$$

and

d) the *azimuthal* equation,

$$\frac{d^2\Phi}{d\varphi^2} = -m^2\Phi\,. \tag{45}$$

Elementary linearly independent solutions of the azimuthal equation (45) are

$$\hat{\Phi}(\varphi) = \Phi_m e^{\pm i(m\varphi+\alpha)}\,, \tag{45a}$$

where Φ_m is the constant factor defining from the normalizing condition, α is an initial phase of the azimuthal state.

5. Polar equation

The polar equation (44) is transformed further by introducing a new variable $\zeta = \cos\theta$. Because $\sin\theta = \sqrt{1-\zeta^2}$ and $d\zeta = -\sin\theta d\theta = -\sqrt{1-\zeta^2}\,d\theta$, therefore,

$$\frac{d\Theta_{l,m}}{d\theta} = \frac{d\Theta_{l,m}}{d\zeta}\frac{d\zeta}{d\theta} = -\sqrt{1-\zeta^2}\,\frac{d\Theta_{l,m}}{d\zeta} \qquad \text{and} \qquad ctg\theta\frac{d\Theta_{l,m}}{d\theta} = -\zeta\frac{d\Theta_{l,m}}{d\zeta}\,. \tag{46}$$

Further,

$$\frac{d^2\Theta_{l,m}}{d\theta^2}=\frac{d}{d\zeta}\left(-\sqrt{1-\zeta^2}\,\frac{\partial\Theta_{l,m}}{\partial\zeta}\right)\frac{d\zeta}{d\theta}=-\zeta\frac{\partial\Theta_{l,m}}{\partial\zeta}+(1-\zeta^2)\frac{\partial^2\Theta_{l,m}}{\partial\zeta^2} \tag{47}$$

And Eq. (44) takes the form,

$$(1-\zeta^2)\frac{\partial^2\Theta_{l,m}}{\partial\zeta^2}-2\zeta\frac{\partial\Theta_{l,m}}{\partial\zeta}+\left(l(l+1)-\frac{m^2}{1-\zeta^2}\right)\Theta_{l,m}=0 \tag{48}$$

This is the differential equation, solutions of which are Legendre's *associated* functions $P_{l,m}$ of the first kind of the power *l* and the order *m*:

$$P_{l,m}(\cos\theta)=\frac{\sin^m\theta}{2^l\,l!}\frac{d^{l+m}}{d(\cos\theta)^{l+m}}\left(\cos^2\theta-1\right)^l. \tag{49}$$

We present them in the form of Legendre's *reduced* functions:

$$\tilde{\Theta}_{l,m}=\frac{(l-m)!}{(2l)!}\sin^m\theta\frac{d^{l+m}}{d(\cos\theta)^{l+m}}\left(\cos^2\theta-1\right)^l,\qquad \tilde{\Theta}_{l,l}=\sin^l\theta. \tag{49a}$$

Wherein,

$$\tilde{\Theta}_{l+1,m}=\cos\theta\tilde{\Theta}_{l,m}-\frac{l^2-m^2}{4l^2-1}\tilde{\Theta}_{l-1,m}. \tag{50}$$

Legendre's reduced functions (49a) are related with Legendre's associated functions $P_{l,m}$ (49) by the following way,

$$\tilde{\Theta}_{l,m}=\frac{2^l\,l!(l-m)!}{(2l)!}P_{l,m}. \tag{51}$$

The first three Legendre's reduced functions have the form,

$$\tilde{\Theta}_{0,0}=1,\qquad \tilde{\Theta}_{1,0}=\frac{1}{2}\frac{d(\cos^2\theta)}{d(\cos\theta)}=\cos\theta,\qquad \tilde{\Theta}_{1,1}=\sin\theta. \tag{52}$$

On the basis of the recurrent relation (50), it is easily to get the other remaining polar functions.

6. Radial equation

The transformation of the radial equation (43) is realized by using the following substitution,

$$R_l = \frac{Z_l}{\sqrt{kr}}. \tag{53}$$

Accordingly,

$$\frac{dR_l}{d(kr)} = -\frac{Z_l}{2(kr)\sqrt{(kr)}} + \frac{1}{\sqrt{(kr)}}\frac{dZ_l}{d(kr)} = 0, \tag{54}$$

$$\frac{d^2R_l}{d(kr)^2} = -\frac{3}{4}\frac{Z_l}{(kr)^2\sqrt{(kr)}} - \frac{1}{(kr)\sqrt{(kr)}}\frac{dZ_l}{d(kr)} + \frac{1}{\sqrt{(kr)}}\frac{d^2Z_l}{d(kr)^2}, \tag{55}$$

and

$$\begin{aligned}\frac{3}{4}\frac{Z_l}{\sqrt{(kr)}} - \sqrt{(kr)}\frac{dZ_l}{d(kr)} + (kr)\sqrt{(kr)}\frac{d^2Z_l}{d(kr)^2} - \frac{Z_l}{\sqrt{(kr)}} + \\ + 2\sqrt{(kr)}\frac{dZ_l}{d(kr)} + \left((kr)^2 - l(l+1)\right)\frac{Z_l}{\sqrt{(kr)}} = 0\end{aligned}, \tag{56}$$

$$\begin{aligned}\frac{3}{4}\frac{Z_l}{(kr)^2} - \frac{1}{(kr)}\frac{dZ_l}{d(kr)} + \frac{d^2Z_l}{d(kr)^2} - \frac{Z_l}{(kr)^2} + \\ + \frac{2}{(kr)}\frac{dZ_l}{d(kr)} + \left((kr)^2 - l(l+1)\right)\frac{Z_l}{(kr)^2} = 0\end{aligned}, \tag{57}$$

$$\frac{d^2Z_l}{d(kr)^2} + \frac{1}{(kr)}\frac{dZ_l}{d(kr)} - \frac{Z_l}{4(kr)^2} + \left((kr)^2 - l(l+1)\right)\frac{Z_l}{(kr)^2} = 0, \tag{58}$$

$$\frac{d^2Z_l}{d(kr)^2} + \frac{1}{(kr)}\frac{dZ_l}{d(kr)} + \left(1 - \frac{(l+1/2)^2}{(kr)^2}l(l+1)\right)Z_l = 0. \tag{59}$$

The final result (59) of the substitution (53) is the equation of *cylindrical functions*. Its elementary potential-kinetic solution is represented by the Hankel function:

$$Z_l = H^{\pm}_{l+1/2}(kr) = J_{l+1/2}(kr) \pm iN_{l+1/2}(kr). \tag{60}$$

For $(kr) >> 1$,

$$H^{\pm}_{l+1/2}(kr) \approx \sqrt{\frac{2}{\pi(kr)}}\exp i\left(\frac{l\pi}{2} + \frac{\pi}{4} + (kr)\right) \tag{61}$$

With taking into account (53) and (60), and the case (61), it is convenient to present the radial solution of the equation (43) in the following form,

$$\hat{R}_l(kr) = \frac{A\hat{e}_l(kr)}{kr} = A\frac{c_l(kr) \pm is_l(kr)}{kr}, \tag{62}$$

where *A* is the constant factor,

$$\hat{e}_l(kr) = \sqrt{\frac{\pi(kr)}{2}} H^{\pm}_{l+1/2}(kr) \text{ is the spherical exponent;} \tag{63}$$

$$c_l(kr) = \sqrt{\frac{\pi(kr)}{2}} J_{l+1/2}(kr) \text{ is the spherical cosine;} \tag{64}$$

$$s_l(kr) = \sqrt{\frac{\pi(kr)}{2}} N_{l+1/2}(kr) \text{ is the spherical sine;} \tag{65}$$

$$c_l(kr) = \sqrt{\frac{\pi(kr)}{2}} J_{l+1/2}(kr) \approx \cos\left(\frac{l\pi}{2} + \frac{\pi}{4} + (kr)\right); \tag{66}$$

$$s_l(kr) = \sqrt{\frac{\pi(kr)}{2}} N_{l+1/2}(kr) \approx \sin\left(\frac{l\pi}{2} + \frac{\pi}{4} + (kr)\right). \tag{67}$$

7. Conclusion

Particular grounds of mathematical physics concerning the wave equation (1) (or (8)) and the equations of its constituents, (42) – (45), to which the spherical realization of the wave equation comes to, have been presented here. All stages of the derivation of two main constituent equations, (51) and (62), of the three-dimensional wave equation (8) were shown herein in detail.

The aforementioned two constituent equations are, correspondingly, the equations for *polar* (θ) and *radial* (*r*) variables. Their solutions (together with solutions of the equation for the azimuthal variable, φ, (45)) define the coordinates of *nodes* and *antinodes* of *standing waves* in the spherical space (that will be discussed further). Knowledge of the given derivation is necessary for understanding the characteristic peculiarities related to the origin of these equations and to understand, taking also into account the DM concepts on the structure of elementary particles, the physical meaning contained in the solutions of (1) that led, ultimately, to uncovering the shell-nodal structure of atoms.

The derivation was realized sequentially by the corresponding transformations of the potential-kinetic gradient $\vec{A}$ of the scalar field $\hat{\Phi}$ of the field exchange potential. Denoting as $\hat{\Psi}$, it has the form (31):

$$\hat{\Psi} = R(kr)\Theta(\theta)\Phi(\varphi)T(\tau) = \hat{\psi}(kr,\theta,\varphi)T(\tau)$$

where

$$\hat{\psi}(kr,\theta,\varphi) = R(kr)\Theta(\theta)\Phi(\varphi)\,. \qquad (68)$$

The resulting solutions: $\hat{R}_l(kr)$, $\Theta_{l,m}(\theta)$, and $\hat{\Phi}_m(\varphi)$, of the equations corresponding to each of the entering in (69) functions: have helped to disclose an internal structure of atoms and to understand what these atoms represent by themselves as physical objects. Remember, we are relying here on an unquestioned concept on the wave nature of their origin, as on the wave nature of the origin of all objects in the Universe, in full agreement with fundamentals of dialectical physics realized in the WM.

Information on the structure of matter (in particular, atoms), which was found thanks to the WM in pure mathematical particular solutions of the wave equation (8), is uncovered, as far as possible, in detail and gradually in the subsequent Lectures of this Volume.

Lecture 2

The Wave Equation Solutions

1. Introduction

One of the particular solutions of the general ("classical") wave equation,

$$\Delta\hat{\Psi} - \frac{1}{c^2}\frac{\partial^2\hat{\Psi}}{\partial t^2} = 0\,, \qquad (1)$$

are *standing sinusoidal spherical waves* described by the product of radial (Bessel), polar (Legendre's), and azimuthal functions [1]. The nodal structure of the standing waves reminds spherical resonant cavities having internal oscillating longitudinal ("electric") and transversal ("magnetic") mode fields [2].

The comprehensive analysis of the solutions of (1), carried out during the development of dialectical physics, led to the *discovery* of the unknown earlier fact that the nodal structure of standing waves in the three dimensional space uniquely determines (repeats) the *structure of matter* at the subatomic, atomic and molecular levels, in particular, the spatial disposition of constituents-nucleons inside the atoms. This discovery completely confirmed the basic concept of dialectical physics on the wave nature of all objects and phenomena in the Universe. Further, in the next Lectures, the nodal structure of the atoms, originating from the solutions, will be demonstrated on the examples of the internal spatial structure, mostly, of carbon and oxygen atoms and some their compounds, including graphene, to which in recent years a special attention is paid.

In the language of dialectical logic (remember the relevant discussions held in L. 10 of Vol. 1), the wave equation of the form (1) means the equality of time double and spatial double negations of $\hat{\Psi}$-image of the physical wave field-space, *i.e.*, (1) represents the dialectical laws of double spatial and double time negations.

Following a consistent logic of the description that we held in our Lectures, the time has come to give now a clear definition of the wave $\hat{\Psi}$-function, entering in the wave equation. Namely, we should know, what the *physical meaning* is contained in the wave $\hat{\Psi}$-function.

And then, uncovering general forms of the solutions presented in previous Lecture (Eqs. (45a), (49), and (62)), we can turn to consideration of the concrete extended expressions for these solutions.

The present Lecture is focused just on these two aforementioned subjects. Let us proceed directly to the first of them – to the definition of the wave function.

2. Physical meaning of the wave function

The wave exchange of matter-space and motion-rest (in short, matter-space-time) is in the nature of all physical phenomena. Accordingly the *probability* of possible states must have as well the wave character and reflect the states of rest and motion. The possibility of rest and motion *gives birth* to the potential-kinetic field of *reality*, where rest (a potential field) and motion (a kinetic field) are inseparable linked between themselves in the unit potential-kinetic field. The mathematical image (measure) of the wave of possibility is the *wave of probability*, which was called in dialectical physics [3] the *phase probability* and denoted by the symbol $\hat{p}$:

$$\hat{p} = p_p + ip_k . \qquad (2)$$

Potential and *kinetic* phase probabilities, p_p and p_k, represent the probability of rest and motion, correspondingly.

The *density of phase probability* $\hat{\Psi}$ describes the distribution of phase probability $\hat{p}$:

$$\hat{\Psi} = \frac{d\hat{p}}{dV} = \frac{dp_p}{dV} + i\frac{dp_k}{dV} = \Psi_p + i\Psi_k , \qquad (3)$$

where dV is an elementary volume of space, $d\hat{p}$ is an elementary phase probability, Ψ_p and Ψ_k are, correspondingly, the potential and kinetic densities of phase probability.

We assume that the phase probability $\hat{p}$ (2) and the density $\hat{\Psi}$ (3) satisfy the wave equation (1), which should be called in a general case the *wave probabilistic equation*. The fact is that the phase probability $\hat{p}$ and its density $\hat{\Psi}$ must describe any wave events. In every concrete case, the character of studying objects and the concrete chosen parameters-measures of the description are determined by these events.

The energy of fields is proportional to the wave amplitudes squared; therefore, the *density of energy* of the field is presented as

$$\frac{dE_p}{dV} = \zeta_p \Psi_p^2, \qquad \frac{dE_k}{dV} = \zeta_k \Psi_k^2, \qquad \frac{dE}{dV} = \zeta_p \Psi_p^2 + \zeta_k \Psi_k^2 , \qquad (4)$$

where dE_p, dE_k, and dE are differentials of the potential, kinetic, and total energy; ζ_p and ζ_k are some coefficients of proportionality depending on the selection of phase probability and on the character of the field.

For the class of fields satisfying the condition, $\zeta_p = \zeta_k = \zeta$, we have

$$\frac{dE}{dV} = \zeta(\Psi_p^2 + \Psi_k^2) = \zeta\left|\hat{\Psi}\right|^2. \qquad (5)$$

Along with the phase probability, we operate with the notion of *energetic probability*. The differential of *energetic probability* dw, by the definition, should be assumed to be proportional to the differential of energy dE,

$$dw = \eta dE, \qquad (6)$$

where η is the coefficient of proportionality. Hence the *densities* of potential, kinetic, and total energetic probabilities are determined as

$$\frac{dw_p}{dV} = \xi\Psi_p^2, \qquad \frac{dw_k}{dV} = \xi\Psi_k^2, \qquad \frac{dw}{dV} = \xi\left|\hat{\Psi}\right|^2, \qquad (7)$$

where $\xi = \zeta\eta$ is the coefficient of proportionality depending on the character of the field and the choice of the wave function $\hat{\Psi}$.

The notion of *energetic probability* is needed, along with phase probability, due to the simple reason: the distributions of *total energy* and *masses* are different (although they are related between themselves in the wave field-space of exchange). We should distinguish them.

The characteristic elements of the *wave probabilistic geometry* – *extremes* and *zeroes* of the functions Ψ_k and Ψ_p – define its discrete structure.

Potential and kinetic extremes are mutually conjugated because the conjugated functions,

$$\hat{\Psi} = \Psi_p + i\Psi_k \qquad (8)$$

and

$$\hat{\Psi} = i(\Psi_p + i\Psi_k) = (-\Psi_k)_p + i(\Psi_p)_k, \qquad (9)$$

satisfy the wave equation. Moreover, these extremes are also "conjugated" to zeroes of the wave function because the kinetic extremes spatially coincide with the potential zeroes and the potential extremes are spatially imposed upon the kinetic zeroes.

The extremes and zeroes of Ψ_k and Ψ_p functions coincide with the extremes and zeroes of their squares, Ψ_k^2 and Ψ_p^2, in three-dimensional space of reality. Therefore, they define the same probabilistic geometry of density of states and the energies related to the extremes and zeroes.

Since the wave functions, $\hat{p}$ and $\hat{\Psi}$, satisfy the same wave equation (1), the extremes and zeroes of phase probability $\hat{p}$ and its density $\hat{\Psi}$ coincide. Hence, in this sense, the functions $\hat{p}$ and $\hat{\Psi}$ are equivalent.

The value of the constant coefficient (the normalizing factor) of the $\hat{\Psi}$-function does not matter because only its extremes and zeros, defining the discrete structure of wave processes (their kinematic spatial geometry), interest us. Therefore, it makes sense to introduce the notion the *potential of probability* (or the *probability potential*) proportional to the wave function, which we also designate by the same symbol $\hat{\Psi}$. At such a definition the potential of probability $\hat{\Psi}$ (just like the density of probability) satisfies the wave probabilistic equation (1).

The potential of probability $\hat{\Psi}$ in the spherical polar coordinates (with the physical polar Z-axis) is represented in the form of the product of the four multiplicative components-functions of probability: $\hat{R}(\rho)$ (where $\rho = kr$), $\Theta(\theta)$, $\hat{\Phi}(\varphi)$, and $\hat{T}(t)$, which represent by themselves the multiplicative components of probability potential.

The radial, polar and azimuth components of the potential of probability form the *spatial amplitude of the potential of probability*

$$\hat{\psi}(\rho,\theta,\varphi) = \hat{R}(\rho)\Theta(\theta)\hat{\Phi}(\varphi). \qquad (10)$$

Thus, the potential of probability $\hat{\Psi}$,

$$\hat{\Psi} = \hat{R}(\rho)\Theta(\theta)\hat{\Phi}(\varphi)\hat{T}(t) = \hat{\psi}(\rho,\theta,\varphi)\hat{T}(t), \qquad (11)$$

is determined by the *product of spatial* and *time potentials of probability*. Their amplitudes are described, in accordance with (1), by the following equations:

$$\Delta\hat{\psi} + k^2\hat{\psi} = 0, \qquad (12)$$

and

$$\frac{d^2\hat{T}}{dt^2} = -\omega^2\hat{T}. \qquad (13)$$

Eq. (12) is called the Helmholtz equation, where $\omega = kc$, and the wave vector k is the constant defined from the boundary conditions. At the atomic and subatomic levels, the k-vector is determined by the fundamental frequency ω_e inherent in these levels, $k = \omega_e / c$.

After the conventional separation of variables, the wave equation (12) falls into the equations of radial $\hat{R}_l(\rho)$, polar $\Theta(\theta)$, and azimuthal $\hat{\Phi}(\varphi)$ components. Solutions and, in the definite extent, the form of the radial equation depend on the concrete problem, which imposes the different requirements on k^2. However, for any model of an object of study, the radial solutions define the characteristic sphere of extremes and zeroes of the radial function. For a variety of problems, it is sufficient to know that such characteristic spheres exist. It is very important for determination of the spatial geometry of studying object.

3. The particular solution of the wave probabilistic equation

The wave equation (1) admits the particular solutions in the form

$$\hat{\Psi}(\mathbf{r},t) = \hat{\psi}(\mathbf{r})e^{\pm i\omega t} \tag{14}$$

where $\hat{\psi}(\mathbf{r})$ is the particular solution of the Helmholtz equation (12),

The wave equatioin (1) describes both the spherical and cylindrical components of function-judgment $\hat{\Psi}$ about the spherical-cylindrical fields of matter-space-time.

The *longitudinal* component of the spherical-cylindrical field is described over a *spherical* realization of the wave equation (1). Since $\hat{\psi}(\mathbf{r}) = \hat{R}(kr)\Theta(\theta)\hat{\Phi}(\varphi)$, the separation of variables leads to one time equation (13), which can be presented in the form as follows,

$$\frac{d^2\hat{T}}{d\tau^2} = -\hat{T} \tag{15}$$

and three equations of the spherical space:

$$\rho^2 \frac{d^2\hat{R}_l}{d\rho^2} + 2\rho\frac{d\hat{R}_l}{d\rho} + (\rho^2 - l(l+1))\hat{R}_l = 0, \tag{16}$$

$$\frac{d^2\Theta_{l,m}}{d\theta^2} + ctg\theta\frac{d\Theta_{l,m}}{d\theta} + \left(l(l+1) - \frac{m^2}{\sin^2\theta}\right)\Theta_{l,m} = 0, \tag{17}$$

$$\frac{d^2\hat{\Phi}_m}{d\varphi^2} + m^2\hat{\Phi}_m = 0, \tag{18}$$

where $\rho = kr$ and $\tau = \omega t$. The time component is usually presented in the form

$$\hat{T}(\omega t) = e^{i\omega t}, \tag{19}$$

hence

$$\frac{\partial^2 \hat{\Psi}}{\partial \tau^2} = -\hat{\Psi}. \tag{18}$$

Using the last equality, the wave equation (1) can be written as

$$\frac{\partial^2 \hat{\Psi}}{\partial \rho_x^2} + \frac{\partial^2 \hat{\Psi}}{\partial \rho_y^2} + \frac{\partial^2 \hat{\Psi}}{\partial \rho_z^2} = -\hat{\Psi}, \tag{19}$$

where $\rho_x = kx$, $\rho_y = ky$, and $\rho_z = kz$, or in the form,

$$\Delta_k \hat{\Psi} - \frac{\partial^2 \hat{\Psi}}{\partial \tau^2} = 0, \tag{20}$$

where

$$\nabla_k \nabla_k = \nabla_k{}^2 = \Delta_k = \frac{\partial^2}{\partial \rho_x^2} + \frac{\partial^2}{\partial \rho_y^2} + \frac{\partial^2}{\partial \rho_z^2}, \tag{21}$$

and

$$\nabla_k = \frac{\partial}{\partial kx}\mathbf{i} + \frac{\partial}{\partial ky}\mathbf{j} + \frac{\partial}{\partial kz}\mathbf{k}. \tag{22}$$

Hence the differential wave equation (1) can be presented also in the following forms:

$$\nabla_k \nabla_k \hat{\Psi} = -\hat{\Psi} \qquad \text{or} \qquad \Delta_k \hat{\Psi} = -\hat{\Psi}. \tag{23}$$

This equation expresses in the language of philosophy the *law of double negation*, which is the *universal law of development* (details are in [3]).

Among numerous solutions of the form (11), there is the solution leading to sinusoidal *spherical standing waves*. Just this solution for the physical wave field-space of spherical structure contains information about the atomic structure, periodicity and symmetry [3]. The spherical polar coordinates are related to the Cartesian system by the following way:

$$x = r\sin\theta\cos\varphi, \qquad y = r\sin\theta\sin\varphi, \qquad z = r\cos\theta. \tag{24}$$

This system is useful if the system has some symmetry about the point of the origin.

The boundary conditions request that the solutions must be regular at $0 \le \theta \le \pi$ and $0 \le \varphi \le 2\pi$. They must also satisfy the condition $Y(\theta, \varphi + 2\pi) = Y(\theta, \varphi)$. The wave number

$k = \frac{\omega_e}{c} = constant$, $0 \le r \le \infty$. With that, ω_e is the *fundamental frequency of the wave field of exchange* (interaction) at the subatomic and atomic levels; it is equal to

$$\omega_e = \frac{e}{m_e} = 1.869162559 \times 10^{18}\ s^{-1}. \tag{25}$$

The function (11) and the corresponding spectrum of the $\rho = kr$ values, obtained under the condition $R(kr) = 0$, form the eigenvalues of the solution. Initial conditions are: $\hat{\Psi}(r,\theta,\varphi,0) = \hat{\psi}(r,\theta,\varphi)$ and $\frac{\partial\hat{\Psi}(r,\theta,\varphi,0)}{\partial\tau} = i\hat{\psi}(r,\theta,\varphi)$.

The general form of the solutions of the wave equation (1) for the spherical (longitudinal, central) component of $\hat{\Psi}$, in spherical polar coordinates, is

$$\hat{\Psi} = \hat{R}_l(kr)\Theta_{l,m}(\theta)\hat{\Phi}_m(\varphi)\hat{T}(\omega t) = \hat{\psi}\hat{T}(\omega t), \tag{26}$$

where $\hat{\psi} = \hat{R}_l(kr)\Theta_{l,m}(\theta)\hat{\Phi}_m(\varphi)$ is the *spatial* factor of the wave function of physical space; $l = 0,1,2,...;\ m = 0,\pm1,\pm2,...,\pm l$

The radial component $\hat{R}_l(kr)$ of the spatial factor describes the density of potential-kinetic probability of radial displacements, the polar component $\Theta_{l,m}(\theta)$ – the polar displacements, and $\hat{\Phi}_m(\varphi)$ – the azimuth displacements.

Under the above conditions, at integer values of the wave number *m*, an elementary solution of the wave equation (12) has the standard form of the product of the solutions for three functions corresponding to three spatial variables: $\hat{R}_l(kr)$ ((62)-(65), L.1), $\Theta_{l,m}(\theta)$ ((49)-(52), L. 1), and $\hat{\Phi}_m(\varphi)$ ((45a), L.1). If we present the number *m* in the form $m = \frac{1}{2}2s$, where $s \in \mathbf{N}$ (natural numbers), the solution of (12) takes the following form:

$$\hat{\psi} = A_l\hat{R}_l(\rho)\Theta_{l,s}(\theta)e^{\pm is\varphi} = A_l\sqrt{\frac{\pi}{2\rho}}H^{\pm}_{l+1/2}(\rho)\Theta_{l,s}(\theta)e^{\pm is\varphi} \tag{27}$$

or

$$\hat{\psi} = A_l\sqrt{\frac{\pi}{2\rho}}(J_{l+1/2}(\rho) \pm iY_{l+1/2}(\rho))\Theta_{l,s}(\theta)e^{\pm is\varphi}, \tag{28}$$

where A_l is the constant factor; $\rho = kr$; $H^{\pm}_{l+1/2}(\rho)$, $J_{l+1/2}(\rho)$ and $Y_{l+1/2}(\rho)$ (or $N_{l+1/2}(\rho)$) are the Hankel, Bessel and Neumann functions, correspondingly.

Two terms in (28) are the potential and kinetic *spatial* constituents of $\hat{\Psi}$ function; they have the following form

$$\hat{\psi}_p = \frac{Ac_l(\rho)}{\rho} = A\sqrt{\frac{\pi}{2\rho}} J_{l+1/2}(\rho)\Theta_{l,s}(\theta)e^{\pm is\varphi}, \tag{29}$$

$$\hat{\psi}_k = \pm\frac{As_l(\rho)}{\rho} = \pm A\sqrt{\frac{\pi}{2\rho}} Y_{l+1/2}(\rho)\Theta_{l,s}(\theta)e^{\pm is\varphi}. \tag{30}$$

The noninteger (fractional) solutions of (12), at $l = m = \frac{1}{2}s$, where $s \in \mathbf{N}$, have the form

$$\hat{\psi} = A\hat{R}_s(\rho)\Theta_s(\theta)e^{\pm i\frac{s}{2}\varphi}, \tag{31}$$

where

$$\hat{R}_s(\rho) = \sqrt{\frac{\pi}{2\rho}} H^{\pm}_{\frac{s}{2}+\frac{1}{2}}(\rho), \tag{32}$$

$$\Theta_s(\theta)e^{\pm i\frac{s}{2}\varphi} = C_s \sin^{\frac{s}{2}}\theta(\cos\frac{s}{2}\varphi \pm i\sin\frac{s}{2}\varphi). \tag{33}$$

The maximal value of (33) is at $\theta = \frac{\pi}{2}$. Therefore, the polar extremes of noninteger solutions are in the equatorial plane *xoy* ($z = 0$, Fig. 2, L.1).

All spatial components are determined with the accuracy of a constant factor *A*, imposed by boundary conditions, which have no influence on the peculiarity of distribution of the *nodes* on radial spheres. The superposition of even and odd solutions defines the *even-odd solutions*. Odd solutions describe the nodes (remember, of sinusoidal spherical *standing waves*), lying in the equatorial plane of atomic space. In this plane, there are also solutions in the form of *rings* in space (graphically shown further) separated by the radial unstable shells. A similar structure is widespread in the Universe. For example, big planets of the solar system have rings of matter on such shells.

It follows from Eq. (33) that the polar extrema of noninteger solutions lie in the equatorial plane. For $s = 1$ only one-half of the azimuthal wave is placed on the equator of an external shell. It defines one extremum and the z-axis of the first-fold symmetry. If $s = 2$ the function in (31) defines two extrema and the second-fold axial symmetry; $s = 3$ results in three extrema and the third-fold symmetry, *etc*.

The half-integer solution at $s = 1$ describe the azimuthal wave of probability in the equatorial plane, which twice rotates around the equator. During a half-period the signs of the

parameters are changed into the opposite sign in such a travelling wave. Upon rotating twice around the equator, the probability wave repeats itself again and hence we can write

$$Y(\theta, \frac{s}{2}\varphi) = Y(\theta, \frac{s}{2}(\varphi + 4\pi)), \tag{34}$$

where $s = 1, 2, 3, ...$ The common requirement of periodicity, namely that $Y(\theta, \varphi) = Y(\theta, \varphi + 2\pi)$, meaning that one complete wave of probability is placed on the equator, does not agree with the aforementioned solutions.

Following the definition accepted in the Wave Model, the complex wave function $\hat{\Psi}$ (28) has the probabilistic sense. Two conjugated real terms, $\hat{\Psi}_p$ and $\hat{\Psi}_k$, of the wave function (28) or (26) represent the *densities of potential* and *kinetic phase probabilities* of occurrence of events in *limited domains* of wave physical spaces [3]. We can write the wave function $\hat{\Psi}$ in the form

$$\hat{\Psi} = \hat{\psi}(x, y, z)\hat{T}(t) = \hat{\Psi}_p + i\hat{\Psi}_k, \tag{35}$$

Both constituents of $\hat{\Psi}$, $\hat{\Psi}_p$ and $\hat{\Psi}_k$, reflect thus the polar opposite features of the function – its potential and kinetic character, respectively.

4. Conclusion

Thus, we have considered the *physical meaning* of the wave $\hat{\Psi}$-function entering in the wave equation (1), and now know what we are dealing with (what we obtain as a result) solving this equation. The wave function $\hat{\Psi}$ expresses the *density of probability* of possible states. We also regard the wave function as the *potential of probability*, as the latter is proportional to the density of probability. Therefore, the potential of probability $\hat{\Psi}$, just like the density of probability, satisfies the wave probabilistic equation (1), which for the above reasons can be called the *wave probabilistic equation*.

The potential and density of probability $\hat{\Psi}$ relate to any wave events, describing them. In every concrete case, the character of studying objects and the *concrete* chosen *parameters-measures* of the description are determined by these events. Another approach to explanation of the physical meaning of the wave function is considered in [4] at analyzing Schrödinger's equation of quantum mechanics.

The boundary and initial conditions needed for obtaining concrete solutions in spherical coordinates were formulated wherein. At the accepted conditions, the resulting particular solutions of the general ("classical") wave equation (1), expressed in the form of the product

of radial (Bessel), polar (Legendre's), and azimuthal functions [1], describe *standing sinusoidal spherical waves*.

The obtained solutions indicate to the binary potential-kinetic character of the wave $\hat{\Psi}$-function, related, in particular, to nodes and antinodes, because it contains the *potential* and *kinetic* spatial terms. Thus, the wave function reflects the polar opposite features of studying phenomena or objects.

The data presented in this and previous Lecture will allow us to understand hereinafter the unambiguous conclusions that were made as a result of analysing the above solutions, which consists in the statement about the discovery of a connection of the spatial disposition of nodes (and antinodes) of the spherical sinusoidal standing waves with the structure of atoms. This means that the presented solutions of the wave equation describe, in fact, the structure of atoms. It is the subject of consideration in the next Lectures.

References

[1] G. A. Korn and T. M. Korn, *Mathematical Handbook for Scientists and Engineers*: *Definitions, Theorems, and Formulas for Reference and Review*, McGraw Hill, 1961.

[2] R. F. Harrington, *Time-Harmonic Electromagnetic Fields*, McGraw-Hill, 1961.

[3] L. G. Kreidik and G. P. Shpenkov, *Atomic Structure of Matter-Space*, Geo. S., Bydgoszcz, 2001, 584 p.; http://shpenkov.com/atom.html

[4] G. Shpenkov and L. Kreidik, "*Schrodinger's Errors of Principle*", Galilean Electrodynamics, 3, 16, 51-56, (2005); http://shpenkov.com/pdf/blunders.pdf

Lecture 3

The Structure of Standing Waves in Spherical Space

1. Radial functions

The obtained solution of the spatial component $\hat{\psi} = \hat{R}_l(\rho)\Theta_{l,m}(\theta)\hat{\Phi}_m(\varphi)$, of the wave function $\hat{\Psi} = \hat{\psi}(\rho,\theta,\varphi)\hat{T}(\omega t)$, where $l = 0,1,2,...$; and $m = 0,\pm 1,\pm 2,...,\pm l$, in the form

$$\hat{\psi} = A_l\sqrt{\frac{\pi}{2\rho}}(J_{l+1/2}(\rho) \pm iY_{l+1/2}(\rho))\Theta_{l,m}(\theta)e^{\pm im\varphi}, \qquad (1)$$

uniquely shows that it describes the kinematic structure of *standing waves* in wave physical space. Namely, the solution (1) yields the spatial geometry of disposition of the specific points (nodes and antinodes) in which the wave $\hat{\Psi}$-function takes the zero and extremal values. We will show it here, uncovering in detail all components of the obtained solution and presenting them in the corresponding graphical forms as far as possible, for clarity.

Principal polar-azimuth *nodes* in spherical polar coordinates define the discrete geometry of the probabilistic *potential* polar-azimuth radial wave shells for $m \neq 0$. They are determined by the elementary solutions:

$$\psi_p = C_\Psi R_l(\rho)\Theta_{l,m}(\theta)\cos(m\varphi + \alpha), \qquad (2)$$

where $C_\Psi = C_{l,m}\Phi_m$ is the constant factor.

The relative radius $\rho = kr$ of the *characteristic* shells, potential or kinetic (the shells with the zero or extremal value of the radial functions $R_l(\rho)$), is defined by the roots of the Bessel functions [1].

Zero values of the wave spherical field of probability define the radial spherical shells of zero probability of radial displacements (oscillations); they are the shells of stationary states - nodes. They are defined by the zeros of the Bessel functions.

The radial functions of *even* solutions ($m = 0, \pm 1, \pm 2, ..., \pm l$) in (1), defining the characteristic potential and kinetic shells, are presented in Table 1 (through their relative values $\frac{\hat{R}_l(\rho)}{A}$) and in Fig. 1.

Table 1. The potential-kinetic radial functions of the even solutions

l	$\hat{R}_l(\rho)/A = \sqrt{\pi/2\rho}(J_{l+1/2}(\rho) \pm iY_{l+1/2}(\rho))$
0	$(\sin\rho \pm i(-\cos\rho))\rho^{-1}$
1	$((\rho^{-1}\sin\rho - \cos\rho) \pm i(-\rho^{-1}\cos\rho - \sin\rho))\rho^{-1}$
2	$[((3\rho^{-2} - 1)\sin\rho - 3\rho^{-1}\cos\rho) \pm i((1 - 3\rho^{-2})\cos\rho - 3\rho^{-1}\sin\rho)]\rho^{-1}$
3	$[((15\rho^{-3} - 6\rho^{-1})\sin\rho + (1 - 15\rho^{-2})\cos\rho) \pm i(-(15\rho^{-3} - 6\rho^{-1})\cos\rho + (1 - 15\rho^{-2})\sin\rho)]\rho^{-1}$
4	$[((1 - 45\rho^{-2} + 105\rho^{-4})\sin\rho + (10\rho^{-1} - 105\rho^{-3})\cos\rho) \pm$ $\pm i(-(1 - 45\rho^{-2} + 105\rho^{-4})\cos\rho + (10\rho^{-1} - 105\rho^{-3})\sin\rho)]\rho^{-1}$
5	$[((945\rho^{-5} - 420\rho^{-3} + 15\rho^{-1})\sin\rho - (945\rho^{-4} - 105\rho^{-2} + 1)\cos\rho) \pm$ $\pm i(-(945\rho^{-5} - 420\rho^{-3} + 15\rho^{-1})\cos\rho - (945\rho^{-4} - 105\rho^{-2} + 1)\sin\rho)]\rho^{-1}$

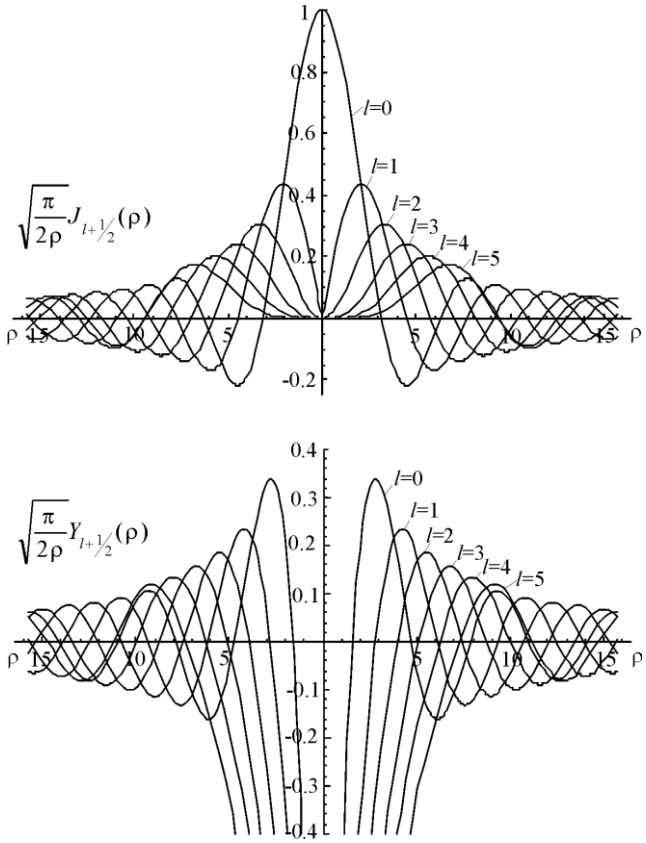

Fig. 1. Plots of the first six radial spherical functions, potential and kinetic.

Two-dimensional images of some potential components of the redial functions, presented in Fig. 1, are shown in Fig. 2.

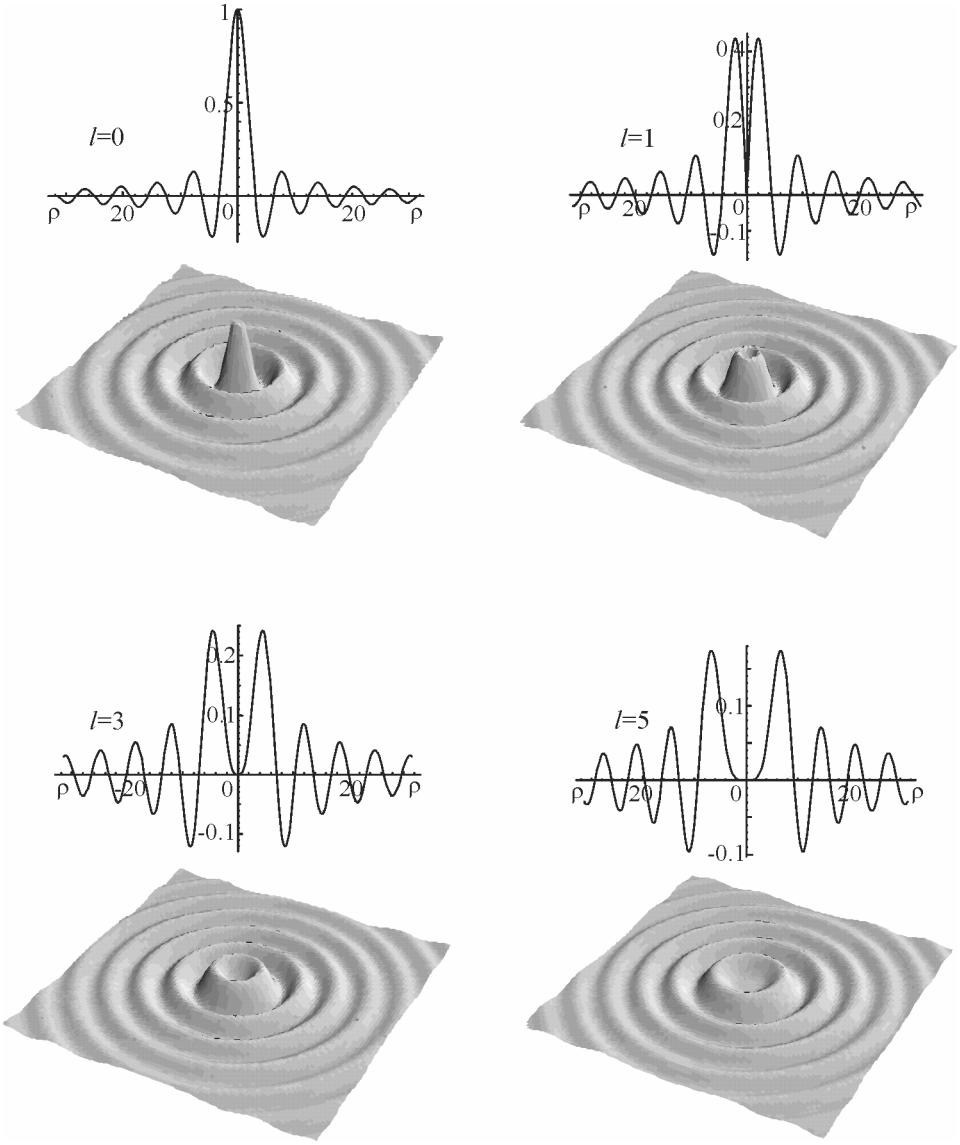

Fig. 2. Two-dimensional images of radial spherical functions $\sqrt{\frac{\pi}{2\rho}}J_{l+1/2}(\rho)$ for $l=0,1,3,5$.

We designate the roots of the zeros and extrema of the radial components, potential and kinetic (see (29) and (30) in L. 2), by the symbols $z_{\nu,q}$ and $z'_{\nu,q}$, respectively, where $\nu = l+\frac{1}{2}$ is the order of the Bessel functions and q is the number of the zero or extremum. We also call the shells, defined by the zeros $z_{\nu,q}$ and extrema $z'_{\nu,q}$, the *characteristic polar-azimuth shells*.

Since $\rho = kr = \frac{r}{\lambda\!\!\!^{-}}$, we obtain the following formulas for the radii of the shells (spheres) of the zeros and extrema: $r_{\nu,q} = \lambda\!\!\!^{-} z_{\nu,q}$ and $r'_{\nu,q} = \lambda\!\!\!^{-} z'_{\nu,q}$. A large set of characteristic shells corresponds to each number *l* of the radial function.

For fixed *l* and *m*, the variable radial number *q* defines the whole class of the geometrically similar shells of the *l*-th radial function.

The conjugate *kinetic* nodes, namely the points of the maxima of motion, are determined by the function

$$\psi_k = C_\Psi R_l(\rho)\Theta_{l,m}(\theta)\sin(m\varphi + \alpha). \qquad (3)$$

2. Polar-azimuthal functions

The polar and azimuth equations, namely ((17) and (18), L. 2), are evidently common (universal) for all models of objects in question, if they are described by the wave probabilistic Eq. (1).

Elementary solutions of the polar equation have the form,

$$\Theta_{l,m}(\theta) = C_{l,m} \cdot P_{l,m}(\cos\theta), \qquad (4)$$

where $C_{l,m}$ is the coefficient depending on the normalization conditions, and $P_{l,m}(\cos\theta)$ are Legendre adjoined functions ((49), L. 1):

$$P_{l,m}(\cos\theta) = \frac{\sin^m\theta}{2^l\, l!}\frac{d^{l+m}}{d(\cos\theta)^{l+m}}\left(\cos^2\theta - 1\right)^l. \qquad (5)$$

The normalization of the polar and azimuthal components is determined by the conditions:

$$\int_0^\pi \left|\Theta(\theta)\right|^2 \sin\theta d\theta = 1 \qquad \text{and} \qquad \int_0^{2\pi} \left|\Phi(\varphi)\right|^2 d\varphi = 1 \qquad (6)$$

The normalized constant $C_{l,m}$ for the polar component (4) is

$$C_{l,m} = \sqrt{\frac{(2l+1)(l-m)!}{2(l+m)!}}. \qquad (7)$$

The elementary linearly independent solutions of the azimuthal equation ((18), L. 2) are

$$\Phi(\varphi) = \Phi_m e^{\pm i(m\varphi+\alpha)}, \qquad (8)$$

where α is an initial phase of the azimuth state. If the first component in the function (8) is potential then the second one is kinetic:

$$\Phi_p(\varphi) = \Phi_m \cos(m\varphi + \alpha), \qquad \Phi_k(\varphi) = \Phi_m \sin(m\varphi + \alpha), \tag{9}$$

Following the normalization condition (6), the normalizing factor of the azimuth potential-kinetic probability in (8) is equal to

$$\Phi_m = \sqrt{\frac{1}{2\pi}}. \tag{10}$$

Thus, the two elementary polar-azimuth functions, potential and kinetic, assume the following form,

$$Y_{l,m}(\theta,\varphi)_p = C_{l,m}\Phi_m\Theta_{l,m}(\theta)\cos(m\varphi + \alpha), \tag{11}$$

$$Y_{l,m}(\theta,\varphi)_k = C_{l,m}\Phi_m\Theta_{l,m}(\theta)\sin(m\varphi + \alpha). \tag{12}$$

Both solutions define the potential-kinetic polar-azimuth function,

$$Y_{l,m}(\theta,\varphi) = C_{l,m}\Phi_m\Theta_{l,m}(\theta)\exp(i(m\varphi + \alpha)). \tag{13}$$

Polar components $\Theta_{l,m}(\theta)$ (4) with the normalizing factor $C_{l,m}$ (7) are presented in Table 2.

Table 2. The polar functions normalized

l	m	$\Theta_{l,m}(\theta)$	l	m	$\Theta_{l,m}(\theta)$
0	0	$\sqrt{2}/2$	4	0	$3\sqrt{2}/16 \cdot (35\cos^4\theta - 30\cos^2\theta + 3)$
1	0	$\sqrt{6}/2 \cdot \cos\theta$		±1	$3\sqrt{10}/8 \cdot \sin\theta\cos\theta(7\cos^2\theta - 3)$
	±1	$\sqrt{3}/2 \cdot \sin\theta$		±2	$3\sqrt{5}/8 \cdot \sin^2\theta(7\cos^2\theta - 1)$
2	0	$\sqrt{10}/4 \cdot (3\cos^2\theta - 1)$		±3	$3\sqrt{70}/8 \cdot \sin^3\theta\cos\theta$
	±1	$\sqrt{15}/2 \cdot \sin\theta\cos\theta$		±4	$3\sqrt{35}/16 \cdot \sin^4\theta$
	±2	$\sqrt{15}/4 \cdot \sin^2\theta$	5	0	$\sqrt{22}/16 \cdot \cos\theta(63\cos^4\theta - 70\cos^2\theta + 15)$
3	0	$\sqrt{14}/4 \cdot \cos\theta(5\cos^2\theta - 3)$		±1	$\sqrt{165}/16 \cdot \sin\theta(21\cos^4\theta - 18\cos^2\theta + 1)$
	±1	$\sqrt{42}/8 \cdot \sin\theta(5\cos^2\theta - 1)$		±2	$\sqrt{1155}/8 \cdot \sin^2\theta\cos\theta(3\cos^2\theta - 1)$
	±2	$\sqrt{105}/4 \cdot \sin^2\theta\cos\theta$		±3	$\sqrt{770}/16 \cdot \sin^3\theta(9\cos^2\theta - 1)$
	±3	$\sqrt{70}/8 \cdot \sin^3\theta$		±4	$3\sqrt{385}/32 \cdot \sin^4\theta\cos\theta$
				±5	$3\sqrt{154}/32 \cdot \sin^5\theta$

To calculate the characteristic polar angles of the functions $\Theta_{l,m}(\theta)$, it is convenient to use the reduced polar functions $\tilde{\Theta}_{l,m}(\theta)$, which are normalized in the following way:

$$\tilde{\Theta}_{l,m}(\theta) = \frac{2^l l!(l-m)!}{(2l)!}\sqrt{\frac{2(l+m)!}{(2l+1)(l-m)!}}\cdot\Theta_{l,m}(\theta) = \\ = \frac{2^l l!(l-m)!}{(2l)!}P_{l,m}(\cos\theta). \tag{14}$$

The recurrence relation connects the normalized polar functions to themselves:

$$\tilde{\Theta}_{l+1,m}(\theta) = \cos\theta\,\tilde{\Theta}_{l,m}(\theta) - \frac{l^2-m^2}{4l^2-1}\tilde{\Theta}_{l-1,m}(\theta), \tag{15}$$

And we have $\tilde{\Theta}_{0,0}(\theta) = 1$, $\tilde{\Theta}_{1,0}(\theta) = \cos\theta$, and $\tilde{\Theta}_{l,l}(\theta) = \sin^l\theta$, if $l = m$.

If the normalizing factor of the azimuth functions (9) is assumed to be equal to the numerical unit, these functions are also called the reduced functions.

The reduced polar potential functions for $l \le 6$ are presented in Table 3.

Table 3. The reduced polar functions $\tilde{\Theta}_{l,m}(\theta)$

l	m	$\tilde{\Theta}_{l,m}(\theta)$	l	m	$\tilde{\Theta}_{l,m}(\theta)$
0	0	1			
1	0	cosθ	5	0	cosθ (cos^{4}θ - 10/9 cos^{2}θ + 5/21)
	±1	sinθ		±1	sinθ (cos^{4}θ - 2/3 cos^{2}θ + 1/21)
2	0	cos^{2}θ - 1/3		±2	sin^{2}θ cosθ (cos^{2}θ - 1/3)
	±1	sinθ cosθ		±3	sin^{3}θ (cos^{2}θ - 1/9)
	±2	sin^{2}θ		±4	sin^{4}θ cosθ
3	0	cosθ (cos^{2}θ - 3/5)		±5	sin^{5}θ
	±1	sinθ (cos^{2}θ - 1/5)			
	±2	sin^{2}θ cosθ	6	0	cos^{6}θ - 15/11 cos^{4}θ +5/11 cos^{2}θ - 5/231
	±3	sin^{3}θ		±1	sinθ cosθ (cos^{4}θ - 10/11 cos^{2}θ + 5/33)
4	0	cos^{4}θ - 6/7 cos^{2}θ + 3/35		±2	sin^{2}θ (cos^{4}θ - 6/11 cos^{2}θ + 1/33)
	±1	sinθ cosθ (cos^{2}θ - 3/7)		±3	sin^{3}θ cosθ (cos^{2}θ - 3/11)
	±2	sin^{2}θ (cos^{2}θ - 1/7)		±4	sin^{4}θ (cos^{2}θ - 1/11)
	±3	sin^{3}θ cosθ		±5	sin^{5}θ cosθ
	±4	sin^{4}θ		±6	sin^{6}θ

The plots of the polar functions $|\Theta_{l,m}(\theta)|$ are shown in Fig. 3. They are valid within the normalizing factor for the reduced functions $\tilde{\Theta}_{l,m}(\theta)$ as well.

The reduced polar-azimuth potential functions, $\tilde{Y}_{l,m}(\theta,\varphi)$, are presented in Table 4. The graphs of the polar-azimuth functions $Y_{l,m}(\theta,\varphi)$ (or $\tilde{Y}_{l,m}(\theta,\varphi)$) are drawn in Fig. 4 (with circumferences, defining the cones of extremal values of polar angles).

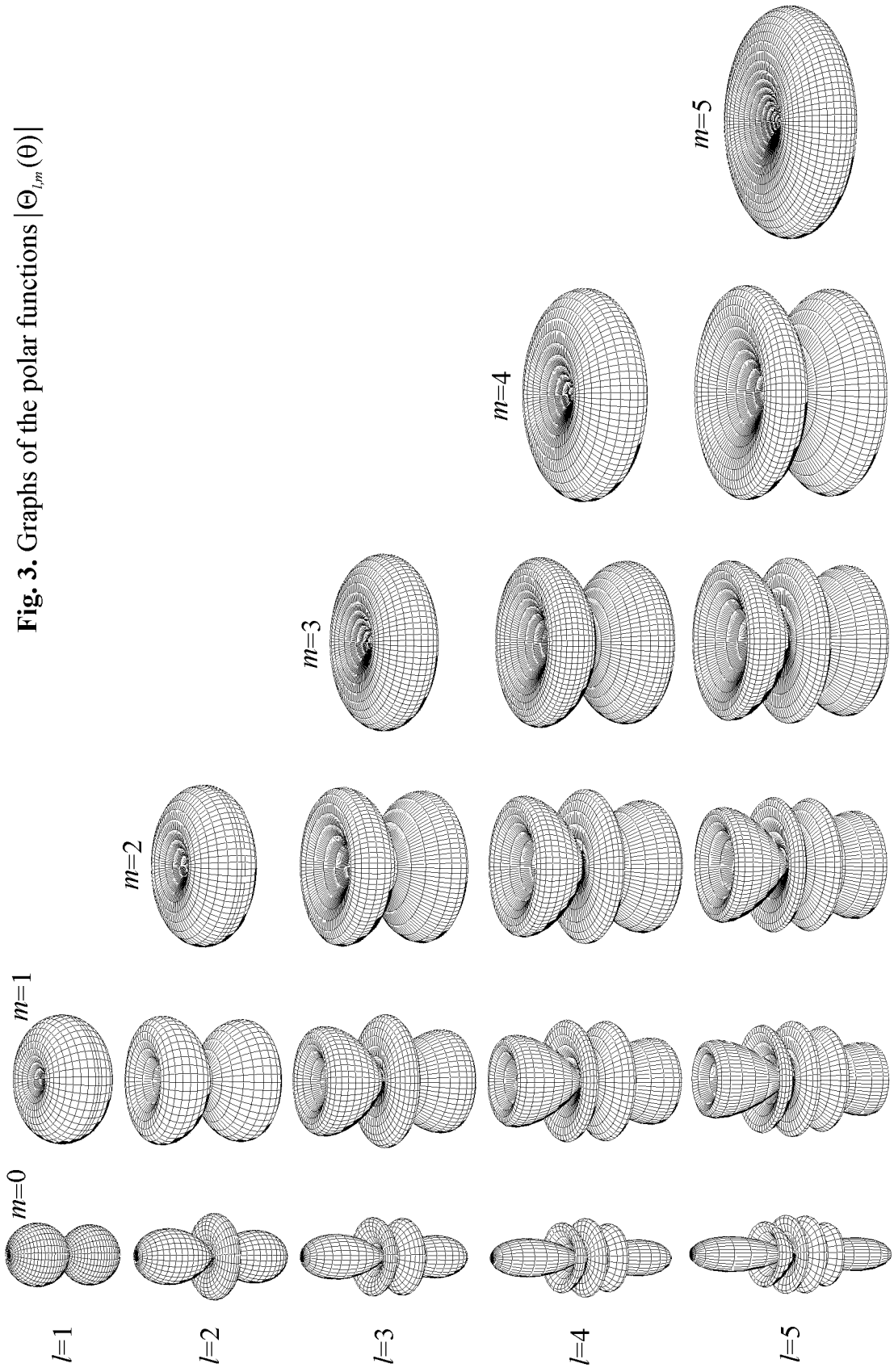

Fig. 3. Graphs of the polar functions $|\Theta_{l,m}(\theta)|$

Table 4. The reduced polar-azimuth potential functions $\tilde{Y}_{l,m}(\theta,\varphi)$

l	m	$\tilde{Y}_{l,m}(\theta,\varphi)=\tilde{\Theta}_{l,m}(\theta)\cos m\varphi$	l	m	$\tilde{Y}_{l,m}(\theta,\varphi)=\tilde{\Theta}_{l,m}(\theta)\cos m\varphi$
0	0	1			
1	0	cosθ	5	0	cosθ (cos^{4}θ - 10/9 cos^{2}θ + 5/21)
	±1	sinθ cosφ		±1	sinθ (cos^{4}θ - 2/3 cos^{2}θ + 1/21) cosφ
2	0	cos^{2}θ - 1/3		±2	sin^{2}θ cosθ (cos^{2}θ - 1/3) cos2φ
	±1	sinθ cosθ cosφ		±3	sin^{3}θ (cos^{2}θ - 1/9) cos3φ
	±2	sin^{2}θ cos2φ		±4	sin^{4}θ cosθ cos4φ
3	0	cosθ (cos^{2}θ - 3/5)		±5	sin^{5}θ cos5φ
	±1	sinθ (cos^{2}θ - 1/5) cosφ			
	±2	sin^{2}θ cosθ cos2φ	6	0	cos^{6}θ - 15/11 cos^{4}θ +5/11 cos^{2}θ - 5/231
	±3	sin^{3}θ cos3φ		±1	sinθ cosθ (cos^{4}θ - 10/11 cos^{2}θ +5/33) cosφ
4	0	cos^{4}θ - 6/7 cos^{2}θ + 3/35		±2	sin^{2}θ (cos^{4}θ - 6/11 cos^{2}θ + 1/33) cos2φ
	±1	sinθ cosθ (cos^{2}θ - 3/7) cosφ		±3	sin^{3}θ cosθ (cos^{2}θ - 3/11) cos3φ
	±2	sin^{2}θ (cos^{2}θ - 1/7) cos2φ		±4	sin^{4}θ (cos^{2}θ - 1/11) cos4φ
	±3	sin^{3}θ cosθ cos3φ		±5	sin^{5}θ cosθ cos5φ
	±4	sin^{4}θ cos4φ		±6	sin^{6}θ cos6φ

The *polar* components $\Theta_{l,m}(\theta)$ of the spatial density of the probability $\hat{\Psi}$ define characteristic parallels of the extrema (principal and collateral) and the zeroes on radial spheres (shells).

The *azimuthal* components $\Phi_m(\varphi)$ define characteristic meridians of extrema and zeroes. Potential and kinetic polar-azimuth probabilities together define the distinctive coordinates (points) of the extrema and zeroes on the corresponding *radial* shells $R_l(\rho)$.

3. The nodal structure of standing waves

The contour plots of the *potential* components of the density of probability ψ_p (for $l=0,1,2,3$) are depicted in Fig. 5. The images presented here are the sections of ψ_p in the plane $x=0$ (for $l=0,1,2,3; m=0,\pm1$), the sections in the *equatorial* plane $z=0$ (for $l=2; m=\pm2$ and $l=3; m=\pm3$), and in the plane *xy* ($z\neq0$, for $l=3; m=\pm2$).

The same solutions, showing the disposition of nodes of standing waves in spherical space (corresponding to $l=0,1,2,3,4,5$), are depicted schematically in Fig. 6. There at the top right are shown also the images of polar $\Theta_{5,2}(\theta)$ and polar-azimuth $Y_{5,2}(\theta,\varphi)$ functions corresponding to the solution for $l=5$ and $m=\pm2$, and the image of the polar-azimuthal function $Y_{5,2}(\theta,\varphi)$ conditionally together with a fixed spherical surface of the radius r_0,

within the radial solution $R_{5,2}(r)$. These images are shown for better understanding the way by which the points, corresponding to the nodes of standing waves (and wave circular formations at $m = 0$) presented in Fig. 6, were arranged in a specific order.

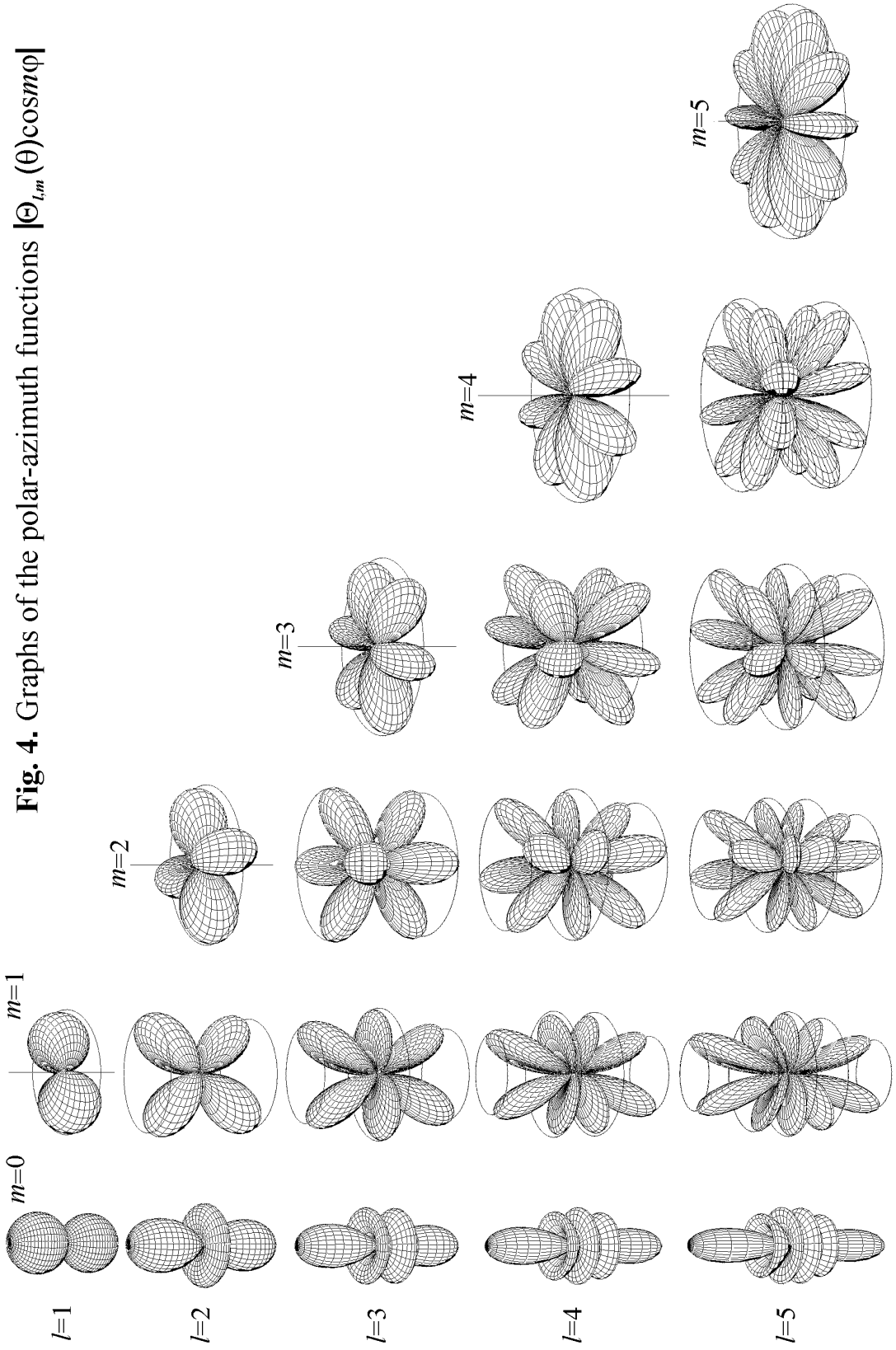

Fig. 4. Graphs of the polar-azimuth functions $|\Theta_{l,m}(\theta)\cos m\varphi|$

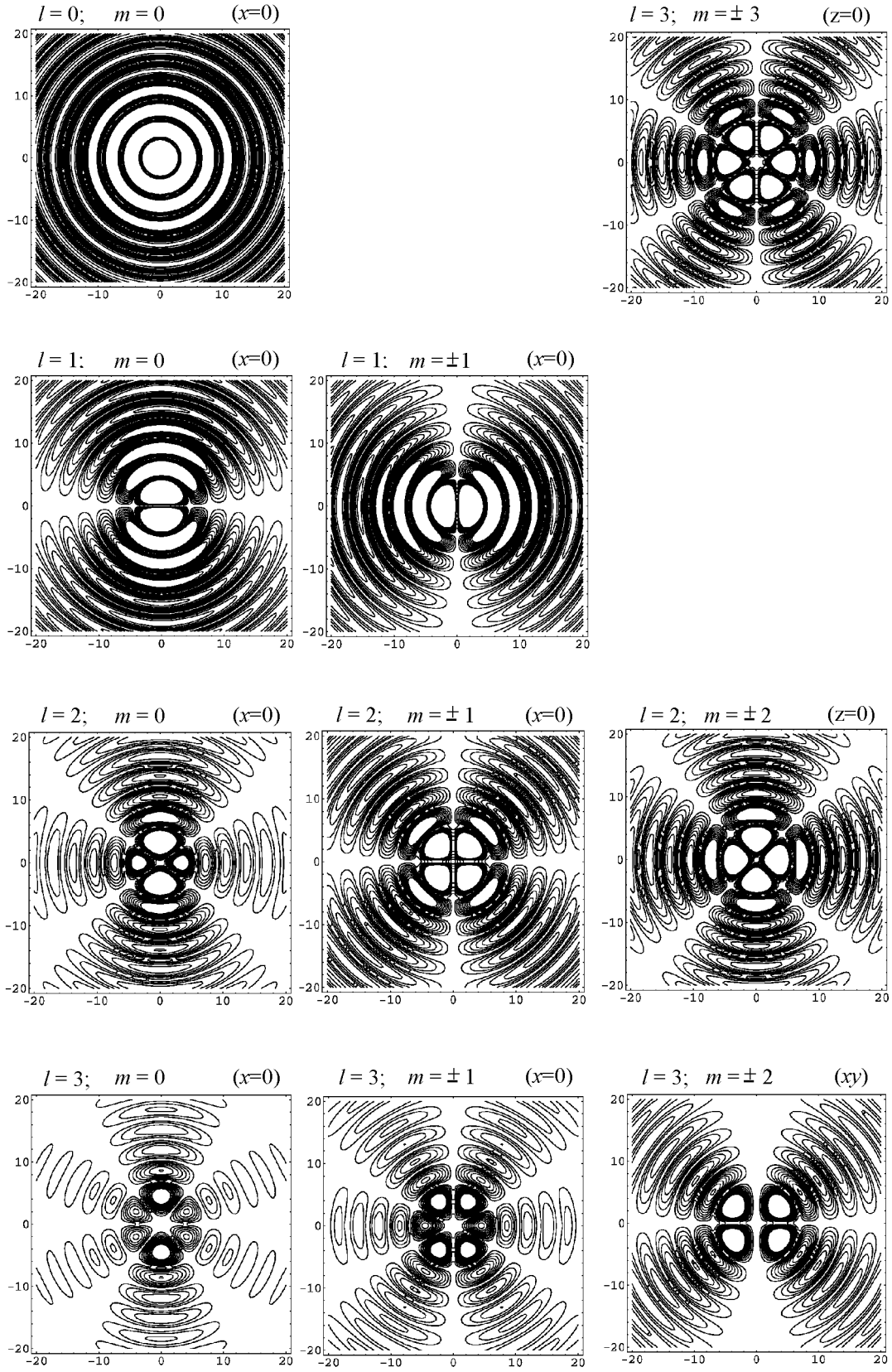

Fig. 5. Contour plots of the sections for the potential density of probability ψ_p in the plane $x=0$ (for $l=0,1,2,3; m=0,\pm1$), in the plane $z=0$ (for $l=2; m=\pm2$ and $l=3; m=\pm3$), and in the plane xy ($z\neq0$, for $l=3; m=\pm2$).

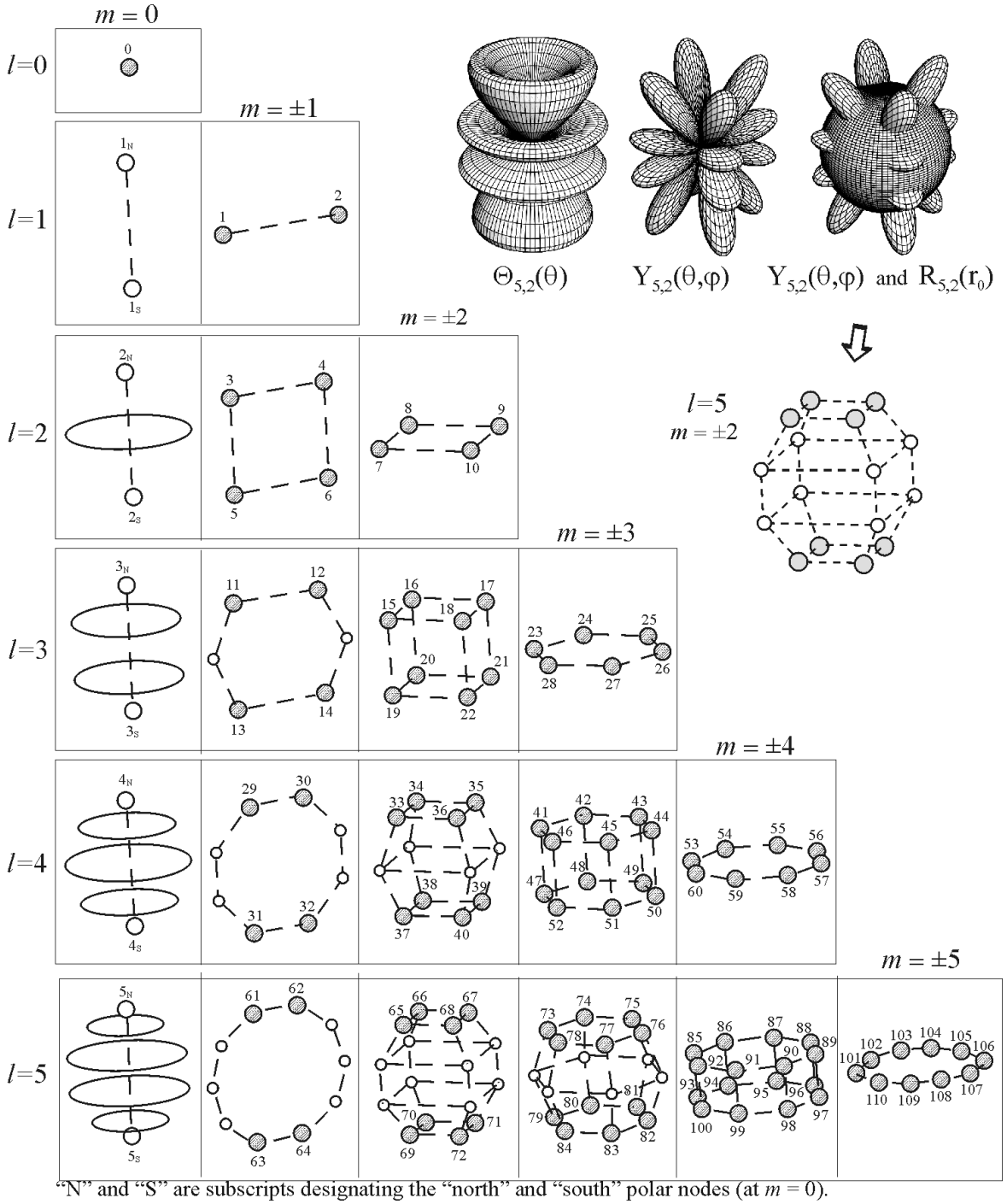

Fig. 6. Solutions $\psi_{l,m}(\rho,\theta,\varphi)_p = C_\Psi R_l(\rho)\Theta_{l,m}(\theta)Cos m\varphi$ for constant r of the probabilistic wave equation $\Delta\hat{\Psi} - \frac{1}{c^2}\frac{\partial^2\hat{\Psi}}{\partial t^2} = 0$ presented so as to indicate the space distribution of the *potential* extrema-nodes (discrete elements of the shell-nodal structure of atoms). The numbers 1, 2, 3, …, 110 are the ordinal numbers of the principal polar-azimuth nodes coinciding with the atomic numbers Z of the elements [3].

Thus, with an example for $l = 5$ and $m = \pm 2$, we see how the presented discrete (nodal) structure of the three dimensional wave space is obtained from the aforementioned solutions for the different wave numbers *l* and *m*.

The plots of the solutions show that there are *principal* (designated in Fig. 6 by shaded points) and *collateral* (designated by the smaller unnumbered hollow points) extrema, which determine, respectively, stable and metastable states of probabilistic events. Principal *potential* polar-azimuth nodes are numbered in Fig. 6 by the ordinal numbers.

Every principal node with the ordinal number Z bounds to a definite extent all previous shells with their nodes. Having the specific spatial structure, every such object is distinguished from all of the others by specific unrepeatable properties. The totality of discrete units (nodes) of the wave probabilistic field is considered to be an element ("atom") of the field.

Now should pay attention to the following fact. It is about the principal difference (mentioned in Sect. 2 of L. 2) existing between the distributions of the two kinds of extrema: (1) the phase probability density $\hat{\Psi}$ and (2) the energy density of wave fields proportional to $\left|\hat{\Psi}\right|^2$: $\frac{dE}{dV} = \zeta(\Psi_p^2 + \Psi_k^2) = \zeta\left|\hat{\Psi}\right|^2$ (Eq. (5), L. 2). This difference is demonstrated in Fig. 7.

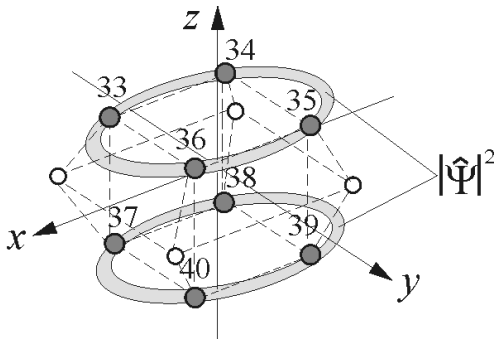

Fig. 7. The distribution of the extrema of probabilistic states $\hat{\Psi}$ (small black and white spheres) and extrema of the total energy proportional to $\left|\hat{\Psi}\right|^2$ (large toroidal circumferences) for the shell with *l* = 4, *m* = ±2.

References

[1] F.W.J. Olver, ed., *Royal Society Mathematical Tables*, Vol. 7, Bessel Functions, part. III, Zeros and Associated Values, Cambridge, 1960.

Lecture 4

Fundamentals of the Periodic Law

1. Introduction

Hundreds of graphical representations of the *Periodic Law* through the *Periodic Table of the Elements* have been designed to present time [1-3] since then as the first periodic table of Dmitri Mendeleev, illustrating periodic trends which he found in the properties of the then-known elements, has been widely recognized after its publication in 1869. Mendeleev's Periodic Table was published in its original form last time in 1906 [4]. Subsequently, all published tables, including the last modern ones, represent the modified and partially distorted reflections, in form and content, of the original. Mendeleev's Table has undergone some principle changes after appearance of relativity theory and resulting rejection of the concept of ether in physics. We will not discuss this topic here. The critical analysis focused on identifying the principal difference of the initial undistorted Periodic Table of Mendeleev compared with the modern versions of the table, one can find in [5].

In spite of a rich diversity of the representations proposed in last years, the patterns of the distorted versions of the Periodic Table have preserved the order established with lapse of time (after aforesaid changes of the original) in the arrangement of the elements *in its groups and periods* have providing no convincing additional information for insight into the nature of the Periodic Law.

Actually, all contemporary variants of the Periodic Table of the Elements are organized on the basis of their *atomic number* (number of protons in the nucleus), so-called "*electron configurations*", and *recurring chemical properties*. In atomic physics and quantum chemistry, the *electron configuration* is the distribution of electrons of an atom or molecule in *atomic* or *molecular "orbitals"*. Thus, currently all explanations of the observed *periodicity* in chemical properties of the elements are based on a quantum-mechanical concept on the *electron configuration* of atoms. In view of the introduced notions, the *key role* at the formation of chemical bonds (their *directions*) in molecular structures is ascribed to the *electron configuration* of the interacting atoms, *i.e.*, to the above "*orbitals*". As concerns *nucleons*, there is no even a hint on any their role in this process.

However, reasonableness of introduction in physics of such subjective notions as the *electron configuration*, *atomic* and *molecular orbitals* (add to them also the notion of *hybridization of the orbitals*) causes the justified doubts in recent years [6].

What is the basis of the aforesaid theoretical notions related to the atomic structure, which are the basis for modern chemistry and, accordingly, used for explanation of the periodicity? In short, the commonly accepted understanding of the periodicity rests on the concepts lying in the foundations of quantum-mechanical (QM) atomic theory (model). The latter has kept the Rutherford-Bohr idea on an existence of a tiny core (*nucleus*) in the centre of an atom.

Further, in the QM theory which is *probabilistic* inherently, there are no circular orbits like of Bohr with orbiting electrons on them. The Bohr orbits were replaced with the so-called *probability density function*, defining the probability of finding any electron of an atom in any specific region around the atom's nucleus. The density of probability is represented by the so-called "*orbitals*" which are regions within the atom where electrons have the highest probability of being found. Thus, denial in principle in the QM of such a notion as the mechanical trajectory, *i.e.*, lack of the notion of orbiting, is a fundamental feature of the QM theory. *Electron orbitals* ("*electron configuration*" or "*electron clouds*") may refer to an "*atomic orbital*", describing the behaviour of an electron in an atom, or a "*molecular orbital*", describing the behaviour of an electron in a molecule.

Since the aforementioned model of atoms (*probabilistic* and *nuclear*) has been accepted in physics, atomic nuclei began studied separately in a newly developing branch of physics – nuclear physics. Remember, the father of *nuclear* physics is rightly considered Ernest Rutherford. Accordingly, the *spatial distribution* of nucleons inside atoms was/is not considering as an urgent problem of researches in *atomic physics*. It does not make sense for the accepted atomic model. Really, according to the latter, all nucleons, densely packed in a minute spatial volume in the center of an atom, form there an extremely dense core called the *nucleus*. Its size, as believe, is in the range of 1.75 fm ($1.75\times10^{-13}\,cm$) for hydrogen ${}^{1}_{1}H$ (*i.e.*, for a single nucleon, proton) to about 15 fm for the heaviest atoms, such as uranium ${}^{238}_{92}U$. The so-called *rms* ("root mean square") *charge radius* ascribed in modern physics to the proton is $r_{p,rms}=0.8775\times10^{-13}cm$. An enormous density of the nucleus of an atom is averaging about $2.3\times10^{14}\ g\times cm^{-3}$.

Having turned with time into a dogma, the nuclear atomic model has never been questioned so far. However, fortunately, during the last several years, as was repeatedly mentioned in these Lectures, it has been found that the particular solutions of the ordinary wave equation, which has been accepted as the basis of the Wave Model (WM):

$$\Delta\hat{\Psi}-\frac{1}{c^2}\frac{\partial^2\hat{\Psi}}{\partial t^2}=0\,, \qquad (1)$$

where the Ψ-function represents the *density of the potential-kinetic phase probability* for the occurrence of events in wave spaces [7, 8], contain information about an *internal* spatial structure (as turned out to be *shell-nodal*) of individual atoms (and elementary crystals) and, hence, about the nature of the periodicity inherent in their behavior.

From solutions of Eq. (1) it follows that *there is no superdense region* in the center of an atom, and, hence, *nucleons* are not s*uperdense* formations as is believed. The nucleons are located in the nodes of the spherical wave shells of an atom, by two per node. As it turned out, the positions of nucleon nodes correlate with the equilibrium disposition of the nodes in elementary crystals. This correlation is proven by the found fact that the *polar-azimuthal* functions, defining angular spatial coordinates of nodes and antinodes of standing waves in spherical space, indicate characteristic directions of atomic planes in crystals, revealing the nature of the *law of constancy of angles* between their facets.

Really, the comparative analysis has shown that the characteristic angles defined just by the polar-azimuthal functions are materialized in characteristic angles observed in different crystal forms of minerals (collected in Table 3.1, pages 232-253 in [9], and Table 1 in [10]). This means that the correctness of the internal spatial shell-nodal structure of atoms (not the electron structure), that has been discovered thanks to the aforesaid solutions, have obtained at once, when solving, the first firm evidence. It should be noted that the aforementioned reproducibility in crystals of the nodal structure of individual atoms, *i.e.*, at the molecular level (for short- and long-range orders), was the first, but not last in a series of the found hereinafter other confirmations of the validity of the shell-nodal atomic model.

Thus, the Wave Model (WM), considering in these Lectures, does not confirm an existence of the superdense atomic nucleus. According to the WM, atoms have the internal ordered *shell-nodal structure* with coupled hydrogen atoms in each of the intra-atomic nucleon nodes. Nucleons (protons and neutrons) have a size of the same order that has the hydrogen atom. Really, the proton radius is $r_p = 0.528421703 \times 10^{-8} cm$ (see Eq. (27) in L. 2, V. 2). This magnitude is on five order more than that one ascribed to the proton in contemporary physics.

The *key role* at the formation of molecules and crystals, *i.e.*, chemical bonds of the *definite directions*, belongs to the spatial configuration of the *internodal bonds* in external wave shells of interacting atoms, but not to the mythical *electron configuration* as it follows from the QM. Electrons define only the *bonds strength, but not their directions*.

Like the atoms at their level, nucleons, in turn, have their *own internal structure* described by the same wave equation (1). This structure is finer in comparison with the intra-atomic nodal structure. The nodal nucleons consist of the finer (subatomic) particles characteristic for the *subatomic level* which is the first among the deeper levels of the Universe, following the atomic level.

The main subject of this Lecture is a continuation of an analysis of the solutions of Eq. (1) carried out in the framework of the Wave Model, where atoms are regarded as the wave formations. This analysis has led to the discovery of the *shell-nodal structure of the atoms* and to the fact that the spatial disposition of the nodes in them repeats the *nodal structure of standing waves* in the spherical space.

The present consideration is focused, in particular, on to elucidation of the nature of Mendeleev's Periodic Law in view of the revealed details about the wave structure of the atoms. The modern version of the Periodic Law is generalized in the well-known Periodic Table widely represented everywhere in different forms. Here, we demonstrate a new version of the table called the *Periodic Table of the Atoms* [11], which is unique as being the first one derived pure theoretically. It displays in a visual form the nature of the Periodic Law which, thanks to the aforesaid comprehensive analysis, for the first time in physics has been revealed in the well-known particular solutions of the wave equation (1).

Thus, we are facing the *discovery* from which it follows that the general ("classical") wave equation describes properly, along with other wave phenomena, the wave structure of the atoms and, hence, the Periodic Law which reflects specific wave features of their behaviour. It should be noted in this connection that the solutions that are analysed here have been known for a long time, but no one could guess so far that they contain also information about the structure of atoms. Only dialectical approach has allowed revealing this fact [7].

2. Nodes of standing waves and nucleon nodes of the atoms

Fig. 6 presented in Lecture 3 is the key graphical image of the obtained solutions. All other forms, namely the Generalized Table of the Elements and the Table of Relative Atomic Masses of the Elements, are the derivatives of it. We will turn constantly to this figure in the present and other Lectures. Therefore, we show the aforesaid image of the obtained solutions here again in Fig. 1.

The obtained distribution of the nodes, presented in Fig. 1, in the standing wave of the spherical space, described by the wave equation (1), also defines the distribution of the particles of matter, if a material space is considered. They have to be positioned in nodal (potential) points of the space, because any particles move toward an equilibrium state.

It should be noted in this connection that the wave equation for atomic spaces is the equation of the microsystems. It does not describe the motion of isolated microobjects, but it describes the wave processes at the definite level of space as a whole, determining the space structures as unified systems.

The question arises as to what kinds of particles are localized in nodes of space at the atomic level: neutrons, protons, electrons, or all together? Analyzing the structure of crystals at the end of the eighteenth century, R.J. Haüy (1743-1822) [12] came to the conclusion that

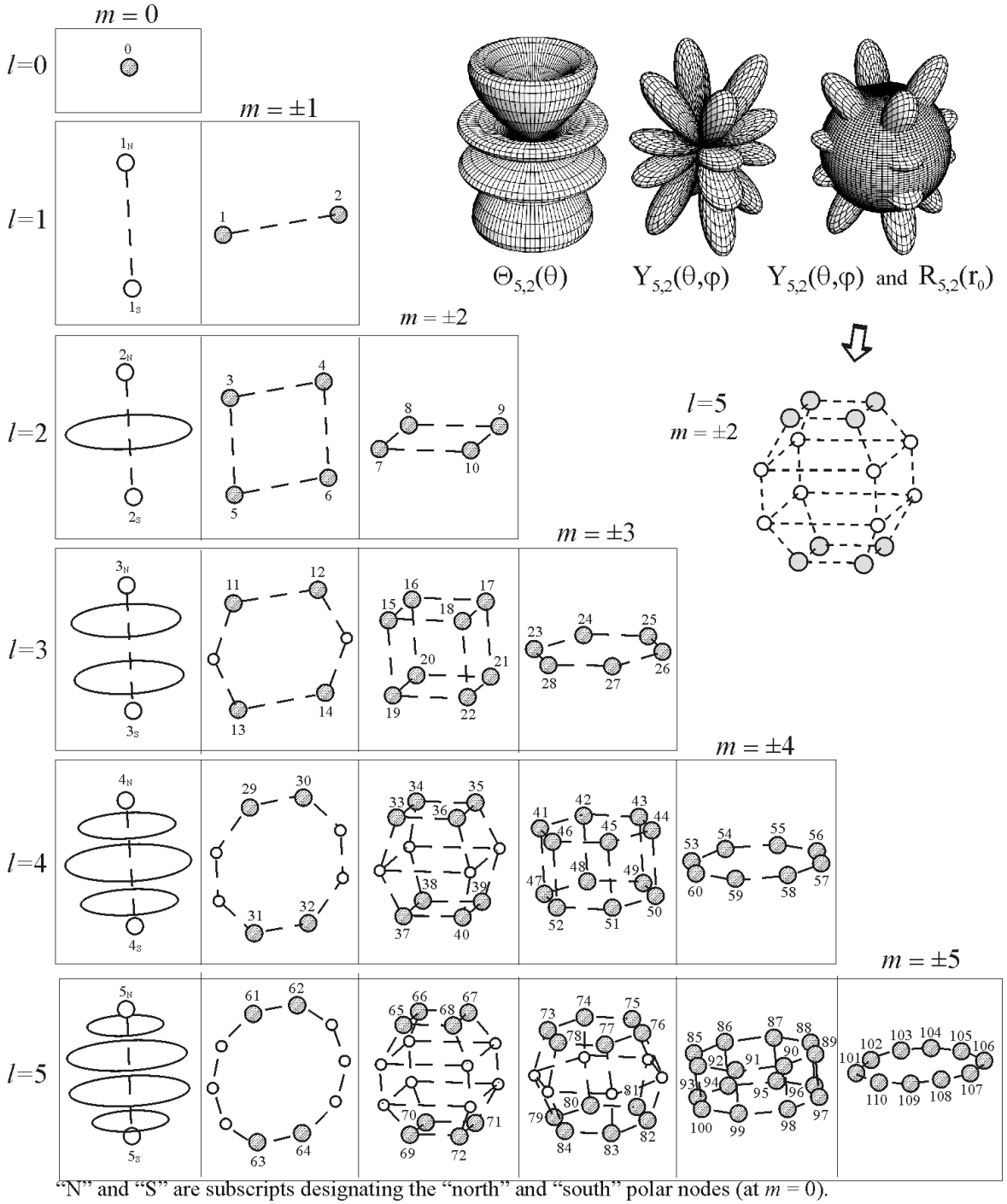

Fig. 1. Solutions $\psi_{l,m}(\rho,\theta,\varphi)_p = C_\Psi R_l(\rho)\Theta_{l,m}(\theta)Cos m\varphi$ for constant r of the probabilistic wave equation $\Delta\hat{\Psi} - \frac{1}{c^2}\frac{\partial^2\hat{\Psi}}{\partial t^2} = 0$ presented so as to indicate the space distribution of the *potential* extrema-nodes (discrete elements of the shell-nodal structure of atoms). The numbers 1, 2, 3, …, 110 are the ordinal numbers of the principal polar-azimuth nodes coinciding with the atomic numbers Z of the elements.

it is necessary to consider atoms as elementary molecules, the internal structure of which determines the crystal structure of solids.

Since the masses of atoms are multiple of the mass of the hydrogen atom mass, it seems reasonable, following Haüy's ideas, to suppose that any atom, like the elementary Haüy molecule, is the hydrogen atom molecule. Actually, it was shown by comprehensive analysis of the direct and indirect consequences of solutions of the wave equation [7] that the nodes of intra-atomic space are filled by hydrogen atoms corresponding to the *protons* and *neutrons.*

Therefore, atoms should be considered as hydrogen atom quasispherical molecules. Thus, it is possible to assume that Fig. 1 shows the actual picture of the distribution of nodes in Haüy's elementary molecules.

Potential *principal* polar-azimuth nodes of the wave space of atoms are characterized by ordinal numbers. These numbers coincide with the ordinal numbers of the elements of the Periodic Table. The number of hydrogen atoms localized in one node is equal to or less than two.

Unnumbered *collateral* nodes are the points in space where the amplitude $\hat{\psi}$ of the probability density of events (concentration of matter in our case) is less than that at principal nodal points. Therefore, the collateral nodes, indicated in Fig. 1 by smaller white circles, are partially vacant; these may provide conditions for the interatomic movement of hydrogen atoms.

For example, one of the isotopes of ${}^{28}_{14}Si$, has four spherical atomic shells, the principal nodes of which are completed (*i.e.*, they contain 28 nucleons), but two collateral nodes of the outer shell ($n = 3$, $m = \pm 1$, see Fig. 1) remain vacant. This latter fact apparently determines the semiconductor properties of silicon. All *polar* nodes (corresponding to $m = 0$) are *potential-kinetic* nodes. They are simultaneously the nodes of rest and motion. Therefore, they cannot be the locations of equilibrium states for the particles of matter settled there.

Integer-fractional shells (Eq. (31), L. 2), which are analogous to mixed fractions in number theory, are complexes of the last integer shells and, subsequently, the groups of half-integer shells. These complexes give a more complete image of the structure of all atoms of the Periodic Table though they are not shown here.

Half-integer solutions occur in the equatorial domain and can have any-fold symmetry. In particular, the five-fold symmetry ($s = 5$), which is strictly forbidden by the mathematical laws of crystallography, was observed in 1984 [13]. Twelve-fold symmetry ($s = 12$) has been found by S. Mae [14]. These (and other "forbidden") symmetries have attracted the special attention of modern researchers [15].

As an example, Fig. 2 presents an image (contour plots of sections) of the distribution of the density of matter at $s = 5$, determined by the function:

$$R_S(\rho_{s,j})\sin^{\frac{s}{2}}\theta\cos(\frac{s}{2}\varphi), \qquad (2)$$

where

$$R_S(\rho) = \frac{1}{\sqrt{\rho}} J_{s/2+1/2}(\rho). \qquad (3)$$

This distribution of the five-fold symmetry has the characteristic arc-rings.

Thus the function $\hat{\psi}$ describes, following an approach developed in dialectical physics by the Wave Model (WM), the *density of probability of concentration of matter* in standing *potential* nodal points of limited domains of the wave physical space of atoms [7], *i.e.*, the wave shell-nodal structure of atoms.

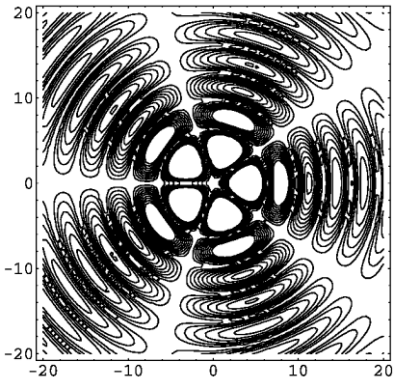

Fig. 2. The equatorial distribution of the density of matter at the subatomic level (s = 5). The symmetry is "strictly forbidden by the mathematical laws of crystallography" [15].

From comparison of quasi-periodicity in completing the shells by nodes (the principal numbers of polar-azimuthal nodes), observed in Fig. 2, and the periodicity in the position of elements in the Periodic Table by groups and rows (the atomic numbers of the elements), it has been easy to come to the understanding that an atom, being considered as a wave formation, represents a system of spherical shells with discrete points-nodes of wave space completed by hydrogen atoms.

It means that atoms, reminding nucleon molecules, have not a customary nucleus as is assumed in case of the standard quantum mechanical (QM) *nuclear* atomic model.

Being essentially different from QM and, respectively, Rutherford-Bohr's model, the new *molecule-like* atomic model, we shall call it *shell-nodal atomic model*, well agrees with well-known experiments that we have already considered (including Rutherford's experiment on dispersion of α- and β-particles in substance [16]). Moreover, it reveals the nature of some phenomena misunderstood until now [17-18], including aforementioned "forbidden" symmetries [15], and the unique conductivity and mobility of charges in two-dimensional crystals of graphene [19-20].

The simplest hydrogen atom ${}^{1}_{1}\mathrm{H}$ (protium) itself – an elementary brick of the Universe at the atomic level (*i.e.*, the basis particle of the atomic level) – has complicated structure as well. It is defined by solutions of the same wave equation (1), but consists of the particles of the deepest subatomic level of the Universe not considered here.

The further analysis of obtained solutions shows that the relative mass of atoms is defined by the total number of H-atoms located in nodes of shells of a concrete atom:

$$A = \sum_k Z_{pk}\eta_{pk} + \sum_i (Z_{gi}\eta_{gi} + Z_{vi}\eta_{vi}) \qquad (4)$$

were k and i are numbers of polar ($m = 0$) and azimuth $m \neq 0$ shells, respectively; Z_{pk} is the number of polar nodes of k-th polar shell; Z_{gi} and Z_{vi} are the number of principal and collateral azimuth nodes, respectively, of i-th azimuth shell; η_{pk}, η_{gi}, and η_{vi} are numbers of multiplicity, *i.e.*, filling the nodes ($\eta = 0, 1$ or 2).

3. Wave shells of some atoms: examples

Using the above mentioned data, we can now turn to the consideration of the shell structure of concrete atoms. At that we do not claim to offer a complete analysis. The completed shells, characterized by the numbers l and m, will be designated by the letter $S_{l,m}$, and the number of nucleons located at the shells will be indicated in brackets. Let us take, for example, the atom of phosphorus with the atomic number 15 and the mass number 31, ${}^{31}_{15}P$. Following the images shown in Fig. 1, the shell structure of phosphorus, limited by the external uncompleted shell of the class $S_{0,1/2}$ with the single polar-azimuthal node of the ordinal number 15, has the following design:

$${}^{31}_{15}P = S_{0,0}(1) + S_{1,0}(0) + S_{1,1}(4) + S_{2,0}(0) + S_{2,1}(8) + S_{2,2}(8) + S_{3,0}(0) + S_{3,1}(8) + S_{0,1/2}(2) \qquad (5)$$

that is presented in Fig. 3 (by the graphical symbols of Fig. 1). Note that the completed external shell $S_{3,2}(16)$ (at $l = 3, m = \pm 2$) corresponds to the titanium atom, ${}_{22}Ti$.

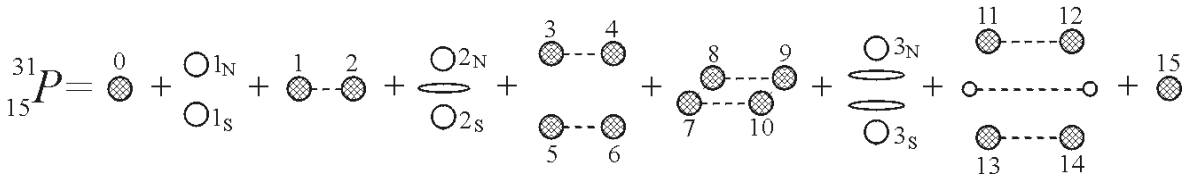

Fig. 3. A symbolic design of the shell structure of phosphorus; 1, 2, 3, ... are numbers of the nodes filled by two hydrogen atoms (nucleons).

The structure of two external shells, $S_{3,1}(8)+S_{0,1/2}(2)$, mainly defines the properties of phosphorus. The shell $S_{3,1}$ has two discrete collateral vacancies. The external shell of phosphorus, corresponding to the half-integer azimuth number $m=\frac{1}{2}s$ $(s=1)$, has one discrete node. $S_{1,1}$ class of shells induces at the external shell one vacant node. Phosphorus ${}^{31}_{15}P$, as follows from the above design, is a highly active atomic structure.

When phosphorus loses its outer shell that occurs under the deuterium or tritium bombardment, it is converted into silicon ${}^{29}_{14}Si$ (of the mass number 29),

$$ {}^{29}_{14}Si = S_{0,0}(1)+S_{1,0}(0)+S_{1,1}(4)+S_{2,0}(0)+S_{2,1}(8)+S_{2,2}(8)+S_{3,0}(0)+S_{3,1}(8), \qquad (6) $$

or ${}^{28}_{14}Si$ with the more symmetric structure (Fig. 4)

$$ {}^{28}_{14}Si = S_{0,0}(0)+S_{1,0}(0)+S_{1,1}(4)+S_{2,0}(0)+S_{2,1}(8)+S_{2,2}(8)+S_{3,0}(0)+S_{3,1}(8). \qquad (7) $$

Silicon is the first element of the periodic table, which has the vacant collateral nucleon nodes in the outer shell (see Fig. 1 at *l*=3, *m*=±1). It provides the motion, in its space, not only of particles, which are much less than nucleons, but also of nodal hydrogen-nucleons themselves. Quantum theory interprets this phenomenon as the motion of "holes".

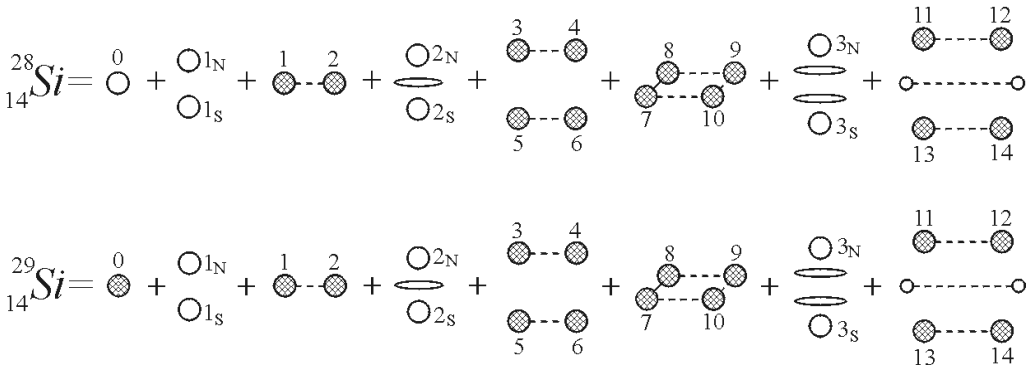

Fig. 4. A symbolic design of the shell structure of silicon ${}^{29}_{14}Si$ and ${}^{28}_{14}Si$.

Other atomic structures with the outer odd shells, including ones formed as a result of superposition of odd asymmetric solutions, are constructed in a similar way.

As has been mentioned above, polar functions of half-integer shells define equatorial orbits in nodes of which can be concentrated matter of deeper subatomic levels. As an example, two images of the same distribution of density of matter at *s* = 12, determined by the function (2), are presented in Fig. 5. This distribution of the twelve-fold symmetry has the characteristic arcs-rings.

Polar-azimuth shells of $\hat{\Psi} = \Psi_p + i\Psi_k$ are subspaces of atomic space. These subspaces, embedded in each other, form the composite multi-dimensional atomic space.

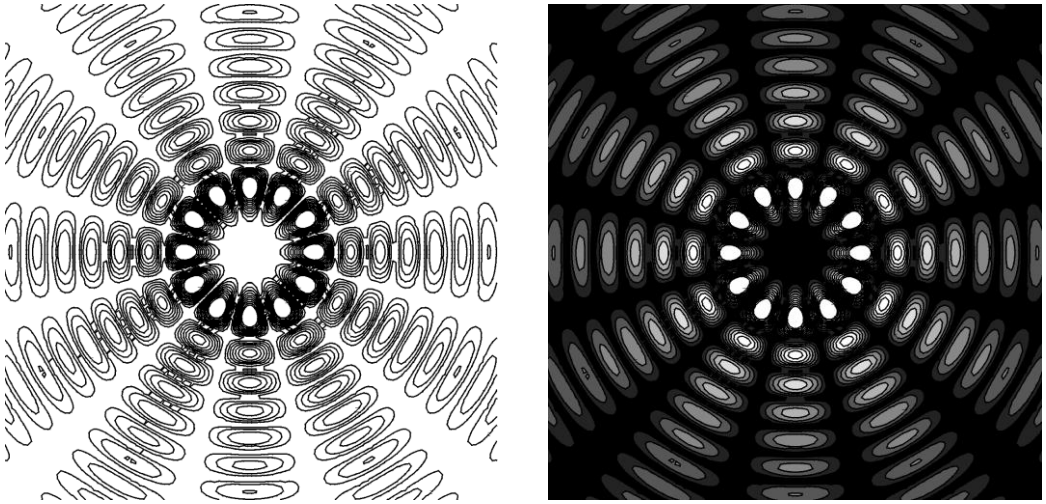

Fig. 5. The equatorial distribution of the density of matter at the subatomic level (s =12).

4. The nature of the Periodic Law

From Fig. 1, it is seen that a definite similarity of the geometry of external shells of abstract atoms occurs. Arranging the atoms with the same or a similar structure of outer shells one under another, in accord with Fig.1, we arrive at the *periodic-non-Periodic Law of spherical spaces.*

If we take the symbols of the real elements of the Periodic Table in their capacity as symbols of probabilistic objects (atoms) as seen in Fig. 1 (so that their ordinal numbers Z coincide with the atomic numbers of real atoms), we arrive at Table 1. We can now speak about a subsequent series of probabilistic elements as “atoms” of the discrete-wave field.

Table 1 reproduces Fig. 1 in the form of the traditional classification of the chemical elements in the order of their atomic numbers. Hence, Table 1 can be regarded as the Generalized Law of Quasi-Periodicity of Atomic Structures in matter-space-time and possibility-reality. We will call it the *Periodic Table of the Atoms of Wave Space*. In essence, we deal now with the unique Periodic Table as being the first and only derived theoretically. The first place in Table 1 takes the *neutron* under the ordinal number 0, designated as $_0$H, corresponding to l = 0 and m = 0.

Thus a whole series of the solutions of Eq. (1) constitutes in essence, speaking another words, *Theoretical Periodic Table of the Atoms* (Table 1) [11], revealing the *correlation of the periodicity of chemical properties of the elements* (clearly ordered first by Mendeleyev) *with the periodical quasi-similarity of the nodal structure of external atomic wave shells*.

Table 1. Theoretical Periodic Table of the Atoms designed on the basis of the particular solutions of the wave probabilistic Equation (1), or the quasi-periodicity as a result of quasi-similarity of the nodal structure of external atomic shells arranged in Fig. 1 and set here at the indicated (by arrows) symbols of the atoms.

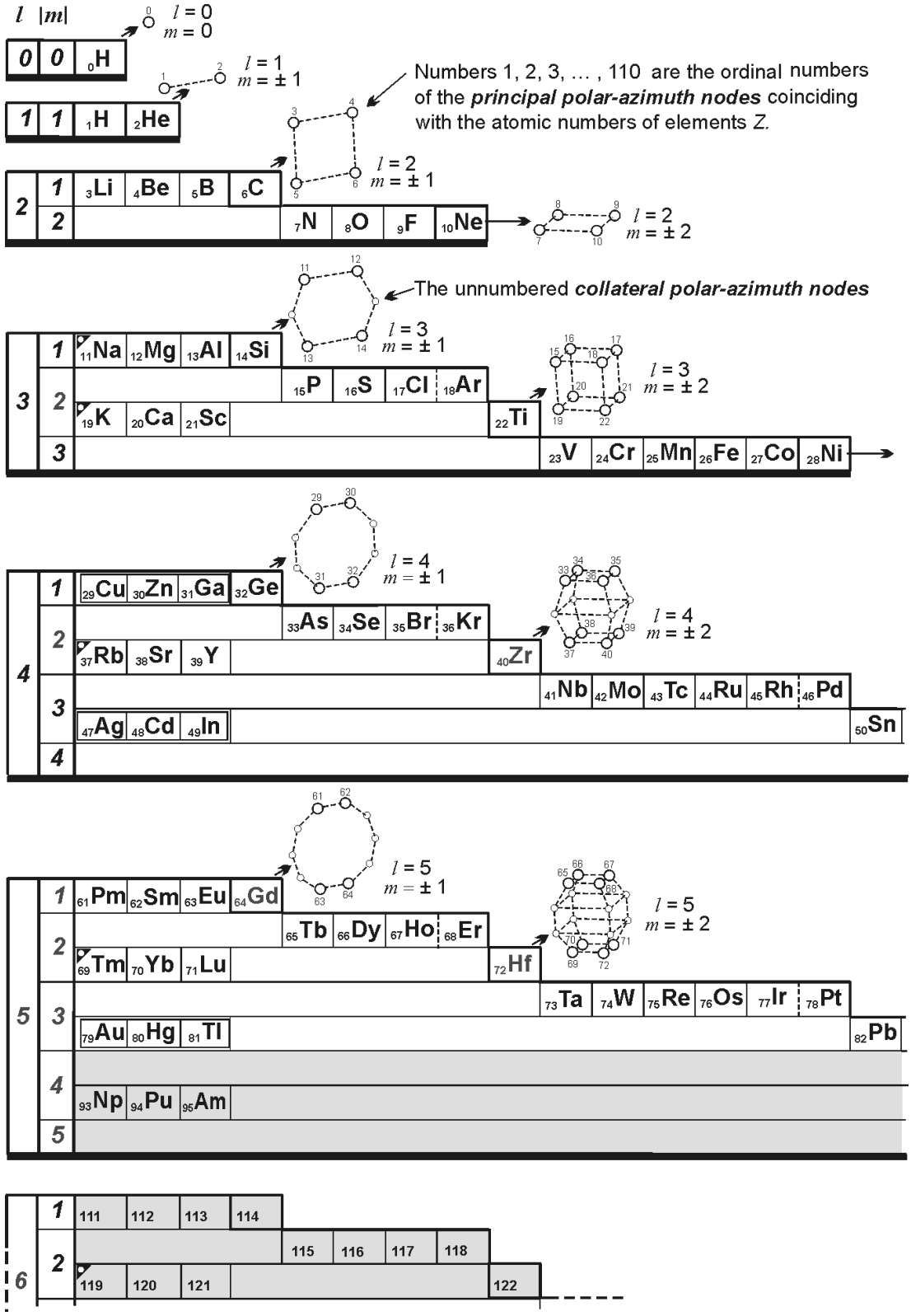

They elucidate, as mentioned before, the nature of symmetries including those "*strictly forbidden by the mathematical laws of crystallography*" [13-15]. Such symmetries attract at present the world-wide attention. In particular, the interest stems partially from the fact that the so-called Penrose tiling (a set investigated by Roger Penrose in the 1970s) exhibits a five-fold rotational symmetry impossible in periodic crystals, just as the structure of certain "quasi-crystal" substances.

The analytical image of an element of probability (an abstract atom) with fully completed external shells and the ordinal numbers

$$Z = 2, 6, 10, 14, 22, 28, 32, 40, 52, 60, 64, 72, 84, 100,... \qquad (8)$$

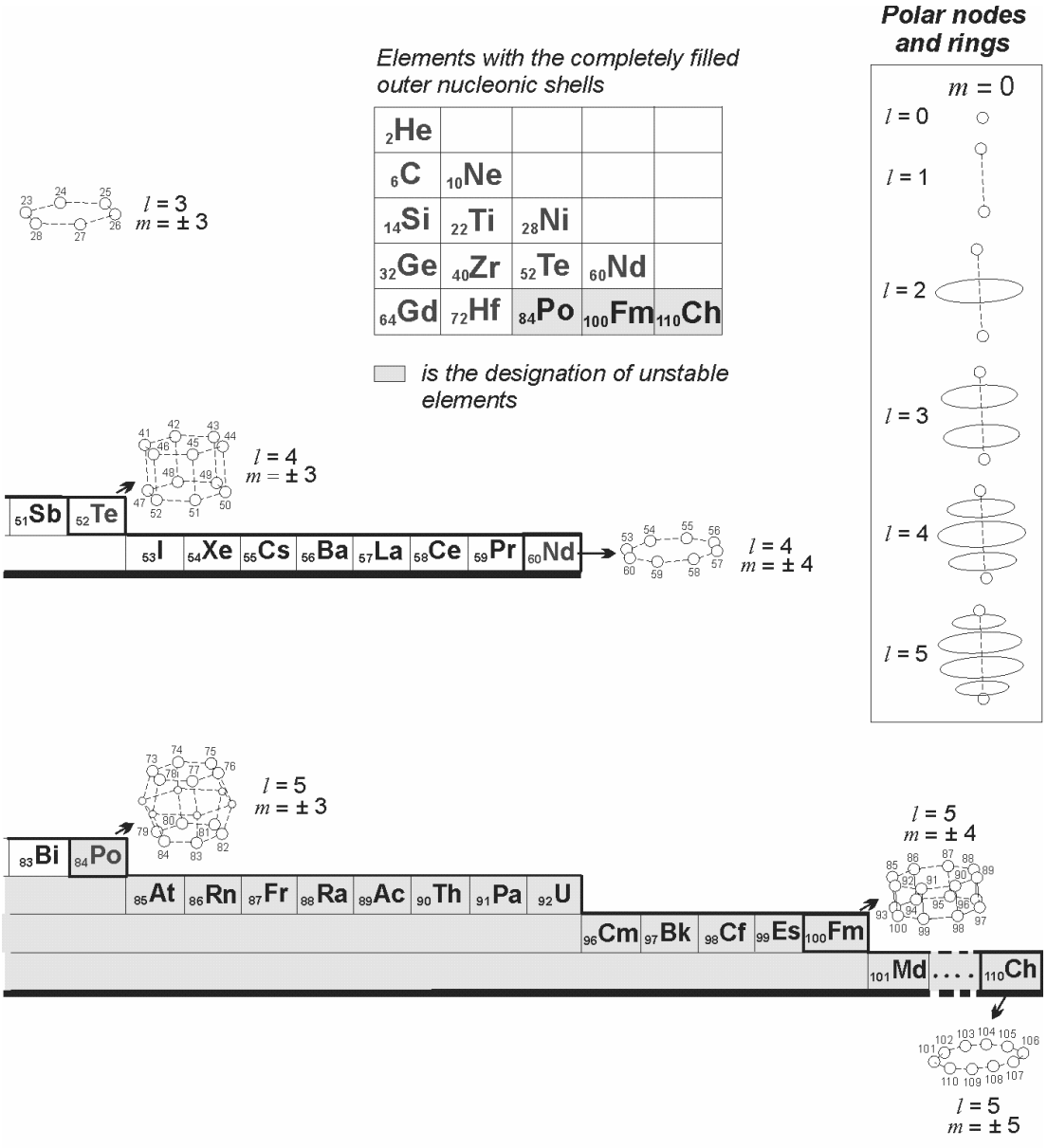

can be presented by the vector of atomic structure of embedded subspaces:

$$\Psi_Z = (\psi_1, \psi_2, ..., \psi_n), \tag{9}$$

where

$$\psi_n = C_\psi R_l(\rho_{l,n})\Theta_{l,m}(\theta)\cos(m\varphi + \alpha). \tag{10}$$

This vector, as the unrealizable sum of fully completed shells ψ_p ((2), L. 3), defined by the integer shells (shells of overtones), can also be written as:

$$\Psi_Z = \psi_1 \oplus \psi_2 \oplus ... \oplus \psi_n = \sum_{k=1}^{n} \psi_k . \tag{11}$$

The sign $\oplus$ expresses in (11) the unrealizable addition and the symbol Σ expresses the sum of the embedded subspaces.

Atomic structures, whose ordinal numbers take up the intermediate positions in the row (8), are represented by fractional (half-integer) external shells. These shells are the shells of undertones.

In the general case, the complete structure of any element (abstract atom) is defined by the following two summations:

$$\Psi_Z = \sum C_\psi R_l(\rho_{l,n})\Theta_{l,m}(\theta)\cos(m\varphi + \alpha_m) \oplus \sum C_s R_s(\rho_{s,j}) \sin^{\frac{s}{2}}\theta \cos\left(\frac{s}{2}\varphi + \beta_s\right) \tag{12}$$

The first sum in Eq. (12) consists of embedded whole shells; the second summation consists of embedded half-integer subshells. Atoms of intermediate spatial forms, which are determined by the odd solutions of Eq. 1 (Eq. (31), L. 2) are located between them.

The sum of the even number of odd solutions defines, in the equatorial plane, the even number of nodes. For instance, the two simplest odd solutions at *s*= 0 with opposite phases,

$$\hat{\Psi} = AR_s\Theta_s(\theta)e^{\pm i\frac{1}{2}\varphi} \qquad \text{and} \qquad \hat{\Psi} = AR_s\Theta_s(\theta)e^{\pm i\left(\frac{1}{2}\varphi+\pi\right)}, \tag{13}$$

describe two nodes in the equatorial plane.

If we add to these two solutions one more similar elementary solution, we obtain three nodes, which can be located on either one or two shells. When located on one shell, they will be disposed at the vertices of an equilateral triangle that can be described as the sum of elementary solutions of the following form:

$$\hat{\Psi} = AR_s\Theta_s(\theta)e^{\pm i\frac{1}{2}\varphi} \qquad \hat{\Psi} = AR_s\Theta_s(\theta)e^{\pm i\left(\frac{1}{2}\varphi+\frac{2}{3}\pi\right)} \tag{14}$$

$$\hat{\Psi} = AR_s\Theta_s(\theta)e^{\pm i\left(\frac{1}{2}\varphi+\frac{4}{3}\pi\right)} \tag{14a}$$

The initial phases, α_m and β_s in Eq. (12), characterize a mutual azimuth orientation of polar-azimuth shells and subshells of the atomic space with respect to the polar Z-axis. They are expressed by the vector of initial phases

$$\alpha = (\alpha_1,...,\alpha_m;\beta_1,...,\beta_s), \tag{15}$$

or for whole and half-integer shells, separately, as

$$\alpha = (\alpha_1,...,\alpha_m;\varnothing), \qquad \text{and} \qquad \alpha = (\varnothing;\beta_1,...,\beta_s) \tag{16}$$

The polar shells (m = 0) are always the whole ones. They have axes of infinite-fold symmetry and, hence, their mutual azimuthal orientation does not matter.

The mutual azimuthal orientation of polar-azimuthal shells and subshells defines the space isomers of atoms. Obviously, the vector of initial phases is the formal argument of the isomers.

As follows from Fig. 1 and Table 1, the wave number l defines the ordinal number of the nucleon layer-period and the number of integral shells in the layer. The total number N_p of *principal* azimuthal nodes (or elements) in the period is

$$N_p = 2l^2, \tag{17}$$

i.e., $N_p = 2, 8, 18, 32, 50, ...$. The number of fractional N_f (half-integer) shells in the layer is:

$$N_f = (2l^2 - l). \tag{18}$$

The total number N_{p+c} of the *principal* and *collateral* azimuthal nodes of an integral outer shell is determined by the following expression:

$$N_{p+c} = (l+1-m)\cdot 2m, \tag{19}$$

where $(l+1-m)$ is the number of extremal circumferences-parallels (see Fig. 4, L. 3) of the shell, which define the extrema of the polar function $\Theta_{l,m}(\theta)$; $2m$ is the number of extrema of the azimuthal function $\Phi_m(\varphi) = \sin m\varphi$, distinguishing on the shell the meridians of azimuthal extrema. The intersection of extremal parallels and meridians defines the nodes. As

was noted previously, the number of nodes of non-integral shells, located in the equatorial plane, (see Eq. (33), L. 2), is equal to *s*.

A general discrete structure of atoms can be presented also by the matrix of nodes of wave spherical space. The *matrix of polar nodes* describes a general *polar* discrete structure of atoms

$$P = [p_0,\ p_1, ...,\ p_i\ , ...], \tag{20}$$

where p_0 is the unitary central node determined by the wave numbers $l = 0$ and $m = 0$, p_i are polar nodes of the *i*-th shell. Analogously, the *matrix of azimuthal nodes* is introduced as

$$S = [s_1, s_2, ..., s_i\ (k_i), ...], \tag{21}$$

where the s_i are *principal* azimuthal nodes and the k_i are *collateral* azimuthal nodes of the *i* shell. The matrix (21) describes a general *azimuthal* discrete structure of atoms.

The sum of polar and azimuthal matrices determines the discrete structure of an atom as a whole:

$$A_z = P + S = \left[P \middle| S\right], \tag{22}$$

where A_z is a matrix of the *polar-azimuthal* discrete structure of an atom with the ordinal number Z. The numerical form of the matrix A_z is as follows:

$$\mathrm{A_z} = \begin{bmatrix} 1 & 0 & 0 & 0 & 0 & \cdot \\ 2 & 2 & 0 & 0 & 0 & \cdot \\ 2 & 4 & 4 & 0 & 0 & \cdot \\ 2 & 4(2) & 8 & 6 & 0 & \cdot \\ 2 & 4(4) & 8(4) & 12 & 8 & \cdot \\ 2 & 4(6) & 8(8) & 12(6) & 16 & \cdot \\ \cdot & \cdot & \cdot & \cdot & \cdot & \cdot \end{bmatrix} \tag{23}$$

Thus, the first column in the matrix (23) contains the number of polar nodes (situated on the Z-axis, see Fig. 1 and Table 1) corresponding to $l = 0, 1, 2, 3, 4, 5, ...$ and $m = 0$, beginning from the only node at $l = 0$. The second column relates to $m = \pm 1$, *etc*. The number of unnumbered collateral nodes is presented in brackets (the first two collateral nodes correspond to $l = 3$ and $m = \pm 1$).

It is to be noted that the elements, which have *collateral nodes* in their outer atomic shells the, are *semiconductors*. The bond energy of nucleons in collateral nodes is lower than that in principal nodes and, hence, the collateral nodes can be vacant. Semiconductors are characterized by both the electron and “hole” conductivity. It is natural to suppose that the

latter kind of conductivity is stipulated by the nucleons located in collateral nodes of the shells.

The first three elements in the row with l = 3, 4, 5 and $m = \pm 1$ (*silicon*, *germanium*, and *gadolinium*) have collateral nodes in the outer shells (see Table 1). The outer shells of *zirconium* and *hafnium* (l = 4 and 5, correspondingly, $m = \pm 2$) have collateral nodes as well. However, the spatial structures (geometry of disposition of the nodes and their number) of zirconium and hafnium differ from the structure of the outer shells of the aforementioned three elements corresponding to $m = \pm 1$.

The last two shells of $_{72}$Hf have six and eight collateral nodes, respectively. The next shell, after the shells of *hafnium*, belongs to the subsequent atoms with Z = 73 - 84, from *tantalum* to *polonium*. It is formed with six *collateral* nodes lying in the equatorial domain. For this reason, *hafnium* must be the strongest absorber of neutrons (hydrogen atoms). This is verified experimentally. Note that the last element in this series, *polonium* $_{84}$Po, is an exceptionally unstable radioactive element that emits α-particles.

The hexagonal cubic structure of the outer shell of *zirconium* defines the discrete structure ("crystal lattice") of its space. Principal nodes of the outer shell predetermine the cubic structure and, together with the collateral nodes, the hexagonal structure of *zirconium*. Experimental data confirms this.

The structure of *hafnium* (l = 5, $m = \pm 2$) is analogous to the *zirconium* structure (l = 4, $m = \pm 2$). Because of the great similarity of their outer shells, both of these elements were formed simultaneously during the formation of the Earth's crust. The outer shell of *hafnium* can be regarded as the exited state of the outer shell of *zirconium*, which under Earth's cooling served as the stable shell. For this reason, *zirconium* and *hafnium* always exist together and scientists were unable to distinguish these elements for a long while.

Comparing the two tables, namely the commonly used Periodic Table (independently of its modern graphic representations) and the Periodic Table of the Atoms (presented in Table 1), we see the difference in the disposition of some of the *heaviest atoms* in them. In particular, in accord with the solutions of the wave probabilistic Equation (1), gadolinium $_{64}$Gd, but not tin $_{50}$Sn and lead $_{82}$Pb, is situated in the same column as carbon $_{6}$C, silicon $_{14}$Si, and germanium $_{32}$Ge. Similarly erbium $_{68}$Er, but not xenon $_{54}$Xe and radon $_{86}$Rn, is in the column with neon $_{10}$Ne, argon $_{18}$Ar, and krypton $_{36}$Kr.

The unique feature of the Generalized Table is that all atoms are arranged in it in accord with the quasi-similarity of their *external* atomic shells. Based on the all above facts and other data (including some not mentioned here), we have the right to state that the aforementioned atoms, together with lanthanides and actinides, find their true places in the Law of Periodicity. Actually, nothing can be said against it, because the *primary* thing is, obviously, the *structure* of individual atoms, and the *consequences* of the structure, to which *chemical properties* relate, are secondary.

An analysis of the results obtained and of the data known in chemistry shows that the chemical bonds, predicted by the outer shell, dominate. Thus, the nodes of all shells in some degree also participate in the formation of chemical bonds. Accordingly, all shells are "valent" ones. Atomic bindings are realized along the bonds of nearest nodes of the external shell and nearby internal shells of interacting atoms. The nodal structure of atoms influences the structure of molecules, i.e., their geometry and interatomic bonds. The formation of molecules is accompanied by the overlapping (mainly two or three multiples) of interacting nodes. These questions were a discussion theme in 2003 at the Eighteenth International Conference on the Interfaces among Mathematics, Chemistry and Computer Sciences [21], and at the Seventh International Conference on Intermolecular and Magnetic Interaction in Matter [22].

Thus, following the *physical* shell-nodal atomic model, atoms represent a system of characteristic spherical shells with nodal points, where the wave function has extremal values, expressing the discrete structure of these shells. The number of potential (or, in equal degree, kinetic) polar-azimuthal extremal points (nodes) indicates the ordinal number of the concrete atom Z. The principal constituents of atoms are hydrogen atoms located in the potential nodes. It should be also noted, in addition, that the simplest atom, namely hydrogen ${}_{1}^{1}H$ (protium) although being an elementary building block of the Universe at the atomic level (i.e., the basis particle of the atomic level), has a complicated structure as well. It is defined by solutions of the same wave equation (1), but consists of the particles from the deeper subatomic levels of the Universe not considered here.

5. Conclusion

The results of the analysis of the particular solutions of the general wave equation (1), finished mainly to 1996 and presented then for the first time in a three-volume book "*Alternative Picture of the World*" [23], led to an important discovery, according to which the atoms have, if they are regarded as the wave formations, the *shell-nodal* structure *identical to the nodal structure of standing waves* in the spherical space, reminding *per se* the *nucleon molecules*. These solutions, represented for the first time in physics in the graphical form as it is implemented in Fig. 1 (which then has been carried over in Table 1) have shown the interesting features of the atoms. Namely, the presented images of their nucleon structure clear manifest the definite regularity in a sequential number of all the existing atoms. This regularity is expressed in the fact of *analogy* (*quasi-similarity*), in the definite extent, of the nodal structure of completed external atomic shells in each group of the atoms (corresponding to each column in Fig. 1) characterized by the different orbital numbers *l* at the same azimuthal number *m*.

Considering the above output, it was natural to assume that the observed *periodicity* in the shell-nodal *structure* of the atoms is the *primary cause of the periodicity* in *chemical*

properties of the corresponding elements, which has long been noticed and formulated as the Periodic Law beginning from the time of Mendeleev's discovery. The Periodic Law states that many of the physical and chemical properties of the elements tend to recur in a systematic manner with increasing atomic number.

The *nodal structure of outer atomic shells*, presented in Fig. 1 and Table 1 in the form of the schematic (conditional) images, *entirely correlates* with the *elementary nodal structure* of molecules and crystals, observed experimentally, and, hence, correlates with their symmetry. This revelation is a result of the comprehensive analysis of those data that to the present time were accomplished, in particular, of the data discussed in [21, 22].

Another important result, justifying in favor of validity of the shell-nodal atomic model and, hence, in favor of rightfulness of wave concepts of dialectical physics on the structure of matter in the Universe, is the following. A description of the *three kinds of fundamental interactions* (excluding *weak*), distinguishing in physics, *from the unit point of view*, that is impossible in principle in modern physics by the Standard Model, became now possible in the framework of the *Shell-Nodal Atomic Model* by the *Universal Law of Exchange* followed from the *Dynamic Model* of elementary particles (DM) [24]; moreover, it is realized logically irreproachably and uncontradictory. The DM is an integral part of the shell-nodal atomic theory of dialectical physics developed by the authors of the capital monograph [7].

The fundamental interactions that we mean, resting on the wave shell-nodal atomic model, are: between the nodal hydrogen atoms belonging to an individual atom (*intra-atomic* internodal bonds, *strong* interactions, considered in modern physics as "*nuclear*"), between the nodal hydrogen atoms belonging to external shells of the different interacting atoms (*interatomic* internodal bonds, *electromagnetic* interactions, *chemical* processes), and the universal interaction between any particles and bodies (*gravitational* interactions). We will discuss this issue and show the corresponding calculations of the above interactions further in a separate Lecture.

The *discrepancy* found between the positions of some elements set in the corresponding groups: in the commonly used Periodic Table (designed on the basis of the *experimental* data) and in the Theoretical Periodic Table (Table 1), is the result of fundamental importance for understanding the true nature of the Periodic Law. We pay attention, in particular, to the position of *gadolinium* $_{64}$Gd (belonging to lanthanides) that have to take a place in the IV group of the Periodic Table, instead of $_{50}$Sn and $_{82}$Pb, together with *carbon*, *silicon* and *germanium*; and the position of *erbium* $_{68}$Er (also related to lanthanides) that should take the place, instead of $_{54}$Xe and $_{86}$Rn, in the VIII group with *neon*, *argon* and *krypton*, *etc.*

The elements-lanthanides of the Periodic Table indicated above with respect to the observed property of the quasi-periodicity are on their true places in the Theoretical Periodic Table (Table 1). Other lanthanides and also actinides, set in the Periodic Table separately, take in Table 1 their proper places as well. We are sure stating about the true ordering of

them in Table 1, because, as was mentioned above, the *structure* of individual atoms is primary for the Periodic Law, and *consequences* of the structure, to which the *chemical properties* relate, are secondary. A revision of the conventional conceptions of physics realized, in particular, in the Periodic Table, in which the position of some elements, including indicated above, call doubts, is inevitable in view of the discovery of the shell-nodal structure of the atoms. As soon it may happen depends on when the Wave Model will be recognized and accepted finally in physics.

Currently, the *Shell-Nodal Atomic Model* and the *Theoretical Periodic Table of the Atoms* (Table 1), as reflecting the objective properties of matter at the atomic level of the Universe, beginning to attract deserving attention of official physics, as evidenced, for example, the invited review articles on this issue published in the books [3, 25]. The arguments presented there and in these Lectures, along with the data presented in some of the other publications indicated in References, are sufficiently substantiated and convincing in order to the overwhelming majority of physicists have recognized the shell-nodal atomic model.

From our point of view, the shell-nodal atomic model deserves a special attention as being a unit real alternative for replacing the modern quantum-mechanical atomic model. The latter exhausted itself completely and its adequacy (validity) causes the justifiable doubts [6, 26-27].

References

[1] K. Saiti (Ed.), *Chemistry and Periodic Table*, Iwanami Modern Chemistry Series, No 5, Iwanami Shoten Publ., 1979.

[2] E. G. Mazurs, *Graphic Representation of the Periodic System During One Hundred Years*, The University of Alabama Press, University, Al., 1974.

[3] *The Mathematics of the Periodic Table*, edited by Rouvray D. H. and King R. B., NOVA SCIENCE PUBLISHERS, NY, 119-160, 2006.

[4] D. I. Mendeleev, *Fundamentals of chemistry*, VIII edition, St. Petersburg, 1906.

[5] V. G. Rodionov, *The Place and Role of the Ether in the True Table of D. I. Mendeleev*, Journal of Russian Physical Thought (JRFM), 2001, №1-12, p. 37-51.

[6] G. P. Shpenkov, *Conceptual Unfoundedness of Hybridization and the Nature of the Spherical Harmonics*, Hadronic Journal, Vol. 29. No. 4, p. 455, (2006); http://shpenkov.com/pdf/HybridizationShpenkov.pdf

[7] L. G. Kreidik and G. P. Shpenkov, *Atomic Structure of Matter-Space*, Geo. S., Bydgoszcz, 2001, 584 p.; http://shpenkov.com/atom.html

[8] G. P. Shpenkov, *An Elucidation of the Nature of the Periodic Law*, Chapter 7 in "*The Mathematics of the Periodic Table*", edited by Rouvray D. H. and King R. B., NOVA SCIENCE PUBLISHERS, NY, 119-160, 2006.

[9]. L. G. Kreidik and G. P. Shpenkov, *Foundations of Physics*; 13.644…*Collected Papers*, Geo. S., Bydgoszcz, 1998, 272 p.; http://shpenkov.com/Found.html

[10] L. G. Kreidik and G. P. Shpenkov, *The Wave Equation Reveals Atomic Structure, Periodicity and Symmetry*, KEMIJA U INDUSTRIJI, Vol. 51, No. 9, 375-384, (2002).

[11] G. P. Shpenkov, *Generalized Table of the Elements*; https://shpenkov.com/periodic_table.html

[12] R.J. Haüy, *Essai d'une Theorie sur la Structure des Crystaux*, Paris, 1784; *Traité Elementaire de Physique*, Paris, Delance et Lesueur, an XII, 1803.

[13] D. Shechtman, I. Blech, D. Gratias, and J.W. Chan, *Metallic Phase with Long-Range Orientation Order and no Translation Symmetry*, Phys. Rev. Lett., 53, No.20, 1984, 1951–1953 (1984).

[14] S. Mae, *Tyndall Figures on Grain Boundaries of Pure Ice*, Nature, 257, No. 5525, (1975).

[15] P. J. Steinhardt and H. C. Jeong, *New Rules for Constructing Penrose Tilings May Shed Light on How Quasicrystals Form*, Nature, Vol. 382, pp. 433–435 (1996); see also http://dept.physics.upenn.edu/~www/astro-cosmo/walker/walker.html

[16] G. P. Shpenkov, *The Scattering of Particles and Waves on Nucleon Nodes of the Atom*, International Journal of Chemical Modeling, Vol. 2, No. 1, (2008).

[17] G. P. Shpenkov, *Conceptual Unfoundedness of Hybridization and the Nature of the Spherical Harmonics*, Hadronic Journal, Vol. 29. No. 4, p. 455, (2006); http://shpenkov.com/pdf/hybridizationshpenkov.pdf

[18] G. P. Shpenkov, *Some Words about Fundamental Problems of Physics*: *Constructive Analysis*, LAMBERT Academic Publishing, p.116 (2012); http://shpenkov.janmax.com/978-3-659-23750-8_eng.JPG amazon.com/words-about-fundamental-problems-physics/dp/3659237507

[19] G. P. Shpenkov, *Anisotropy of Unstrained Pristine Graphene*; http://shpenkov.com/pdf/GrapheneAnisotropy.pdf

[20] G. Shpenkov (Author): *Method for Manufacturing Nano Electronic Devices Made From 2D Carbon Crystals Like Graphene and Devices Obtained with this Method*. International Application Published under the Patent Cooperation Treaty (PCT). International Application No.: PCT/EP2010/052298. International Publication No.: WO/2010/097393. https://register.epo.org/application?number=EP10707863&lng=en&tab=main

http://www.wipo.int/pctdb/en/wo.jsp?WO=2010097393&IA=EP2010052298&DISPLAY=STATUS

[21] G. P. Shpenkov, *Intra-Atomic Structure of Carbon and Its Compounds*, The Eighteenth International Conference on the Interfaces Among Mathematics, Chemistry and Computer Sciences, Abstracts, p. 79, Dubrovnik, Croatia, 2003.

[22] G. P. Shpenkov, *The Role of Electrons in Chemical Bonds Formations* (In the Light of Shell-Nodal Atomic Model), Report at the Seventh International Conference on Intermolecular and Magnetic Interaction in Matter (2003); published in MOLECULAR PHYSICS REPORTS 41, 89-103, (2005).

[23]. L. G. Kreidik and G. P. Shpenkov, *Alternative Picture of the World*. Vol. 1, "*Mathematical Expression of the Main Categories of Philosophy and Logic, Kinematics and Dynamics of Exchange*", p. 158; Vol. 2, "*Structure of Space of the Universe, Electrostatic and Electromagnetic Fields, Particles and Exchange in the Electromagnetic Field*", p. 164; Vol. 3, "*Atomic Structure of Matter-Space-Time and Physical Properties of Substance, Physics and Philosophy*", p. 186; Geo. S., Bydgoszcz, 1996.
http://shpenkov.com/Alt.html

[24] L. Kreidik and G. Shpenkov, *Dynamic Model of Elementary Particles and the Nature of Mass and 'Electric' Charge*, "Revista Ciencias Exatas e Naturais", Vol. 3, No 2, 157-170, (2001); http://shpenkov.com/pdf/masscharge.pdf

[25] G. P. Shpenkov, *Physics and Chemistry of Carbon in the Light of Shell-Nodal Atomic Model*, Chapter 12 in "*Quantum Frontiers of Atoms and Molecules*", edited by Putz M. V., NOVA SCIENCE PUBLISHERS, New York, 277-323, 2011.

[26] L. Kreidik and G. Shpenkov, "*Important Results of Analyzing Foundations of Quantum Mechanics*", Galilean Electrodynamics & QED-East, Special Issues 2, 13, 23-30, (2002); http://shpenkov.com/pdf/QM-Analysis.pdf

[27] G. Shpenkov and L. Kreidik, "*Schrodinger's Errors of Principle*", Galilean Electrodynamics, 3, 16, 51-56, (2005); http://shpenkov.com/pdf/blunders.pdf

Lecture 5

The Nature and Structure of Isotopes

1. Introduction

The Wave Model, including the shell-nodal atomic model based on the particular solutions of the wave equation and the dynamic model of elementary particles, accounts for all physical phenomena related to the atomic structure [1]. In particular, in previous Lecture, we have analyzed the fundamental regularities inherent in the atoms having the shell-nodal structure. They consist in repeatability in the definite extent of disposition of the nodes on successive wave atomic shells. These regularities led to revealing the nature of Mendeleev's Periodic Law and, on this basis, to the correct arrangement of the atoms reflecting this Law in the form called the Theoretical Periodic Table of the Atoms.

Now, we will show how such a wave atomic model reveals the nature of atomic isotopes. In view of the obtained solutions, we will give the answers to the following principal questions. What is the internal structure of all isotopes of an atom: natural stable and unstable, and synthesized short-lived? How does the wave atomic model predict the complete variety of all possible isotopes, including the ultimate ones, lightest and heaviest, for all atoms of the Periodic Table?

The "*electron structure* (*configuration*)" of atoms, which is a major outcome of Schrödinger's quantum-mechanical atomic theory, is unable to explain the nature of isotopes in principle and, hence, give no answers to the above questions. In accord with the definition accepted in modern physics, isotopes are atoms that have the same number of protons, but the different number of neutrons in own *nuclei*. The nuclei of some isotopes are unstable. They emit radiation and break down to form smaller nuclei.

The above statements express only the experimental fact about existence of the same atoms with different masses. At that, the given definition, characterizing isotopes, is formulated considering the quantum-mechanical *nuclear* model of atoms (QM). However, accepting the concept on an existence of the atomic nuclei, the modern theories of physics (atomic and nuclear) nothing can say about how the nucleons in each of all atomic isotopes are disposed spatially inside their nuclei. Let us take, for example, one of the stable isotopes

of the nickel atom $^{58}_{28}Ni$ having 58 nucleons. How 58 nucleons are disposed in its nucleus? For modern physics, it is an unsolvable problem in principle. Why? Yes because there is no nuclei. The nuclear model of atoms is wrong. This assertion follows not only from analysis of all the data on this matter [1- 3], but even from the point of view of common sense.

Really, following the QM, an atom consists of a central nucleus of about $10^{-13} cm$ radius filled with Z protons and A–Z neutrons, and Z electrons, moving around the nucleus in an atomic space prescribed by a radius of order $10^{-8} cm$. From this it follows that linear sizes of an atom and its nucleus (where, as believe, practically the whole atomic mass is concentrated) relate approximately as $10^5 : 1$ and their volumes as $10^{15} : 1$.

Thus, in essence, the quantum-mechanical atom represents an empty space occupied with continuously moving relatively light electrons to which the key role is ascribed in forming the whole variety of substances, molecular and crystalline structures. Let us imagine an atom scaled up to $10^3\ m^3$. The heavy nucleus of an unimaginable density (more than $10^{14}\ g \cdot cm^{-3}$) in its center will look like an invisible mote of about $10^{-3}\ mm^3$. Obviously, the common sense opposes such an image of nature at the atomic level.

Following the wave shell-nodal atomic model, originating from the particular solutions of the wave equation, each atom has the strictly definite internal nodal structure (see Fig. 1 and Table 1, L. 4). On the basis of a comprehensive analysis of individual peculiarities of the nodal structure inherent to each atom, the mystery of the origin of atomic isotopes is revealed in a natural way.

Hydrogen atoms are the main structural units of the atom. In stable atoms, they are located mainly in potential nodes of the corresponding spherical shells. The total number of the nodes in an abstract atom, its nodal measure, as a totality of probabilistic discrete units, can be easy counted up from solutions presented in the form of images of these nodes depicted in Fig. 1 of L. 4.

The number of the nodes, which, in principle, can be filled with matter (particles), and *multiplicity* η of their possible filling define the relative mass of the atom, A. As was already noted (in previous Lecture, see Eq. 4 there), the relative mass of an atom is defined by the total number of hydrogen atoms located in the nodes (excluding kinetic) of the corresponding shells of a concrete atom in accord with the following formula:

$$A = \sum_k Z_{pk}\eta_{pk} + \sum_i (Z_{gi}\eta_{gi} + Z_{vi}\eta_{vi}), \qquad (1)$$

where *k* and *i* are the numbers of polar ($m = 0$) and azimuthal ($m \neq 0$) shells, respectively; Z_{pk} is the number of *polar potential-kinetic* nodes of *k*-th polar shell; Z_{gi} and Z_{vi} are the number of *potential principal* and *collateral* polar-azimuthal nodes, respectively, of the *i*-th polar-azimuthal shell; η_{pk} , η_{gi}, and η_{vi} are the numbers of the multiplicity, *i.e.*, filling the nodes η.

The *node multiplicity* η is equal to the number of hydrogen atoms in the node. For atoms of space and matter η is equal to 0, 1 or 2:

$$\eta = \begin{Bmatrix} 0 \\ 1 \\ 2 \end{Bmatrix}. \qquad (2)$$

A successive series of solutions of the wave equation of matter-space-time is naturally determined by the *ordinal numbers* of principal polar-azimuthal nodes, which are a natural bound of each elementary solution. These solutions are realized in objective space in the form of atoms of matter-space.

Thus, an existence of the different nodes and multiplicity of their filling in the wave shells of the atoms (see Fig 1, L. 4) are the main reason for an existence in Nature of different atomic isotopes, stable and unstable (radioactive), and the reason of possibility for synthesizing the many other short-lived isotopes inherent in every atom. We mean the filling of both the numbered *principal potential polar-azimuthal* nodes and unnumbered *potential collateral* nodes, and also the numbered *polar potential-kinetic* (axial) nodes.

We will demonstrate now the filling of the above nodes on concrete examples. Our consideration is focused mainly on an internal structure of all possible isotopes of the carbon and oxygen atoms. The given atoms form a great variety of compounds and are the most studied atoms among all atoms. Therefore, we assume that for the present consideration the choice just of these atoms is optimal.

2. Shell-nodal structure of carbon and its isotopes

According to the obtained solutions, characteristic shells of the carbon atom are defined by the following quantum numbers: $l = 0, 1, 2$ and $m = 0, \pm 1$.

Radial functions of the even solutions (9), defining the characteristic shells of the carbon atom, are presented in Table 1 (through their relative values R_l /A) and drawn in Fig. 1.

Table 1. The radial functions of even solutions for the carbon atom.

l	$\hat{R}_l(\rho)/A = \sqrt{\frac{\pi}{2\rho}}\left(J_{l+1/2}(\rho) \pm iY_{l+1/2}(\rho)\right)$
0	$(\sin\rho \pm i\,(-\cos\rho))/\rho$
1	$((\rho^{-1}\sin\rho - \cos\rho) \pm i\,(-\rho^{-1}\cos\rho - \sin\rho))\,\rho^{-1}$
2	$[((3\rho^{-2} - 1)\sin\rho - 3\rho^{-1}\cos\rho)) \pm i\,((1 - 3\rho^{-2})\cos\rho - 3\rho^{-1}\sin\rho))]\,\rho^{-1}$

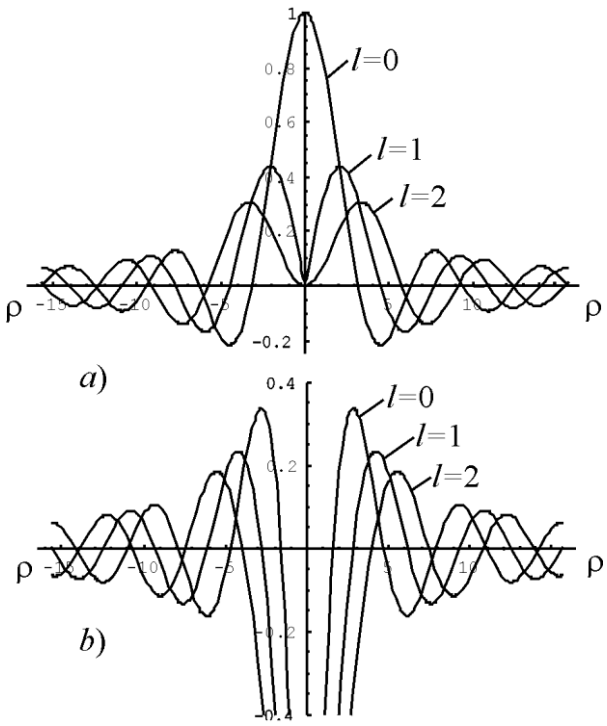

Fig. 1. Plots of the radial spherical functions of the carbon atom: potential $\sqrt{\frac{\pi}{2\rho}}J_{l+1/2}(\rho)$ (*a*) and kinetic $\sqrt{\frac{\pi}{2\rho}}Y_{l+1/2}(\rho)$ (*b*).

The reduced polar-azimuth potential functions, $\tilde{Y}_{l,m}(\theta,\varphi)$, for the carbon atom are presented in Table 2; their graphs are drawn in Fig. 2.

Contour plots of the potential components of density of probability ψ_p for the carbon atom are presented in Fig. 3. Pictures presented in this Figure are the sections of ψ_p (*i.e.* the sections of the product of the three functions: radial $R_l(\rho)$, polar $\Theta_{l,m}(\theta)$, and azimuthal $\Phi_m(\varphi)$) in the plane $x = 0$.

Table 2. The reduced polar-azimuth potential functions $\tilde{Y}_{l,m}(\theta,\varphi)$ of the carbon atom

l	m	$\tilde{Y}_{l,m}(\theta,\varphi)=\tilde{\Theta}_{l,m}(\theta)\cos m\varphi$
0	0	1
1	0	$\cos\theta$
	± 1	$\sin\theta\cos\varphi$
2	0	$\cos^2\theta - 1/3$
	± 1	$\sin\theta\cos\theta\cos\varphi$

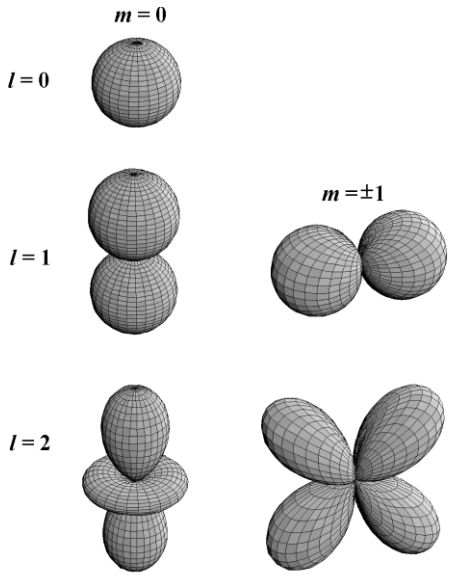

Fig. 2. Graphs of the polar-azimuthal functions $\left|\Theta_{l,m}(\theta)\cos m\varphi\right|$ of the carbon atom.

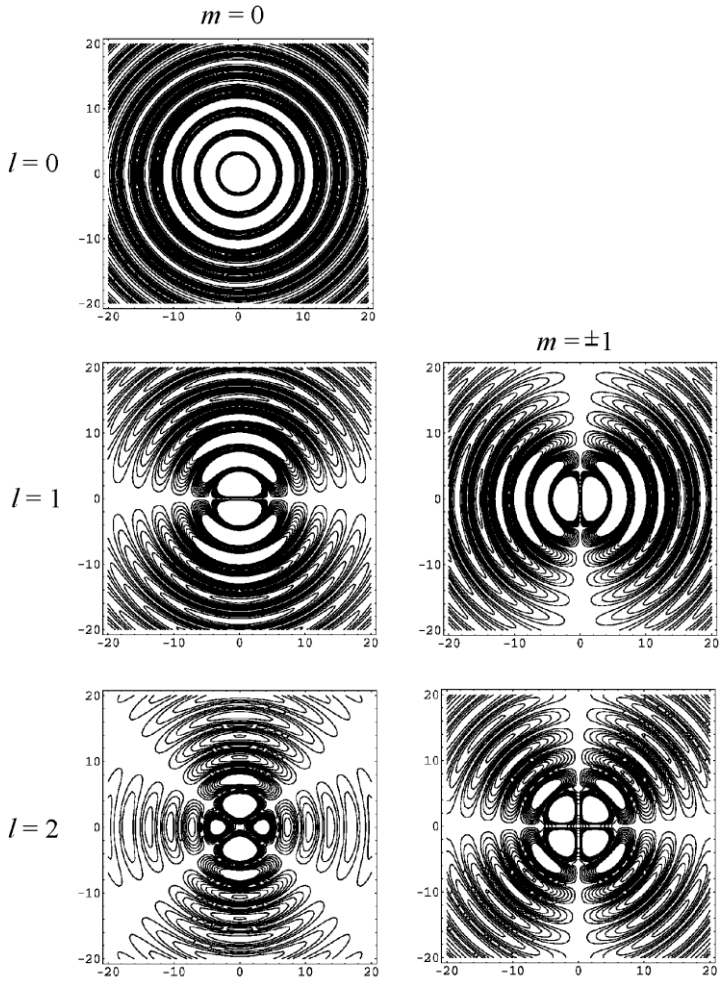

Fig. 3. Contour plots (an interference image) of the sections for the *potential* density of probability ψ_p in the plane $x = 0$ for the space of the carbon atom.

It should be noted that the pictures depicted in Fig. 3 are, in accord with the particular solutions of the wave equation, the interference images of modes of standing waves in the three-dimensional spherical space.

A characteristic feature of the shell at $l = 2$, $m = 0$ is an existence of a toroidal vortex-ring. Obviously, the latter plays an important role in physical and chemical processes at the atomic and molecular levels. We assume that it is responsible for some of the unique properties of *graphene* – an atomic size thickness layer of *graphite* – observed in last years. Therefore, we show this ring once more in Fig. 4 in the two projections: for the section along the *z*-axis (in a plane perpendicular to the plane (*x*, *y*), as in Fig. 3), and additionally for the section $z = 0$ in a plane (*x*, *y*).

The next peculiarity of the solution is an existence of the nodes along the z-axis which we call polar nodes. The 2*n* and 2*s*, "north" and "south", polar nodes, corresponding to $l = 2$, are indicated in Fig. 4.

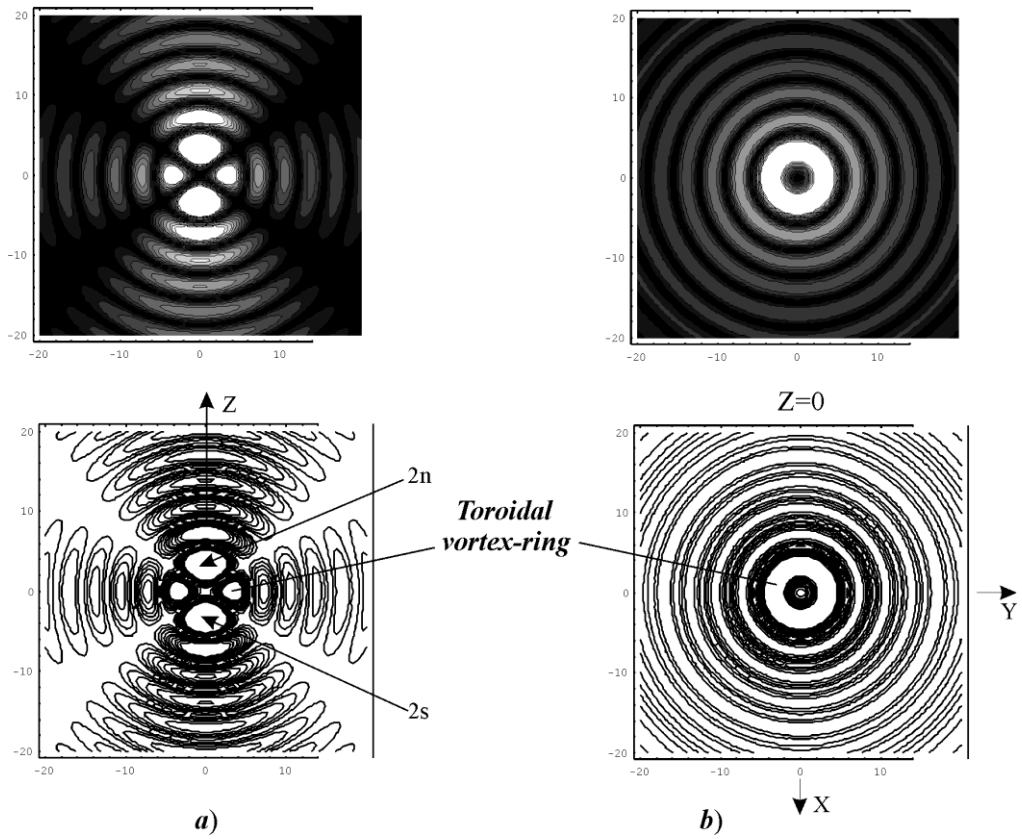

Fig. 4. The solution $\psi_p = C_\psi R_l(\rho)\Theta_{l,m}(\theta)\cos(m\varphi + \alpha)$ of the wave equation $\Delta\hat{\psi} + k^2\hat{\psi} = 0$ for the spherical shell of the carbon atom characterized by the wave (quantum) numbers $l = 2$, $m = 0$: (*a*) for a section along the *z*-axis (in a plane perpendicular to the plane (*x*, *y*)), (*b*) for a section $z = 0$ in a plane (*x*, *y*); 2*n* and 2*s* are, respectively, the "north" and "south" polar nodes belonging to the shell.

The solutions $\psi_{l,m}(\rho,\theta,\varphi)_p = C_\psi R_l(\rho)\Theta_{l,m}(\theta)\cos m\varphi$ for $r = const$ of the probabilistic wave equation presented in the form indicating the relative space disposition of *potential* extremes-nodes – discrete elements of the shell-nodal structure of the carbon atom – are drawn schematically in Fig. 5. Numbers 1, 2, 3, …, 6 are the ordinal numbers of the principal polar-azimuth nodes coinciding with the atomic numbers of the elements *Z* of the Periodic Table.

Thus, Fig. 5 demonstrates an unfolded schematic image of spatial arrangement of the potential *nodes* (and the toroidal *vortex-ring*) on the concrete wave spherical shells (corresponding to the definite value of *l*) and subshells of the shell (corresponding to the definite value of *m*); these nodes and the toroid constitute the carbon atom. In light of the shell-nodal structure, the carbon atom is in essence one of the *elementary molecules of hydrogen atoms* (as all of the remaining atoms of the Periodic Table, excluding the hydrogen atom itself).

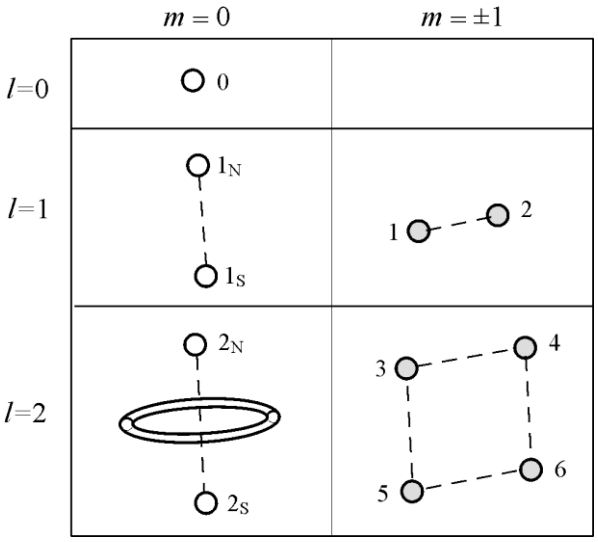

Fig. 5. The schematic drawing of the nodes and a toroidal vortex ring in the carbon atom: 0, 1_N, 1_S, 2_N, 2_S is the ordinal number of the polar *potential-kinetic* nodes (located along the z-axis, $m = 0$); 1, 2,…, 6 is the ordinal numbers of principal polar-azimuthal *potential* nodes. The nodes 1 and 2 belong to the internal spherical shell, $l = 1$; the nodes 3, 4, 5, and 6 are located on the external spherical shell, $l = 2$.

The unfolded shell-nodal structure of carbon $^{12}_{6}C$ and its polar-azimuth functions are shown in Fig. 6. The carbon atom has a central empty node ($m = 0$, $l = 0$) and four spherical shells: two shells ($m = 0$; $l = 1, 2$) with four empty potential-kinetic *polar nodes* and one *ring*, two shells ($m = \pm 1$; $l = 1, 2$) with six completed *potential polar-azimuth nodes* and six

empty *kinetic polar-azimuth nodes*. The last (kinetic nodes or antinodes) are shown neither in figures of previous Lectures nor Fig. 6. Antinodes are the places of intensive motion and nucleons cannot be in rest in them. Six potential polar-azimuth nodes (at $m = \pm 1$) are each filled with two hydrogen atoms and lie in one plane: two potential nodes are in the inner shell (l = 1) and four such nodes are in the outer shell (l = 2). Six empty kinetic nodes (not shown here) lie on kinetic radial (spherical) shell in a perpendicular plane with respect to the plane of disposition of the potential nodes.

The main mass of hydrogen in Nature at all its levels is in coherent states, in particular, in the form of coupled atoms – hydrogen molecules H_2. Note that at the megalevel, in the cosmos, about one half of all stars form (star) pairs. Paired hydrogen atoms, filling polar-azimuthal nodes, provide the equilibrium state of atomic shells. The *condition of coupling*, inherent in the hydrogen atoms located in the nodes of individual atoms, is probably inherent also for individual atoms themselves at the formation of molecules and crystals; we shall turn to this subject later.

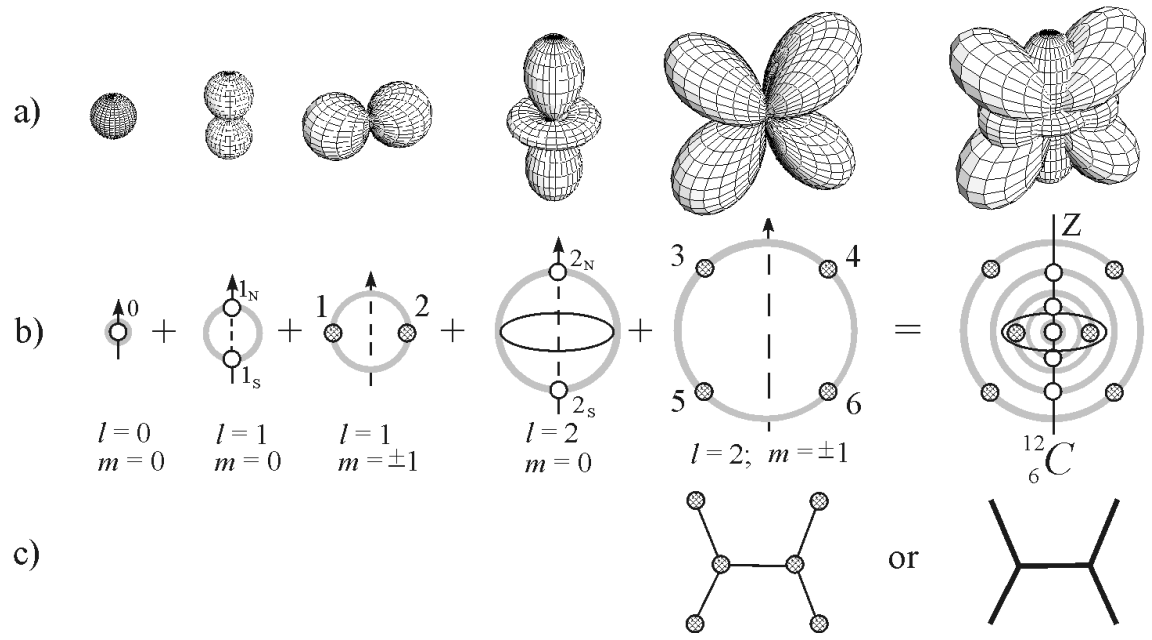

Fig. 6. (a) Plots of the potential polar-azimuth functions $\Theta_{l,m}(\theta)\mathrm{Cos}m\varphi$ ($l = 0, 1, 2$; $m = 0, \pm 1$), (b) the extremal points of their angular spatial positions (defining the position of the nodes) on the potential radial shells $R_l(\rho)$, and (c) the symbolic designation of the shell-nodal structure of the carbon atom.

Since all potential polar-azimuth nodes with hydrogen atoms inside them are situated in the same plane, the structure of the carbon atom, being spherical like every atom, looks like a plane. Thus because of the specific geometry of the location of the nodes, carbon atoms can

form the *plane hexagonal structure* of graphite. The symbolic designation of carbon ⋊ (Fig. 6c) reflects such a plane geometry of arrangement of its six *principal* polar-azimuth nodes and shows the shortest directions of exchange (interaction) between them. Accordingly, each carbon atom is associated in shell-nodal atomic model with one of the exo-pentagonal bonds of the truncated icosahedron.

The same individual properties characteristic for all isotopes of an atom, *i.e.*, for those atoms characterized by the same ordinal number *Z* and different mass number *A*, are defined by the same fixed (unchanged) structure of their external atomic shells. While the structure of the shells is not broken, the properties are saved even when the principal polar-azimuth nodes of the *external shells* are not completed with the paired hydrogen atoms, *i.e.*, when each of their nodes contain only one hydrogen atom. Naturally, such a state will not be equilibrium and is a temporal state characterized by a lifetime. Thus, the geometry of *external* polar-azimuth shells and hence specific strong intra-atomic bindings between nodes in such isotopes do not change only during the lifetime of unstable, in this case, atom.

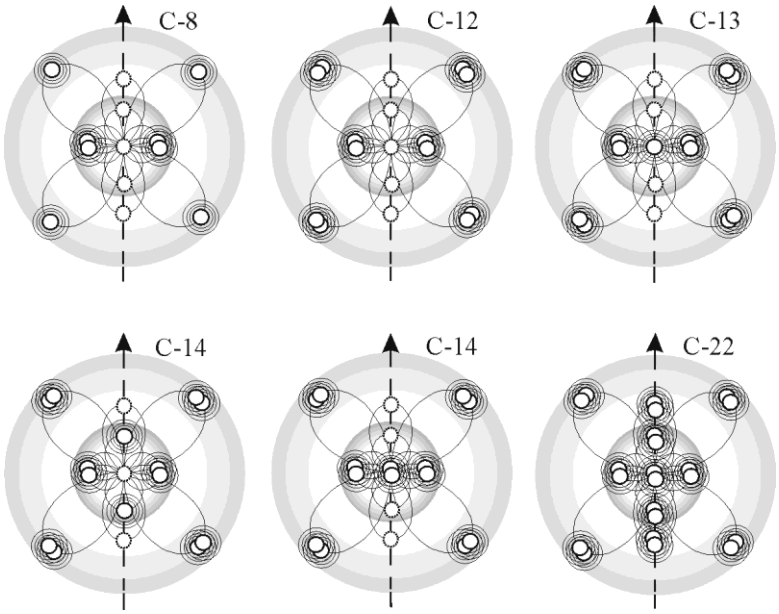

Fig. 7. The filling of the potential nodes with hydrogen atoms in the stable isotopes of carbon – ${}^{12}_{6}\mathrm{C}$, ${}^{13}_{6}\mathrm{C}$, ${}^{14}_{6}\mathrm{C}$, and in two of its unstable isotopes (lightest and heaviest, respectively) – ${}^{8}_{6}\mathrm{C}$ and ${}^{22}_{6}\mathrm{C}$.

Hence, following the shell-nodal structure depicted in Fig. 6, the uniquely possible lightest unstable isotope of carbon is ${}^{8}_{6}\mathrm{C}$ with the mass number 8 (the total number of H-atoms). The order of filling the nodes in this isotope is exhibited in Fig. 7. Of course, the structures with incompletely filled principal potential nodes cannot be equilibrium, and as metastable states they are characterized by a definite lifetime.

Carbon is made up of isotopes with masses 12, 13 and 14. An isotope of carbon $^{13}_{6}\mathrm{C}$ can be obtained under the condition of filling the central vacant node in the carbon $^{12}_{6}\mathrm{C}$ with one hydrogen atom as shown in Fig. 7. This isotope is stable. Apparently, a specific configuration of internal fields and internodal bindings in $^{13}_{6}\mathrm{C}$ provides the stable state of the single hydrogen atom in the central polar-azimuthal potential-kinetic node.

The two possible structures of carbon $^{14}_{6}\mathrm{C}$ (Fig. 7) can be formed by filling the central node with two hydrogen atoms or by filling two vacant nodes of the first polar shell ($l = 1, m = 0$) with one hydrogen atom per node. Both these structures of the isotope are unbalanced, for this reason the carbon isotope $^{14}_{6}\mathrm{C}$ is unstable, radiogenic. Nevertheless, this is a long-lived isotope. Its half-life is 5730±40 years, apparently, because of a specific symmetry of the filled nodes and, hence, due to a specific symmetrical structure of its resulting binding fields.

The maximal mass number of carbon cannot exceed 22 in any way. This fact follows from the aforementioned solutions. The total number of its nodes (excluding purely kinetic ones not shown in the figures), axial *potential-kinetic polar* and *principal potential polar-azimuth*, is 11, and multiplicity η cannot exceed 2; hence, $11 \times 2 = 22$.

Actually, the carbon $^{22}_{6}\mathrm{C}$ is the heaviest artificially produced short-lived isotope of carbon [4]. It is obtained forcibly by filling all vacant polar nodes (by the neutron exposure on accelerators) with paired hydrogen atoms, as is shown in Fig. 7. The matrix of polar-azimuth discrete structure of carbon (see a matrix of the nodes (23), L. 4) $\left|\mathrm{C}_{l,m}\right|$ and matrices of filing its nodes by hydrogen atoms for the above (Fig. 2) cases have the following forms:

$$\left|\mathrm{C}_{l,m}\right| = \begin{vmatrix} 1 & 0 & 0 \\ 2 & 2 & 0 \\ 2 & 4 & 0 \end{vmatrix}; \qquad (3)$$

$$\left|^{12}_{6}\mathrm{C}\right| = \begin{vmatrix} 0 & 0 & 0 \\ 0 & 4 & 0 \\ 0 & 8 & 0 \end{vmatrix}; \quad \left|^{8}_{6}\mathrm{C}\right| = \begin{vmatrix} 0 & 0 & 0 \\ 0 & 4 & 0 \\ 0 & 4 & 0 \end{vmatrix}; \quad \left|^{22}_{6}\mathrm{C}\right| = \begin{vmatrix} 2 & 0 & 0 \\ 4 & 4 & 0 \\ 4 & 8 & 0 \end{vmatrix} \qquad (4)$$

Remember, in the matrices of the nodes, the *columns* correspond to the azimuthal number: $m = 0$, $m = \pm 1$, $m = \pm 2$, $m = \pm 3$, ..., *i.e.*, to the ordinal number of wave atomic *subshells;* the *rows* correspond to the number of the radial functions: $l = 0, 1, 2, 3, 4, 5, \ldots$, *i.e.*, to the ordinal number of the wave atomic *shells*.

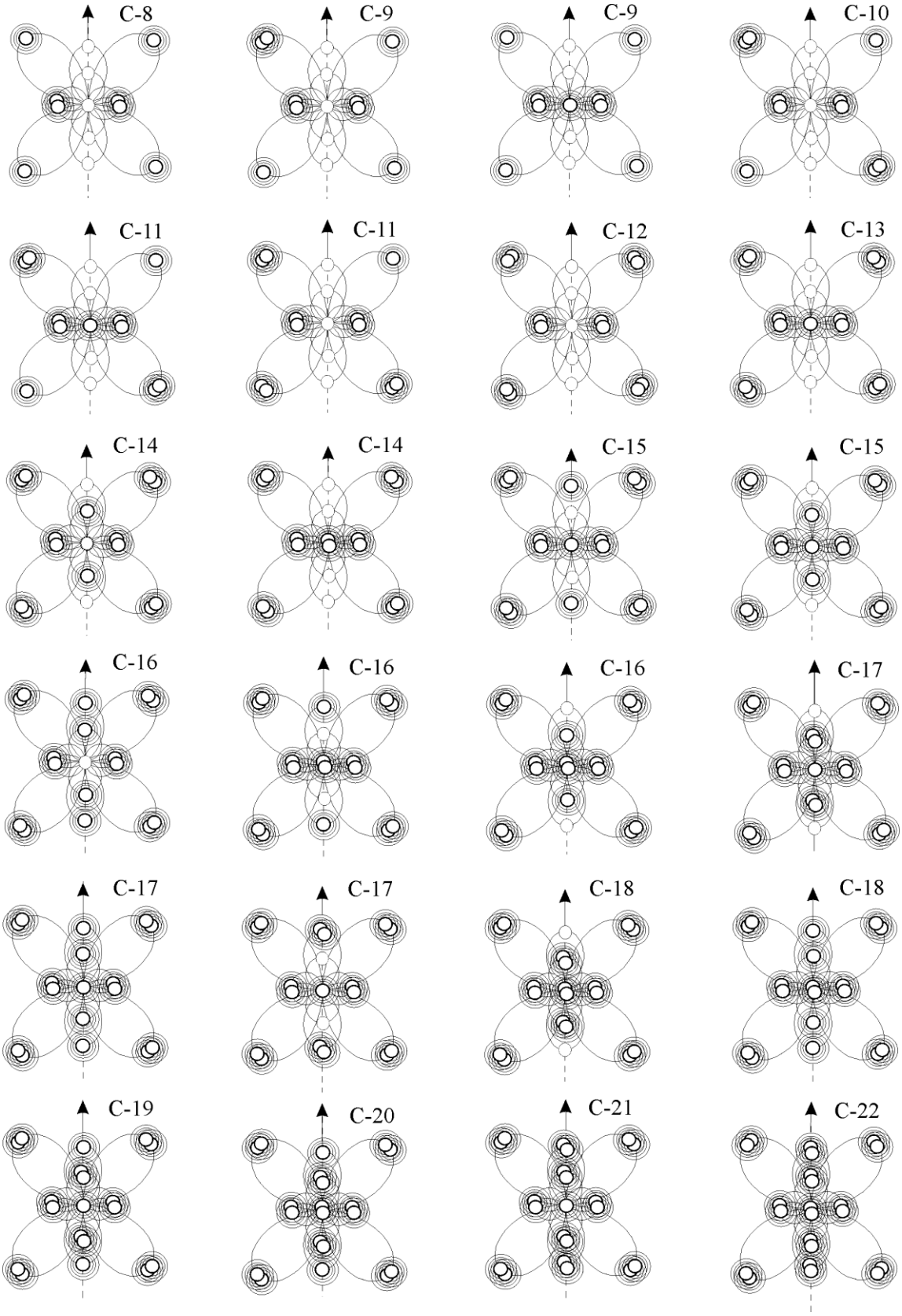

Fig. 8. A schematic image of the nodal structure of all possible isotopes of carbon, from lightest ${}^{8}_{6}\mathrm{C}$ to heaviest ${}^{22}_{6}\mathrm{C}$, arising from the particular solutions of the wave equation.

The above described filling of only *external* nodes by one hydrogen atom, in the lightest unstable isotope of carbon, is inherent in *lightest isotopes* of the most of atoms with *integer external* shells:

$$Z = 2,\ 6,\ 10,\ 22,\ 28,\ 40,\ 52,\ 60,\ 64,\ 72,\ 84,\ 100,... \qquad (5)$$

Silicon and germanium, $Z = 14$ and $Z = 32$, respectively, having completed external shells, $l = 3,\ m = \pm 1$ and $l = 4,\ m = \pm 1$, are exceptions. Why? The external integer shells of silicon and germanium contain *collateral nodes* that differ these atoms from $_{6}$C, $_{10}$Ne, $_{22}$Ti or $_{28}$Ni (see Fig.1, L. 4). The rest of atoms, including oxygen $_{8}$O, have *half-integer external* shells lying in the equatorial plane.

The shell-nodal structure of all possible isotopes of the carbon atom (from lightest to heaviest), originated from the solutions of the wave equation, is shown in Fig. 8.

3. Shell-nodal structure of oxygen and its isotopes

The spatial shell-nodal structure of the oxygen atom $^{16}_{8}$O and its polar-azimuth functions, originating from the shell-nodal atomic model (in full conformity with the solutions depicted in Fig. 1 (L. 4), are drawn in Fig. 9.

The oxygen atom has one more shell compared with the structure of carbon. It is a half-integer external shell ($l = m = \frac{1}{2}s;\ s = 2$) with two of its potential polar-azimuth nodes (the seventh and eighth) lying in the equatorial plane. They can be either in the same plane or a perpendicular plane with respect to the disposition of the rest nodes, as shown in Fig. 3b.

Note again that all of the empty *kinetic polar-azimuth nodes* (not shown in Fig. 9) are in the plane perpendicular to the plane containing the potential nodes. Obviously, the polar nodes disposed on the axis of symmetry, namely the Z-axis, are simultaneously potential and kinetic.

Since all nodes inside the oxygen atom are situated in the same plane (we refer to the first variant of the solutions presented in Fig. 9a), the spherical structure of oxygen atom looks like a plane. Thus, because of the specific geometry of disposition of its nodes, oxygen atoms can form the *plane hexagonal structure* pertinent, in particular, in snow crystals [5]. The symbolic designation of oxygen depicted in Fig. 9c reflects such a plane geometry of the arrangement of its eight *principal* polar-azimuth nodes and shows the shortest directions of exchange (interaction) between them.

The structure of all possible isotopes of the oxygen atom, as every atom in the shell-nodal atomic model, is uniquely defined by the multiplicity of filling both external potential polar-

azimuthal nodes and polar potential-kinetic nodes. The relative masses of the isotopes calculated on this basis completely coincide with the experimental data.

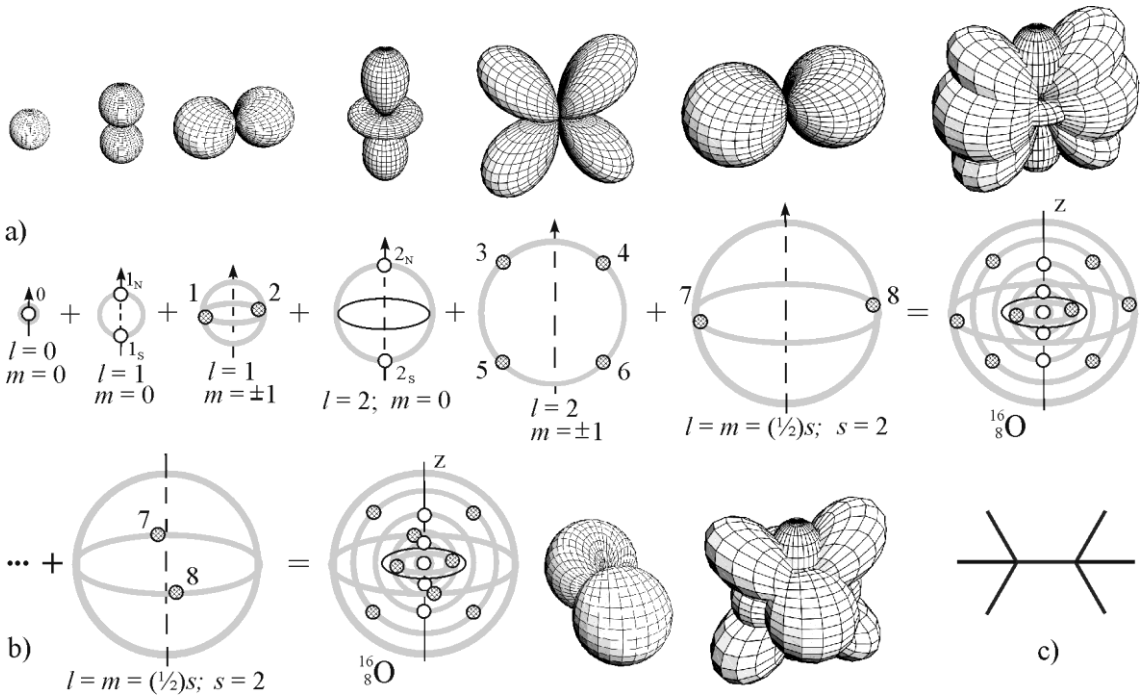

Fig. 9. Plots of the polar-azimuth functions $\Theta_{l,m}(\theta)\mathrm{Cos}(m\varphi+\alpha)$ ($l=0,1,2$; $m=0,\pm1$) and their extremal points on radial extremal shells $R_l(\rho)$ of the oxygen atom: (a) $\alpha=0$; (b) $\alpha=\pi/2$ for the external half-integer shell at $l=m=(1/2)s$ and $s=2$; (c) the symbolic designation of oxygen (at $\alpha=0$).

Let us consider the filling of *external* nodes by hydrogen atoms in the lightest unstable *isotope of oxygen*. The oxygen atom has the *half-integer external* shell $l=m=\frac{1}{2}s$, where $s=2$, with two nodes, 7-th and 8-th (see Fig. 9). Nate that the fully completed external shell at $l=2;\ m=\pm2$ correspond to the neon atom (turn to L. 4, see Fig. 1 and Table 1 there). The nearest completed integer shell of oxygen is its internal shell at $l=2; m=\pm1$. Resting upon the experimental isotope data, one can state that even if a part of nodes of the aforementioned nearest integer shell does not contain coupled hydrogen atoms the character of strong bindings temporarily keeps as well.

We can now suppose that half of the nodes of the last integer shell of oxygen have coupled hydrogen atoms and another half contains single hydrogen atoms. Then, following the shell-nodal structure depicted in Fig. 9, the uniquely possible lightest unstable isotope of oxygen is $^{12}_{8}\mathrm{O}$ with the mass number 12 (corresponding to the total number of hydrogen

atoms in the isotope). The order of arrangement and filling of the nodes in this isotope is demonstrated in Fig. 10.

It is possible as well that there is an additional unstable structure of $^{12}_{8}O$ (not shown in Fig. 10) in which the last integer shell (l = 2, m = ±1) contains one hydrogen atom in each of its four nodes and the external half-integer shell is filled fully by paired hydrogen atoms.

The isotope of oxygen $^{17}_{8}O$ can be obtained under the condition of filling the central vacant node in the stable isotope $^{16}_{8}O$ with one hydrogen atom. Filling the central node with two hydrogen atoms or two vacant nodes of the first polar shell ($l=1, m=0$) by one hydrogen atom per node, we arrive at the two possible structures of the oxygen isotope $^{18}_{8}O$ (Fig. 10). Both isotopes, $^{17}_{8}O$ and $^{18}_{8}O$, are stable because of symmetry (as is the isotope of carbon $^{13}_{6}C$).

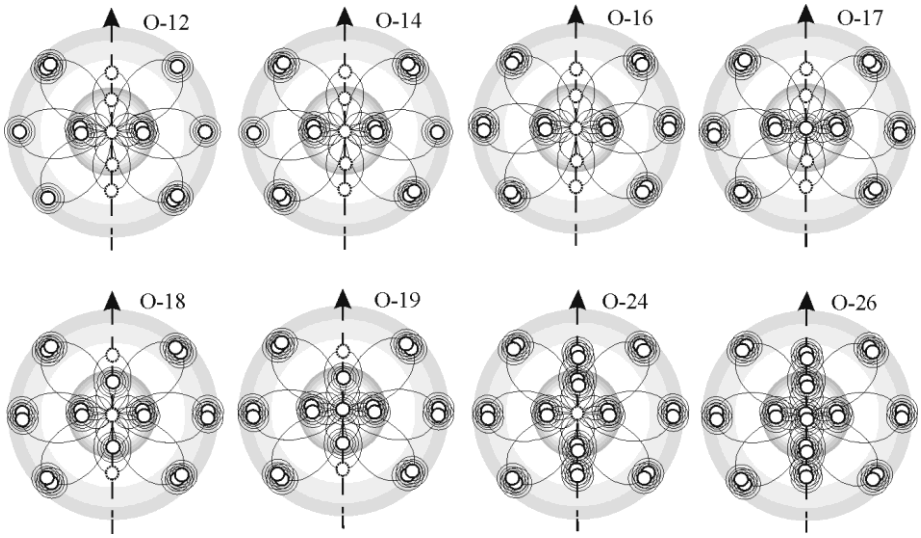

Fig. 10. The shell-nodal structure of some isotopes of oxygen following from the solutions of the wave equation: 3 stable isotopes ($^{16}_{8}O$, $^{17}_{8}O$ and $^{18}_{8}O$) and 5 short-lived unstable isotopes (including lightest $^{12}_{8}O$ and heaviest $^{26}_{8}O$).

From these solutions it also follows that the maximal mass number of oxygen is 26: the total number of all its nodes (excluding kinetic) is 13 and the maximal multiplicity of their filling is η=2. Actually, the oxygen $^{26}_{8}O$ is the heaviest artificially produced short-lived isotope of oxygen [4]. It is obtained forcibly by filling all of the vacant polar nodes with paired hydrogen atoms as is shown in Fig. 10.

The matrix of nodes of oxygen $\left|O_{l,m}\right|$ and the matrices of filing its nodes by hydrogen atoms for the above cases have the forms:

$$\left|O_{l,m}\right| = \begin{vmatrix} 1 & 0 & 0 \\ 2 & 2 & 0 \\ 2 & 4 & 2 \end{vmatrix}; \qquad \left|{}^{16}_{8}O\right| = \begin{vmatrix} 0 & 0 & 0 \\ 0 & 4 & 0 \\ 0 & 8 & 4 \end{vmatrix}; \qquad \left|{}^{14}_{8}O\right| = \begin{vmatrix} 0 & 0 & 0 \\ 0 & 4 & 0 \\ 0 & 8 & 2 \end{vmatrix} \qquad (6)$$

$$\left|{}^{12}_{8}O\right| = \begin{vmatrix} 0 & 0 & 0 \\ 0 & 4 & 0 \\ 0 & 6 & 2 \end{vmatrix} \quad \text{or} \quad \left|{}^{12}_{8}O\right| = \begin{vmatrix} 0 & 0 & 0 \\ 0 & 4 & 0 \\ 0 & 4 & 4 \end{vmatrix}; \qquad \left|{}^{26}_{8}O\right| = \begin{vmatrix} 2 & 0 & 0 \\ 4 & 4 & 0 \\ 4 & 8 & 4 \end{vmatrix} \qquad (7)$$

The peculiarity of filing the nodes in the lightest oxygen isotopes also occurs with the lightest isotopes of the remaining atoms with *half-integer* external shells (at least as far as ${}^{67}_{35}\mathrm{Br}$, which has been confirmed experimentally). The same situation is realized with the lightest isotopes of silicon and germanium, ${}^{22}_{14}\mathrm{Si}$ and ${}^{58}_{32}\mathrm{Ge}$, having *integer* external shells; they were obtained experimentally as well. Integer external shells of silicon and germanium contain *collateral nodes* that differs these atoms from C, Ne, Ti and Ni. Two nodes of their next to last integer shell have uncoupled hydrogen atoms, along with all of the uncoupled nodes of the external shell.

4. All variety of atomic isotopes

Let us look at one more example, this time nickel ${}_{28}\mathrm{Ni}$. Nickel is heavier than the atoms considered above; it contains two *collateral* nodes in one of its internal subshells (see Fig. 6). The matrix of nodes of nickel $\left|\mathrm{Ni}_{l,m}\right|$ (its two collateral nodes at $l = 3$, $m = \pm 1$ are indicated in brackets) and two matrices of nodal filling of its short-lived lightest and heaviest isotopes, ${}^{56}_{28}Ni$ and ${}^{78}_{28}Ni$ (obtained experimentally as well), are as follows:

$$\left|Ni_{l,m}\right| = \begin{vmatrix} 1 & 0 & 0 & 0 \\ 2 & 2 & 0 & 0 \\ 2 & 4 & 4 & 0 \\ 2 & 4(2) & 8 & 6 \\ 2 & 0 & 0 & 0 \end{vmatrix} \qquad (8)$$

$$\left|{}^{56}_{28}Ni\right| = \begin{vmatrix} 0 & 0 & 0 & 0 \\ 0 & 4 & 0 & 0 \\ 0 & 8 & 8 & 0 \\ 0 & 8(0) & 16 & 6 \\ 0 & 0 & 0 & 0 \end{vmatrix} \qquad \left|{}^{78}_{28}Ni\right| = \begin{vmatrix} 2 & 0 & 0 & 0 \\ 4 & 4 & 0 & 0 \\ 4 & 8 & 8 & 0 \\ 4 & 8(4) & 16 & 12 \\ 4 & 0 & 0 & 0 \end{vmatrix} \qquad (9)$$

The relative masses of the isotopes of all of the atoms of the Periodic Table, originating from the particular solutions of the wave equation [6], are graphically presented in Fig. 11 (in accord with the matrices of filling and Eq. (1)).

The extent of deviation from the maximal nodal fillings of both *external half-integer* shells and the next to the last *integer* shells are responsible for the *lightest isotopes*, presented in Figure 11 above ${}^{67}_{35}Br$.

The lightest isotopes of the heavier atoms, below ${}^{67}_{35}Br$, are exhibited in the Figure only for the case when all their *integer* potential polar-azimuthal shells remain undisturbed (their nodes are entirely completed by paired hydrogen atoms), as it takes place, *e.g.*, for the isotope of oxygen ${}^{14}_{8}O$ (see Eq. (6) and Fig. 10)).

The *maximal* relative masses of all isotopes, shown in Fig. 11, are uniquely possible because of the strictly limited number of nodes in every atom, defined by the particular solutions of the wave equation $\Delta\hat{\Psi} - \frac{1}{c^2}\frac{\partial^2\hat{\Psi}}{\partial t^2} = 0$ (see the matrix of nodes (Eq. (23), L. 4)), and owing to their limited filling (the multiplicity η cannot exceed 2, see Eq. (2)).

Thus, owing to the different filling η (2) of the various nodes with hydrogen atoms: *potential principal* nodes of external integer and half-integer polar-azimuthal shells, *potential-kinetic polar* nodes, and *potential collateral* nodes (the latter define the metastable states), the same probabilistic element (atom) can be realized in real space with different relative masses. Accordingly, any atom of the probabilistic wave field, having the characteristic nodal structure, is represented by a series of its own isotopes in accord with the formula (1).

Based on all of the above data we can confidently say that the *nodal structure* of the wave atomic spaces along with the *peculiarity of different types of the nodes* and, hence, *different multiplicities of their filling*, define the nature and structure of all isotopes.

A comparative analysis shows that not all *isotopes* of the atoms, predicted by the obtained solutions and shown in Figure 11, were produced experimentally.

5. Natural and synthesized isotopes of hydrogen

The question may arise at everyone, what isotopes of hydrogen follow from the shell-nodal atomic model, and what is their shell-nodal structure? As known, in 2003 it was announced about synthesising the 7-th isotope of hydrogen ${}^{7}_{1}H$ at RIKEN's RI Beam Science Laboratory [7, 8]. The half life of 2.3×10^{-23} seconds, ascribed to this supposed isotope, was not purely derived from experimental data; it was estimated, in fact, from “systematic trends”. The announced finding was not confirmed independently in none other laboratory.

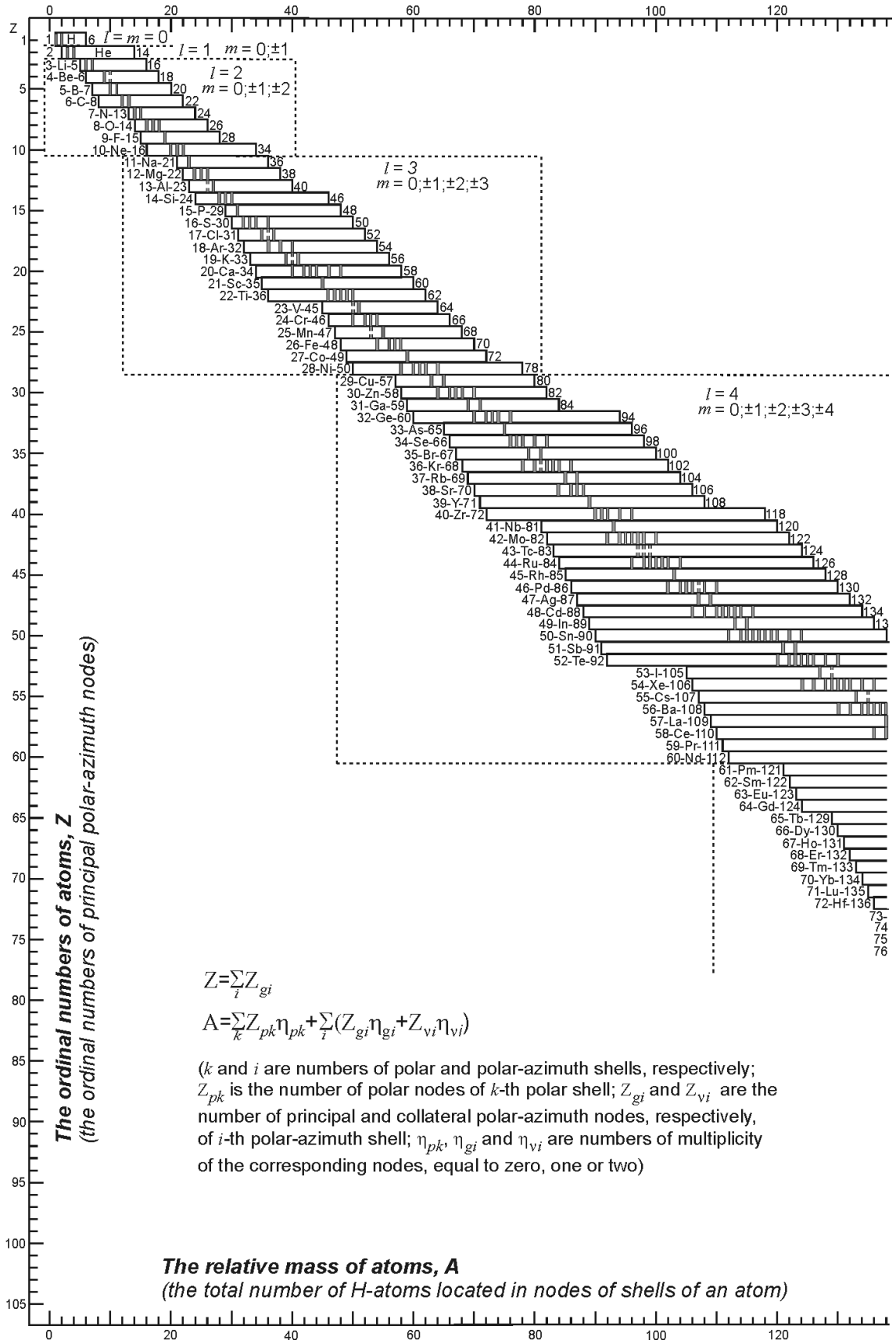

Fig. 11. The complete set of the isotopes derived from the particular solutions of the wave equation.

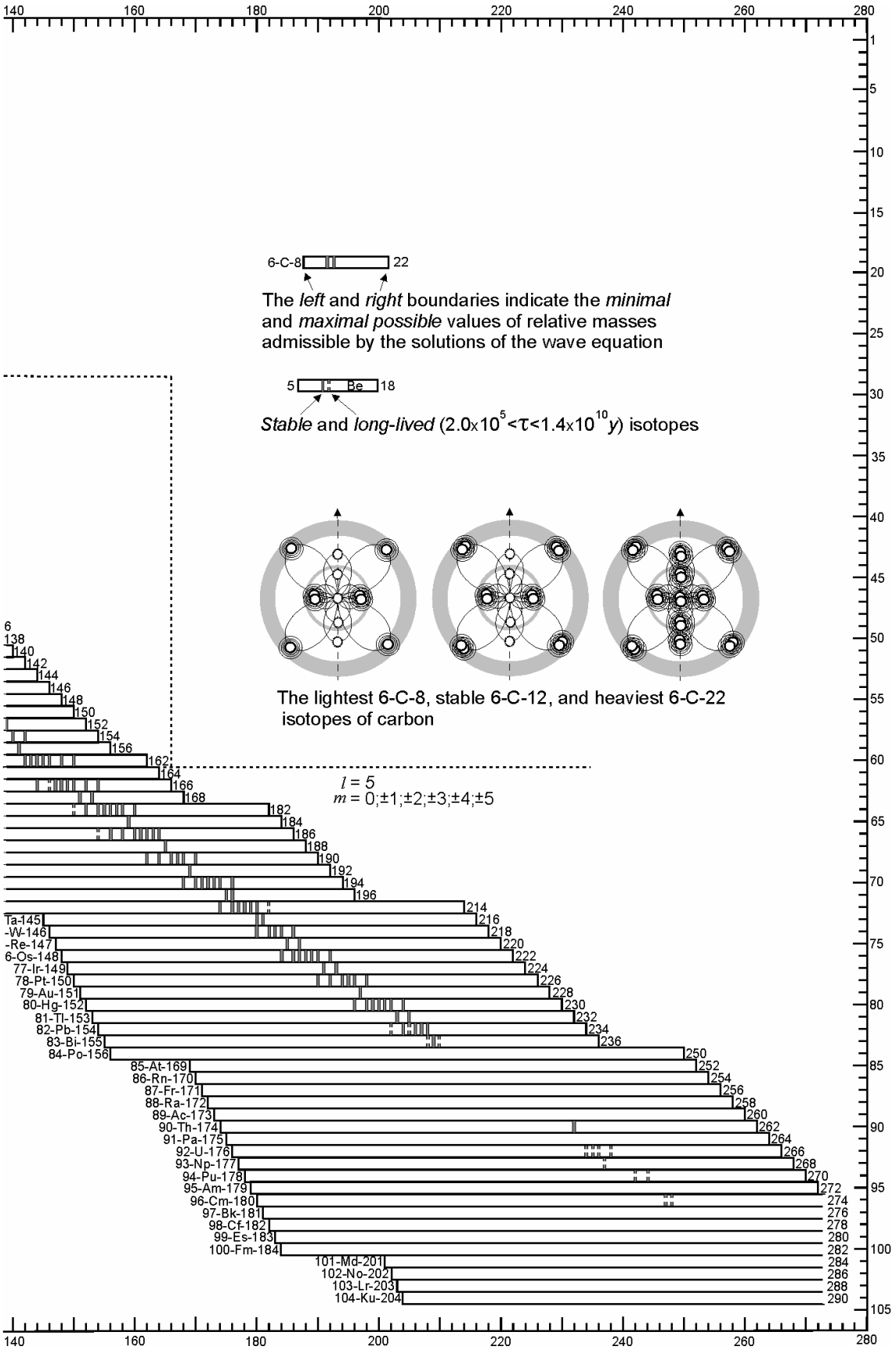
6-C-8 22
The *left* and *right* boundaries indicate the *minimal* and *maximal possible* values of relative masses admissible by the solutions of the wave equation
5 Be 18
Stable and *long-lived* ($2.0 \times 10^5 < \tau < 1.4 \times 10^{10}$ *y*) isotopes
The lightest 6-C-8, stable 6-C-12, and heaviest 6-C-22 isotopes of carbon
l = 5
m = 0;±1;±2;±3;±4;±5
Ta-145
-W-146
-Re-147
6-Os-148
77-Ir-149
78-Pt-150
79-Au-151
80-Hg-152
81-Tl-153
82-Pb-154
83-Bi-155
84-Po-156
85-At-169
86-Rn-170
87-Fr-171
88-Ra-172
89-Ac-173
90-Th-174
91-Pa-175
92-U-176
93-Np-177
94-Pu-178
95-Am-179
96-Cm-180
97-Bk-181
98-Cf-182
99-Es-183
100-Fm-184
101-Md-201
102-No-202
103-Lr-203
104-Ku-204

However, this fact agrees with the results obtained from the solutions of the wave equation for the hydrogen atom, in the framework of the shell-nodal atomic model. According to the latter, the hydrogen atom has 5 *nodes* (see Fig. 12): three potential-kinetic *polar*: 0, 1_N, 1_S, and two *polar-azimuthal*, one of them is *potential* 1 and another – *kinetic*, the last not shown in the presented Figures. Hence, from the latter it follows that potentially the hydrogen atom can have maximum 8 isotopes (at maximal multiplicity η=2 and excluding filling the kinetic node). Let us show this.

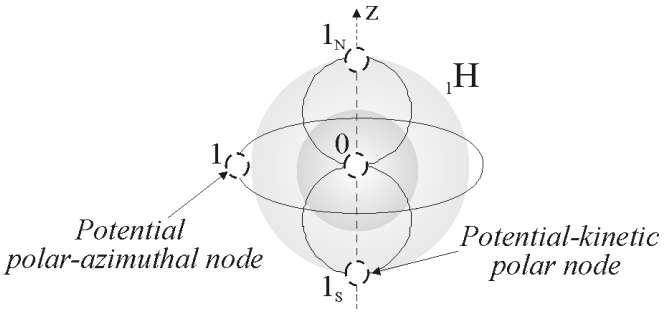

Fig. 12. A scheme of the nodes of the hydrogen atom according to the solutions of the wave equation; the node 1 is the first of the *principal* polar-azimuthal nodes whose ordinal numbers coincide with the *atomic numbers* of the elements of the Periodic Table.

The first place in *Theoretical Periodic Table of the Atoms* (Table 1 in L. 4) under the ordinal number 0 takes the *neutron* designated as $_0$H. It corresponds to the solution of the wave equation at $l = 0$ and $m = 0$ resulted in *one node* (see, *e.g.*, the nodes depicted in Fig. 5).

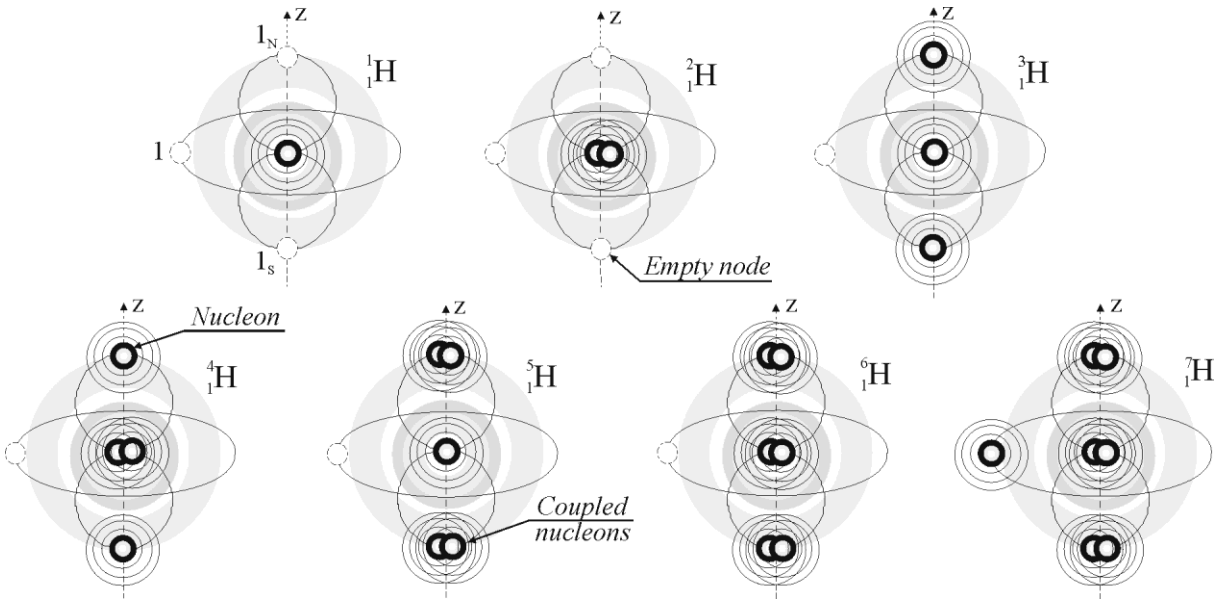

Fig. 13. The filling of the nodes with nucleons in the wave shells of the seven of the total eight possible isotopes of the hydrogen atom.

The *hydrogen atom* $_1$H has the ordinal number 1 corresponding to the solution at $l = m =$ 0 and $l = 1$, $m = \frac{1}{2}s$ at $s = 1$ (a half-integer equatorial shell of the subshell at $m = \pm 1$, see Figures 5 and 12 and also Fig. 1 in L.4). Having, according to the solutions, the nodes indicated in the above Figures, nucleons will fill the nodes respecting as far as possible the higher symmetry as shown in Fig. 13. Of course, if we can fill the half-integer shell ($s = 1$) with coupled nucleons (to maximal multiplicity $\eta = 2$), we will arrive at the last extremely unstable of the possible synthetic isotopes of hydrogen, $^{8}_{1}H$.

The variants of filling the nodes can be different for the same isotopes. For example, the isotope $^{3}_{1}H$ can have also the form like $^{2}_{1}H$ with additionally filled by a nucleon one of the polar nodes, 1_N or 1_S, *etc*.

The probability of forming the half-integer shell at $s = 1$ (not shown in the Figure) and filling the only node on it has little likelihood, therefore we not show it here. The $^{1}_{1}H$ (protium), $^{2}_{1}H$ (deuterium), and $^{3}_{1}H$ (tritium) are three naturally occurring isotopes, among them tritium is unstable (a half-life is 12.32 years). Other, highly unstable isotopes have been synthesized in the laboratory but not observed in Nature.

6. Isotopes of helium

The *helium atom* $_2$He of the ordinal number 2 has completely filled shells corresponding to the solutions at $l = 0$, 1 and $m = 0, \pm 1$ (see Fig. 5). The total number of the nodes, excluding kinetic, but including potential-kinetic polar nodes 2_N and 2_S related to the solution at $l = 2$ and $m = 0$, is 7 (Fig. 14).

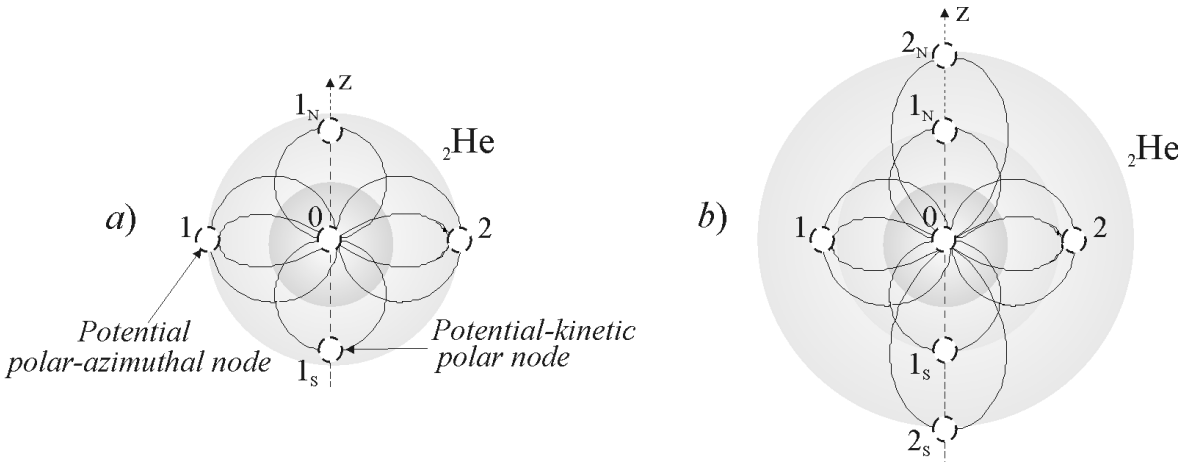

Fig. 14. A scheme of the nodes of the helium atom without (*a*) and with (*b*) taking into account the two potential-kinetic polar nodes, 2_N and 2_S, located on the Z-axis of the wave spherical shell corresponding to the solution at $l = 2$ and $m = 0$.

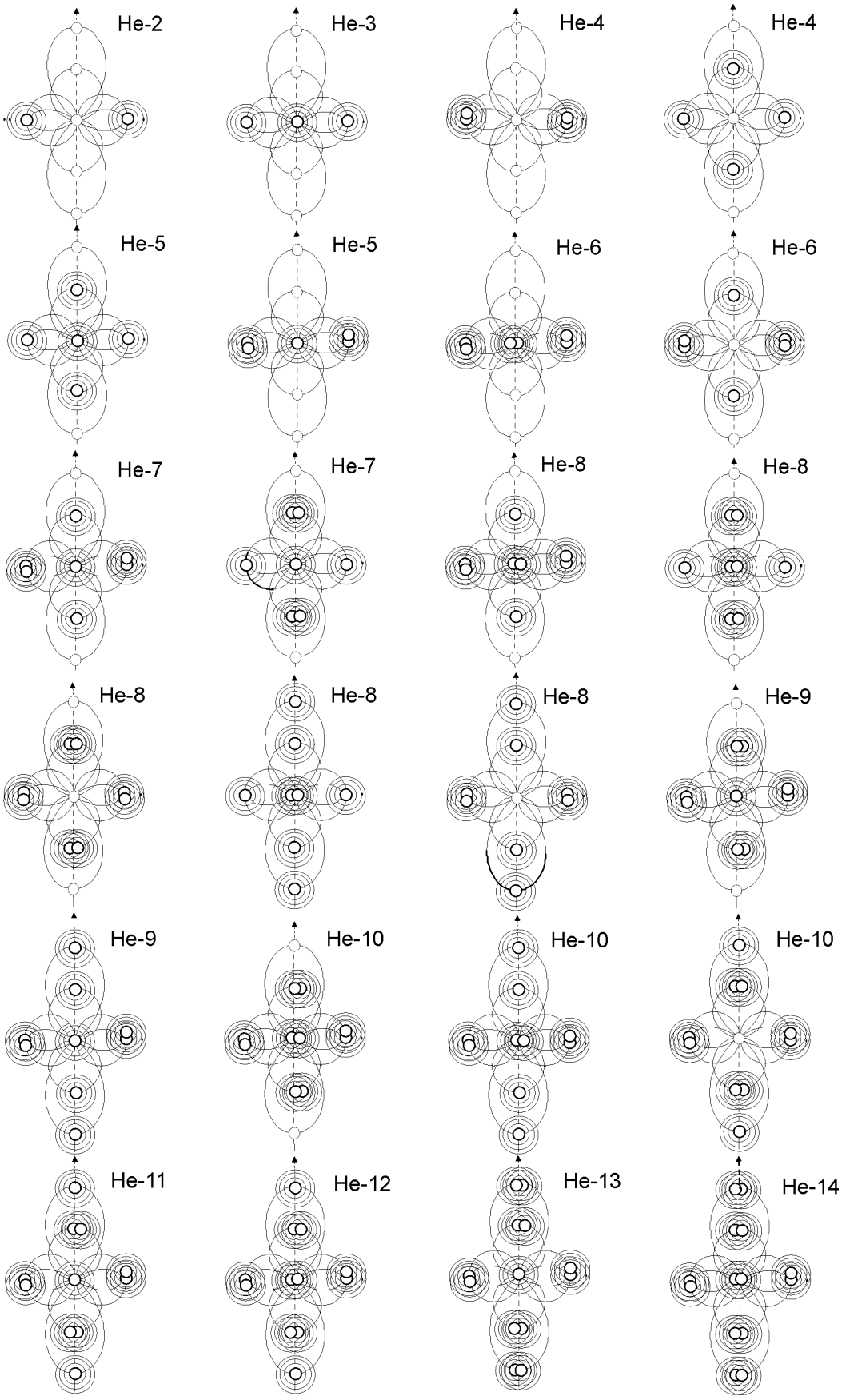

Fig. 15. A scheme of filling the nodes in possible isotopes of the helium atom admitted by the particular solutions of the wave equation.

We must consider the above polar nodes in spite of they are related to the next shell (belonging to the atoms with ordinal numbers from 3 up to 10). The matter is that these nodes are on the axis of symmetry Z and their possible shortest-time filling at the corresponding conditions (at synthesizing in a laboratory), making the helium atom superheavy, will not influence on its individual properties which are defined (as for any atoms) exceptionally by the structure of the external polar-azimuthal shells.

The potential polar-azimuthal nodes under the ordinal numbers 1 and 2 are the first of the principal potential polar-azimuthal nodes coinciding with the atomic numbers of hydrogen and helium, respectively.

The continuous contour lines in Fig. 14 of the polar-azimuthal functions of the helium atom (in accordance with theis images depicted in Fig. 2) relate to the solutions at $l = 0, 1$ and $m = 0, \pm 1$. They indicate the spatial position of the nodes and a toroidal wave vortex.

Having, according to the solutions, the nodes indicated in the Figure, nucleons will fill the nodes respecting as far as possible the higher symmetry as shown in Fig. 15.

To present time there are 9 known isotopes of helium. Among them, the isotopes ${}^{3}_{2}He$ and ${}^{4}_{2}He$ are stable. The remaining isotopes are short-lived with different half-lifes. The lightest isotope ${}^{2}_{2}He$ (known as a diproton) is an extremely unstable isotope of helium, so that its half-life even was not estimated. The nodes of its external polar-azimuthal shell (see Fig. 15) are half-filled that makes it impossible to keep this shell unchanged at least for some reasonable in time instant.

The heaviest synthesized radioisotope ${}^{10}_{2}He$, obviously, corresponds to the complete filling of all of the nodes in the shell-nodal structure of helium depicted in Fig. 14a. However, in accord with the shell-nodal atomic model, other variants of filling the nodes are also possible as demonstrated in Fig. 15. In these cases, it takes place the participation of the polar nodes, 2_N and 2_S, of the external shell related to the solutions at $l = 2$, $m = 0$ (see Fig. 14b). Thus, as follows from the shell-nodal structure, the heaviest isotope of helium is likely ${}^{14}_{2}He$.

7. Conclusion

Thus, in accord with the approach developed within the Wave Model of dialectical physics, an atom represents a system of the spherical shells with discrete points-nodes of wave space filled with the hydrogen atoms to which we refer *neutron*, *proton* and *hydrogen atom* ${}^{1}_{1}H$ (*protium*).

The same probabilistic element (an atom) can be realized in the real space with different relative masses due to the different filling η with hydrogen atoms of its nodes of the different types. We mean the *principal potential* nodes of external integer- and half-integer polar-

azimuth shells, the *potential-kinetic polar* (axial) nodes, and the *potential collateral* nodes (the latter are the sites of metastable states). Accordingly, any atom of the probabilistic wave field, having each the specific nodal structure inherent just in this individual atom only (see the matrix of the nodes (23) in L. 4), is represented by a series of its own isotopes in full agreement with the formula (1) and the multiplicity η (2) of filling each of the nodes in its shells.

This implies that atoms do not have a nucleus as is customary assumed in the quantum-mechanical nuclear atomic model. Actually, the reconsideration of Rutherford's experiments on scattering of α- and β-particles in matter has shown that the supposition on an existence of a superdense nucleus in the centre of an atom has been insufficiently substantiated and its acceptation, as follows from the data published in the last two decades, turned out to be mistaken [1-3].

We see, thus, that having the wave *shell-nodal structure*, the new *molecular-like* (*multicentric*) atomic model essentially differs from the *nuclear* (*monocentric*) quantum-mechanical and Rutherford-Bohr atomic models. Accordingly, dialectical physics contrary to modern (official) physics explains all physical phenomena in a different way.

In particular, by now with taking into account the shell-nodal structure of the atoms and the dynamic model of elementary particles, some of the well-known phenomena were essentially reconsidered. As a result, it was revealed the nature of the phenomena ununderstandable in the framework of the Standard Model of modern physics and explained the true nature of the phenomena misunderstood until now [3] (some of them were considered in previous Lectures contained in a given series of the Volumes). All these facts underline an advantage of the *wave concepts* lying in the foundation of the new atomic model.

It is to the point to note here that contrary to particular solutions of the general ("classical") wave equation $\Delta\hat{\Psi} - \frac{1}{c^2}\frac{\partial^2\hat{\Psi}}{\partial t^2} = 0$ which uncover the wave shell-nodal structure of matter (atoms), the quantum-mechanical "solutions" of Schrödinger's equation led, as turned out groundlessly, to the *subjective* notion of "*electron structure"* ("*electron configuration"*) of atoms. It was the great conceptual error [9]. For this reason, it is quite natural that Schrödinger's solutions, as erroneous, *do not give any information about the nature and structure of atomic isotopes*.

Thus, the revealing of the nature and structure of all possible isotopes is a very important result which, along with many other unique data already obtained in the framework of the Wave Model, confirms the *reliability of the solutions* that led to the discovery of the shell-nodal structure of the atoms. Evaluation of *intrinsic* and *extrinsic* binding energies between, respectively, the filled nodes in the individual shell-nodal structures (*intra-atomic bonds*) and between the filled nodes belonging to different interacting atoms (*interatomic bonds*) confirms also this conclusion. We will consider the latter issue further in these Lectures.

References

[1] L. G. Kreidik and G. P. Shpenkov, *Atomic Structure of Matter-Space*, Geo. S., Bydgoszcz, 2001, 584 p.; http://shpenkov.com/atom.html

[2] G. P. Shpenkov, *The Scattering of Particles and Waves on Nucleon Nodes of the Atom*, International Journal of Chemical Modelling, Vol. 2, No. 1, (2008).

[3] G. P. Shpenkov, *Some Words about Fundamental Problems of Physics*: *Constructive Analysis*, LAMBERT Academic Publishing, p.116 (2012);
amazon.com/words-about-fundamental-problems-physics/dp/3659237507
http://shpenkov.com/pdf/Book-2011-Eng.pdf

[4] G. Audi and A.H. Wapstra, *The 1995 Update to the Atomic Mass Evaluation*, Nuclear Physics A595, Vol. 4, p. 409-480, December 25, 1995; R.R. Kinsey, et al., *The* NUDAT/PCNUDAT *Program for Nuclear Data*. Data extracted from NUDAT database (Jan. 14/1999).

[5] W.A. Bentley and W.J. Humphreys, *Snow Crystals*, McGraw-Hill, New York and London, 1931.

[6] G. P. Shpenkov, *Relative Atomic Masses of the Elements*, 2001;
https://shpenkov.com/isotopes_table.html

[7] Y. B. Gurov *et al*, *Spectroscopy of Superheavy Hydrogen Isotopes in Stopped-Pion Absorption by Nuclei*, Physics of Atomic Nuclei 68 (3), p. 491–497, (2004).

[8] A. A. Korsheninnikov *et al*, *Experimental Evidence for the Existence of 7H and for a Specific Structure of 8He*, Physical Review Letters 90 (8): 082501, (2003).

[9] G. P. Shpenkov, *Conceptual Unfoundedness of Hybridization and the Nature of the Spherical Harmonics*, Hadronic Journal, Vol. 29. No. 4, p. 455, (2006);
http://shpenkov.com/pdf/HybridizationShpenkov.pdf

Lecture 6

Carbon Compounds

1. Introduction

At the beginning of this Lecture it seems important to recall briefly the fundamental concepts and existing circumstances that led to the discovery of the *shell-nodal structure* of the atoms. And then we will proceed to consider the possible variants and *peculiarities of the interatomic bindings* implemented when forming some of the elementary hydrocarbon compounds and most common allotropes of carbon, taking into account, naturally, the shell-nodal structure of the carbon atom.

All in the Universe at all its levels, including micro- and mega-, is in incessant oscillatory-wave motion and, hence, has the wave nature. Wave fields of all objects are overlapped herewith. All in the Universe follows the law of rhythm and is in natural harmony. Accordingly, the natural harmonic bond exists between all fields, including electromagnetic and gravitational, like between any objects and phenomena.

Recognizing without any doubts the wave nature of the Universe, it is not so difficult to come to the conclusion that all phenomena and objects in the Universe at all levels, including subatomic, atomic, and molecular, behave obeying the wave laws. This means that they are described by the universal ("classical") wave equation,

$$\Delta\hat{\Psi} - \frac{1}{c^2}\frac{\partial^2\hat{\Psi}}{\partial t^2} = 0\,. \qquad (1)$$

Taking this statement into account, accepting it completely without any doubts, some of the purely mathematical solutions of the wave equation were undergo to the comprehensive analysis. This was made in order to disclose objective information about the structure and behaviour of matter existing, most likely, in the solutions, as we expected, and which till now was "hidden" from physicists (since no one earlier did not notice there it).

Performing this analysis, we were confident in a positive result of the analysis for many reasons. One of them is the fact that the physical meaning of some particular solutions of the wave equation has turned out a white spot in science. Why? The wave nature of *all*

phenomena, fields, and objects in the Universe was not regarded in physics as a self-evident truth (and still is not regarded as such by majority, unfortunately). That is, universality of the wave nature of the Universe was not recognized as the universal being and, hence, this fundamental feature was not considered, in general, as the primordial obligatory conceptual basis in developing the physical theories. For this reason, the wave concept was not included in a series of basic postulates of modern physics theories, *i.e.*, in the foundation of the Standard Model. This is why, in particular, the modern physics still cannot find any relation between gravitational and electromagnetic fundamental interactions, and, hence, cannot build a unified field theory (UFT). Accordingly, intellects of most physicists-atomists were/are focused (almost for a century) not on the general wave equation (1) and its solutions, but just on Schrödinger's equation, designed for describing quantum mechanical behaviour, and its controversial "solutions". Up to now, no one raised the question, is whether Schrödinger's equation the viable alternative to the general wave equation, for cognition of atomic structure, or not?

As it turned out with time, quantum mechanics with the Schrödinger equation was unable to withstand the fair criticism, and eventually it was revealed that its solutions, really, are erroneous. The main reason is that the quantum mechanical equation itself invented by Schrödinger, as turned out, with fatal flaws is erroneous originally, being intrinsically contradictory. Therefore, it is unable to describe correctly the wave processes at the atomic level in principle that is clearly shown, for example, in the analytic articles [1-3]. The indicated works, devoted to an analysis of the Schrödinger equation and his so-called "solutions", are subjected all time (after their publication) to the undiminishing interest of physicists, judging by feedback; and the conclusion to which the authors of these articles have come is now recognized by majority as well-grounded and fair.

In result of the aforementioned analysis carried out profoundly enough, it was found that the well-known particular solutions of the general wave equation (1) de facto, as we have assumed, contain information about the structure of matter and about such fundamental regularities in Nature which were unknown earlier [4, 5]. Namely, the main discoveries obtained in result of the analysis, about which we would like to recall once more in this Lecture, concerning the structure of matter and physical processes running in Nature, are the following.

1. Atoms are the wave formations.

2. As the wave formations, atoms have a quasi-spherical shell-nodal structure coincident with the nodal structure of standing waves formed in local volumes of the three-dimensional wave space-field. Actually, each atom with $Z \geq 2$ represents one of the elementary molecules of the hydrogen atoms (to which we refer *proton*, *neutron* and *protium* ${}_1^1H$). In view of the stated above, it should be noted that the Periodic Table of the Atoms represents, in essence, the *Periodic Table of the Elementary Molecules*.

3. Every *potential* polar-azimuthal node in spherical shells of the atoms contains not more than two nucleons.

4. Along the Z-axis of the atom (in spherical polar coordinates), there are potential-kinetic polar nodes (which are the nodes of rest and motion simultaneously). These nodes are not filled with nucleons in the most abundant and stable atoms.

5. Exchange (interaction) between the filled nodes inside and outside of the atoms is realized on the fundamental frequency of exchange at the atomic and subatomic levels,

$$\omega_e = 1.869162559 \times 10^{18}\ s^{-1}. \qquad (2)$$

In accord with the Dynamic Model [6], the fundamental frequency (2) is equal to the pulsation frequency of elementary particles.

6. Exchange at the megalevel (gravitational exchange) is realized by exchange gravitational charges q_g at the fundamental frequency inherent in the pulsating particles at this level,

$$\omega_g = 9.158082264 \times 10^{-4}\ s^{-1}. \qquad (3)$$

7. The electromagnetic, strong and gravitational exchanges (interactions) are realized by the exchange charges of electrons and nucleons, respectively. The exchange charges of a particle, q_e or q_g, are defined as the product of its associated mass m and the corresponding fundamental frequency, ω_e or ω_g:

$$q_e = m\omega_e \quad g \cdot s^{-1}. \qquad q_g = m\omega_g \quad g \cdot s^{-1} \qquad (4)$$

The above enumerated features cardinally change the common view on the structure and behaviour of matter. This is in a violent discrepancy with present-day concepts which are the base of the Standard Model of modern physics, including atomic physics. The first information on the above discoveries has appeared in 1996 in the book (of limited edition) entitled “Alternative Picture of the World” [7].

However, in spite of appearance of the aforementioned unique discoveries and convincing proofs of their reality, the basic concepts of modern theory of atoms, judging on mainstream publications, are not yet reconsidering and do not undergo any changes. Apparently, it happens because of the strong conservatism inherent in science. With this, the relatively too short period of time, beginning from 1996, has passed ever since in order to the above information became well-known and seriously perceived, a fortiori, at absence of extensive publicity.

For these reasons the modern atomic theory based on Schrodinger’s equation “solutions” still continues to be considered as before, almost dogmatically, as the only true and unchanged.

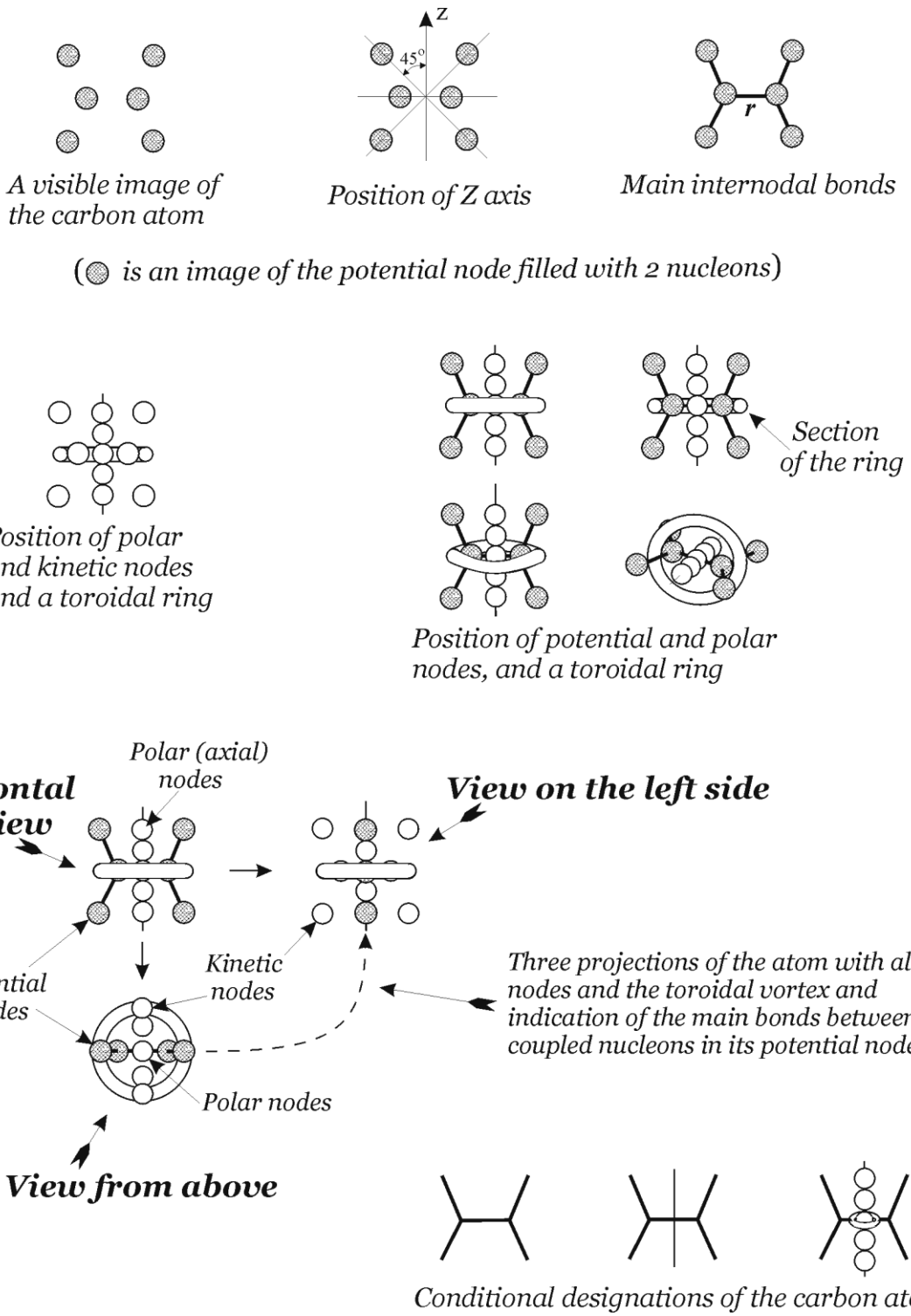

Fig. 1. The shell-nodal structure of the carbon atom.

Let us turn now to the main subject of the present Lecture. With regard to the carbon atom, the schematic images of principal elements of its shell-nodal structure, considered in previous Lectures and collected here together, are shown in Fig. 1. Note again that all six potential polar-azimuthal nodes (denoted by dark circles) are in the same plane. The corresponding kinetic nodes are in the plane perpendicular to the plane of potential nodes.

2. Formation of bindings in hydrocarbon compounds

Thus, in accord with the shell-nodal atomic model, the *carbon atom* is an elementary molecule of the hydrogen atoms, having the ordinal number $Z = 6$ that coincides with the number of principal potential polar-azimuthal nodes in its shell-nodal structure.

A carbon frame is the basis for hydrocarbon molecules. An *external shell* of the carbon atom ${}^{12}_{6}C$ ($l = 2,\ m = \pm 1$) having four potential polar-azimuthal nodes (the numbers 3 – 6; see Fig. 1, L. 4) is entirely completed with the coupled hydrogen atoms. The next subshell ($m = \pm 2$) of the same shell, $l = 2$, with four empty nodes belongs to the neon atom, *Ne*. An atomic number of neon Z = 10 is equal to the number of its principal potential polar-azimuthal nodes. Neon has all completely filled subshells (at $m = \pm 1,\ m = \pm 2$) of the shell $l = 2$. Intermediate solutions (atomic numbers Z = 7, 8, and 9) relate, respectively, to the atoms of N, O, and F. All they have half-integer external shells with polar-azimuthal nodes lying in the equatorial plane.

The four empty nodes of the next external shell belonging to neon, which is outside the completed shell of the carbon atom, are in an equatorial plane as shown in Fig. 2*a*,*b* (designated by dotted lines). This shell outside the carbon atom is simultaneously a vacant shell for the carbon environment. It plays the role in forming molecules. Four empty nodes of the shell can absorb H-atoms from the outside. By this way, the chemical level of bonds is realized and hydrocarbon molecules are formed as a result. Accordingly, this shell is called the *improper* shell of carbon.

Thus, when the *improper* shell is drawn into a process of interchange (interaction) with hydrogen, hydrocarbon molecules are formed. The resulting structure of the improper shell repeats the discrete nodal structure (topology) of the external shell of the corresponding atom to which this shell is proper (in our case it relates to the neon shell). In a case of chemical adsorption of four hydrogen atoms by the nodes of the aforementioned improper shell of carbon, the methane molecule CH_4 is formed as shown in Fig. 2*c*.

The conditional designations of the structures under consideration are drawn on the right side of the figures. A structural analog of the methane molecule is the neon atom (Z = 10). The latter has the same topology of the disposition of nodes as the methane molecule CH_4 drawn in Fig. 2*c*. However, external nodes of the neon atom have fully completed equatorial nodes by *coupled* hydrogen atoms. Moreover, they are *strongly* bound with the rest nodes of neon in comparison with the *chemical* level bonds of the nodes in the improper shell of the carbon atom filled with *single* atoms, resulted in the formation of methane molecules.

The next possible nodal structure of CH_4, when two nodes of the improper shell absorb the coupled hydrogen atoms, H_2, is shown in Fig. 2*d*.

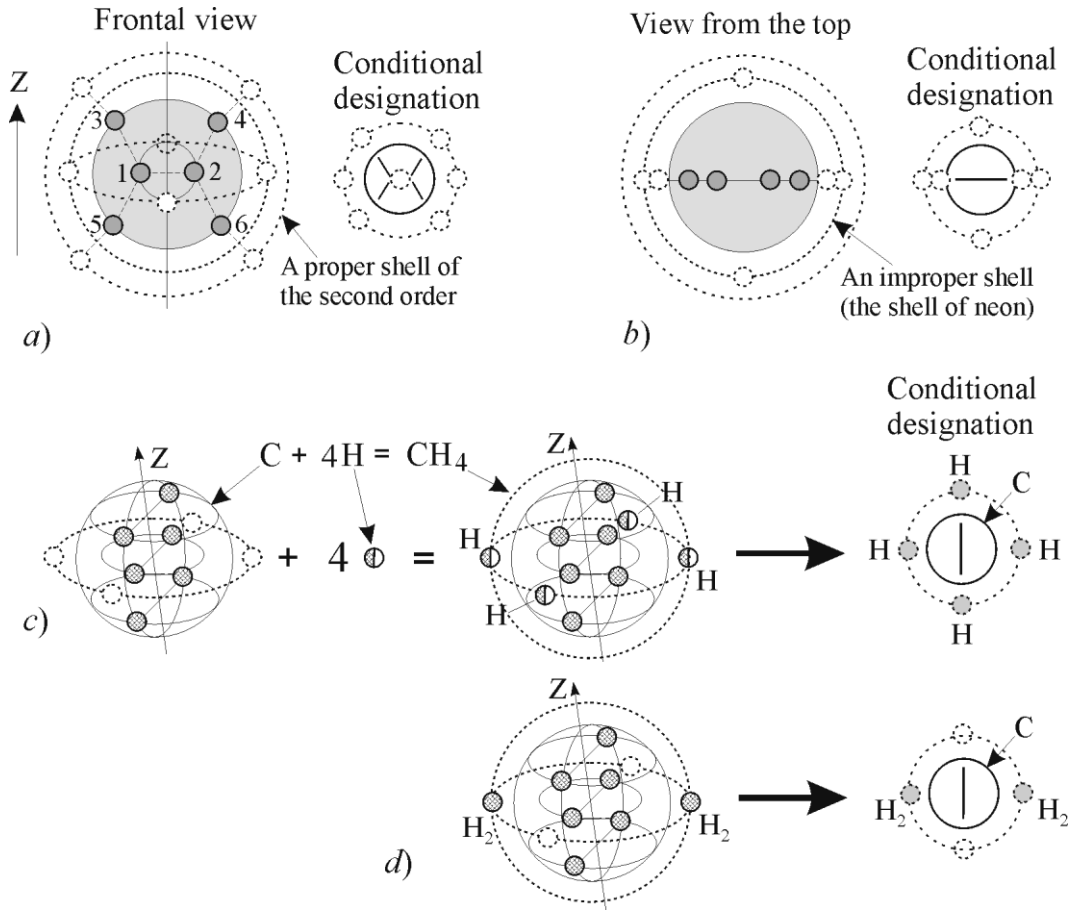

Fig. 2. A schematic images of the carbon structure (*a*, *b*) with indication by dotted lines of two nearest empty proper and improper spherical shells and their potential polar-azimuthal nodes; the possible ways (*c*, *d*) of the formation of the methane molecule CH_4 with participation of the improper shell of carbon. (Polar nodes are not shown here.)

Further, the radial solutions of the wave equation (1) give a series of radial shells (see Fig. 1, L. 3) slowly damped in amplitude (in the radial direction), with alternating zero amplitude values determined by a series of zeros of Bessel functions [8]. These shells are the *proper shells* for the atom *of the second, third, etc. order*. The nearest (second order) *proper* polar-azimuthal shell of carbon ($l = 2$, $m = \pm 1$), following the first order completely filled external shell, with four empty nodes of the same polar-azimuth angular orientation, is shown in Fig. 2*a*,*b* by dotted lines. The nodes of the second order proper shell of carbon are in a perpendicular plane with respect to the aforementioned nodes lying in an equatorial plane of the improper shell.

A case of the participation of the second order *proper* radial shell in the formation of molecular bonds, resulted in a *plane* structure of the disposition of all potential constituents in methane molecule, is shown in Fig. 3.

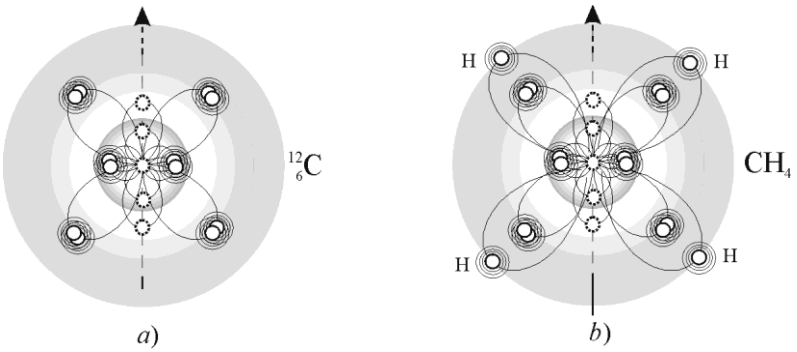

Fig. 3. An internal structure of the carbon atom $^{12}_{6}C$ (*a*) , and a possible polar-azimuthal structure of methane molecule CH_4 (*b*); all chemically adsorbed individual hydrogen atoms are in the same plane with the completely filled with coupled hydrogen-atoms proper potential nodes of carbon.

The possible structure of the carbon frame in some hydrocarbon compounds is demonstrated in Fig. 4. Under the formation of a great number of carbon based molecules with C–C bonds, two- and three-multiple overlapping of polar-azimuthal nodes belonging to different interacting carbon atoms (or carbon dimer molecules) takes place. An overlapping of polar-azimuth nodes is realized along the external and internal bonds of external and internal atomic shells, respectively, belonging to contacting carbon atoms, as shown in Fig. 4.

Two-multiple overlapping of the nodes of carbon atoms, characteristic for a homologous series of saturated hydrocarbons and having the general formula $C_nH_{2(n+1)}$, is shown in the first row in Fig. 4. The three-multiple overlapping of the nodes of carbon atoms is shown in the second and third rows in Fig 4. The mixed three-multiple overlapping of the nodes of nearby carbon atoms and, partially, of the nodes of carbon atoms with carbon dimer molecules C_2 is demonstrated with an example of the formation of C_6H_{10} and C_8H_{12} molecules. The complete three-multiple overlapping of pairs of the coupled hydrogen atoms (*i.e.*, of carbon dimer molecules, C_2) in graphite, fullerenes, diamond will be shown in the next sections.

From Fig. 4 it follows that among cyclic hydrocarbons C_nH_{2n} (cycloalkanes), where $n \geq 3$, the more stable is cyclohexane C_6H_{12}. An equilibrium topology of the structure of atomic bindings in all six bound carbon atoms is not deformed; hence cyclohexane is not a strained compound. The most deformed intra-atomic bindings in carbon (with respect to the equilibrium structure originated from solutions of the wave equation (1)) are observed in cyclopropane C_3H_6 and cyclobutane C_4H_8. This is why these compounds are highly strained ones. They have maximal superfluous enthalpy (formation heat) among cycloalkanes: 37.674 and 26.377 *kJ/mol*, respectively; for comparison, cyclohexane has 0 *kJ/mol*.

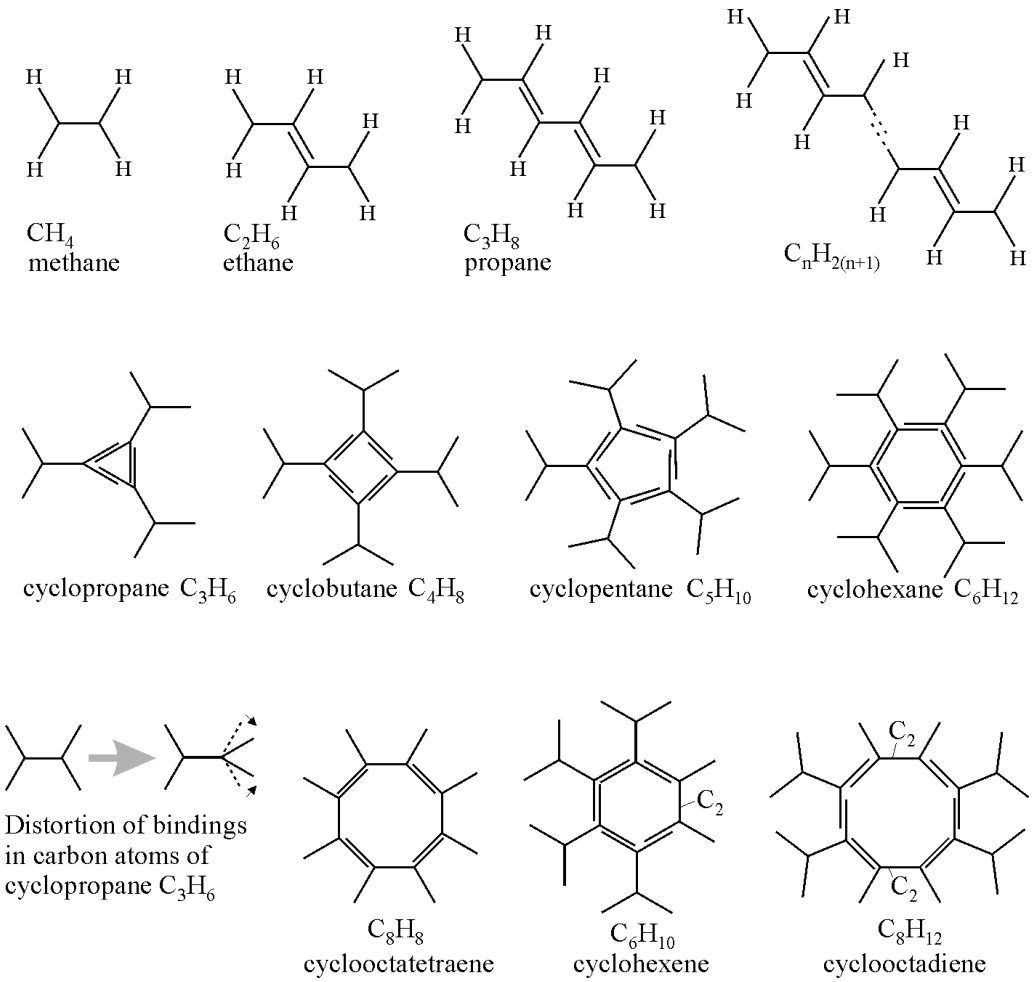

Fig. 4. The structure of bindings of carbon frames in some typical hydrocarbon compounds based on the shell-nodal atomic model.

A scheme of overlapping of the nodes of two carbon atoms resulted in the formation of the C_2 molecule is shown in Fig. 5. Two-multiple overlapping of atomic nodes leads to the nodes contained every by the four hydrogen atoms per node. Just the same number it has the helium atom ${}^{4}_{2}He$ belonging to one of the balanced atomic structures (along with neon and argon). For this reason, we can suppose that the latter fact (coupling) provides, apparently, the more stable thermodynamic state of C_2 with respect to C, *i.e.*, to the state that has an individual carbon atom.

An overlapping occurs with both carbon atoms and carbon dimers (see Fig. 6). In gaseous carbon compounds (as for example, in ethane C_2H_6, Fig. 6*a*, see also Fig. 4), the single carbon atoms are overlapped as a rule. Dense carbon compounds, as for example benzene C_6H_6 (Fig. 6*c*), are formed from carbon dimers C_2. And such compounds, as for example cyclohexane C_6H_{10} and cyclooctadiene C_8H_{12} (see Fig. 4), are composed both from single carbon atoms, C, and carbon dimers, C_2; their positions are indicated in Fig. 4.

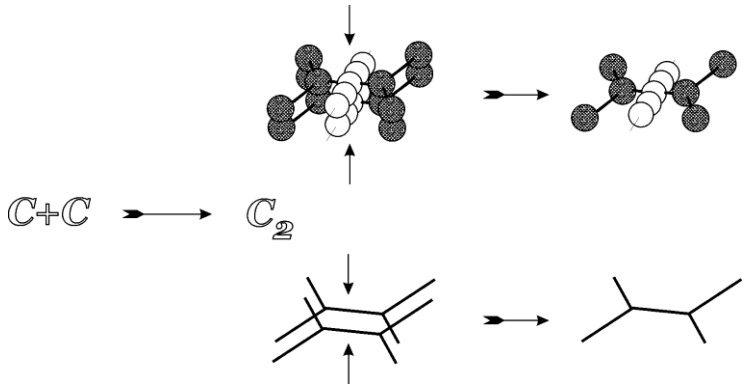

Fig. 5. Formation of the carbon diatomic molecule C_2: overlapping ("confluence") of all approaching nodes (and toroidal rings not shown here) of two carbon atoms in the unit whole. (A symbolic image of C_2 does not differ from the symbolical designation of a single C atom drawn in Fig. 1).

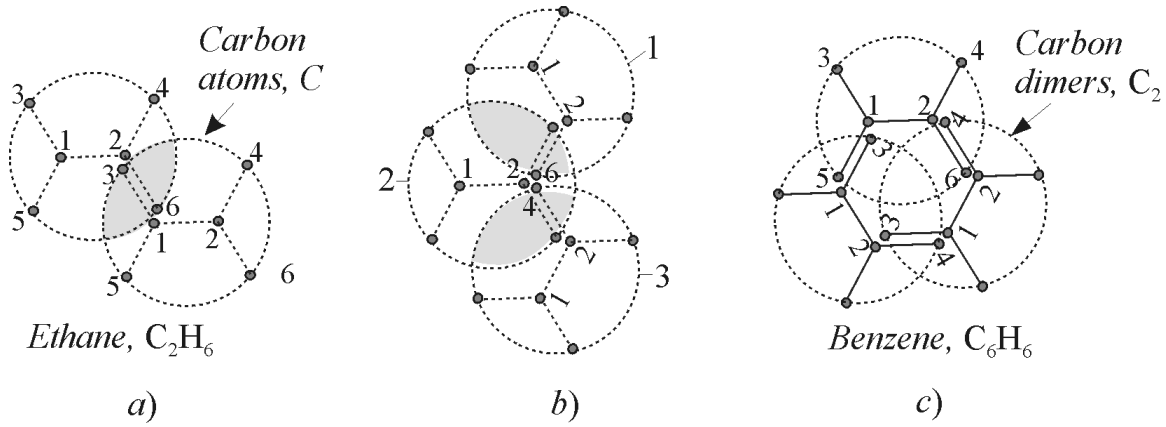

Fig. 6. A schematic view showing the two-multiple overlapping of the potential polar-azimuthal nodes at the formation of the C–C bonds in ethane C_2H_6 (*a*) and a fragment of the three-multiple overlapping of the nodes realized in cyclohexane C_6H_{12} (*b*); the case of two-multiple overlapping of the nodes of three carbon dimmer molecules C_2 along the closed circle (*c*) (the formation of C_2–C_2 bonds in benzene C_6H_6).

The direction of interatomic bonds between the nodal hydrogen atoms of interacting carbon atoms in hydrocarbon compounds and the character of overlapping of their potential polar-azimuthal nodes for the case of single carbon atoms is demonstrated in Fig. 6*a* (two-multiple overlapping) and Fig. 6*b* (three-multiple overlapping); and for the case of two-multiple overlapping of interacting carbon dimmers – in Fig. 6*c*.

A fragment of three-multiple overlapping of single carbon atoms realized in cyclohexane C_6H_{12} (depicted in Fig. 4) is shown in Fig. 6*b*. In this case, one internal node of each of the 6 carbon atoms is overlapped with two external nodes belonging to two nearby carbon atoms. For example, as shown in Fig. 6*b*, the internal node 2 (of the 2nd atom) is overlapped with the

external node 4 (of the 3rd atom) and with the external node 6 (of the 1st atom), and so on around the circle.

Two-multiple overlapping of carbon dimers resulted in a closed hexagonal ring with six vertices-nodes is characteristic feature for the carbon frame of the benzene molecule (Fig. 6*c*). In this case, each internal node (1 and 2) of each of three dimers is overlapped with one external node belonging to a nearby dimer (as, *e.g.*, 1 with 5, or 2 with 4, *etc*., as shown in the figure).

A three-multiple overlapping of the nodes of carbon dimmers, C_2, is realized at the formation of carbon crystals, we will show this below. Note that the three-multiple overlapping of the nodes of carbon dimers corresponds to the six-multiple overlapping of the nodes of carbon atoms (contained two coupled hydrogen atoms per node).

From the figures presented above it follows that, at the formation of compounds, the internal nodes, 1 and 2, of connecting atoms never overlap between themselves. In all cases these nodes are overlapped only with the nodes belonging to external shells of nearby attached atoms, as for example, it is shown in Fig. 6*a*, where an *internal* node 2 (or 1) of one carbon atom is overlapped with the *external* node 3 (or 6) of a nearby attaching atom.

A schematic view of self-binding (assembling) of two-dimensional carbon compounds such as graphene and benzene is presented in Fig. 7. If one considers that the lattice parameters accepted for them, including graphite, are true, these compounds are formed on the basis of carbon dimmers C_2.

Nature uses the method of self-assembly, self-organization that resulted in complexity of nature. The structure of crystals is strongly deterministic. In particular, characteristic feature of graphene, related to the two-dimensional crystals, is the fact that all its constituent carbon dimer molecules, C_2, are arranged in such a way that all their polar potential-kinetic (axial, empty in ^{12}C) nodes form the straight continuous parallel chains along a crystallographic direction coincident with directions of all joined Z-axes of linked dimers. It means that graphene is the crystallographically and, hence, physically anisotropic crystal. Apparently, owing to such a structure, presented in Fig. 7, graphene possesses unusual physical and chemical properties observable experimentally [9].

A carbon frame of the benzene molecule, C_6H_6, has the form of a flat hexagonal ring, which is closed without a strain. Its formation from carbon dimmers C_2 and the resulting structure are demonstrated in Fig. 7. An ideal conjunction of all bonds conditions a high stability of benzene rings. It is well-known that the benzene molecule behaves as a closed superconductor. Apparently, this feature occurs due to the junction around its center of three chains of empty polar potential-kinetic nodes which serve as the specific channels for motion of charges without resistance.

Thus, unique physical properties of graphene and benzene molecules are determined, apparently, by the nodal structure formed in result of the characteristic internodal bindings of interacting dimers as shown schematically in Fig. 7.

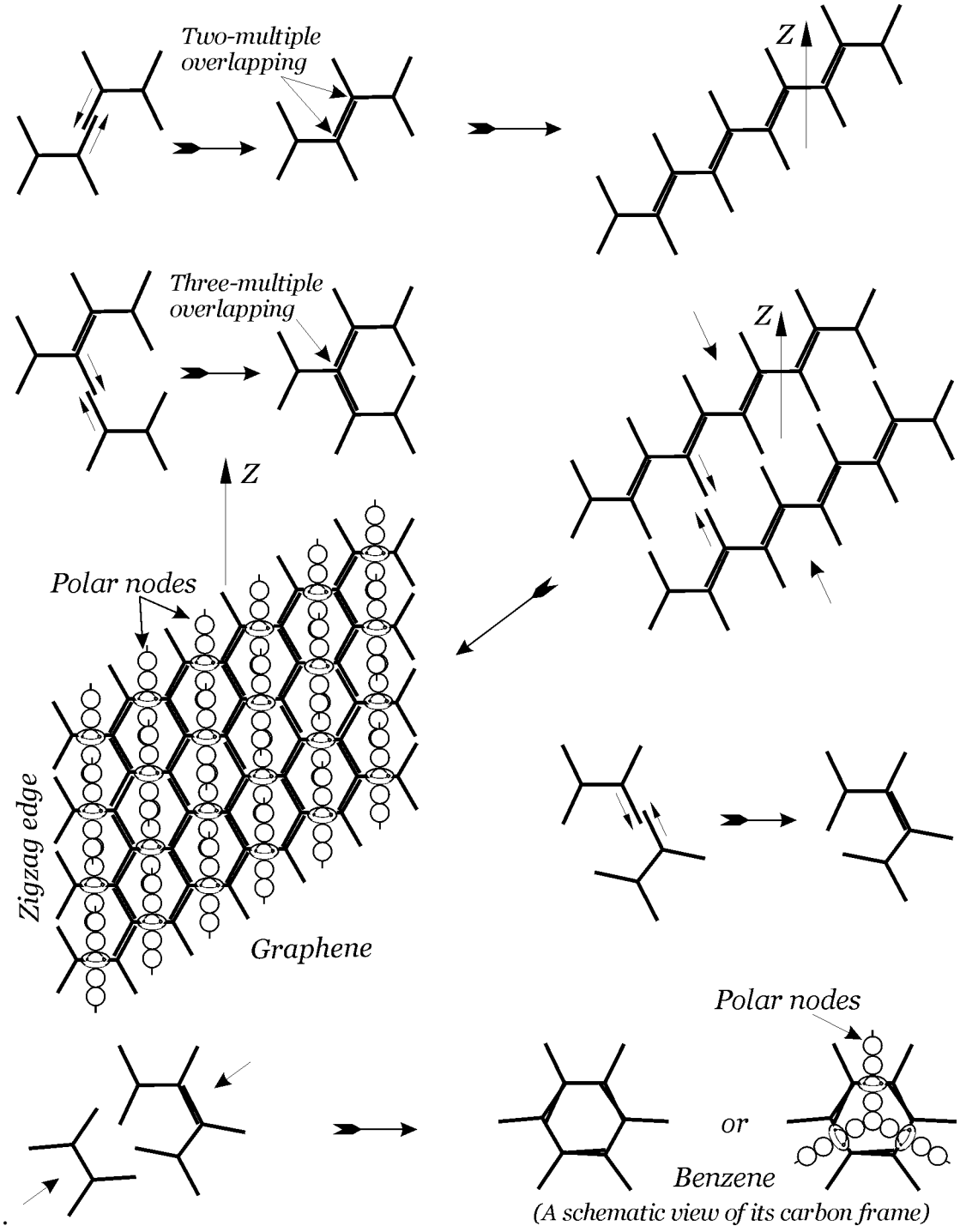

Fig. 7. A schematic view of self-binding (assembling) of two-dimensional carbon compounds.

We see that the *structural* features of carbon compounds, which we have already considered, are naturally and logically explained in the framework of shell-nodal atomic model originated from the solutions of the wave equation (1).

3. Graphite and fullerenes

Graphite is a modification of carbon crystallized in the laminated hexagonal structure. A unit cell of graphite consists of three layers (Fig. 8a). The atoms of carbon on the top layer and bottom layer are at the same lateral positions. The middle layer is shifted relative to the top and bottom layers.

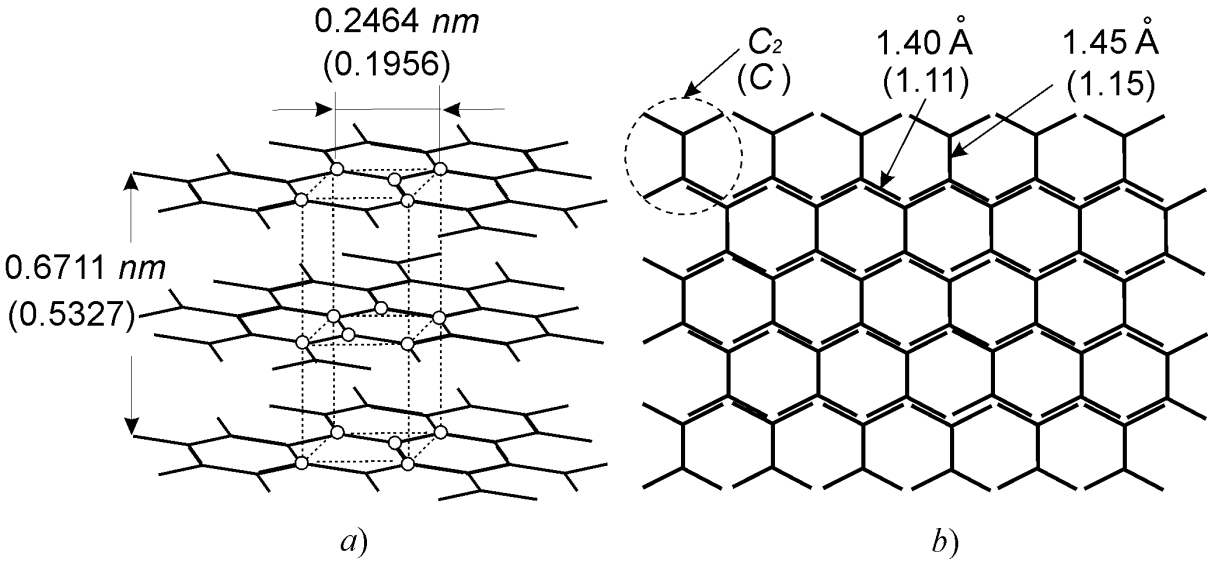

Fig. 8. An elementary cell of graphite **(***a*); the structure of bindings in a layer of graphite (called graphene) (*b*).

We will follow the shell-nodal pattern of the carbon atom expressed graphically by the symbol ⋋ (Fig. 1). The same designation is applied to the carbon molecule C_2 (see Fig. 5). At present we cannot say what kind of carbon is responsible for the formation of graphite, atomic, C, or molecular, C_2. There are a few objective reasons for this. In particular, there are suppositions that the C_2 radical is responsible for the formation of graphite [10]. Moreover, it was found experimentally that the carbon dimer C_2 is in fact the major observable product of C_{60} fragmentation. It is stated that being a very effective growth species, C_2 can rapidly incorporate into the diamond lattice leading to high-film growth rates [11].

Our calculations of lattice parameters, the results of which are presented in Fig. 8, call the question: what are elementary "bricks" in graphite, C or C_2? The correct answer to this question is possible to obtain only after additional research for excluding any doubts, including the uncertainty noted above.

Following the shell-nodal atomic model and assuming that the lattice constants of crystals accepted in modern physics are precise and congruent to reality, we should conclude that an elementary "building block" in carbon crystals, including graphite, is the diatomic molecule of carbon, C_2. However, the validity of this statement calls the doubt because the accepted lattice parameters were obtained by the existed method of their evaluation, which takes into account the quantum-mechanical nuclear (*mono*-centre) model of the atoms. The latter differs essentially from the shell-nodal (*multi*-centre) atomic model.

Under accepted designations of C and C_2, hexagonal layers of graphite have the structure shown in Fig. 8. The overlapping of the nodes of external nucleon shells of carbon atoms (or carbon dimmers) is realized orderly along the strong bindings existed between internal and external nodes of each of the nearby carbon atoms (or carbon dimers). In this figure, lattice constants of graphite indicated in brackets correspond to imaginary lattice parameters if one accounts that the crystal lattice is formed from the single carbon atoms, C.

When we consider C_2-based structure of graphite, we have *six-multiple overlapped* atomic nodes (except of boundary nodes) with 12 overlapped hydrogen atoms in each *nodal point* of the crystal formed, thus, from the nodes belonging to three linked carbon *dimers*.

Now let the structure presented in Fig. 8 is formed from the single carbon atoms, C. In this case it takes place the *three-multiple overlapping* of all nodes of all bound *carbon atoms*, *i.e.*, we deal with overlapping of each internal node of an *atom* with external nodes of nearby atoms (excepting boundary atoms where the two-multiple overlapping of external nodes occurs, see Fig. 9).

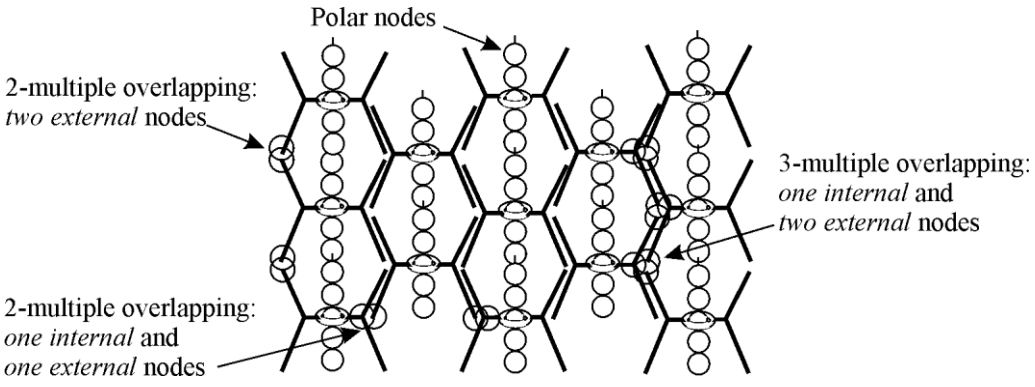

Fig. 9. Two- and three-multiple overlapping of the nodes characteristic for linked carbon dimmers C_2 in graphene – the one-atom-thick layer of graphite.

It means that every (except boundary) nodal point of the crystal (which is attributed in X-ray structural analysis to an atomic node), where it takes place overlapping the nodes, belongs to three individual carbon atoms, ${}^{12}_{6}C$, as depicted in Fig. 9. Each of the six nodes of the carbon atom contains two coupled hydrogen atoms; hence, in this case each nodal point of the

crystal is the place of overlapping the 6 hydrogen atoms, but not 12 as it take place in the case of overlapping the carbon dimers.

Thus, taking into account the above reasoning on the *C*-based structure of graphite, we should distinguish among the nodal point representing in shell-nodal atomic model the three-multiple overlapped atomic nodes (with the 6 overlapped hydrogen atoms), belonging to three different carbon atoms C, and the nodal point representing in the standard quantum mechanical (nuclear) atomic model one carbon atom C holding 12 nucleons (hydrogen atoms) localized, as is believed, in its nucleus.

At present, after the definite progress in obtaining in laboratory conditions of one-atom-thick layers of graphene [9] and developing the corresponding technologies for manipulation with nanoscale objects such as graphene, the latter has became intensively studied worldwide.

The two types of two-multiple overlapping are realized in graphene on its characteristic edges only, which are called, respectively, zigzag- and armchair-like edges. Unsaturated two-multiple overlapped external nodes of carbon atoms C (or carbon dimers C_2) on these edges, especially zigzag-like edges, must have unusual physical and chemical properties, *i.e.*, must behave similarly to chemical radicals. Actually, as follows from the experiments, zigzag-like edges of graphene nanoribbons have unique electronic state and chemical reactivity that distinguishes them, in properties, from the basic part of graphene with saturated bonds.

An average density of graphite is $2.26\, g \cdot cm^{-3}$. At the above density and three-multiple overlapping of the nodes of *single* carbon atoms, lattice constants of graphite must have the following values: $a = 0.1956\, nm$ and $c = 0.5327\, nm$ (shown in Fig. 8 in brackets). An average length of the C–C bonds corresponding to these parameters is equal to $0.111\, nm$ and $0.115\, nm$.

However, the presented above values do not coincide with the officially accepted lattice parameters for graphite shown in Fig. 8 without brackets: $a = 0.2464\, nm$ and $c = 0.6711\, nm$. The C–C bond lengths, corresponding to the latter values, are equal to $0.140\, nm$ and $0.145\, nm$. These data completely coincide with the theoretical data calculated for the case when the crystal lattice is formed with use of C_2 molecules, as the elementary basic units, having shell-nodal atomic structure.

Thus, the complete coincidence of calculated parameters with the table (accepted) values is achieved if we will take into account the previous coupling of individual carbon atoms between themselves leading to the formation at first of diatomic molecules of carbon C_2. And only then just these molecules take part, as basic elementary units, in the formation of the crystals. In this case we have the six-multiple overlapping of the nodes resulted in the 12 overlapped hydrogen atoms per nodal point in the crystal. We arrive, thus, at the coincidence of the aforementioned parameters with the accepted values. It is a quite real case because the coupling (resulted, *e.g.*, in H_2, N_2, O_2, *etc.*) is the natural property of matter at all levels.

Remember, the coupling of hydrogen atoms, *constituents of atoms*, occurs as well *at the subatomic level* inside intra-atomic nodes.

Overlapping the nodes of two carbon atoms resulted in the formation of the C_2 molecule, shown in Fig. 5, apparently provides the more stable thermodynamic state inherent in the diatomic systems, to which belongs the carbon dimer molecule, with respect to the state that have the single atoms.

Now let us turn to the next case of bindings in graphite and other carbon compounds, which is also noteworthy. The lattice constants of graphite shown in brackets in Fig. 8 can prove to be verisimilar because of the following highly plausible situation. The existing X-ray and neutron scattering analysis (along with others methods) of crystals and molecules is not so simple matter in spite of using the modern computers and perfect techniques. The gauging of diffraction images takes into account the *atomic model*, officially accepted in physics, and the *density of substance* known from the experiment.

The modern solid-state theory based on the QM atomic model identifies each nodal point in a crystal lattice (or a molecule) with one atom, which is regarded as the only center of scattering of incident particles or waves in the atom. Therefore, investigators regard the position of every peak of electron density, in X-ray crystallography analysis when determining lattice parameters, as relating to the position in a crystal of a definite node identified to a single atom [12].

A precise calculation of atomic positions and lengths of interatomic bonds uses the *iterative* method. The last is based on *comparison* and *fitting* of *measured* and *calculated* (proceeding from the accepted atomic model) intensity of reflected beam so as long as will not be achieved an *adequate correspondence of two sets of the values*.

However, if only the X-ray analysis will be based on usage of shell-nodal (*i.e.*, *multi-center* or *molecule-like*) atomic model, the gauging could be different, depending on the multiplicity of overlapping of atomic nodes belonging to various atoms. It means that the three-multiple overlapping of the nodes of three *carbon atoms*, just as presented in Fig. 8, can be also real. However, we have above noticed that if lattice constants of crystals accepted in physics are precise and congruent to reality then an elementary "building block" of graphite is the C_2 *diatomic molecule*, but not the carbon atom C.

The schematic images of the formation of carbon compounds presented here in all figures show that the interatomic (intermolecular) bindings in graphite, and hence in graphene, are realized along the bonds between the nodes belonging to the external shell and the nodes of the nearby internal shell of each atom. Every hexagonal circle of nodal points in the two-dimensional crystal having the 4 double bindings is surrounded with the 6 similar hexagonal circles. We see also that single bindings between the 1^{st} and 2^{nd} nodes of internal shells (responding to $l=1,\ m=\pm 1$; see Fig. 6) *nowhere overlap*.

As the consequence of the specific shell-nodal structure of the constituent carbon atoms, the characteristic feature of the formed graphene is its *crystallographic anisotropy*. The polar nodes on Z-axes of all bound elementary carbon formations (C_2) form the straight parallel continuous chains of these nodes. Their direction is perpendicular to a line of the bonds between the 1st and 2nd internal nodes (see Fig. 6 and 9).

In order to verify the above described peculiarities of nodal bindings in carbon compounds, similar those which was found in graphite, it is interesting to consider the structure of other carbon compounds. Let us turn now to the structure of fullerenes considering them in the light of the shell-nodal atomic model as well (Fig. 10).

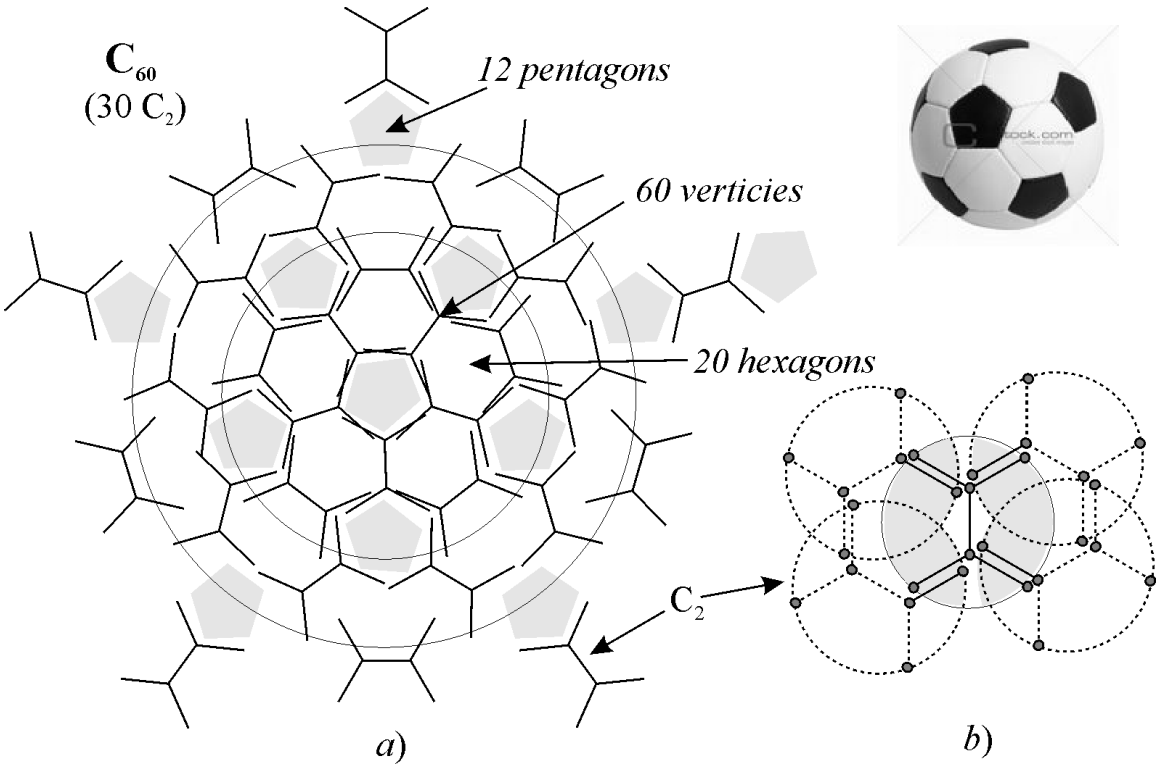

Fig. 10. An unfolded structure of buckminsterfullerene C_{60} (*a*); a fragment showing the overlapping of the nodes belonging to 5 spherical molecules C_2 resulted in three-multiple overlapping of their nodes in two vertices (nodal points) (*b*).

Fullerenes are regarded as a molecular form of a pure carbon (a kind of microclusters) representing a high symmetrical structure hollow inside. They are formed by the regular polygons of strained atomic bindings because of their bending under the formation of cage-like structure of carbon atoms, characteristic for fullerenes.

The most known among fullerenes is C_{60} molecule (called buckminsterfullerene), which is well detected by mass-spectrograph. The complicated structural analysis has led to the

conclusion that this molecule has 60 vertices, and their bindings form 20 hexagons and 12 pentagons. Such a structure reminds in form a football pattern (Fig. 10).

If one follows the shell-nodal atomic model then we should accept that elementary "building bricks" of the C_{60} molecule must be carbon dimers C_2, but not carbon atoms C.

The spherical closed pentagonal/hexagonal monomolecular shell has the rotational symmetry of order 5 forbidden in crystallographic space of plane symmetry group and highest possible icosahedral point-group symmetry [13].

The conclusion about the structure of buckminsterfullerene, accepted in physics, rests on the concept of quantum mechanical (mono-center) atomic model, according to which one node of a crystal lattice corresponds to one atom containing all its nucleons in a nucleus (12 nucleons in the case of carbon).

Let us suppose that the aforementioned spherical structure with 20 hexagons and 12 pentagons is realized on the basis of shell-nodal atomic model with use of 30 carbon atoms, but not carbon molecules C_2, in the capacity of elementary "bricks" (they are designated by the same symbol $\asymp$, see Fig. 1 and 5). In this case, the above structure of 60 vertices, depicted in Fig. 10 in the unfolded form, will be characterized by the *three-multiple overlapping* of all the nodes of the atoms similarly as it is shown in the case of the graphene structure. As a result, we will arrive at the hypothetical C_{30} molecule, because only 30 carbon atoms are needed for the formation of 60 such vertices (nodal points). However, this case contradicts to the mass-spectrographic data which uniquely justify in favor of C_{60} molecule.

The only *six-multiple overlapping* the nodes belonging to 6 carbon atoms (having the shell-nodal structure) leads to the formation of C_{60} molecule; in every of 60 vertices-nodes of buckminsterfullerene. This is realized on the basis of coupled carbon atoms, *i.e*. dimers C_2, participating as elementary structural units at the formation of C_{60}, just like it takes place, apparently, at the formation of all crystal structures on the basis of carbon, including graphite considered above. Thus, the symbol $\asymp$ in Fig. 10 represents two coupled carbon atoms, the carbon dimer C_2. Just then we have the right to state that the above structure, ascribed to C_{60} molecule, really belongs to the latter. The length of "single" bindings in such C_{60} molecule is $1.45\times10^{-8}\ cm$, "double" bindings – $1.40\times10^{-8}\ cm$, as in graphite in the same case formed from the coupled carbon atoms.

Assuming that the case of three-multiple overlapping the nodes belonging to carbon atoms, but not carbon dimer molecules, is real then we should recognize that the molecule C_{60} called buckminsterfullerene has actually 120 vertices and some other cage-like structure than usually accepted as shown in Fig. 10. This is very likely because of possible errors at an extremely complicated procedure of deciphering the intricate diffraction images of C_{60} molecule (as, generally, all fullerenes), and mainly due to the aforementioned gauging, accomplished with taking into account the nuclear (*mono-center*) structure of atoms. Thus, at the current stage of the development of atomic physics, we cannot exclude completely that

the structure presented in Fig. 10 with 60 vertices is an image of the C_{30} molecule, but not C_{60}.

The overlapping of atomic shells at the formation of molecular and crystal carbon structures occurs along the directions of bindings between the nodes belonging to two shells, external and nearest internal, both for graphite and fullerenes. Internal bindings of the internal shell of carbon atoms (between the nodes 1 and 2, corresponding to $l = 1$ and $m = \pm 1$ (Fig. 6) overlap only once at the coupling of carbon atoms resulted in the formation of carbon dimers (see Fig. 5).

4. The shell-nodal structure of diamond

All variety of the results which follows from the solutions of the wave equation (1), as applied to the carbon space, is not limited by the already considered examples. We will not analyze all other here. However, it makes sense to analyze now the peculiarity of forming an elementary *tetrahedral* structure inherent in diamond crystals taking into account the shell-nodal structure of constituent basic units, which can be (as in the case of hexagonal graphite) either individual carbon atoms C or carbon dimer molecules C_2.

Diamond is a modification of carbon crystallized in a face-centered cube. The coordination number of diamond is 4. Therefore the structure of diamond is more friable in comparison with cubic structures characteristic for metals. Diamond can be artificially obtained from graphite under $1300-1600^0 C$ temperature and $4.5-8.0\,GPa$ pressure.

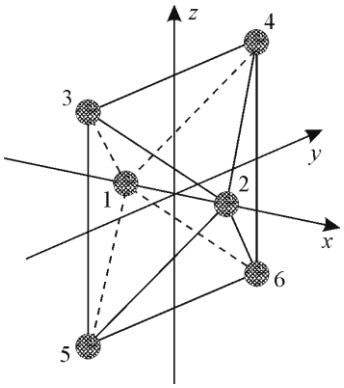

Fig. 11. The octahedral structure of the carbon atom ($\alpha = \pi/2$).

If an internal shell of the carbon atom, containing two nodes (numbered as 1 and 2), will be rotated at right angle relative to the plane of outer four nodes, we obtain the carbon atom in the octahedral form (Fig. 11). The solutions of the wave equation of space determining the principal potential polar-azimuthal nodes in spherical polar coordinates, $\psi_p = C_\psi R_l(\rho)\Theta_{l,m}(\theta)\cos(m\varphi+\alpha)$, allow such a position of the internal nodes (1 and 2) by specifying the corresponding initial phase. The value of the azimuth angle entered in the

above wave function, corresponding to the solution related to the internal shell, originally taken as zero, must be equal in this case to $\alpha=\pi/2$.

We can also set another value of α, for example, $\alpha=\pi/4$. Most likely, as follows from analyzing the possible variants of bindings leading to the tetrahedral structure, that the latter value of α for the solution related to the internal shell is realized in diamond crystals. Recall that we base in this analysis on the shell-nodal structure of the carbon atom.

Let us show now the scheme of forming the tetrahedral bindings for the above case.

The disposition of all polar-azimuth nodes in one plane (inherent in the carbon atom under normal conditions, see Fig. 12a, and keeping in graphite) does not keep under high pressure and temperature. As a result the one-planar disposition of all atomic nodes characteristic for hexagonal layers of graphite is broken.

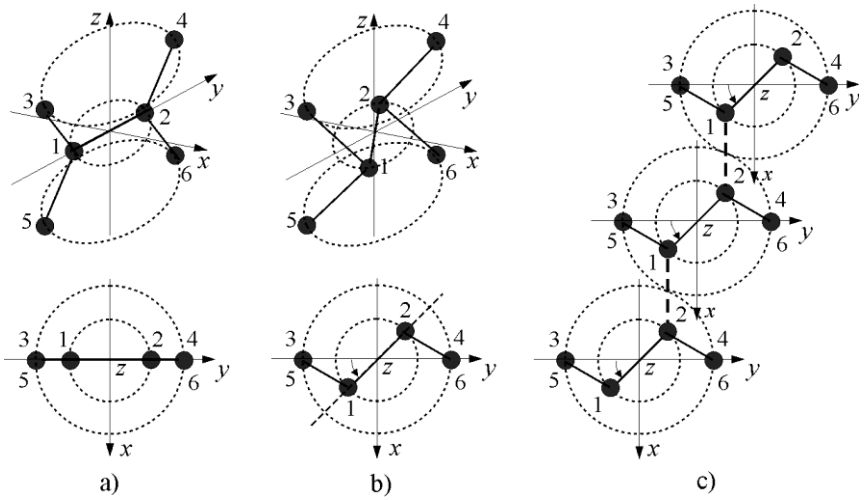

Fig. 12. A plane structure of the carbon atom (a) (and molecule C_2 as well); a shifted (turned) position of an internal shell with the nodes 1 and 2 around the z-axis by the phase angle $\alpha = \pi/4$ (b); the bindings (marked by broken lines) (c) between the shifted internal nodes 1 and 2, belonging to different carbon dimmers, resulted in a face-centered cubic structure of diamond.

The planes of the location of the 1st and 2nd internal polar-azimuth nodes (which coincide in hexagonal graphite with the plane of the location of all external nodes, 3 – 6) can be turned around the Z-axes in all basic units (C or C_2) by the angle of about $\pi/4$; naturally, together with the internal shells to which these nodes belong. The given turns are carried out, thus, with respect to the plane of the disposition of the rest external polar-azimuth nodes belonging to the outer shells as shown in Fig. 12b for an individual carbon atom (or an dimer). The relevant particular solution of the wave equation (1) admits the resulting structure by setting the corresponding initial phase, *i.e.*, taking the value of the azimuthal angle to be equal to $\alpha=\pi/4$.

As a result the directions of all internodal bonds, initially lying in the same plane, are changed (see Fig. 12b). The *plane hexagonal* structure of graphite layers is transformed into the *wavy hexagonal* structure, which enables bindings between them in the volume face-centered cubic structure. The direct interaction with the formation of bindings between the 1st and 2nd nodes, drawn by broken lines in Fig 12c, of different *coupled* carbon atoms (if bindings are realized with participation of carbon *dimers*), belonging to nearby layers, is realized in this case.

We see that hexagonal disposition of the nodal points is characteristic for both crystal forms, for graphite and diamond. However, if hexagonal circles are *planar* in graphite, they are *wavy* in diamond (Fig. 13b,c). The bindings between the deformed (wavy) neighboring hexagonal layers, leading to the formation of the tetrahedral diamond structure, are shown by dashed lines in Fig. 13c.

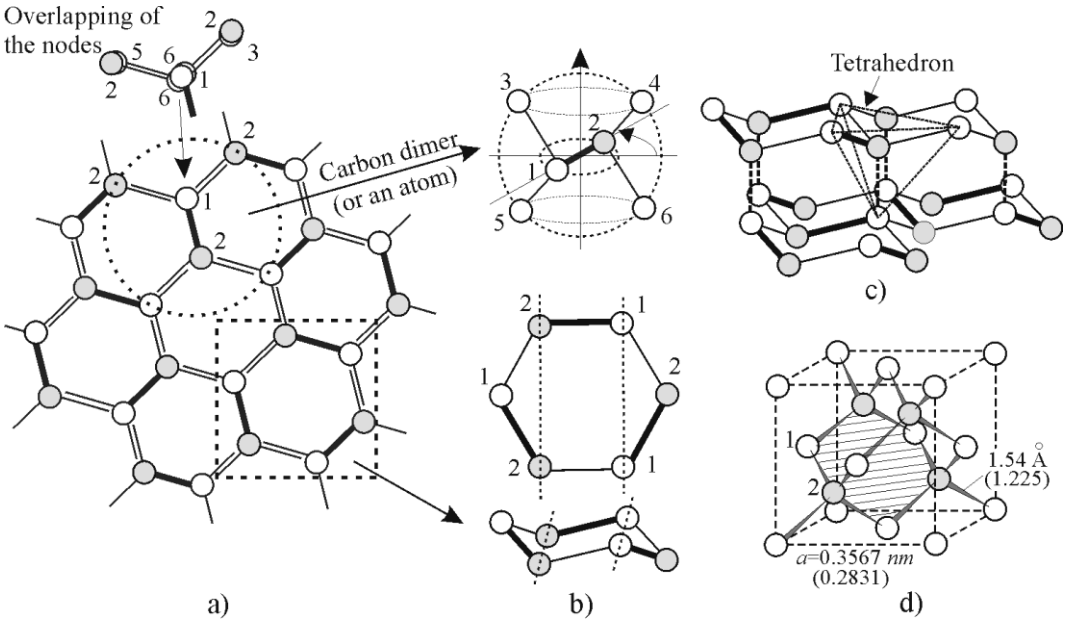

Fig. 13. The hexagonal-wavy structure of crystallographic planes in diamond (a); a hexagonal-wavy circle built from 3 carbon units (carbon atoms, C, or dimmers, C_2) (b); the bindings (marked by dashed lines) between hexagonal-wavy layers resulted in the face-centered cubic structure (c); an elementary cell of diamond (d).

Thus, the specific *hexagonal* structure originated from the specific topology of the disposition of nodes in the carbon atom, pronounced in graphite, keeps in diamond in general terms and distinctly in its crystallographic planes (Fig.13). The next similarity relates to the same pattern and multiplicity of overlapping the nodes in diamond realized just as it occurs in graphite. Peculiarities of overlapping in graphite were considered in a preceding section. Therefore, because they have the same character in diamond, we will not explain this again.

Note, however, that the lattice parameters of diamond presented in brackets in Fig. 13 (just like the corresponding parameters of graphite presented in Fig. 8) correspond to a hypothetical case of the participation, presumably, the individual carbon atoms, as elementary basic units when forming the diamond lattice. A three-multiple overlapping of atomic nodes, containing each the coupled hydrogen atoms and belonging to different carbon atoms, takes place in nodal points of the crystal in this case.

The crystallographic parameters of diamond crystals indicated without brackets in Fig. 13d coincide in value with the data accepted in physics. They correspond to the case of three-multiple overlapping the neighboring nodes of carbon dimer molecules C_2.

Repeat again in conclusion that if only the structural analysis would be based on the shell-nodal (*i.e.*, multi-center or molecule-like) atomic model, the gauging would be different; depending on the condition of what is accepted in the capacity of elementary "building blocks" for the formation of corresponding crystal lattices – individual carbon atoms or carbon dimer molecules, C or C_2.

At present assuming, as in the case of graphite, that the lattice constants of crystals accepted in physics are precise and congruent to reality, we must accept that elementary "building blocks" in diamond (as, generally, in all carbon crystals) are diatomic molecules of carbon, C_2. They are considered here as two carbon atoms coupled in such a way that their corresponding nodes pairwise completely mutually overlap as shown in Fig. 5.

5. Conclusion

It stands to reason that the "genetic code" of structural variety in Nature is, obviously, "hidden" inside the atoms. A comprehensive analysis of the particular solutions of the wave equation (1) has revealed the structure of this "code". An atom, as the wave formation, represents a system of spherical shells with discrete *points-nodes* of wave space. From all the nodes and antinodes, the *principal nodes* (potential polar-azimuthal) of stable atoms are filled with coupled hydrogen atoms, *i.e.*, an atom represents a molecular formation from the hydrogen atoms. In view of this, the hydrogen atoms only (proton, neutron and protium, ^1H) are the atoms in the true sense of the word. Discovered in result of the analysis, the internal shell-nodal structure of the atoms is specific for each atom. Such a structure represents the definite molecular formation which defines all individual properties of an atom, atomic isotopes and molecules formed from the atoms (figuratively speaking, like the structure of a DNA molecule that contains the genetic information for a living organism).

Thus, from solutions of the ordinary wave equation (1) in spherical polar coordinates it follows that the atoms (except the hydrogen atoms) represent by themselves *quasi-spherical molecules*. They are reminiscent of R.J. Haüy's elementary molecules [14]. Their internal shell-nodal structure uniquely determines the structure of matter at the molecular level.

The hydrogen atoms – basic constituents of all other (molecule-like) atoms – prevail over electrons more than by three orders both in value of mass and exchange charges (at both levels, atomic and gravitational). Therefore, it was natural to assume that the role of the hydrogen atoms localized in atomic nodes is determinative at the formation of interatomic bonds. If so, then the nodal hydrogen atoms must be responsible for forming the certain spatial structure of a molecule. Actually, the structure of molecules and crystals depends on the shell-nodal structure of *external wave shells* of interacting atoms. The mechanism of chemical bindings, where the hydrogen atoms play the defining role, is quite natural; it is in compliance with logic and common sense.

Electrons are the particles of the second order with respect to nucleons in hierarchy of the "elementary" particles of the Universe. Naturally, therefore, that they play the secondary role in interatomic exchange (interaction). Really, in accordance with the shell-nodal atomic model, set forth first in 1996 [7], electrons define only the strength (we will show this further), but not directions of chemical bonds, and, hence, they do not exert determining influence on the form of molecules and crystals, as it is considered in modern physics and chemistry.

The chemical bindings are realized in interatomic space *along the characteristic directions* defined by the topology of internodal (strong) bindings inherent in each of interacting atoms; more precisely, by the spatial disposition of the (strong) bonds between the intra-atomic nodes belonging to *two external shells* in each of the interacting atoms. The latter is clearly seen in all Figures above, at all of the depicted images for widely known carbon compounds presented in this Lecture. Thus, the main role in the formation of molecules and crystals, built on the basis of the molecule-like atoms, belongs to the nodal hydrogen atoms.

Assuming that the data on the lattice constants accepted in physics are precise and congruent to reality, we must conclude that an elementary "building block" of graphite (and, hence, graphene, fullerene and some other carbon compounds like benzene, *etc*.) is the C_2 diatomic molecule. In this case, however, we found ourselves face to face with the following arisen problem required its resolution.

The matter is that presently for the precise calculation of atomic positions and lengths of interatomic bonds it is used the *iterative* method. The latter is based on *comparison* and *fitting* of the *measured* and *calculated* intensity of a reflected beam so as long as will not be achieved an *adequate correspondence of two sets of the values*. And what is ultimately important therewith in principle, it is the fact that at *calculating the intensity* of a reflecting beam *each node* of a crystal or a molecule, which *reflects* the beam, is identified with a *single* atom. That is, the *nuclear* model of the atoms is taken into account at the aforesaid calculations. The resulting calculated values are subjected further to the subsequent fitting with the measured intensity by the iterative method. Thus, the nuclear atomic model is used

as the *required principle* (as absolute condition) in creating the corresponding computer programs for the automatic processing of the measurement data to determine the lattice parameters.

It is obvious, if only the X-ray analysis would be carried out taking into account the *shell-nodal* structure of the atoms, *i.e.*, the *multi-center molecule-like* atomic model, the gauging would have been different. It will depend on the different multiplicity of overlapping of atomic nodes belonging to the interacting units: either the single atoms C or diatomic molecules C_2, realized at the formation of different carbon compounds, molecules and crystals.

This means that the standard lattice parameters, including parameters of graphite and diamond presented without brackets, respectively, in Figures 8 and 13, should be reconsidered. In view of the shell-nodal atomic model, the above parameters relate to the crystals formed from the diatomic molecules of carbon, C_2, whereas in view of nuclear atomic model they are formed from carbon atoms, C. Accordingly, one needs to *recalculate the intensity* of a reflected beam (used in the iterative method) with taking into account the *shell-nodal* (multi-center) atomic model and considering therewith each of the two variants of bindings in the crystals realized with either elementary basic units, C or C_2.

In other words, we should know, which of two possible versions of the three-multiple overlapping of the nodes takes place in reality: with participation of carbon atoms C or diatomic molecules of carbon C_2. In general, one should verify also the lattice parameters of the substances used as the standard for comparison to check the truthfulness of lattice parameters defined for unknown earlier substances by the iterative method.

Thus, we are interested in revealing all peculiarities, related to the shell-nodal structure of the atoms and their compounds, which were denoted in this Lecture. Any results of the inevitable verification of lattice constants of the crystals, including that above discussed, will be ultimately informative. They will favor the more profound insight into all peculiarities of the Wave Model, on the whole, which is developed to replace the Standard Model dominating currently in physics.

References

[1] L.G. Kreidik and G.P. Shpenkov, *Important Results of Analyzing Foundations of Quantum Mechanics*, GALILEAN ELECTRODYNAMICS & QED-EAST, Vol. 13, SI No. 2, 23-30, (2002); http://shpenkov.com/pdf/QM-Analysis.pdf

[2] G.P. Shpenkov and L.G. Kreidik, *Schrodinger's Errors of Principle*, GALILEAN ELECTRODYNAMICS, Vol. 16, No. 3, 51 - 56, (2005);
http://shpenkov.com/pdf/Blunders.pdf

[3] G.P. Shpenkov, *Conceptual Unfoundedness of Hybridization and the Nature of the Spherical Harmonics*, HADRONIC JOURNAL, Vol. 29. No. 4, p. 455, (2006); http://shpenkov.com/pdf/HybridizationShpenkov.pdf

[4] L. Kreidik and G. Shpenkov, Atomic Structure of Matter-Space, Geo. S., Bydgoszcz, 2001, 584 p.; http://shpenkov.com/atom.html

[5] George P. Shpenkov, *A Comparison of Two Models in Physics: DM (new) and SM (used currently)*; http://shpenkov.com/dmds.html

[6] Leonid. G. Kreidik and George P. Shpenkov, *Dynamic Model of Elementary Particles and the Nature of Mass and "Electric" Charge*, REVISTA CIENCIAS EXATAS E NATURAIS, Vol. 3, No 2, 157-170, (2001); http://shpenkov.com/pdf/masscharge.pdf

[7] L.G. Kreidik and G.P. Shpenkov, *Alternative Picture of the World*, Vol. 1-3, Bydgoszcz, 1996.

[8] F.W.J. Olver, ed., *Royal Society Mathematical Tables*, Vol. 7, Bessel Functions, part. III, *Zeros and Associated Values*, Cambridge, 1960.

[9] A.K. Geim, K.S. Novoselov, *The Rise of Graphene*, Nature Naterials 6, 183-191 (2007).

[10] H.C. Shik, et al., *Diamond and Related Materials* 2, Elsevier Science Publishers B. V., Amsterdam, (1993), 531.

[11] D.M. Gruen, at al, *Turning Soot Into Diamonds With Microwaves*, Proceedings of the 29th Microwave Power Symposium, Chicago, Illinois, July 25-27, 1994.

[12] Russell S. Drago, *Physical Methods in Chemistry*, W.B. Saunders Company, 1977.

[13] R.E. Smalley, *The Third Form of Carbon*, "Naval Research Reviews", December (1991), p. 3-14.

[14] R.J. Haüy, *Essai d'une Theorie sur la Structure des Crystaux*, Paris, 1784; Traite Elementaire de Physique, Paris, Imp. Delance et Leueur, an XII, 1803.

Lecture 7

Specific Features of Graphene

1. Introduction

We believe that it is not superfluous to recall and emphasize at the beginning the fact that discovery of the shell-nodal structure of atoms was not a fruit of an occasional imagination or a conscious fiction of the authors. It was a result of profound analysis of the well-known in mathematics particular solutions of the wave equation. The discovery has crucial importance for the entire foundation of physics because it changes our common view on the structure of atoms and molecules. In particular, the shell-nodal atomic model enabled to understand the true cause of unusual properties observed in one of the crystalline allotropes of carbon – graphene.

Graphene is a carbon-based two-dimensional one-atom thickness crystal (a gigant plane molecule) that exhibits unique physical properties. Its supposed application in electronic industry will enable increasing the density packing for electronic components in nanoelectronic devices acompanied with reducing the power consumption per component. The noted above application open a wide perspective for use of graphene in nanotechnology, to produce a new generation of electronic devices of nano and molecular sizes, the more so that modern Si-based technology is approaching its natural limits. Specific mechanical and chemical properties of graphene allow its use also in other industries.

We verified from different sides and by different ways the main discoveries made in result of the aforementioned analysis, which were brought up for discussions in these Lectures. We mean discoveries of the dynamic wave nature of elementary particles and wave shell-nodal structure of the atoms, unknown earlier new fundamental parameters (constants) and new phenomena, and other findings related with the new basic notions of dialectical physics. We consider the Wave Model developing in the framework of the dialectical approach as an alternative to the Standard Model of modern physics.

The aforesaid verifications concern thus, generally, the wave structure and behavior of matter at the atomic and subatomic levels. The obtained results completely confirm correctness and validity of the valuable information disclosed in the solutions of the wave equation, *i.e.*, reality of the made discoveries.

A single layer of graphite, called graphene, having a two dimensional hexagonal lattice gave us, fortunately, because of the one-atom thickness, a new unique possibility for the direct verification of reality the wave shell-nodal structure of the atoms. By this way we have examined once more veracity of the fundamental theoretical concept of dialectical physics [1] postulating the wave nature of the Universe and, hence, the wave nature of matter.

In this Lecture we will focus on the description of the structure of graphene and its conductivity anisotropy first predicted by the author, which after that indeed was found in graphene. Conditioned by peculiarity of the wave shell-nodal structure, anisotropic behavior is a natural phenomenon in graphene. You will see this.

So let us proceed now to the consideration of this matter.

2. The shell-nodal structure of graphene

A schematic plan view of a graphene sheet is shown in Fig. 1. It demonstrates bindings between carbon constituent units and an invisible (by electron microscopes) part of the graphene structure related to polar nodes (empty in ^{12}C). These nodes form the so-called "ballistic channels" along the Z-axis. There are also shown three types of edges characteristic for the two-dimensional crystal lattice of graphene.

The fact that we do not see the polar nodes does not quite mean that these nodes do not exist. For example, we do not see wind, but it exists. We know about it from the effects which wind causes. About the polar nodes we have learned directly from the corresponding solutions of the wave equation, and their existence was confirmed further by different ways. In particular, forced filling these nodes (which are the nodes of rest and motion simultaneously, *i.e.*, they are potential-kinetic) with hydrogen atoms causes appearing the short-lived atomic isotopes (considered already in L.5).

The unique properties observed in graphene experimentally are also, mainly, caused by an existence of such nodes. Conditioned by the polar nodes characteristic for the shell-nodal structure of the atoms, these properties of graphene are explained now, logically and noncontradictory, without fictional hypotheses. The latter became, unfortunately, commonplace in physics.

The form of edges in graphene differs essentially depending on their orientation in a crystal with respect to the united Z-axes of the orderly bound carbon atoms that is clearly seen in Fig. 1.

Due to an ideal conjugation of all nodes and internodal bonds, the total energy of all bonds in an ideal lattice of graphene is minimal; such is the nature of the formation of all compounds. So in the event of a deviation from the aforementioned regularity, occurred for some reason, a loss of (deviation from) thermodynamic stability takes place that results in appearance of the metastable defects.

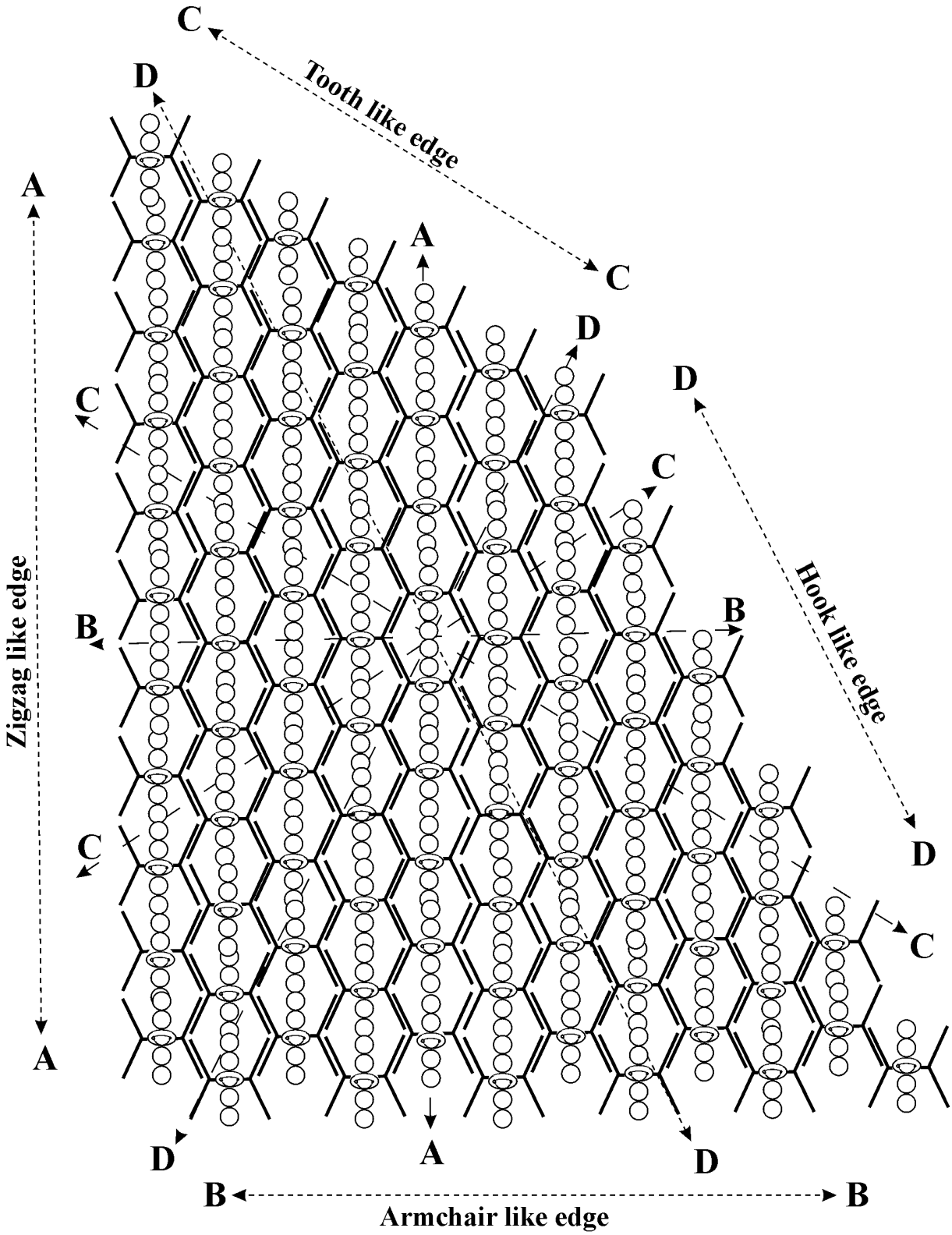

Fig. 1. The shell-nodal structure of graphene and its characteristic edges.

Typical metastable defects inherent in graphene are two pairs of five- and seven-member rings of carbon nodes (pentagon-heptagon (5-7) defects) called Stone-Wales (SW) defects. The main stages of their formation are schematically shown in Fig. 2*a-d*. These defects spontaneously appear in a hexagonal graphene lattice and remain stable for a time. In an electron microscopy conditions, under influence of heating by an electron beam, the defects lifetime is about several or tens of seconds depending on electron energy.

It should be noted that all nodes of the basic constituent units (carbon atoms C or carbon diatomic molecules C_2) are in a plane, but each of the carbon units, as a whole, has a spherical spatial structure with two principal spherical shells, internal and external. The 2 internal nodes and 4 external nodes belong, respectively, to these shells.

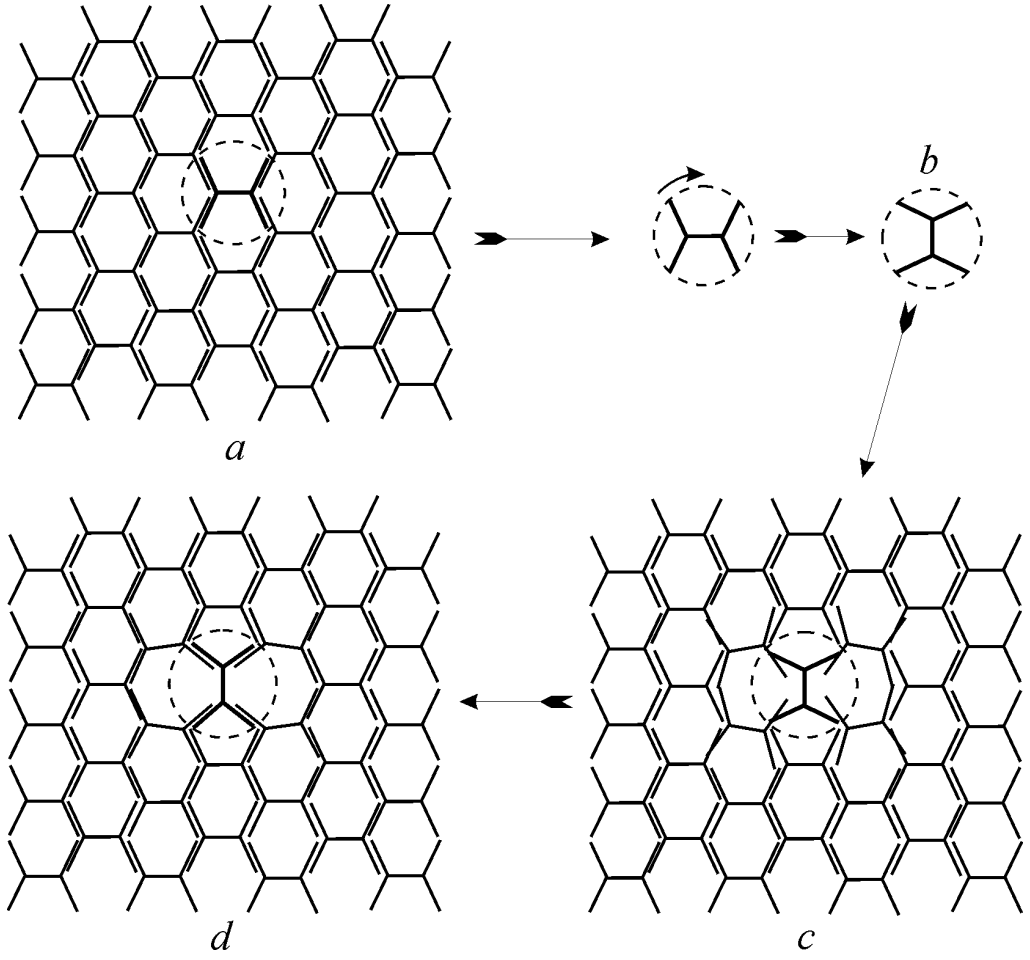

Fig. 2. The formation of the pentagon-heptagon (SW) defects in graphene.

Before beginning the consideration of the mechanism responding for the formation of the defects, let's agree to denote the carbon atom C, representing the elementary molecular formation of 12 hydrogen atoms, located by 2 in every of 6 principal polar-azimuthal nodes by the short abbreviator 6-NEM that means the *six-nodal elementary molecule* of the hydrogen atoms.

As was discussed in previous Lecture, at present we cannot say what kind of carbon is responsible for the formation of graphite (and, hence, graphene): atomic, C, or molecular, C_2. Therefore, assuming that the lattice constants of crystals accepted in modern physics are precise and congruent to reality, we have concluded that an elementary "building block" of carbon crystals is the diatomic molecule of carbon, C_2. In view of this, the carbon dimer C_2 having, naturally, the double number of the above constituents of 6NEM, we will denote for distinction by the short abbreviator 6-NED that means the *six-nodal elementary dimer* molecule of the hydrogen atoms.

A process of the formation of the defect is the following. All 6-NED and their nodes continuously oscillate around an equilibrium state with amplitude depending on the temperature. At room temperature graphene is stable, and Fig. 2*a* shows schematically an unperturbed fragment of its lattice before an appearance there of the defect. A dashed circle indicates the disposition of the 6-NED selected for consideration. Under influence of the electron beam, of a definite dose and voltage, the temperature of the 6-NED increases and, hence, amplitude of oscillations of the selected unit, as the whole, and its nodes also increases.

As was noted in [2], "*The maximum energy that can be transformed from an* 80 keV *electron to a carbon atom is* 15.6 eV, *which is below the threshold for knock-on damage but sufficient to form multiple SW defects*". The appeared perturbation results in weakening of internodal bonds that can lead to turning of the 6-NED in the plane around the axis passed through its center of symmetry perpendicularly to this plane as shown in Fig. 2b.

Fig. 2*c* shows a relative position of the 6-NED just after turning at the angle of $\pi/2$. All internodal bindings in ECNFs are elastic, and deformation (bending) of them in the turned 6-NED and the surrounded 6-NEDs is resulted in a new configuration of metastable bonds, in an appearance of a joined pair of pentagon-heptagon (SW) defects as shown in Fig. 2*d*. An appeared defect is metastable because all bonds newly formed are strained in some extent because of bending from thermodynamically equilibrium state. Therefore the above-described process shown in Fig. 2 is reversible.

After a relaxation time the defect disappears and by the reverse way returns to the unperturbed ideal graphene lattice. A schematic view of dynamics of the SW defect appearance shown in Fig. 2*d* completely agrees with the direct experimental images presented in the above-referred article published in Nano Letters [2] (in Figs. *3a-d*, herein). As noted in the referred article, an explanation of the origin of SW defects "*is important for basic understanding of this novel material as well as for potential electronic, mechanical, and thermal applications*".

The resulting formation of another complex metastable defect, like shown in Fig. 2, but with 4 pairs of five- and seven-member rings of carbon nodes is shown in Fig. 3. The latter completely agrees with the direct experimental images of such a kind of the defects shown in

[2] (in Figs. 3h,I). Here we see the 3 6-NEDs turned in plane by the different in value angles from their equilibrium states so that directions of their Z-axes are essentially changed. Their positions are market by the dash circles.

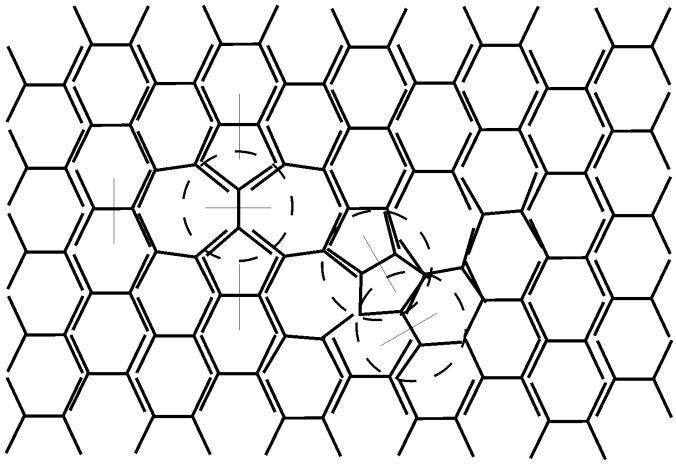

Fig. 3. The scheme of bindings at forming the complex metastable defect in graphene.

So an appearance and disappearance of the defects in graphene means that the 6-NEDs are mobile being in a continuous oscillatory motion. Their nodes only rebuild their bonds with neighboring nodes, so that in this case the 6-NEDs do not escape. A relatively low excitation of the graphene crystal structure is needed to stimulate the process of self-treatment of arisen defects. After relaxation, a graphene lattice returns to an ideal unperturbed stable state.

3. Graphene nanoribbons

Graphene nanoribbons, abbreviated GNRs, are strips of graphene with ultra-thin width (<50 nm) (Fig. 4).

It is usually believed that the electronic states of GNRs largely depend on the edge structures (armchair or zigzag). In particular, it is repeated in the literature that graphene nanoribbons can have different conductivity character depending on edge character. However, such a conclusion is the traditional fallacy of many. In particular, the wording in [3] (page 1, "*A GNR can be metallic or insulator, depending on its width and two edges*"), is erroneous concerning both statements: about the "*depending*" and "*insulator*". Missunderstanding the phenomenon is due to ignorance the true structure of graphene.

In accord with the shell-nodal atomic model, the "*edge character*" is the effect, but not the cause of the "*different conductivity character*". The properties of graphene and graphene nanoribbons, including "*different conductivity character*", depend only on the crystallographic structure and physical properties of graphene crystal as a whole.

The "*different conductivity character*", like the "*edge character*", depends only on a certain orientation of the main crystallographic axis in graphene crystal, including a graphene nanoribbon, the Z axis (see Fig. 1). The form of edges is a secondary thing.

If a nanoribbon is cut out in such a way that the Z axis of the crystal is found to be along a nanoribbon, parallel to its lateral edges, then these edges have a *zigzag form*. If the Z axis is perpendicular to lateral edges of nanoribbon, then these edges have an *armchair form*. If the Z axis forms an angle of 60^o or 120^o with respect to lateral edges, then these edges have a C-like (or tooth-like) form.

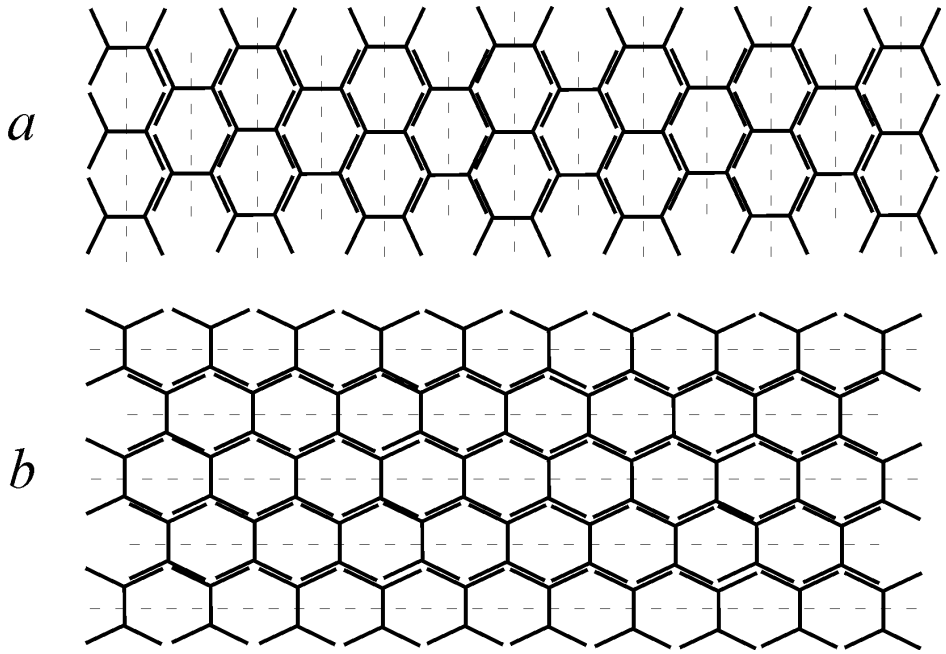

Fig. 4. Armchair (*a*) and zigzag like (*b*) types of graphene nanoribbons.

Note that the identification of the orientation of the Z axis in a graphene sheet, especially because the characteristic edges practically are not clearly seen on SEM images, must be provided as the first step before fabrication of electronic devices with required parameters on its basis.

Graphene nanoribbons cut from a graphene sheet with the different orientation of the Z-axis, on which are empty polar nodes (forming the "ballistic channel" for moving electric charges without resistance), with respect to the edges are shown in Fig. 5.

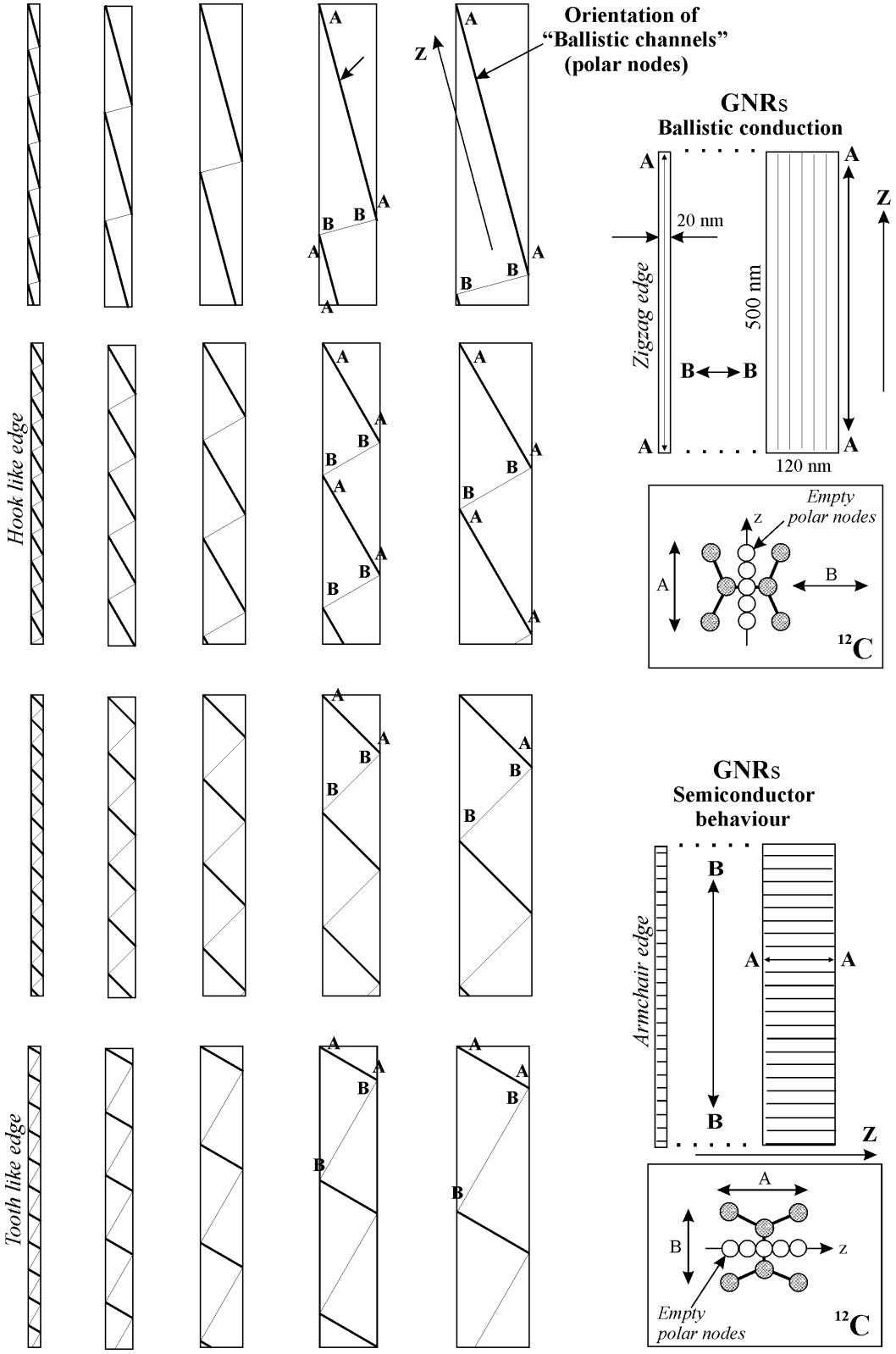

Fig. 5. Graphene strips (nanoribbons, GNRs) having the different orientations (A-A) of the Z-axis ("ballistic channels") in respect to their edges and different widths.

There are four main directions of cutting out the graphene sheets which yield nanoribbons with 3 basic types of edges (Fig. 1). The first cutting direction (A-A) is along the Z axis (*i.e.*, along the "ballistic channels"); it results in *zigzag edge* nanoribbons as shown in Fig. 4b. The second direction of the cutting out process (B-B), perpendicular to the Z axis, yields nanoribbons with characteristic *armchair edges* (Fig. 4a). The cutting out of nanoribbons along the third and fourth crystallographic directions(C-C), symmetrical with respect to the Z axis (under the angles of $\pm 60^{o}$), lead to nanoribbons with *tooth-like edges*.

In the case of cutting along the D-D directions (Fig. 1), we can obtain nanoribbons with *hook-like* edges. However, such edges being extremely unstable (because of extremely high chemical reactivity of broken free bonds on the edge, on the background of thermal vibrations of nodes and internodal bonds) can be spontaneously transformed due to a *self-treatment* into a more thermodynamically stable state which have the edges, zigzag- and tooth-like.

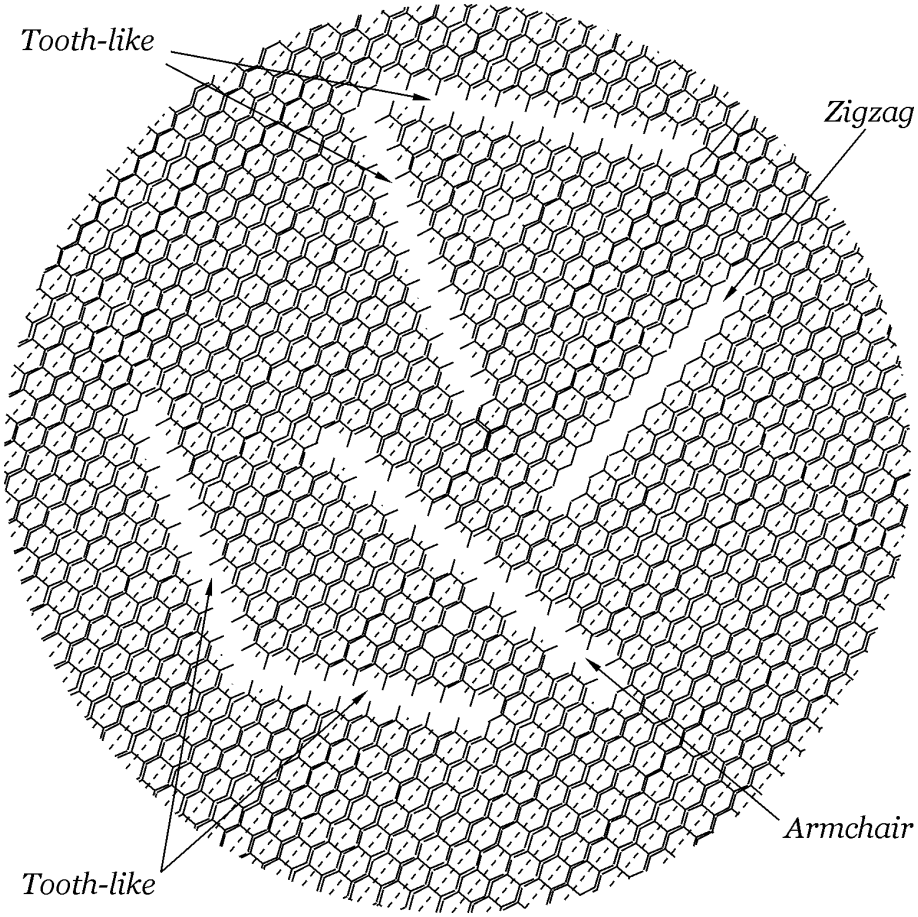

Fig. 6. The main directions of spontaneous etching in graphene (armchair and tooth-like), and a desired pattern of etching strictly along "ballistic channels" resulted in zigzag-like edges of the etched path.

The *zigzag*-like edge formed along the Z axis is the *more stable* edge because the nodes of the boundary constituent units, 6-ECDs, are double overlapped on the edge. Then, in the order of decreasing the stability of edges, we have a *tooth-like* (or C-like) edge. In this case, one node of each of the boundary 6-ECDs is free, counterbalanced. The *armchair* edge is *even less stable* because of two nodes of each of the boundary 6-ECDs are free, counterbalanced. Armchair edges have markedly higher chemical reactivity then tooth-like or zigzag edges.

This is why spontaneous anisotropic etching of single-layer graphene, for example, by thermally activated nanoparticles is, mainly, observed strictly along the angles formed by the cuts to be either 60^o or 120^o [4-6]. The directions of supposed spontaneous etching with respect to the Z-axes (depicted by the dotted lines) of the orderly bound 6-NEDs in the hexagonal lattice of graphene are shown in Fig. 6.

4. Anisotropy of unstrained pristine graphene

Thus, in accord with the shell-nodal atomic model, graphene is structurally anisotropy that follows from the data considered in previous Lectures and clear seen in all presented above Figures. Actually, looking at such a structure everyone will say without doubts that graphene is anisotropic. The shell-nodal structure of graphene has the *two-fold axis of rotational symmetry*. Hence, the physical properties of graphene must be anisotropic in a plane perpendicular to this axis.

According to modern notions, the hexagonal lattice of graphene, a two dimensional hexagonal crystal, has a high order symmetry axis, *six fold*. The hexagonal structure of graphene as it is usually considered in modern physics is presented in Fig. 7. The three identical crystallographic directions (1-1, 2-2, and 3-3) and three perpendiculars to them (depicted by dashed lines) are drawn here.

Obviously, looking at this pattern of graphene, everyone can conclude that each of the two pairs of the indicated directions, actually, are structurally equitable. Hence, the physical properties of graphene must be isotropic in a plane perpendicular to its *six-fold axis* of rotational symmetry, in full agreement with the basic symmetry theory [7].

Thus, thanks to graphene we have arrived at the situation when we can verify the validity of new concepts on the structure of atoms, and by this way to confirm the conclusion on invalidity of modern theoretical notions concerning the structure of matter at the atomic and subatomic levels. The first property dependent on the crystallographic anisotropy, which can easy verify in graphene, is its electric conductivity.

An examination of likely conductivity anisotropy in pristine unstrained graphene has never been undertaken, and a question about such tests has never been raised among researchers. An existence of natural anisotropy of graphene was not only unknown, but even is not discussed a possibility itself of this phenomenon, as completely unacceptable, craze.

As we have said above, at first glance a talk about an existence of natural conductivity anisotropy in graphene seems nonsensical. Looking at the structure shown in Fig. 7, one can conclude that all three indicated directions are equitable and electric conductivity of graphene measured along these directions must be the same.

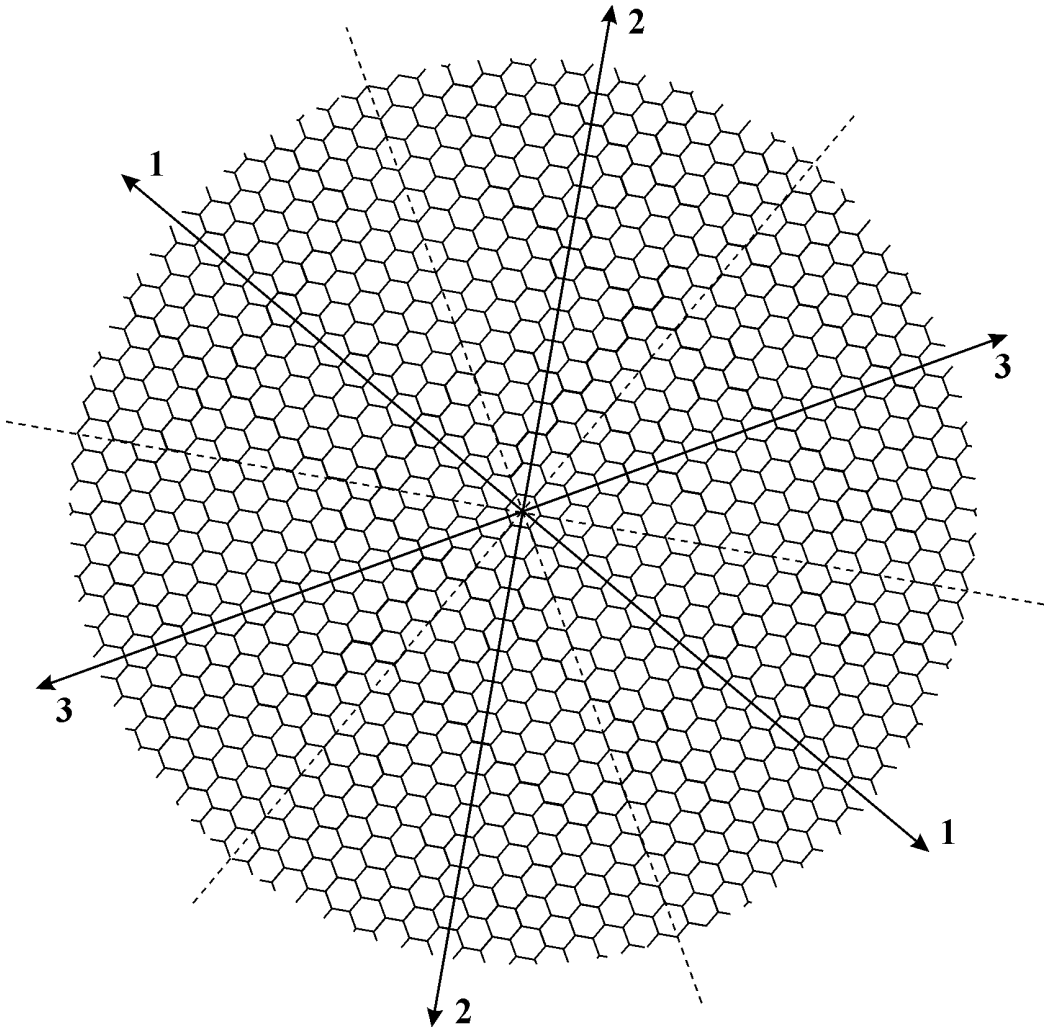

Fig. 7. The honeycomb lattice of graphene.

However, according to the shell-nodal structure of the carbon atom, it makes sense. Polar potential-kinetic nodes along the Z-axis (empty and, therefore, invisible in structural analysis) form together an empty channel allowing the ballistic motion of electric charges in graphene. They divide the hexagonal cell formed of potential nodes filled with nucleons (and, hence, visible in structural analysis) onto two symmetrical halves. Conductivity along the ballistic channel must be higher than in perpendicular direction.

In this connection it should be noted the following. Graphene flakes (sheets) obtained by different ways and, moreover, not being sufficiently isolated from its environment in order to be considered as free-standing, have many different kind defects and impurities. Consequently, the pure ballistic motion, observed in suspended pristine graphene membranes,

is not ideal in some cases (for example, in an attempt to implement the device on such graphene) because of scattering of electrons on the defects during their motion.

The fact that we do not see empty polar nodes forming the ballistic channel does not quite mean that these nodes do not exist. Modern technological means are too imperfect at present to observe all peculiarities of the structure of matter at the atomic level.

The laboratory tests conducted in 2010, have confirmed the existence of conductivity anisotropy [8], *i.e.*, the validity of theoretical solutions, and, hence, the correctness of the shell-nodal structure of carbon atoms and their specific ordering in the hexagonal lattice as shown schematically in all posted figures.

The method of measurements is clearly seen from a scheme shown in Fig. 8.

Importantly, the accepted method of *the test on conductivity anisotropy* allows providing an instant control of the quality of electric contacts to the disc-shaped graphene plates, directly during measuring the resistances. Hence, this method can be used as *the method of the tests on applicability* of the technology of making the electric contacts on graphene.

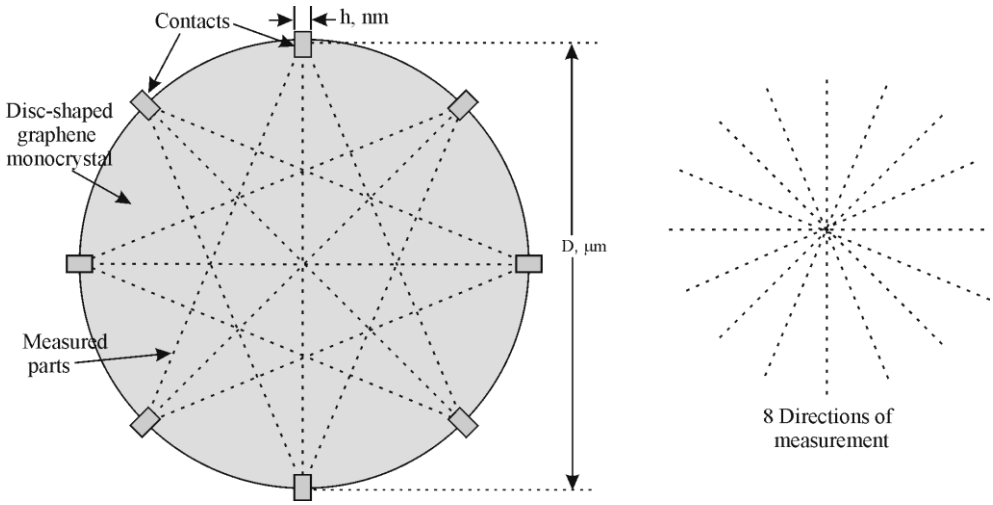

Fig. 8. A measurement scheme.

It is obvious that in the case of unstrained pristine graphene monocrystals (having none structural defects) and perfectly plated contacts to them, the resistances of the parallel pair of identical conductive paths of the same geometrical configuration must be equal in value (within error margins). What type of the parallel symmetrical (with respect to a diametrical line) pairs of resistances we mean is shown in Fig. 9. Here, as an example, are shown the identical parts (in configuration, form) of a graphene plate at measuring the voltage between 8-5 and 1-4 contacts at the definite constant current flowing through these parts.

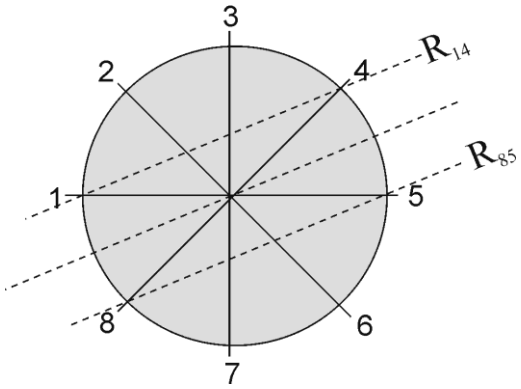

Fig. 9. A parallel pair of identical conductive paths of the same geometrical configuration.

If relatively large differences (variations) of resistances measured between the two symmetrical parallel (identical) parts extending between the indicated contacts will be found on structurally perfect graphene plates, the technological flaws of making the contacts on graphene plates must be carefully analysed, and the corresponding technology must be improved or replaced by another. A typical scanning electron microscope image of the disk-shaped graphene test sample with 8 contacts is shown in Fig. 10.

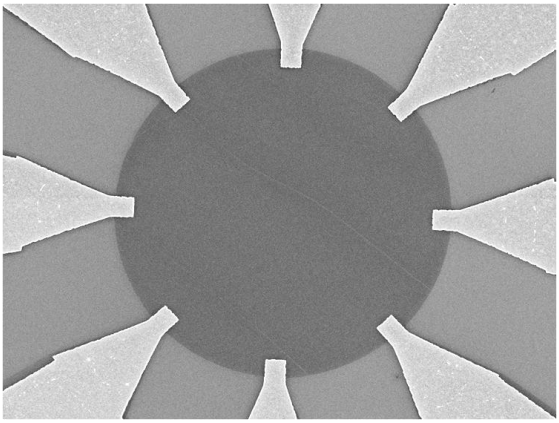

Fig. 10. The SEM image of the tested graphene device.

Not controlled variations (fluctuations) of any parameters, which can be caused by possible imperfect technological conditions, existed in the laboratory during fabrication of the tested samples, naturally can influence on the obtained results. However, as a rule, fluctuations are characterised by a chaotic (random) distribution, which superimposes upon the investigated dependences (if such really exists), does not changing the latter.

Pristine unstrained graphene, obtained by a mechanical exfoliation method (the “scotch tape technique” on HOPG graphite), was used for the tests. The first tests were carried out on three samples of disk-shaped monatomic-thick graphene layers with diameters of 10 μm (Dev. 4), 7 μm (Dev. 2), and 5 μm (Dev. 5). The most commonly used substrate for graphene

devices is SiO_2; it was used also for the fabrication of the test devices. An angular dependence of resistance in a plane of the graphene plates was measured.

A typical *polar diagram* of conductivity anisotropy, R = f(φ), of the test samples of an *unstrained pristine* graphene layer, monoatomic in thickness, has a characteristic elliptical form, as presented in Fig.11 for Dev. 4 measured at two temperatures, 4.2 and 295 K. For all first three tested samples [8], the found angular dependence in a plane of graphene monolayers is clearly seen on the background of insignificant random variations of absolute values of resistances in some directions.

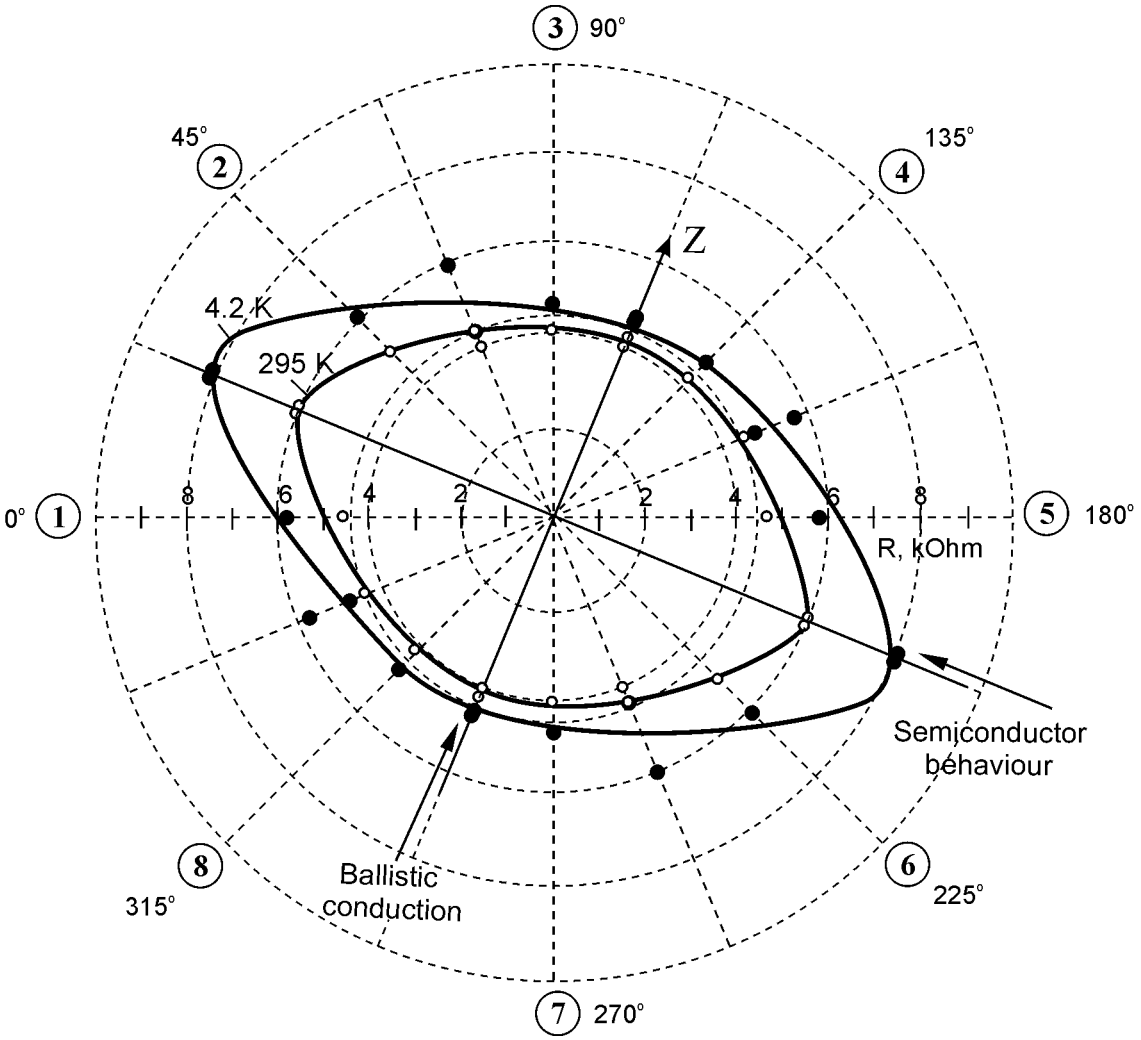

Fig. 11. Anisotropy of resistance (*R, kOhm*) in a plane of a hexagonal graphene monolayer of the device Dev. 4, prepared in the form of a circular-shaped plate of the diameter of *D*=10 *μm*; a width of contacts is *h*=580 *nm* (V_g=24 *V*; *T*=4.2 *K*, *I*=1 *nA*; *T*=295 *K*, *I*=100 *nA*).

In another graphical form, the angular dependence of conductivity R = f(φ) in a plane of a graphene monolayer of the graphene device Dev. 4, obtained at the room temperature

(T=295 K), is presented in Fig. 12. At this figure it is also shown, in small circles, all 8 directions of measurements corresponding to each of the obtained values of the resistance R.

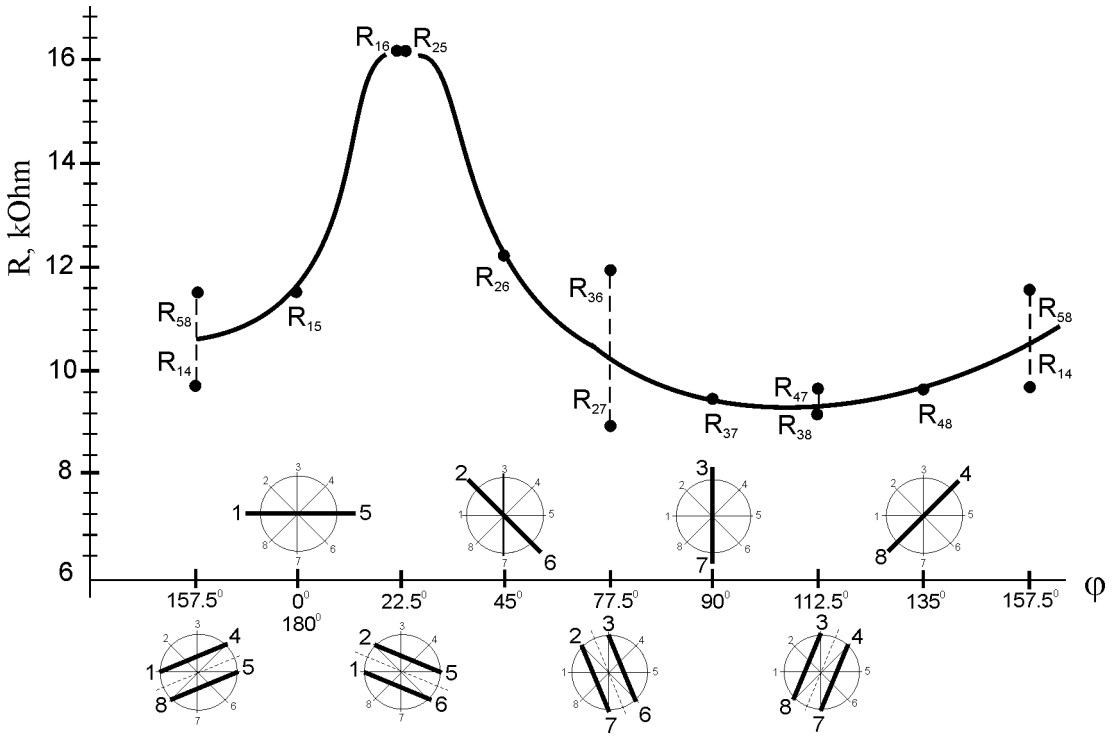

Fig. 12. The angular dependence of conductivity R = f(φ) in a plane of a graphene monolayer of the graphene device Dev. 4: the diameter D=10 μm, the width of contacts h=580 nm, T=4.2 K, I=1 nA.

As follows from the data obtained, the temperature dependence of graphene conductivity *occurs like in a metal* along the major axis of anisotropy coinciding with the Z-axis. It is the A-A direction indicated in Fig. 1. However, we cannot say about *metallic conductivity* of graphene. It is not a suitable term for characterization of the *ballistic electron transport* found in pristine graphene. Graphene conduct electricity better than metals due to the phenomenon known as ballistic transport. Ballistic transport occurs when an electron is able to travel without being impeded by atoms, molecules, defects or impurities within the transport medium. The ballistic motion does not fit within the theory of metallic conductivity, in principle. Unlike known metals, graphene exibits superior thermal and electrical conductivity, and extraordinary high room temperature carrier mobility.

A mechanism of the ballistic transport of electrons observed in graphene differs from the mechanism responsible for the electron transport in metals. By its nature and due to the extremely high magnitude of carrier mobility, the ballistic motion in graphene is, in essence, one of the previously unknown forms of high conductivity in solids exibited in a wide

temperatures range, including the room temperature. And now we can add to the above properties one more property that the ballistic motion is realized at the certain crystallographic direction due to graphene anisotropy. Thus, the expression „metallic conductivity" is confused with the essense of the conductivity running in graphene.

In a direction perpendicular to the major axis of anisotropy (the B-B direction indicated in Fig. 1) graphene exhibits *semiconducting properties*. This follows from the character of the obtained temperature dependence in this direction.

The extent of anisotropy, defined as the maximal ratio of resistances measured in mutually orthogonal directions between corresponding pairs of contacts, is far beyond the possible random deviations and errors for all tested samples. Maximal anisotropy of 84%, at the temperature 4.2 K, and 50%, at 295 K, was found in Dev. 4 which has a bigger size (diameter 10 μm) with respect to other tested samples.

Resistance R is inverse proportional to conductivity σ: $R \sim 1/\sigma$. Resistance and, hence, conductivity in a plane along the *axis* of symmetry (identical with the Z-axis), which is the *minor axis* of anisotropy of resistance, does not depend practically on temperature in the range from 4.2 K to 295 K. This feature follows from the data of measurement for Dev. 4 at both temperatures. In this direction graphene behaves as possessing *ballistic charge transport properties* (referred usually to its "*metallic*" conductivity properties). An insignificant change of resistances with the temperature along the Z-axis, clear distinguishable in Fig. 11, can be conditioned by different phenomena, for example, by the influence of the SiO_2 substrate and environment, *etc*.

Conductivity along the *major axis* of anisotropy of resistance (along transverse diameter, perpendicular to the Z-axis) depends on the temperature. This feature is clearly expressed in Fig. 11 at both polar diagrams of resistances obtained at the temperatures 4.2 K and 295 K. This means that in this direction graphene behaves as having *semiconducting properties*.

Graphene anisotropy is confirmed by the fact, that graphene nanotubes, rolled up form of graphene, have either conductivity, metallic or semiconducting. It means that the rolling up of graphene is realized mainly along two crystallographic directions: along the Z-axis and in the perpendicular to it direction.

The extent of anisotropy, in value, in dependence on the size of tested devices is shown graphically In Fig. 13. The observable tendency shows that in devices of the bigger size (diameter) with respect to sizes of tested devices, we can wait yet bigger values of anisotropy exceeding 2.0.

Obtained nanotubes have the minimal energy of state. The rolling-up of graphene sheets runs spontaneously at the high temperature conditions; it is not yet controlled process. The rolling up in other directions, apparently, is thermodynamically unfavourable unstable

process, which does not provide the minimal energy of state for the formation of such systems (graphene nanotubes).

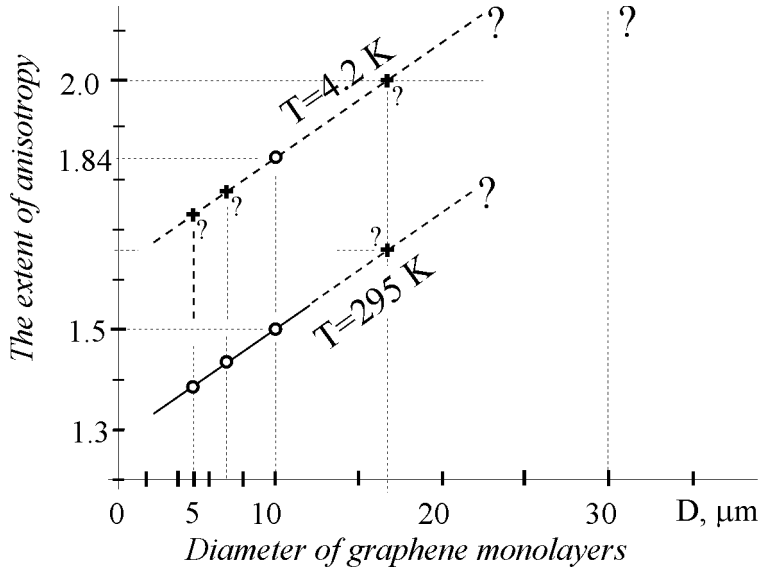

Fig. 13. The extent of anisotropy in tested graphene devices: Dev. 5 (D=5 μm), Dev. 2 (D=7 μm), and Dev. 4 (D=10 μm).

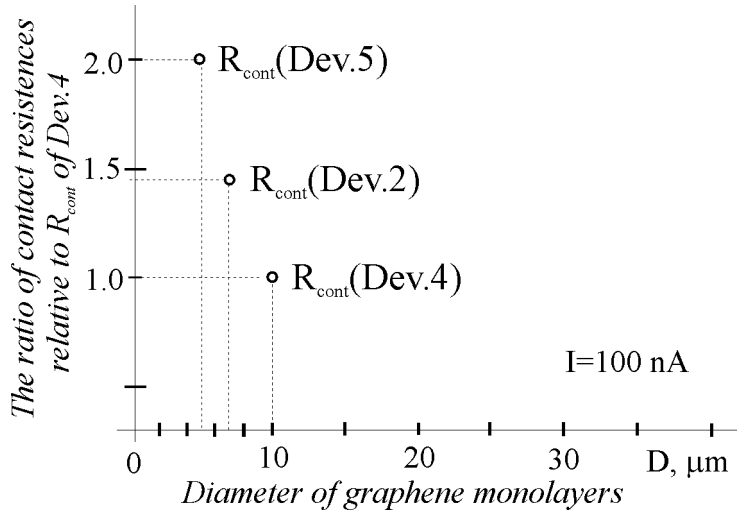

Fig. 14. The relation between contact transient resistances of tested graphene devices with respect to contact resistance of Dev. 4.

Note, that the tendency shown in Fig. 13 is found on samples which are distinguished not only by the size, but also by the different transient resistances of their contacts, at the constant current, because of the different width (and hence, areas) of their contacts (see Fig. 14): h=580, 400, 290 nm, respectively, in Dev. 4, Dev. 2, and Dev. 5. Therefore, on the basis of the limited data obtained, it is impossible to predict precisely enough a variation of the extent of anisotropy in dependence on the size of graphene and the area of contacts plated on it.

At more optimal conditions of the fabrication of the test devices and optimally fitted measurement parameters, the anisotropy can reach the more significant values (undoubtedly exceeding 84% found in Dev.4). Especially best results on the degree of anisotropy one can wait from future tests on a suspended (free-standing) graphene, where the negative influence (affect) of the substrate on physical properties of graphene will be excluded. More ideal will be tests accomplished by non-contact methods, for example, optical methods of sample analysis, *etc*.

Coming back to Fig. 7, we can conclude that the hexagonal lattice of graphene presented there reflects only the observable part of its structure. Therefore, we do not see any difference between three indicated crystallographic directions (1-1, 2-2, 3-3) and three identical directions indicated by dashed lines.

5. Conclusion

According to the modern notions, it is generally accepted that the hexagonal lattice of graphene, a two-dimensional crystal, with the structure shown in Fig. 7, has the high-order axis of rotational symmetry, *six-fold*. Hence, the physical properties of graphene, in particular, electrical conductivity, must be isotropic in a plane perpendicular to this axis, in full agreement with the basic symmetry theory [7].

However, in accord with the solutions of the wave equation, *atoms* have the *shell-nodal structure*; that is, they represent nucleon molecules. They have the different symmetries, strictly definite inherent in each individual atom. The specific feature of the carbon atom is the fact that its shell-nodal structure has the *two-fold axis* of rotational symmetry. This implies that graphene, consisting of carbon atoms, if they are orderly bound in the lattice in a certain manner as shown in Figs. 1 and 6, is, apparently, an *anisotropic crystal*.The first laboratory tests have confirmed this statement.

There are many evidences in favour of the shell-nodal structure of the atoms found in result of the comprehensive analysis of the particular solutions of the Helmholtz wave equation [1]. All peculiarities, conditioned by the nodes order just in a two-dimensional lattice of graphene, lead to *a series of predictions* naturally arising as a consequence of the aforesaid structure. The conducted tests confirmed, in particular, the prediction of conductivity anisotropy caused by an existence and the specific arrangement of *invisible* empty polar nodes relative to the *visible nodal points* in graphene crystal. Remember that the visible *crystal nodes* are formed in result of overlapping the coupled hydrogen atoms being in polar-azimuthal nodes belonging to the interacting (linkable) carbon units, 6-NEDs (six-nodal elementary dimer molecules of the hydrogen atoms); they form the visible bone of graphene (Fig. 1). Thus, a one-atom thick layer of graphite, having a two-dimensional hexagonal lattice, gave the unique chance allowed the direct verification of the reality of such a nodal structure.

Thus, an existence of the unknown earlier intrinsic property of graphene, the conductivity anisotropy, following from the crystallographic anisotropy of its lattice predicted theoretically, has been proven experimentally.

On the basis of shell-nodal atomic model, all specific features of graphene are naturally explained, logically and noncontradictory, for example, such properties of graphene nanoribbons (GNRs) as: "*length and width dependent resistance scaling in GNRs*", "*the averaging hopping length between localized states*", why "*the charge transport is dominated by hopping through localized state*", what are "*localized states*" themselves [9]. The new atomic model uncovers also, why "*graphene is...an interesting mix of a semiconductor...and a metal...*" [10]; and so on. We will not analyze the aforementioned statements, caused by ignorance of the true structure of graphene, in the framework of this Lecture. You can do it easy now yourself.

Graphene anisotropy explains logically the fact that graphene nanotubes, rolled-up form of graphene, have either conductivity, metallic or semiconducting. The rolling-up of graphene is realized mainly along two crystallographic directions [11]: along the major axis (the Z-axis) and in perpendicular to it direction. Obtained nanotubes have the minimum-energy state in these cases. The rolling-up of graphene sheets runs spontaneously at the high temperature conditions; it is not yet controlled process. The rolling-up in other directions is thermodynamically unfavorable unstable process which does not provide the minimum-energy state. And such carbon systems (graphene nanotubes) with an asymmetric crystallographic orientation with respect to the cylindrical axis of nanotubes are not forming.

Ignorance about an existence of the anisotropy conditions a random orientation of graphene sheets in experiments conducted to present and, as a result, leads to diversity, jumble, and lack of coordination (confusion) in numerous experimental data obtained in different laboratories.

Obviously, after the first trial tests described here, the comprehensive studying of the found anisotropy should be continued. For this purpose it is necessary to provide complete tests on graphene plates of less and bigger sizes (diameters), at low and high temperatures (4.2 and 295 K), low current (1 nA and less), having different areas (widths) of electric contacts, *etc*.

One needs also to provide the continuous resistance readings during a slow heating of samples from 4.2 K to 295 K approximately over the 10 K (or 20 K) temperature interval. The resistance reading should be carried out along such an angular direction, corresponding to the maximal obtained value of resistance, *i.e.*, along the major axis of the found resistance anisotropy (perpendicular to the Z-axis, see Fig. 11). The resistance readings will allow drawing the following dependence,

$$\ln \sigma = f\left(T^{-1}\right), \qquad (1)$$

and, accordingly, to define the *forbidden band gap*, E_g, in tested graphene monolayers.

Thus, as follows from the particular solutions of the general wave equation, atoms do not correspond to the Rutherford-Bohr model. They have the shell-nodal structure and resemble molecules composed of coupled nucleons (hydrogen atoms) that fill up potential nodes of the spherical shells of the atoms. Accordingly, atoms are not monocentric in their internal structure. Such a structure, verified from different sides during the period beginning from the publication of the book in 1996 [12], was confirmed directly experimentally in unstrained pristine graphene by the found anisotropy predicted in this two-dimensional crystal. The anisotropy behavior is conditioned by the shell-nodal structure of graphene constituents – carbon atoms and their specific ordering in the hexagonal lattice.

Thousands years people thought about, what is atom? Now scientists must come back again to this topic. They should verify the findings of dialectical physics which are the subject of discussion in these Lectures, and, accordingly, independently carefully analyze the well-known particular solutions of the general wave equation to be convinced about truthfulness of the unknown earlier physical meaning contained in them and disclosed at last, as shown in these Lectures, within the Wave Model.

Note also that with the development of high-tech on graphene, its crystallographic anisotropy must be taken into account to exclude arbitrary spatial setting of graphene layers on substrates with respect to the direction of their axis of anisotropy [8]. The controlled crystallographic orientation of graphene sheets is needed for fabrication on their basis of identical nanoscale devices with the strictly definite set-up parameters. This condition is an obligatory first step in high-tech based on use of monocrystalline materials, *i.e.*, is a self-evident technological operation.

References

[1] L. Kreidik and G. Shpenkov, *Atomic Structure of Matter-Space*, Geo. S., Bydgoszcz, 2001, 584 p. http://shpenkov.com/atom.html

[2] J.C. Meyer, C Kisielowski, R Erni, MD Rossell, MF Crommie, A Zettl, *Direct imaging of lattice atoms and topological defects in graphene membranes*, Nano letters, 2008, 8 (11), 3582-3586.

[3] Q. Liang and J. Dong, *Superconducting switch made of graphene-nanoribbon junctions*, Nanotechnology 19 (2008) 355706 (7pp).

[4] S. S. Datta, D. R. Strachan, S. M. Khamis, A. T. C. Johnson, *Crystallographic Etching of Few-Layer Graphene*, Nano Lett. 2008, **8** (7), pp 1912-1915.

[5] L. Ci, Z. Xu, L. Wang, W. Gao, F. Ding, K.F. Kelly, B.I. Yakobson, and P.M. Ajayan, *Controlled nanocutting of graphene*, Nano Res. **1**, 116-122 (2008).

[6] N. Severin, S. Kirstein, I.M. Sokolov, J. P. Rabe, Nano Lett., *Rapid trench channeling of graphenes with catalytic silver nanoparticles*, 2009, 9 (1), 457-61.

[7] Robert E. Newnham, *Properties of Materials: Anisotropy, Symmetry, Structure*, Oxford University Press, 2005.

[8] G. Shpenkov, *Anisotropy of Graphene*: Test Results, 2010; https://register.epo.org/application?documentId=ES2PMPUZ5321FI4&number=EP10707863&lng=en&npl=false . Supplementary data to "*Method for manufacturing nano electronic devices made from 2D carbon crystals like graphene and devices obtained with this method*". Int. Appl. No.: PCT/EP2010/052298; Publ. No.: WO/2010/097393; https://register.epo.org/application?number=EP10707863&lng=en&tab=main

[9] Melinda Y. Han, Juliana C. Brant, and Philip Kim, *Electron Transport in Disordered Graphene Nanoribbons*, Phys. Rev. Lett. **104**, 056801 (2010).

[10] A.H. Castro Neto, F. Guinea, N. M. R. Peres, K. S. Novoselov and A. K. Geim, *The electronic properties of graphene*, Rev. Mod. Phys. **81**, 2009.

[11] Graphene Nanoribbons; http://shpenkov.com/pdf/nanoribbons.pdf

[12] L.G. Kreidik and G.P. Shpenkov, *Alternative Picture of the World*, Vol. 1-3, Bydgoszcz, 1996.

Lecture 8

Oxygen Compounds

1. The shell-nodal structure of oxygen and neon atoms

The *oxygen* atom has an external subshell, of the shell l = 2, completed by half and, therefore, containing only two polar-azimuth nodes (7 and 8, Fig. 1) filled each by the coupled hydrogen atoms.

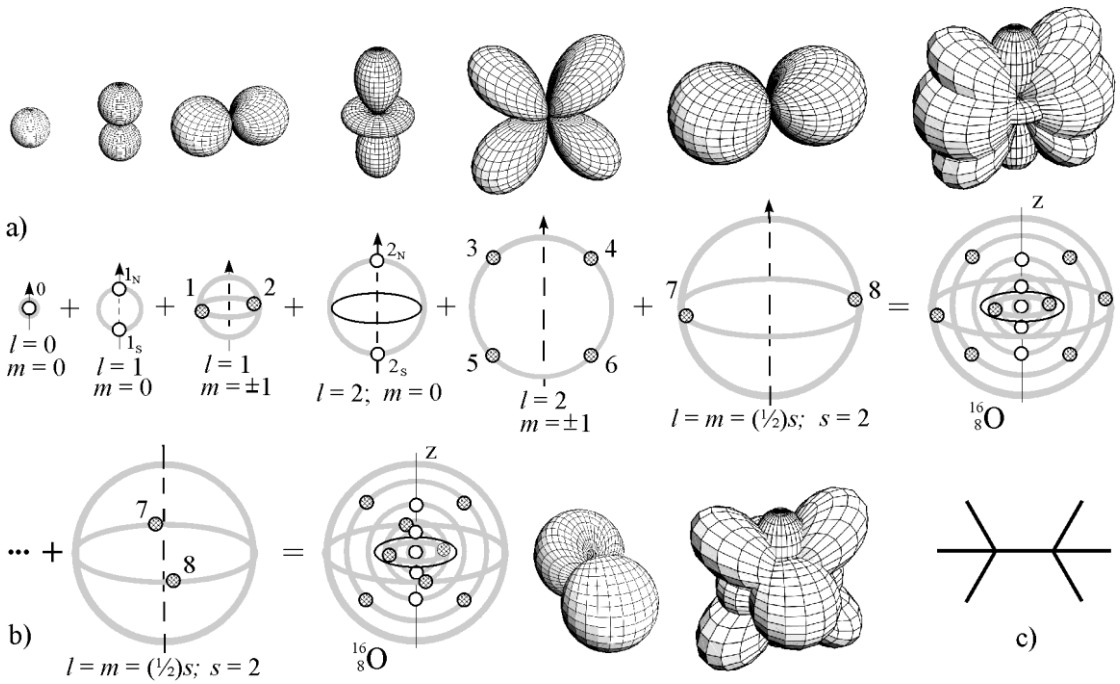

Fig. 1. Plots of the polar-azimuthal functions $\Theta_{l,m}(\theta)\cos(m\varphi+\alpha)$ $(l=0,1,2;\ m=0,\pm1)$ and the disposition of the nodes defined by these functions on radial shells $R_l(\rho)$ of the oxygen atom: $\alpha=0$ (a) and $\alpha=\pi/2$ (b) for the external half-integer shell at $l=m=s/2$ and $s=2$; (c) the symbolic designation of oxygen ${}_8O$ (at $\alpha=0$).

This uncompleted subshell relates to the half-integer solution (Eq. (31), L. 2) of the order $l+1/2$ where $l=m=(1/2)s$ and $s=2$,

$$\hat{\psi} = A\hat{R}_s(\rho)\Theta_s(\theta)e^{\pm i\frac{s}{2}\varphi} \qquad (1)$$

As all uncompleted (noninteger, fractional) shells, the external subshell of oxygen lies in the equatorial plane.

An outer subshell of the shell l = 2, completed by one quarter, $s = 1$, laying also in the equatorial plane, belongs to the *nitrogen* atom $_7$N.

The next uncompleted external subshell at $s = 3$ of the shell l = 2 belongs to the *fluorine* atom $_9$F.

The entirely completed (*i.e.*, *integer*) external subshell responding to the solution for $m = \pm 2$ of the same shell, l = 2, (see Fig. 6 in L. 3) has the neon atom $_{10}$Ne. This shell contains the four completed external potential polar-azimuthal nodes (numbered as 7, 8, 9, and 10 in Fig. 2). The next subshell, m = 0, with two empty polar nodes, of the shell l = 3 also belongs to the neon atom.

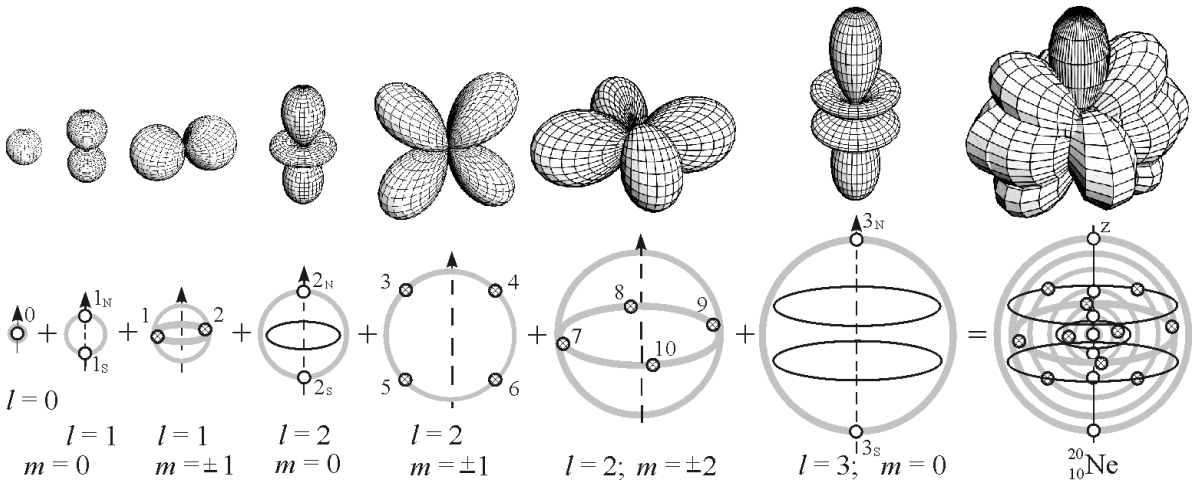

Fig. 2. Plots of the polar-azimuth functions and their extremal points on the corresponding radial shells of the neon atom.

The half-integer external subshell of oxygen is intermediate between the entirely completed external integer shell of carbon (l = 2, $m = \pm 1$) and the shell of neon (l = 2, $m = \pm 2$).

Thus, the mentioned above three atoms, having fractional external polar-azimuth subshells of the shell l = 2 (with one, two, and three nodes, respectively), are uncompleted structures with respect to the entirely completed integer shell of the atom with Z = 10 (having four completed nodes in the external subshell) and characterized by the wave numbers l = 2 and $m = \pm 2$,.

However, the external shell with four equatorial nodes (at $l = 2$, $m = \pm 2$), being filled with coupled hydrogen atoms belonging to the neon atom – one of the balanced atomic formations, is, simultaneously, the resulting *balanced shell for molecular compounds* formed on the basis of the aforementioned atoms having noninteger external shells: N, O, and F (their atomic numbers Z are equal, respectively, to 7, 8, and 9).

Therefore, the external subshell, fully completed in the case of neon, as being its *proper* shell, is considered for *nitrogen*, *oxygen* and *fluorine* – individual atoms having unfinished fractional external shells, as their *improper* shell. The *deficient nodes*, needed to finish building of the aforementioned fractional external shells to the fully completed state (characteristic to neon), are the *active centers* of adsorption of hydrogen atoms from environment for the above atoms.

2. The shell-nodal structure of oxygen compounds

The filling of the deficient (vacant) nodes of the improper shell with hydrogen atoms (single, or nodal bound with a nearby node in a molecule-like atom) occurs without breakdown of individuality, *i.e.*, without destroying the distinctive pattern of *strong bonds* inherent in each of the atoms, including the aforementioned *nitrogen*, *oxygen* and *fluorine* having uncompleted shells. This provides the *chemical* (electromagnetic) level of interatomic bonds occurring with participation of the deficient nodes.

A new atom is not formed when nodes of the *improper* shell are drawn into a process of exchange (interaction). A molecule with the structure, repeating the nodal structure of the atom having the balanced external shell, is formed in this case.

In particular, the water molecule H_2O is formed under adsorption of individual hydrogen atoms by two vacant nodes (drawn by dotted circles in Fig. 3) of the improper shell of the oxygen atom, ${}^{16}_{8}\mathrm{O}$.

The obtained molecule of water has a three-dimensional spatial disposition of the nodes with respect to the single-plane disposition of all filled nodes in oxygen. A structural analog of the H_2O molecule is the short-lived neon isotope ${}^{18}_{10}\mathrm{Ne}$ (1672 *ms* half-life). This isotope has the same spatial *disposition* of the nodes and *multiplicity* of filling all the nodes just like it has H_2O. However, of course, the four nodes of the external shell of the above isotope and the water molecule have the different coupling strength structure with the rest of their nodes that distinguishes the formed water molecule from the neon isotope: interacting atoms are not destructed at the formation of molecules, their individuality is saved.

We see that the shell-nodal structure of an individual water molecule is not completed entirely – its two external nodes are filled on half, they contain by one hydrogen atom. Therefore this structure is not entirely equilibrium. Such a structure will continuously aspire

to form bindings with other water molecules by joining their half-completed nodes till the coupling of hydrogen atoms in them will not be achieved.

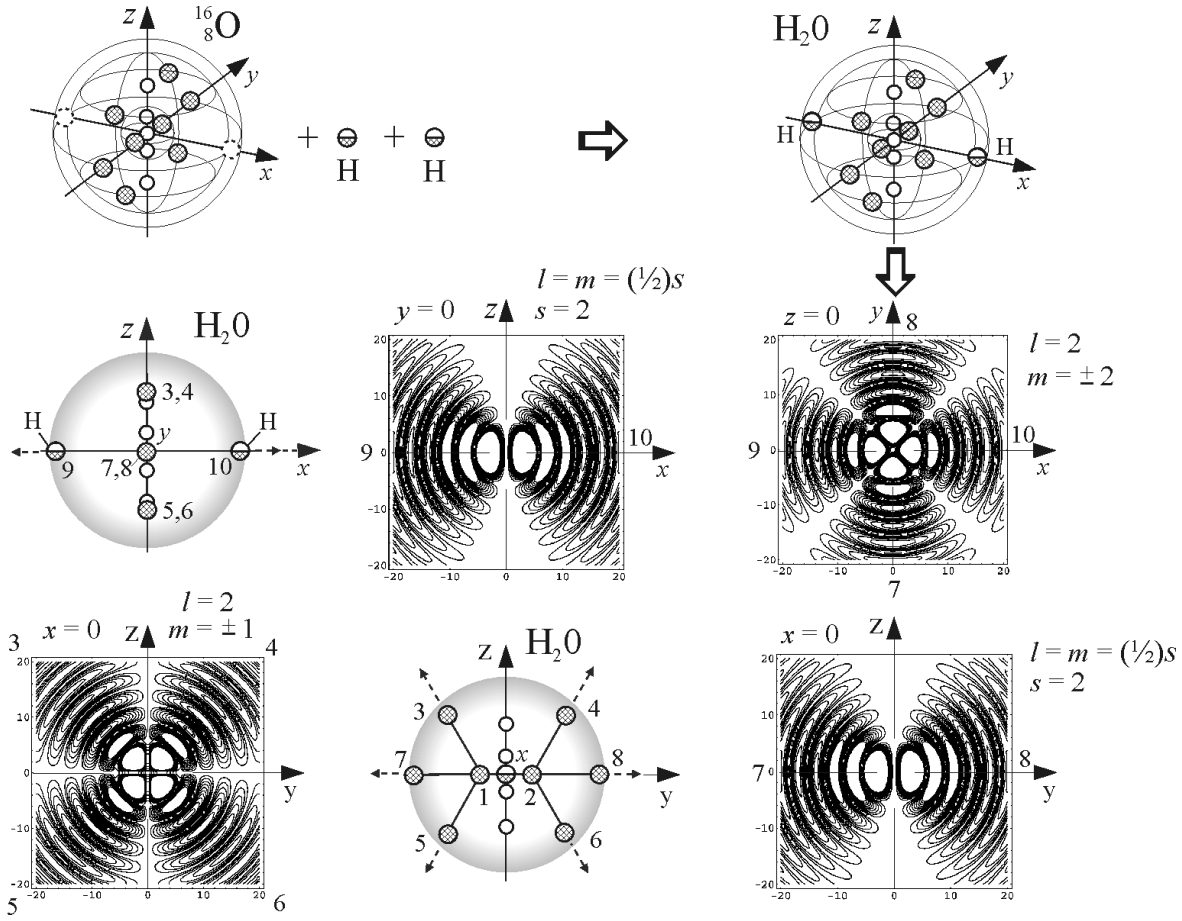

Fig. 3. Conditional drawings of the formation of water molecule H_2O and the density of probability (contour plots) $\hat{\Psi}$ of localization of substance (hydrogen atoms) in external shells for the planes $x = 0$, $y = 0$, and $z = 0$; the arrows indicate the directions of external bindings inherent in the water molecule.

If we take a look at the water molecule in the direction along the *x*-axis, we find the hexagonal structure of disposition of its nodes defining the six radial directions of exchange (interaction) in the plane $x = 0$. They are designated by the six smaller arrows in Fig. 3. Two other directions of exchange, perpendicular to the plane $x = 0$, are along the *x*-axis.

The characteristic nodal structure of H_2O stipulates the great variety of possible internodal bonds between water molecules and, accordingly, the great structural variety of molecules and crystals. Such a structure defines numerous symmetric-asymmetric hexagonal forms of snowflakes, the short-range order of liquid water and long-range crystalline order of ice, dynamic and thermodynamic anomalies of water, *etc*. Water is the most abundant

compound on the Earth and a major constituent of all living organisms. It is still the most enigmatic liquid on the Earth, apparently, because of the shell-nodal structure of the oxygen atom.

Remember, the $\hat{\Psi}$ function define the probability density of any wave events (L. 2). The radial solutions of the wave equation give a series of slowly damped in amplitude, in radial direction, radial shells with alternating zero values, responding to a series of the roots of the solutions defined by Bessel functions $J(\rho)$ and $Y(\rho)$ [1]:

$$\hat{R}_l(\rho)/A = \sqrt{\pi/2\rho}(J_{l+1/2}(\rho) \pm iY_{l+1/2}(\rho)), \qquad (2)$$

where $\rho = kr$ is the relative radius, A is the constant factor. The sections of some of the $\hat{\Psi}$ functions shown in Fig. 3 demonstrate this.

The noninteger solutions at $l = m = (1/2)s$ ($s = 0, 1, 2, 3, \ldots$) give the following potential constituents $\psi_s(\rho_{s,j}, \theta, \varphi)_p$ of the spatial function $\psi(\rho, \theta, \varphi)$,

$$\psi_s(\rho_{s,j}, \theta, \varphi)_p = C_\Psi R_s(\rho_{s,j}) \sin^{s/2}\theta \cos(s/2\,\varphi + \alpha), \qquad (3)$$

where $\rho_{s,j}$ are the radii of the characteristic noninteger j-shells defined by the function $R_s(\rho)$.

The nearest radial shell in a series of the j-shells at $s = 2$, following the completely filled basic external half-integer shell, has two empty nodes of the same polar-azimuth orientation (coordinates). A picture of the distribution of the probability density in this case (in a plane $y = 0$) is shown in Fig. 3. The nearest radial j-shell, following the completely filled integer shell at $l = 2; m = \pm 1$, has four empty nodes. A picture of the density of probability (a section in a plane $x = 0$) for this case is shown also in Fig. 3. The aforementioned uncompleted j-shells are the *proper* empty radial shells of the *second order*. Their empty nodes take part (along with nodes of the improper shell) in the formations of snow crystals, short- and long-range order of water, *etc*.

Because of peculiarities of the shell-nodal structure, formation of oxygen molecules (just like any molecules) can be realized by different ways. Fig. 4a demonstrates one of the possible structures of the oxygen molecule O_2 where it is realized the two-multiple overlapping of three completed nodes each of two bound oxygen atoms.

Another possible structure of oxygen molecule O_2, formed with participation of improper nodes, is shown in Fig. 4*b*,*c*. The overlapping (joining) of completed proper and empty improper external nodes leads in this case to the three-dimensional spatial disposition of the filled nodes in the obtained oxygen molecule.

The *partial filling*, by three fourths, of equatorial shells of bonded and partially joined oxygen atoms, with hydrogen atoms, is realized here. So that only three nodes of the four nodes needed to have the equilibrium shell, characteristic in Ne, are filled in them. Two improper nodes (shown by dotted circles in Fig. 4c) remain uncompleted, empty. The resulting structure, as not fully completed, is not entirely equilibrium. This stipulates its chemical activity to form the bonds with hydrogen atoms both single and nodal belonging to other atoms and molecules, first of all those of them having the non-equilibrium external shells.

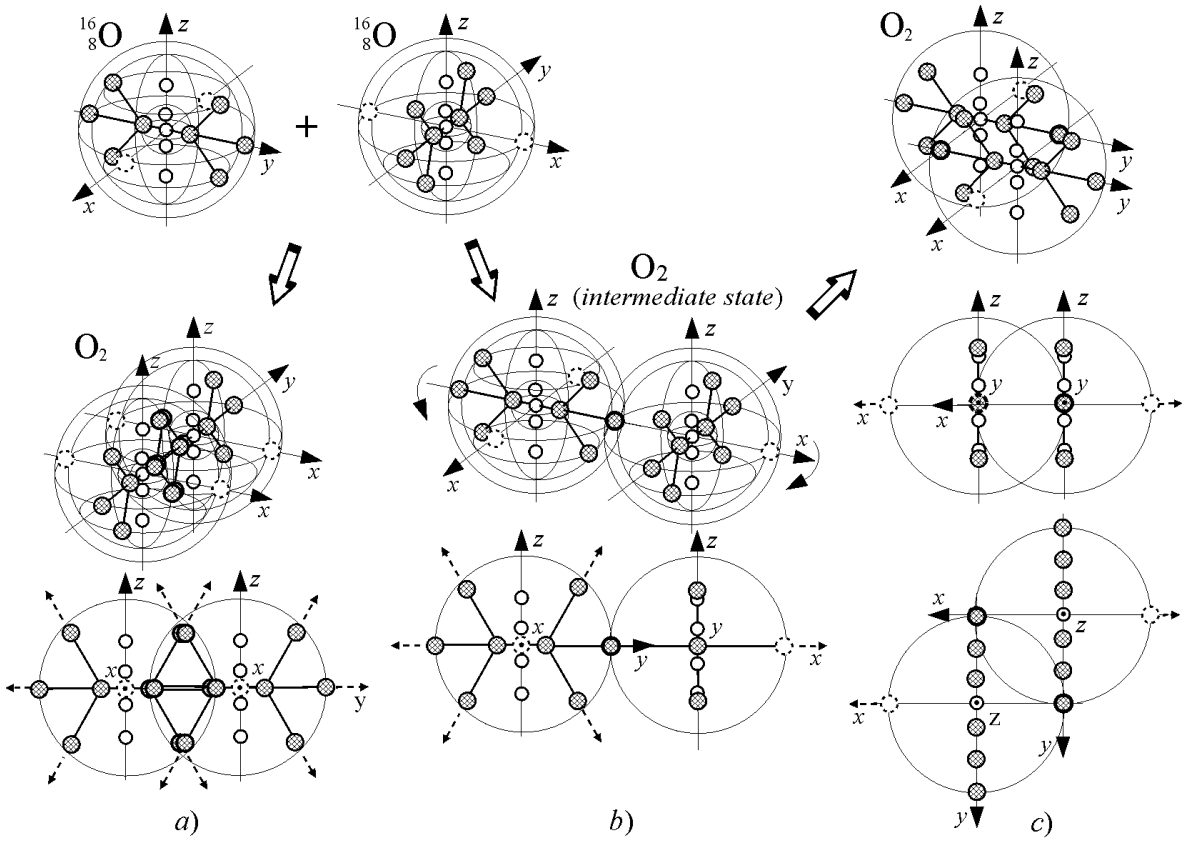

Fig. 4. Two possible ways of forming the oxygen molecule O_2: (*a*) by mutual two-multiple overlapping each of the three completely filled nodes of two oxygen atoms; (*b*,*c*) by overlapping the proper completed nodes with improper empty nodes.

A comparison of the structure of oxygen compounds presented here with the structure of carbon compounds, considered in previous Lectures, allows noting the following.

The characteristic feature of carbon bonds in all innumerable carbon compounds is, along with two-multiple overlapping of the completed nodes, the three-multiple overlapping of all nodes of the constituent carbon atoms. The three-multiple overlapping takes place in all cyclic carbon compounds and in the well-known crystallographic forms of carbon: graphite, diamond, fullerenes, and graphene.

Remember, three-multiple (or two-multiple) overlapping of the nodes in compounds means that the resulting nodal point in them belongs, respectively, to the nodes belonging to three (or two) individual atoms. And taking into account the coupling of the hydrogen atoms in the nodes, every such a point contains 6 (or 4) the overlapped hydrogen atoms. The 12 hydrogen atoms in the nodal point of carbon compounds will be, at the three-multiple overlapping, in the case when elementary components of the compounds are carbon dimer molecules. We have considered this subject in L. 6.

The overlapping occurs in such a way, in all cases with oxygen and carbon atoms, that the resulting interatomic bindings are realized just *along the intra-atomic strong bonds* existing between external nodes, belonging to the external shell, and conjugated internal nodes of the nearby internal shell each of interacting atoms.

The next peculiarity is that single bindings between the 1st and 2nd nodes of the internal shell (corresponding to $l=1,\ m=\pm1$) nowhere overlap.

In Fig. 5 we present one more way (shown) of the formation of oxygen molecule O_2 and other oxygen compounds, in addition to the presented above.

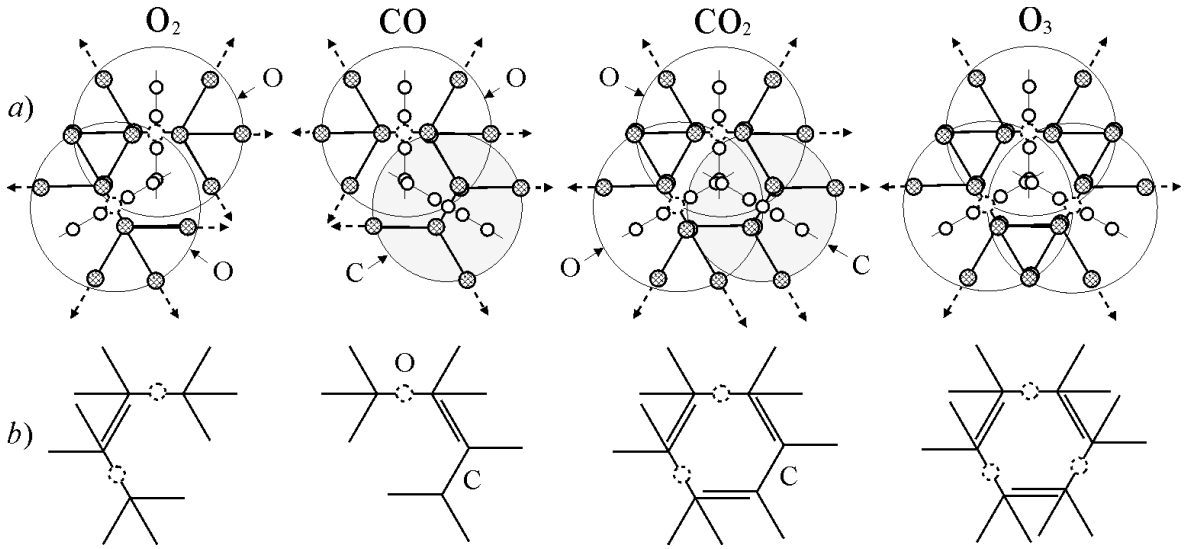

Fig. 5. (*a*) One more possible way of the formation of oxygen molecule O_2 and possible structures of carbon oxide CO, carbon dioxide CO_2, and ozone O_3; (*b*) the symbolic designation of the oxygen compounds characterized by two-multiple overlapping of the interatomic nodes.

This way is characterized by the *two-multiple overlapping* of the completed nodes *along* the *internodal strong bindings*. Such overlapped bonds, apparently, are realized, as shown in Fig. 5, at forming the spatial structure of the O_2, CO, CO_2, and O_3 molecules. Take attention

at the perfect symmetry of trioxide (ozone O_3). It has *three improper nodes* above and *three improper nodes* below the plane of the disposition of completed nodes, *i.e.*, above the opposite sides of the plane. They are shown here by the dotted circles. The two improper nodes belonging to the individual oxygen atom $^{16}_{8}O$ were shown above in Figs. 3 and 4 (and are shown below in the next figures). Their existence makes this compound is very active. Actually, as well-know, ozone is a powerful oxidant. It is much less stable than the diatomic allotrope of oxygen and breaks down in the lower atmosphere to normal dioxide.The analogous interatomic bindings (just like above considered for oxygen and carbon compounds) take place for nitrogen oxides. As an example, the formation of two hypothetical structures of nitrous oxide N_2O is shown in Fig. 6*a*,*b*.

.

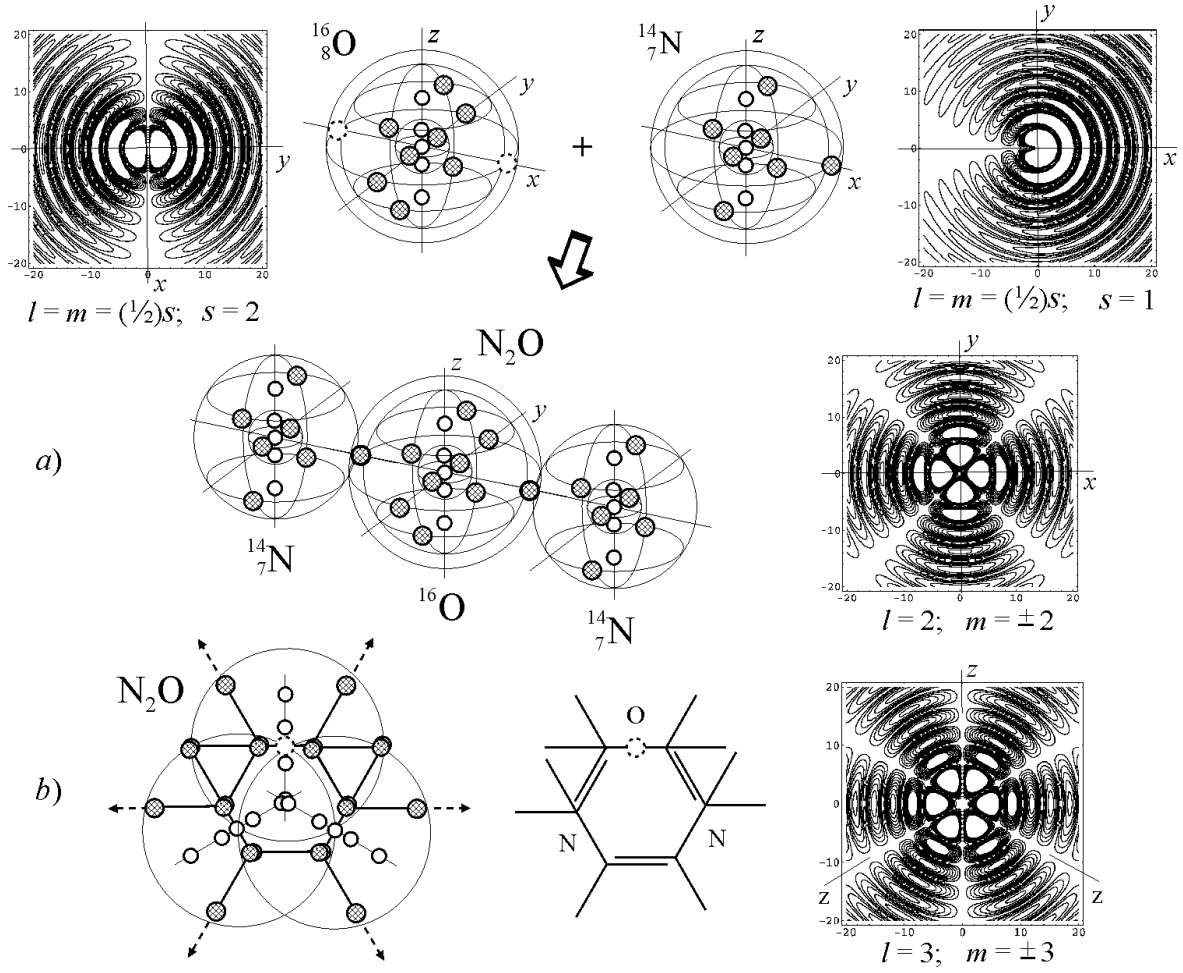

Fig. 6. Two possible ways (*a*, *b*) of the formation of nitrous oxide N_2O and the density of probability $\hat{\Psi}$ (contour plots) drawn for the external equatorial shells of separate atoms $^{16}_{8}O$ and $^{14}_{7}N$ (the upper row, left and right) and for the selected parts of the joined shells.

The first structure (Fig. 6a) is presented in the unfolded form. Two associated nitrogen atoms (left and right) have rotational degrees of freedom (around the joined nodes). They will form additional bonds, turning about up to overlapping either single nodes or pairs of nodes belonging to their internal shell (at $l = 2,\ m = \pm 1$) with corresponding conjugated (approached) nodes of two external shells of oxygen.

The next but very enlightening example with Al_2O_3 structure in unfolded and closed forms, admissible by the solutions, is presented in Fig. 7.

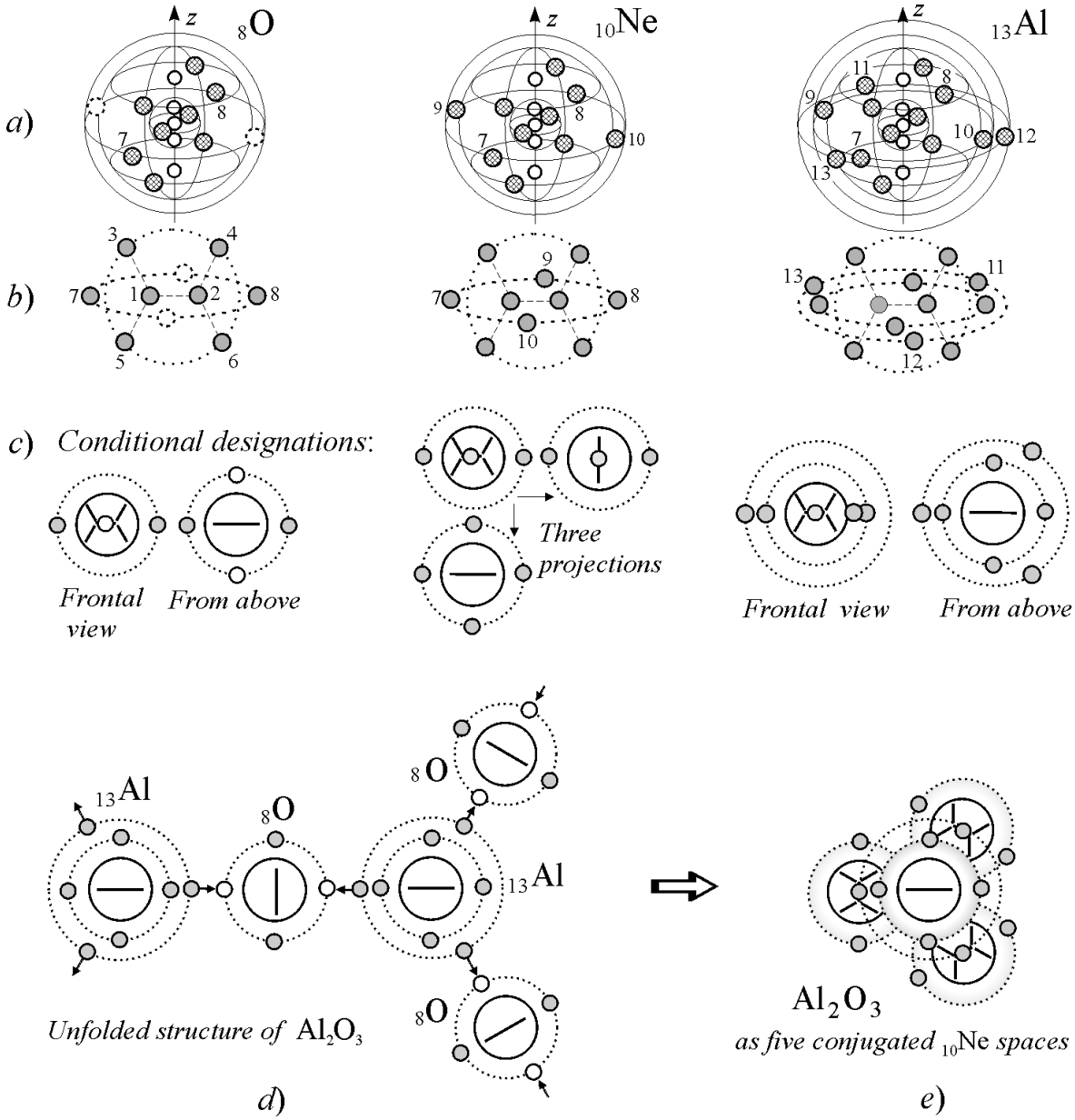

Fig. 7. The shell-nodal structure of the ${}_8\mathrm{O}$, ${}_{10}\mathrm{Ne}$, and ${}_{13}\mathrm{Al}$ atoms (*a*, *b*) and their conditional designations (*c*) for different projections; the unfolded (*d*) and closed (*e*) structure of bindings in Al_2O_3.

Improper vacant nodes of every from three conjugated oxygen atoms (designated as small hollow circles in Fig. 7c,d) join with external nodes of two aluminum atoms, as indicated in Fig. 7d by arrows. We see the perfect compact arrangement of all nodes of two aluminum atoms (up and down, Fig. 7e)) and three oxygen atoms resulted in the stable neutral structure, as if five individual neon spaces were tightly embedded and bound together (reminiscent of a perfect fitted cogged joint).

The structure of the atoms with completely filled atomic shells is defined by the superposition of embedded *whole* shells; the structure of the rest atoms includes the *fractional* external shells (we have considered this issue in more detail in L. 4). The superposition of atomic structures, graphically demonstrated here, is provided by more complicated solutions to the wave equation, which define the structure of molecules and crystals.

3. Conclusion

Thus, basing on the shell-nodal structure of the atoms, disclosed in the particular solutions of the wave equation, an existence of sets of all possible *structural* forms in chemical compounds (the structural diversity) become naturally and logically explainable.

The true structure of the atoms was and still is an open question in natural science. A unified theory of atoms has not been built so far. In the framework of quantum-mechanics (QM), the problem on the comprehensive complete description of atomic structure is unsolvable in principle. The QM is an abstract-mathematical theory. It was being developed on the basis of a series of the abstract postulates to describe first of all an optical spectrum observable in the hydrogen atom. The fit of the calculations to the experimental data became its major method. At the present, the QM represents a theory, which deals mainly with the so-called "*electron structure*" ("*electron configuration*") of atoms. The spatial structure of the atoms is *terra incognita* for QM.

The structure of the main atomic constituents (*protons* and *neutrons*), which are considering in modern physics as the superdense particles, and an internal structure of a tiny atomic nucleus (with respect to the whole atom), where, as believe, these particles are placed, are the realm of other branches of modern physics. As a consequence, the nature and structure of atoms and their isotopes are still an unsolved mystery for physics. Accordingly, we assume that the nature of Mendeleev's Periodic Law, reflecting the observed regularity in the behavior of the atoms at their interaction with each other, caused by the specific atomic structure inherent in each of them, but yet unknown, is not properly understood for this reason.

From the particular solution of the wave equation for the spherical wave space it follows that all atoms, having the shell-nodal structure, are elementary molecules of the *hydrogen*

atoms (to which we refer *proton*, *neutron*, and *protium*). Only the *hydrogen atoms*, as the *single-centre* elementary wave formations, are *atoms* in the full sense of the word. That is why we call all rest of the atoms Z-*nodal elementary molecules* of the hydrogen atoms, Z-NEMs. This definition reflects the fact that the *atomic number* Z each of the atoms in the Periodic Table *is equal to (defines, indicates) the number* of principal (potential or kinetic) *polar-azimuthal nodes* in all shells of the atom.

The spatial structure of the *molecule-like* atoms recalls the spherical resonant cavities [2] which are also described by Bessel functions. It means that all types of elementary lattices represent (repeat), in essence, elementary nodal structures of standing waves in a limited three-dimensional wave physical space. For the spherical space, the standing wave structure was presented schematically in Fig. 6 of L. 3.

The wave concept on the atomic structure is based on recognizing, as an axiom, the *wave nature* of the Universe and, hence, the wave nature of matter. Respectively, in accord with this axiom, the general *wave equation*, which describes all wave processes, must describe also the structure of matter at all levels of the Universe, including atomic and subatomic, that is the subject of the present Lectures. A key role for the development of the shell-nodal atomic model belongs also to the *Dynamic Model* of elementary particles, atomic constituents, which led to the discovery of a series of the fundamental physical constants unknown earlier [3]. These constants made it possible to calculate the corresponding parameters characteristic for the atomic and subatomic wave formations and fields of their interactions.

The shell-nodal (*multi-center*) atomic model, developed on the basis of the wave concept, reveals the nature of different symmetry inherent in crystals, including the symmetries found in quasi-crystals "*strictly forbidden by the mathematical laws of crystallography*" [4-6], and the nature of the Periodic Law. The understanding of the regularity observed in properties of the atoms allowed arranging them in the *Periodic Table of the Atoms* in a new form presented in L. 4.

The periodicity in chemical properties of the elements is a result of the disclosed *quasi-similarity* of the nodal structure of *external shells* of the atoms. Taking into account the latter, some of the heavier elements and all rare-earth elements get their true places in the aforementioned Periodic Table. Moreover, taking into account the multiplicity of filling the nodes, the nature (structure) of all possible atomic isotopes (already known and not yet observed) was naturally revealed as a result.

It should be stressed also that, together with other ways, the interatomic wave exchange (interaction) at the formation of chemical bindings is realized along the intra-atomic strong bonds existed between all the nodes in each of the interacting atoms. With this, these intra-atomic strong bonds overlap without being destroyed. The same condition is fulfilled at the formation of carbon compounds (considered in previous Lectures) [7].

The overlapping strength is realized by the elementary quanta of the rate of mass exchange, *i.e*., by exchange charges of electrons. It means that the main role at the formation of interatomic bindings in molecules and crystals belongs to major constituents of the atoms – the nodal hydrogen atoms. Electrons play the secondary role; they define only the chemical bonds strength, which we call *additive* in respect to strong ("nuclear") bonds called *multiplicative*. We will consider the above notions in the next Lecture devoted to the derivation of the bonds strength.

Finally, it should be noticed that the disclosed shell-nodal structure of the atoms represents, figuratively speaking, something like the "genetic code", which defines, in a definite extent, the structural diversity, symmetry, and periodicity in Nature.

References

[1] F. W. J. Olver, ed., *Royal Society Mathematical Tables*, Vol. 7, Bessel Functions, part. III, Zeros and Associated Values, Cambridge, 1960.

[2] R. F. Harrington, *Time-Harmonic Electromagnetic Fields*, McGraw-Hill, 1961.

[3] L. Kreidik and G. Shpenkov, *Dynamic Model of Elementary Particles and the Nature of Mass and 'Electric' Charge*, "Revista Ciencias Exatas e Naturais", Vol. 3, No 2, 157-170 (2001); http://shpenkov.com/pdf/masscharge.pdf

[4] D. Shechtman, I. Blech, D. Gratias, and J.W. Cahn, *Metallic Phase with Long-Range Orientational Order and No Translational Symmetry*, Phys. Rev. Lett. **53**, 1951–1953 (1984).

[5] S. Mae, *Tyndall Figures at Grain Boundaries of Pure Ice*, Nature **257**, 382-383 (1975).

[6] P. J. Steinhardt and H. C. Jeong, *A Simpler Approach to Penrose Tiling with Implications for Quasicrystal Formation*, Nature **382**, 433–5 (1996).

[7] G. Shpenkov, *The Role of Electrons in Chemical Bond Formation*, Molecular Physics Reports **41**, 89-103 (2005).

Lecture 9

Intra-atomic and Interatomic Binding Energies

1. Introduction

Derivation of binding energy of nucleons in deuterium, tritium, helium ${}^{4}_{2}He$, and carbon ${}^{12}_{6}C$ atoms and interatomic bindings in molecules in the light of the shell-nodal atomic model are presented in this Lecture. It is shown that the internal structure of nucleons at the level of constituent g-particles recalls the shell-nodal structure of silicon of the nucleon level. The calculated binding energies well agree with the binding energies commonly estimated from the mass-energy equation as the mass defect.

Recall briefly the basic information that is needed in this Lecture devoted to the derivation of binding energies. Shell-Nodal Atomic Model (SNAM) allows explaining the structure of matter at atomic and subatomic levels in a more logical and simple way. The model is based on particular solutions of the ordinary wave equation in spherical polar coordinates and on the Dynamic Model of Elementary Particles (DM).

As follows from the SNAM, atoms are molecules of the hydrogen atoms, which are by two in the principal potential nodes of spherical shells. Radii of the shells are defined by the roots of Bessel functions.

The wave function $\hat{\Psi}$,

$$\hat{\Psi} = \hat{R}_l(kr)\hat{Y}_{l,m}(\theta,\varphi)\hat{T}(\omega t) = \Psi_p + i\Psi_k, \qquad (1)$$

of the wave equation

$$\Delta\hat{\Psi} - \frac{1}{c^2}\frac{\partial^2\hat{\Psi}}{\partial t^2} = 0, \qquad \text{or} \qquad \Delta\hat{\Psi} + k^2\hat{\Psi} = 0, \qquad (2)$$

has the form

$$\hat{\psi} = A_l\sqrt{\pi/2\rho}(J_{l+1/2}(\rho) \pm iY_{l+1/2}(\rho))\Theta_{l,s}(\theta)e^{\pm is\varphi}, \qquad (3)$$

where A_l is the constant factor; $\rho = kr$; $H^{\pm}_{l+1/2}(\rho)$, $J_{l+1/2}(\rho)$ and $Y_{l+1/2}(\rho)$ (or $N_{l+1/2}(\rho)$) are the Hankel, Bessel and Neumann functions, correspondingly, $k = \frac{2\pi}{\lambda} = \frac{\omega}{c}$ is the wave number. It is the particular solution corresponding to integer values of the wave number m ($m = \frac{1}{2}2s$ and $s \in N$) the kinematic structure of *standing spherical waves* in wave physical space and the shell-nodal structure of the atoms with fully completed external shells..

All spatial components are determined with the accuracy of a constant factor *A*, imposed by boundary conditions, which have no influence on the peculiarity of distribution of the *nodes* on radial spheres. The superposition of even and odd solutions defines the *even-odd solutions*. Odd solutions describe the nodes, lying in the equatorial plane of atomic space. In this plane there are also solutions in the form of *rings* in space.

$\hat{\Psi}$ -Function represents any parameter of the *wave* field such as, for example, potential-kinetic displacement, potential-kinetic speed, physical potential-kinetic probability, *etc*.

The radial component $\hat{R}_l(kr)$ of the wave function $\hat{\Psi}$ (1), representing the density of potential-kinetic phase probability [1], describes the radial field of displacements of the wave parameter, which the $\hat{\Psi}$-function represents in the wave equation. The polar component $\Theta_{l,m}(\theta)$ describes the polar displacements, and $\hat{\Phi}_m(\varphi)$ describes the azimuth displacements.

The potential solutions define the coordinates of rest, whereas the conjugate kinetic solutions define the coordinates of maxima of motion. Thus, the potential solutions give us the spatial coordinates of equilibrium domains (nodes of standing spherical waves) in the wave atomic space.

Thus, we should distinguish two solutions, potential and kinetic; do not mixing them. Rest and motion (nodes and antinodes) are the two *qualitatively different* states. Kinetic harmonics are the same, in form, as potential harmonics, but they are displaced in space in the radial direction and turned in the azimuthal direction, around the z-axis, with respect to potential harmonics (just like $\cos m\varphi$ with respect to $\sin m\varphi$ so that the kinetic extrema are between the corresponding potential extrema (as alternated nodes and antinodes in standing waves).

The geometry of characteristic states on radial shells is expressed by extrema and zeros of the polar-azimuthal components of the $\hat{\Psi}$-function. A schematic form of the *potential* solutions of the $\hat{\Psi}$-function for $l = 0, 1, 2, 3$, which relate to the shells of the atoms under consideration, are shown schematically in Fig. 1 (it is a part of the solutions presented in Fig. 6 of L. 3,).

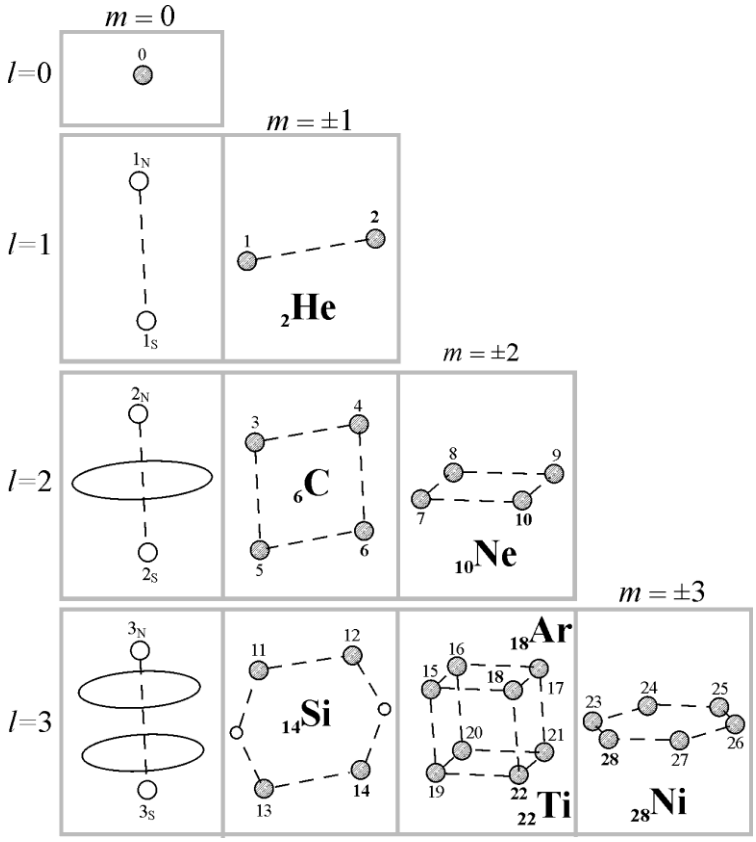

Fig. 1. A schematic view of the solutions $\psi_{l,m}(\rho,\theta,\varphi)_p = C_\Psi R_l(\rho)\Theta_{l,m}(\theta)Cosm\varphi$ of Eq. (2) presented in the form indicating the spatial disposition of principal *potential* polar-azimuthal nodes in the atomic shells; their ordinal numbers 1, 2, …, 28 coincide with atomic numbers.

The standing wave structure presented in Fig. 1 uniquely determines the shell-nodal structure of the atoms in the range of hydrogen ($_1$H) to nickel ($_{26}$Ni). The atoms having *completed outer shells* and $_{12}$Ar, which has a *half-integer outer shell* with four nodes lying in equatorial plane as $_{10}$Ne, are indicated herewith.

2. The shell-nodal structure of helium ^4_2He, and carbon $^{12}_6C$

The completely realized polar-azimuthal *n*-th potential shell (with potential nodes) is defined, in accordance with solutions of the wave equation (2), by the function

$$\Psi_{l,m}(\rho_{l,n},\theta,\varphi)_p = C_\Psi R_l(\rho_{l,n})\Theta_{l,m}(\theta)\cos(m\varphi+\alpha), \qquad (4)$$

where $\rho_{l,n}$ is the relative radius of the *n*-th external radial shell. The geometry of angular disposition of nodes is determined by polar-azimuthal functions $\Theta_{l,m}(\theta)\cos(m\varphi+\alpha)$. The latter and their sections are presented in Fig. 2 for hydrogen, helium, and carbon atoms. In the case of carbon atom, two configurations of functions, $\Theta_{1,1}(\theta)\cos\varphi$ and $\Theta_{1,1}(\theta)\cos(\varphi+\pi/2)$,

different by initial azimuthal phases ($\alpha = 0$ and $\alpha = \pi/2$), are shown in Fig. 2. The octahedral structure ($\alpha = \pi/2$) is, apparently, realized in the diamond structure of carbon.

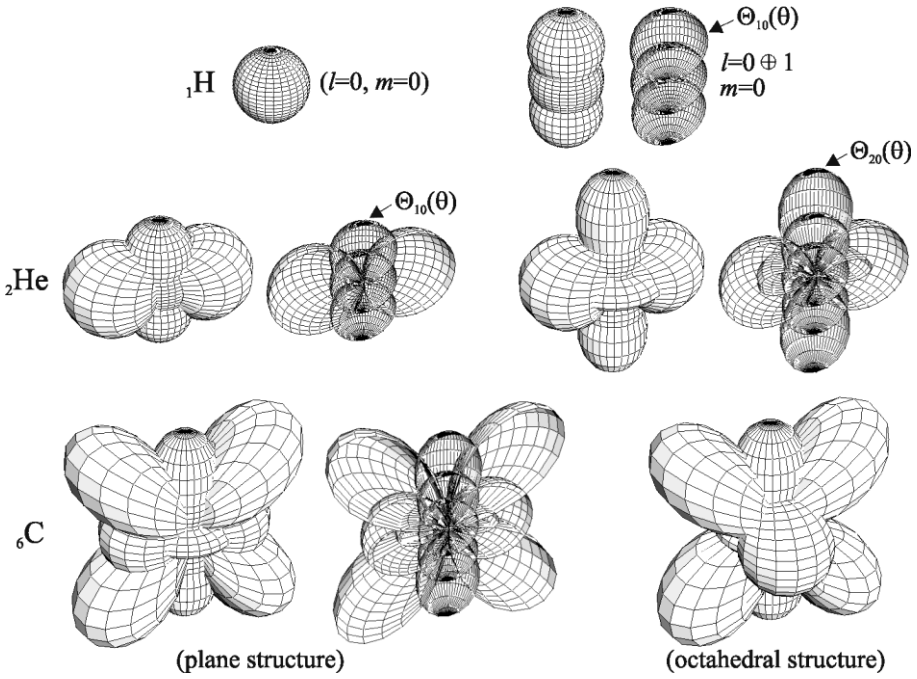

Fig. 2. The structure of potential polar-azimuthal functions (integer solutions) for hydrogen $_1H$, helium $_2He$, and carbon $_6C$.

The nodal structure of ^4_2He and $^{12}_6C$, originated from (4), is conditionally shown in Fig. 3. The carbon's nodal structure is depicted with the plane disposition of its six principal polar-azimuth nodes ($\alpha = 0$). All principal polar-azimuthal nodes in the stable isotopes, which are presented in this figure, are filled with paired nucleons - say H-atoms (to which we refer the hydrogen atoms, protons and neutrons). Polar nodes are situated at the polar azis z, forming something like "spinal" of atoms.

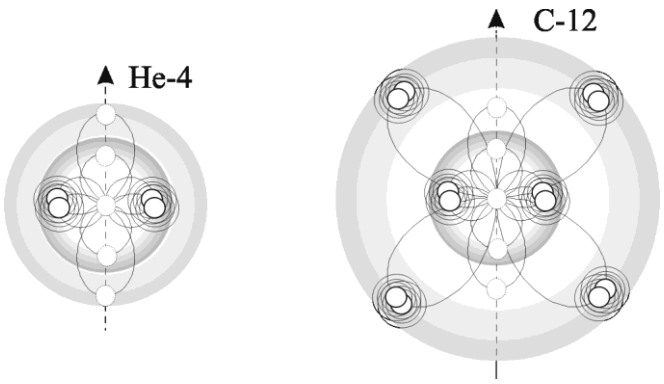

Fig. 3. The nodal structure of helium ^4_2He and carbon $^{12}_6C$.

The nodal structure of carbon isotope $^{12}_6C$ and its polar-azimuth functions are shown also in Fig. 4. The carbon atom has the central empty node (m = 0, l = 0) and four spherical shells:

two shells (m = 0, l = 1, 2) with four empty *potential-kinetic polar nodes* (situated along the z-axis) and one *ring*, two shells ($m = \pm 1; l = 1, 2$) with six completed *potential polar-azimuth nodes* and six empty *kinetic polar-azimuth nodes* (the lasts are not in Fig. 1 and in other figures).

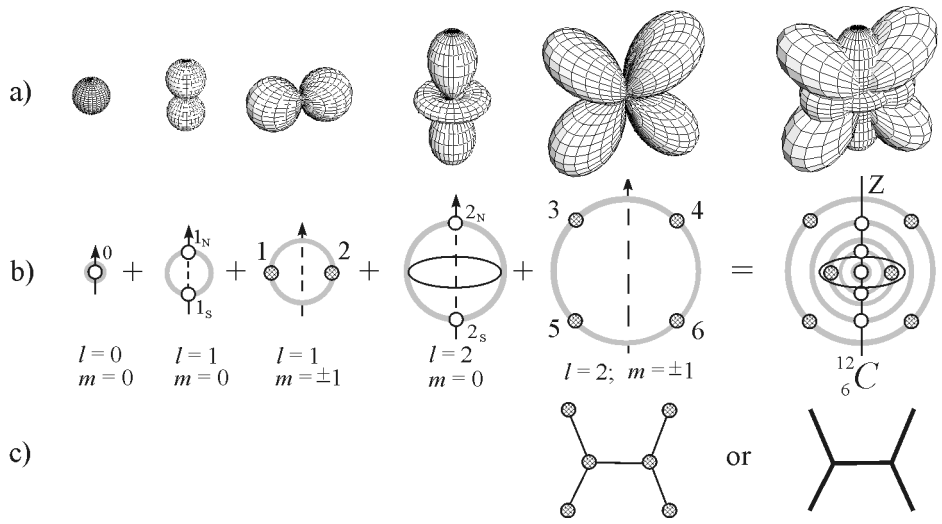

Fig. 4. Plots of potential polar-azimuth functions $\Theta_{l,m}(\theta)\mathrm{Cos}m\varphi$ ($l = 0, 1, 2$; $m = 0, \pm 1$) (a), their extremal points on radial extremal shells $R_l(\rho)$ (b), and the symbolic designation of carbon $_6$C (c).

Six potential polar-azimuth nodes (at $m = \pm 1$), completed every by two H-atoms, lie in one plane: two potential nodes are in the inner shell (l = 1) and the four ones are in the outer shell (l = 2). Six empty kinetic nodes (not shown here) lie in a perpendicular plane with respect to the plane of disposition of potential nodes, on kinetic radial shells.

Hydrogen is mainly in coherent states in Nature, in particular, in the form of coupled atoms – hydrogen molecules H_2. Paired H-atoms, filling polar-azimuth nodes, apparently provide for the stable state of atomic shells. The *condition of coupling*, observed in nature, is inherent not only for H-atoms in nodes of individual atoms, but probably also for individual atoms themselves in solids, liquids, and molecules built on their basis.

The distance r between nodes is defined by roots of Bessel functions $z_{n,m} = kr$, as follows from solutions (3) of the wave equation (2).

3. The energy of exchange

The derivation of binding energy of nucleons, located in nodes of atoms, rests on the Law of Universal Exchange, which originates from the Dynamic Model of Elementary Particles

(DM). Therefore, we will recall now the formula of exchange used for calculations of binding energies here.

As follows from the DM [2], the law of central exchange has the form

$$F = \omega^2 \frac{m_1 m_2}{4\pi\varepsilon_0 r^2}, \tag{5}$$

where ω is the fundamental frequency of exchange, m_1 and m_2 are associated masses defined by the formula $m = \frac{4\pi r^3 \varepsilon_0 \varepsilon_r}{1 + k_e^2 r^2}$, $\varepsilon_0 = 1 g \cdot cm^{-3}$ is the absolute unit density. This law lies at the foundation of nature. If $\omega = \omega_e$, $\omega_e = e/m_e = 1.869162505 \cdot 10^{18}\ s^{-1}$, this law describes exchange (interactions) at the atomic and subatomic levels:

$$F_e = \omega_e^2 \frac{m_1 m_2}{4\pi\varepsilon_0 r^2}. \tag{6}$$

A particular case of the law (5) is the law of universal gravitation, which we present in the form

$$F_g = \omega_g^2 \frac{m_1 m_2}{4\pi\varepsilon_0 r^2}, \tag{7}$$

where ω_g is the fundamental frequency at the gravitational (mega) level of the Universe, *i.e.*, the fundamental gravitational frequency. Its magnitude, defined on the basis knowing the value of the gravitational constant $G = 6.6742 \cdot 10^{-8}\ cm^3 \cdot g^{-1} \cdot s^{-2}$, is equal to

$$\omega_g = \sqrt{4\pi\varepsilon_0 G} = 9.1581 \cdot 10^{-4}\ s^{-1}. \tag{8}$$

The existence of the *gravitational frequency* ω_g and, hence, the corresponding *gravitational radius* of elementary particles $\lambda\!\!\!^{-}_g = c/\omega_g = 327.35\,Mkm$ shows the indissoluble bond of micro- and mega-objects of the Universe in the unit complex of the Infinitely Small and Infinitely Big, as the coexisting polar oppositions.

According to the DM, and the law of the universal exchange (6), the energy of exchange (interaction) of particles is defined, at atomic and subatomic levels, by the formula

$$E = \omega_e^2 \frac{m_1 m_2}{8\pi\varepsilon_0 r}, \tag{9}$$

where $\omega_e m_1 = q_1$ and $\omega_e m_2 = q_1$ are exchange charges of interacting particles. We will use just this formula at the derivation of internodal binding energies of nucleons in atoms.

4. The binding energy of helium ${}^{4}_{2}He$

The binding energy of nucleons in atoms is attributed to three causes and consists of:

(*a*) the binding energy of paired nucleons in nodes, *i.e.*, in essence, it is the energy of deuterons;

(*b*) the binding energy of nucleon nodes with atomic shells to which these nodes belong; and

(*c*) the energy of internodal exchange (interaction) of nucleons.

The derivation of the **first** constituent of the binding energy (*a*) on the basis of the DM and SNM with use of Eq. (9), we will consider latter at the derivation of the binding energy of deuterium. Here, in order to take into account the binding energy of deuterium, we will use the value obtained from the mass defect formula:

$$\Delta E = c^2 \Delta m \tag{10}$$

A deuteron is the nucleus of a deuterium atom, and consists of one proton and one neutron. The mass of the constituents is

$$m_p + m_n = 1.007276 + 1.008665 = 2.015941 amu\,. \tag{11}$$

The atomic mass of the deuteron D (^{2}H) is 2.013553 *amu*; hence, the mass difference is $\Delta m = 0.002388\, amu$. Thus, according to (10), a deuteron's binding energy is

$$E_D = c^2 \Delta m = 2.224\, MeV\ . \tag{12}$$

The **second** constituent of the binding energy (*b*) is defined from the following conditions. In a *spherical atomic field*, radial amplitudes of oscillations of *H*-units in nodes of the *n*-th atomic shell are determined by the expression

$$\hat{A}_s = A\hat{e}_l(kr)/kr \tag{13}$$

originated from solutions of (2) for the radial function $\hat{R}_l(kr)$. Then, the energy of oscillations takes the form [1]:

$$E_s = \frac{m_p \omega^2 A_s^2}{2} = \frac{1}{2} h\nu = \frac{m_p \omega^2}{2}\left(\frac{A}{kr}\right)^2 e_l^2(kr) = \frac{m_p c^2 A^2}{2r^2} e_l^2(kr)\,, \tag{14}$$

where m_p is the mass of *H*-unit. Obviously, that

$$h = 2\pi m_p \upsilon_s A_s = 2\pi m_p \omega \left(\frac{A}{kr}\right)^2 e_l^2(kr) = \frac{2\pi m_p c A^2}{kr} e_l^2(kr)\,, \tag{15}$$

where

$$e_l(kr) = |\hat{e}_l(kr)| = \sqrt{\frac{\pi kr}{2}\left(J^2_{l+½}(kr) + Y^2_{l+½}(kr)\right)}, \tag{16}$$

$J_{l+½}(kr)$ and $Y_{l+½}(kr)$ are the Bessel functions.

At $n = 0$, in the wave zone ($kr = 1$), we have

$$h = 2\pi m_p c A^2 / r_0 . \tag{17}$$

From this, we define the constant *A*:

$$A = \sqrt{\frac{hr_0}{2\pi m_p c}} . \tag{18}$$

In the wave zone, $r_0 = ƛ_e$, then assuming that the radial action for the mass m_p is $h = 2\pi m_p \upsilon ƛ_e$, we arrive at

$$A = \sqrt{\frac{hr_0}{2\pi m_p c}} = ƛ_e \sqrt{\frac{\upsilon}{c}} . \tag{19}$$

If one assumes further the speed υ to be equal to the Bohr speed, the constant *A* takes the value of

$$A = 1.370113189 \cdot 10^{-9}\, cm . \tag{20}$$

Accepted suppositions lead to the following energy of the *H*-unit in a node, at $m_p = m_u$ (atomic mass unit):

$$E_s = \frac{m_u \omega^2 A_s^2}{2} = \frac{m_u \omega^2 A^2}{2(kr)^2} e_l^2(kr) = \frac{\pi\left(J^2_{l+½}(kr) + Y^2_{l+½}(kr)\right)}{2kr} \frac{m_u \omega^2 A^2}{2} . \tag{21}$$

At the level of the fundamental frequency ω_e, we have

$$w_u = \frac{m_u \omega_e^2 A^2}{2} = 3398.72\ keV \tag{22}$$

and

$$E_s = \frac{m_u \omega_e^2 A_s^2}{2} = \frac{w_u}{z_{l,s}^2} e_l^2(z_{l,s}) , \tag{23}$$

where $z_{l,s} = kr$ is the root of Bessel functions [3] .

The binding energy (23) is only an estimation of the bond of an atomic shell with the *n*-node, because it was obtained on the basis of a series of suppositions, which should be regarded as preliminary axioms. A transition from one *n*-shell into another is defined by the energy of transition:

$$\Delta E_s = w_u \left(\frac{e_p^2(z_{p,m})}{z_{p,m}^2} - \frac{e_q^2(z_{q,n})}{z_{q,n}^2} \right). \tag{24}$$

The root $z_{l,s} = y_{0,1} = 0.89357697$ defines the equilibrium distance

$$r_{He} = y_{0,1} \lambda\!\!\!^{-}_e = 1.433196073 \cdot 10^{-8}\ cm \tag{25}$$

between two polar-azimuthal nodes on the external atomic shell of helium ${}^4_2He$ (see Fig. 3). Hence, according to (23), the binding energy of a nucleon node with the atomic shell in helium is

$$E_{shell} = \frac{w_u}{y_{0,1}^2} e_0^2(y_{0,1}) = 3.92109\,MeV\ . \tag{26}$$

The **third** constituent of the binding energy of helium (*c*), the energy of internodal exchange, is determined by the formula (9). The *quantum* of internodal nucleon exchange, $q = m\omega_e$, under formation of internodal bonds at the nucleon ("nuclear") level, is the *nucleon's exchange charge*. It means that the *exchange charge* of two such quanta maximum, by one per every node (proton's or neutron's exchange charge), can take part in the internodal exchange. Then, at $r = r_{He}$ (25), $\omega_e = 1.869162505 \cdot 10^{18}\ s^{-1}$, and the proton's exchange charge $q_p = m_p \omega_e$, where

$$m_1 = m_2 = m_p = 1.67262171 \cdot 10^{-24}\ g \tag{27}$$

is the associated mass of a proton, we have the energy of exchange (per two pairs of nucleons)

$$E_{exch} = \omega_e^2 \frac{m_p^2}{8\pi\varepsilon_0 r_{He}} = 16.91883553\,MeV\ . \tag{28}$$

Hence, the exchange binding energy per nucleon is

$$E_{exch/n} = E_{exch} / 4 = 4.229708883\,MeV\ , \tag{29}$$

and per single internodal nucleon bond (pair),

$$E_{exch/b} = E_{exch} / 2 = 8.459417765\,MeV\ . \tag{30}$$

For estimation, we take into account the double bond between nodes in helium-4 realized by the elementary quantum of internodal nucleon exchange. It means that two pairs of nucleons participate in the internodal bond, so that the whole value (28) must be taken in this case.

As a result, the binding energy of helium atom ${}^{4}_{2}He$ obtained as the sum of three constituents: (12), (26), and (28), is defined by the expression

$$E_{He,atom} = 2E_D + 2E_{shell} + E_{exch} \tag{31}$$

and equal to

$$E_{He,atom} = 2 \cdot 2.224 + 2 \cdot 3.92109 + 16.91883553 = 29.209\,MeV. \tag{32}$$

In the shell-nodal atomic model there is not such a notion as a nucleus. The value (31) was obtained for the helium atom as a whole independently of an existence of two electrons in the helium atom. The contribution of two electrons in the binding energy is insignificant. The energies of electron bond with proton (ionization energies) and of interelectron exchange (interaction) are very small in comparison with the energy of internucleon exchange. Actually, according to the formula of exchange (9), we have

$$E_{e-exch} = \omega_e^2 \frac{m_e^2}{8\pi\varepsilon_0 r_{He}} \approx 5.24\,eV\,, \tag{33}$$

where $\omega_e m_e = e = 1.702691627 \cdot 10^{-9}\ g \cdot s^{-1}$ is the exchange charge of an electron. The energy obtained naturally defines the difference between the two energies of ionization of the helium atom:

$$E_{e-bond} = E_{ion}^{(2)} - E_{ion}^{(1)} = (54.42 - 49.18)\,eV = 5.24\,eV\,. \tag{34}$$

Thus, finally, at the subtraction of energy of two electrons $2E_e = 2m_e c^2$ from (32), the binding energy of helium ion ${}^{4}_{2}He^{-2}$ ("nucleus") is

$$E_{He,ion} = E_{He,atom} - 2E_e = 29.209 - 2 \cdot 0.510998902 \approx 28.187\,MeV\,. \tag{35}$$

If we substitute the neutron's mass $m_n = 1.67492728 \cdot 10^{-24}\ g$ in place of m_p in (27), we will arrive at

$$E_{He,ion} \approx 28.23\,MeV\,. \tag{36}$$

Resulting magnitudes, (35) and (36), almost coincides with the binding energy

$$\Delta E_{He} = c^2 \Delta m \approx 28.3\,MeV \tag{37}$$

obtained for the helium nucleus on the basis of the formula on the mass defect.

5. The binding energy of carbon $^{12}_{6}C$

Basing on solutions of Eq. (2), we must take into account only those shortest internodal bonds in the carbon atom $^{12}_{6}C$ which distinguish by the shortest distances between wave shells of internodal nucleons. Angular directions of such bonds are in more or less extent conditioned by the space geometry of polar-azimuthal functions (see Figs. 2 - 4). Only along these directions shown in Fig. 5*a* the chemical bonds between nucleon nodes of different atoms are realized at formation of molecules and crystals [4].

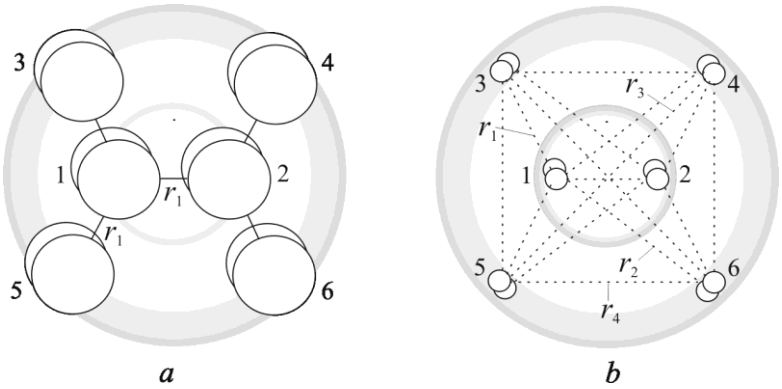

Fig. 5 The geometry of internodal nucleon ("nuclear") bonds in the carbon $^{12}_{6}C$ atom (a) and characteristic internodal distances (b) (between their centers) defined by the roots of Bessel functions.

Five internodal bonds responsible for the binding energy in the carbon atom have the same length $r_1 \approx 2.7 r_0$ (where r_0 is the Bohr radius), defined by the root of Bessel functions $y_{0,1}$ (as in the case of the helium atom):

$$y_{0,1} = 0.89357697, \qquad r_1 = y_{0,1}\lambda\!\!\!^{-}_e = 1.433196073 \cdot 10^{-8}\ cm \tag{38}$$

All other characteristic internodal distances in the carbon atom, shown in Fig. 5*b*, are not arbitrary as well. They are defined, as r_1, by the roots of Bessel functions. This is justified by regularities of wave processes, described by the Bessel functions that influence the strictly definite structure of the material spaces at all level:

$$y_{1/2,1} = 1.57079633 \qquad r_2 = y_{1/2,1}\lambda\!\!\!^{-}_e = 2.519379088 \cdot 10^{-8}\ cm$$

$$j_{0,1} = 2.40482556 \qquad r_3 = j_{0,1}\lambda\!\!\!^{-}_e = 3.857067342 \cdot 10^{-8}\ cm \tag{39}$$

$$j'_{1,1} = 1.84118378 \qquad r_4 = j'_{1,1}\lambda\!\!\!^{-}_e = 2.953049879 \cdot 10^{-8}\ cm$$

As in the case of the helium atom, three constituents of the binding energy must be taken into account. The first one, considering the coupling of two nucleons in a node in the form of deuteron, gives us the deuteron's binding energy E_D of 2.224 *MeV* (12) per node.

The second constituent of the binding energy takes into account the bond of a node with the atomic shell where this node is located. According to (23) and (24), for the 1st and 2nd nodes (Fig. 5) situated at the internal atomic shell (the shell of helium), we have $z_{l,m} = y_{0,1}$ and $E_{\text{int},shell} = 3.92109\,MeV$ (26).

Transitions of nucleons from the internal shell to the external shell, where four nodes are located, are defined by the formula of energy of transitions (24). For $z_{p,m} = y_{0,1}$ and $z_{q,n} = y_{1/2,1}$, we have $E_{trans} = 2.54363\,MeV$. The binding energy for every of four nodes of external shell is

$$E_{ext,shell} = \frac{w_u}{y_{1/2,1}^2} e_{1/2}^2(y_{1/2,1}) = 1.37745\,MeV\,. \qquad (40)$$

The third constituent of the binding energy of the carbon atom ${}^{12}_{6}C$, the energy of internodal exchange, is determined by the formula (9). According to the latter, an elementary binding energy, caused by exchange interaction between two nodes a distance r_1 apart, is

$$E_{exch} = \omega_e^2 \frac{m_p^2}{8\pi\varepsilon_0 r_1} = 16.91883553\,MeV \qquad (41)$$

(as in the case of the helium atom (28)).

The exchange energy (41) (of the quantum of nucleon exchange $q_p = m_p\omega_e$) of the 1st node (Fig. 5*a*) expends on three equal bonds with 2nd, 3rd, and 5th nodes; and the 2nd node, with 1st, 4th, and 6th nodes. Hence the binding energy per node (we mean 1st and 2nd nodes here) is

$$E_{exch,1} = (1/3)E_{exch} = 5.639611843\,MeV/node\,. \qquad (42)$$

Every node of the 3rd, 4th, 5th, and 6th nodes are connected only with one node (1st or 2nd). Hence, the binding energy per node (for nodes from 3rd to 6th) is

$$E_{exch,2} = (1/2)E_{exch} = 8.459417765\,MeV/node\,. \qquad (43)$$

Thus, we have the following internodal binding energies between the nodes of the numbers (1-2):

$$E_{exch,1-2} = 2E_{exch,1} = 11.27922369\,MeV/bond\,; \qquad (44)$$

the numbers (3-1), (5-1), (4-2), (6-2):

$$E_{exch,3-1} = E_{exch,1} + E_{exch,2} = 14.09902961 MeV / bond \quad (45)$$

Thus, the total energy of internodal exchanges is

$$E_{\text{int},exch} = E_{exch,1-2} + 4E_{exch,3-1} = 67.67534212 MeV . \quad (46)$$

A resulting sum of all constituents of binding energy of the carbon atom $^{12}_{6}C$, calculated for q_p: (12), (26), (40), and (46), is

$$E_{C,atom} = 6E_D + 2E_{\text{int},shell} + 4E_{ext,shell} + E_{\text{int},exch} = 94.37132212 MeV . \quad (47)$$

(Calculations for the exchange charge of a neutron $q_n = m_n \omega_e$ give 94.48781375 *MeV*).

At subtraction of the energy of four valent electrons, $4E_e = 2.022 MeV$, from (47), we arrive at the energy of the carbon ion $^{12}_{6}C^{-4}$,

$$E_{C,ion} = E_{C,atom} - 4E_e = 92.34932212 MeV . \quad (48)$$

Thus, the binding energy of the carbon ion $^{12}_{6}C^{-4}$, obtained here on the basis of shell-nodal atomic model and the DM, is in well agreement with the binding energy of the carbon nucleus $^{12}_{6}C$ equal to $92.488 MeV$, calculated from the formula on the mass difference, $\Delta E = c^2 \Delta m$.

For the derivation described above, the used value of the first constituent of the binding energy of helium and carbon atoms, 2.224 *MeV*, originates from the well-known formula $E_D = c^2 \Delta m$ (12). It is the binding energy of deuteron D ($^{2}_{1}H$). We have the right to take this value assuming that according to shell-nodal atomic model the coupled protons and neutrons in nodes are in the form of deuteron.

We will show further that the binding energy of deuteron E_D is also derived on the new basis accepted in this work, just like the derivation of the binding energy of helium and carbon atoms. This aim is achieved on the basis of the supposition that solutions of the wave Eq. (2), resulted in the shell-nodal structure of atomic and interatomic (crystal or molecular) spaces (Fig. 1), are also valid for the subatomic (intra-nucleon) space. It means that basic constituents of atoms, protons and neutrons, have the same shell-nodal internal structure depicted graphically in Fig. 1. In this connection, we will explain first of all our point of view on the nucleon structure and answer to the question: what particles of the subatomic level are the main “building bricks” for nucleons?

Let us proceed to elucidate now this question as it is solved in the framework of the Dynamic Model of Elementary Particles.

6. The g-lepton structure of proton and neutron

The spectrum of associated masses, following from the DM, is considered in detail in L. 11 and L. 12 of Vol. 3. In dependence on the character of exchange, we distinguish the masses in the longitudinal exchange (at motion-rest in the cylindrical field of matter-space-time), the masses in the transversal exchange (transversal oscillations of the wave beam), and the masses in the tangential exchange (at motion-rest in the cylindrical space-field).

We have come to the conclusion that the result obtained gives the reason to assume that *g*-lepton is a highly stable particle, which possibly is a constituent (like a nucleon for atoms) of protons, neutrons, and other elementary particles of this series. If only this is true, then on the basis of g-lepton and the periodic law of space [5], it is possible to compose the spectrum of elementary particles. In such a spectrum, *g*-lepton is hydrogen analog, γ-quantum is deuterium analog, μ-meson is tritium analog, π-meson is helium analog, *etc*.

The *g*-lepton has the following elementary charge

$$q_g = \varepsilon_0 hc / e = 68.5e\,. \tag{49}$$

The division of the charge q_g by the fundamental frequency ω_e gives its associated mass:

$$m_g = 68.5 m_e\,. \tag{50}$$

Evidently, *g*-lepton and the Dirac monopole *g* are the same particle. At that time, the mass of the monopole was determined incorrectly, therefore, *g*-lepton was not rendered due attention.

The radius of its sphere, defined from the formula of associated masses ((21), V. 2, L. 2) $m_g = \dfrac{4\pi r_g^3 \varepsilon_0 \varepsilon_r}{1 + k_e^2 r_g^2}$, at the condition $k_e^2 r_e^2 << 1$, $\varepsilon_0 = 1\, g \times cm^{-3}$, and $\varepsilon_r = 1$ (at the field level), is equal to

$$r_g = \left(m_g / 4\pi\varepsilon_0\right)^{1/3} = 1.706 \cdot 10^{-9}\ cm \approx 4 r_e\,. \tag{51}$$

We see that r_g is very close to the rational golden section of the fundamental metrological period Δ:

$$r_g \approx \frac{5}{8} 2\pi \lg e \cdot 10^{-9}\, cm\,. \tag{52}$$

Accepting the supposition that nucleons (protons and neutrons) consist of g-leptons, we must recognize that nucleons represent by themselves, by analogy with atoms of the nucleon level, the silicon of the g-lepton level of the atomic number 14 (having 14 nodes according to solutions of Eq. (2) presented in Fig. 1). Indeed, let the mass of g-lepton will be precisely multiple to a quarter of the fundamental period, with respect to the electron mass m_e,

$$m_g = (1/4)2\pi \lg e \cdot 10^2 \, m_e = 68.21881769 \, m_e . \qquad (53)$$

The masses of proton and neutron are, correspondingly,

$$m_p = 1836.1526675 m_e \qquad \text{and} \qquad m_n = 1838.683645 m_e . \qquad (54)$$

Hence, it is clear that the mass number of nucleons at the g-lepton level must be rather more than 27, because of the relation,

$$m_n / m_g = 26.95273397 , \qquad (55)$$

with taking into account an essential value of the binding energy of g-leptons influenced on the resulting mass of nucleons.

On this basis, we assume that protons and neutrons represent, respectively, at the g-lepton level, two stable isotopes analogous, in nodal structure, to the silicon isotopes, ${}^{28}_{14}Si$ and ${}^{29}_{14}Si$. Their nodal structure, in full agreement with solutions of the wave equation (2) (Fig. 1), is presented in Fig. 6. The polar-azimuthal functions of ${}_{14}Si$ and spatial disposition of its spherical shells and potential nodes are shown in Fig. 7.

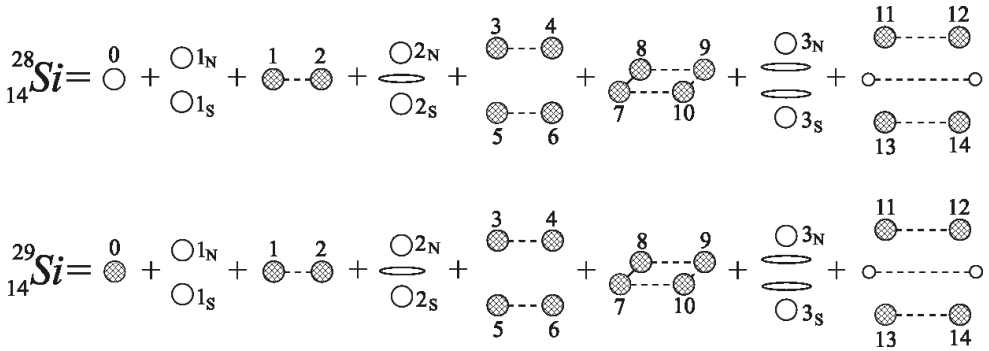

Fig. 6. A symbolic design of the shell-nodal structure of silicon, ${}^{28}_{14}Si$ and ${}^{29}_{14}Si$, in accordance with the shell-nodal structure of atoms shown in Fig. 1.

Thus, we regard a neutron of the ${}^{29}_{14}Si$ structure, in the above meaning, as one of the unstable isotopes of protium (the simplest hydrogen atom ${}^{1}_{1}H$). The neutron contains additionally one g-lepton in comparison with the proton of the ${}^{28}_{14}Si$ structure. We assume that this g-lepton is in the central polar *potential-kinetic* node (such nodes are metastable places for constituent particles) and forms with an electron a *g-e* pair (see Fig. 8).

As follows from calculations, the paired electron of the central node is responsible for the negative magnetic moment of the neutron. The neutron is a stable isotope only in a bond state

with other neutrons, like $^{29}_{14}Si$. It decays during $\tau = 1000\,s$ to a proton (the $^{28}_{14}Si$ analogous), an electron, and a neutral g-lepton (an antineutrino $\tilde{\nu}$ of nuclear physics):

$$n \rightarrow p + e^{-} + g\,. \qquad (56)$$

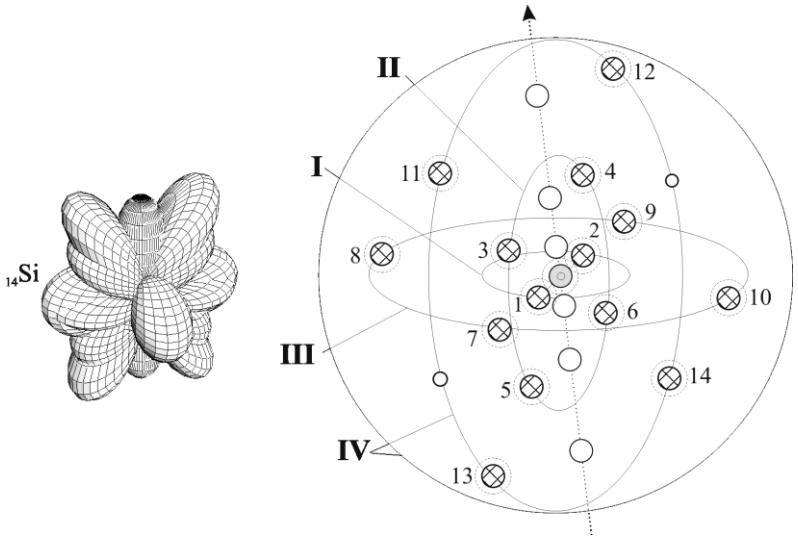

Fig. 7. The structure of polar-azimuthal functions (at the left), and the space arrangement of the 14 polar-azimuthal nodes in four (**I – IV**) spherical shells of $_{14}Si$.

The shell-nodal structure of $^{28}_{14}Si$ (and $^{29}_{14}Si$) (Fig. 6 and 7) is more complicated than the shell-nodal structure of $^{12}_{6}C$ (Fig. 4), because it has two shells and eight nodes more (at $l = 2, m = \pm 2$ and $l = 3, m = \pm 1$). An internal shell (I) with two polar-azimuthal nodes (1, 2) is the shell of the helium atom (see Fig. 3). The second internal shell (II) is the external shell of the carbon atom. The third shell (III) is the external shell of the neon atom. The shell IV is the external shell characteristic for the silicon atom.

According to SNAM, the unrepeatable (specific) structure of external shells mainly defines individual properties of atoms distinguishing them from each other. The external shell of $_{14}Si$ has two collateral nodes not completed by nucleons in the isotopes of silicon under consideration. Silicon is the first element of the periodic table with such nodes (unnumbered in Fig. 1 and other figures), which are metastable states judging from the fact that amplitudes of polar-azimuthal functions determining their positions on shells are essentially smaller that corresponding amplitudes of principal (numbered in presented figures) nodes. This feature provides the motion, in its internal space, not only of particles, which are much less than nucleons, but also the motion of nodal nucleons themselves. Quantum theory interprets this phenomenon as the motion of "holes".

A neutron has the negative magnetic moment of the value

$$\mu_n = -0.96623640(23)\cdot 10^{-26}\ J\cdot T^{-1} \qquad (57)$$

(according to the CODATA [6]). This magnitude is approximately in 1.46 times less in absolute value than the (positive) magnetic moment of a proton. A simplified picture of the neutron g-lepton structure with the surrounding field looks conditionally as it is depicted graphically in Fig. 8.

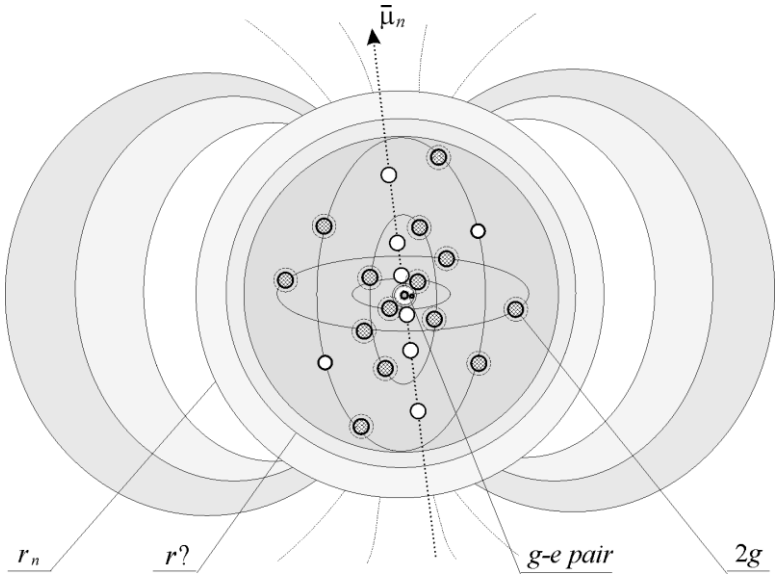

Fig. 8. A neutron as an analogous of the silicon atom $^{29}_{14}Si$ with the surrounding field; r_n is the neutron outer shell; g-*e* is the g-lepton-electron pair; *r*? is the inner radius of the neutron shell; 2*g* is the condition designation of 14 principal polar-azimuthal *potential* nodes completed with coupled *g*-leptons (the 29th g-lepton coupled with an electron is in the central polar *potential-kinetic* node, on the z-axis); $\bar{\mu}_n$ is the magnetic moment of the neutron.

According to the formula of mass defect (10), the binding energy of a proton, consisted of 28 g-leptons, is to be

$$\Delta E(p) = c2\Delta m = c^2(28m_g - m_p) = 62.79769638\,MeV\ , \qquad (58)$$

so that the binding energy per g-lepton is

$$\varepsilon(p) = \Delta E(p)/A(p) = 2.242774871 MeV\ , \qquad (59)$$

where $A(p) = 28$ is the mass number of a proton at the g-lepton level.

The corresponding values for a neutron ($A(n) = 29$) are

$$\Delta E(n) = c^2(29m_g - m_n) = 71.36715712\,MeV\ , \qquad (60)$$

$$\varepsilon(n) = \Delta E(n)/A(n) = 2.460936452\,MeV\ . \qquad (61)$$

Now, resting on the shell-nodal g-lepton structure of nucleons, we can proceed to derive the binding energy of deuterium and tritium regarding them as the junction, respectively, of two and three g-lepton systems (pairs)

7. The binding energy of deuterium ${}^{2}_{1}H$ and tritium ${}^{3}_{1}H$

At the joining of two H-atoms, of a neutron and the hydrogen atom ${}^{1}_{1}H$ (protium), the deuterium atom ${}^{2}_{1}H$ is formed. The process of joining results in the penetration of spaces of one nucleon into another, so that the partial overlapping of spherical shells of both nucleons occurs. With this, all g-lepton nodes (Fig. 8), filled with coupled g-leptons, of one nucleon and corresponding nodes of another nucleon draw together at the distance *r* defined by solutions of the wave equation (2) (*i.e.*, by the roots of Bessel functions). As a result, 28 helium structures on the basis of binding of approached pairs of coupled g-leptons, like that one shown in Fig. 9, are formed.

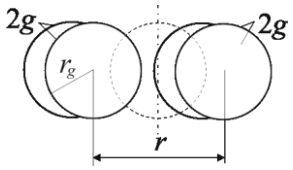

Fig. 9. The helium structure formed on the basis of binding of two g-lepton nodes.

The distance *r* between the nodes is defined by roots of Bessel functions

$$z_{m,n} = kr. \tag{62}$$

The unknown value in this expression is the wave number *k* equal to the inverse value of the wave radius $\lambda\!\!\!^{-}$,

$$k = 1/\lambda\!\!\!^{-}. \tag{63}$$

The wave radius $\lambda\!\!\!^{-}$ defines the characteristic radii of elementary spherical and cylindrical surfaces described by Bessel functions with zero and extremal values. As we saw above, at the *nucleon level*, $k = 1/\lambda\!\!\!^{-}_{e}$, where $\lambda\!\!\!^{-}_{e} = 1.603886538 \cdot 10^{-8}\, cm$ originates from the DM. The wave radius of the value $\lambda\!\!\!^{-}_{e}$ is responsible for the arrangement of *nucleons* in atoms, and hence in crystals, molecules, *etc*. at the definite absolute distances. Accordingly, it is not a random coincidence that the wave diameter of

$$2\lambda\!\!\!^{-}_{e} \approx 3.2 \cdot 10^{-8} cm \tag{64}$$

is equal, in average, to lattice parameters of crystals. Thus, the wave radius at the nucleon level $\lambda\!\!\!^{-}_{n}$ is equal to (coincides with) the fundamental wave *radius of exchange*

$$\lambda\!\!\!^{-}_{n} = \lambda\!\!\!^{-}_{e} = c / \omega_e , \tag{65}$$

it defines the principal parameters of atomic spaces. Note that

$$\omega_e = e / m_e \tag{66}$$

is the fundamental *frequency of exchange* at the atomic and subatomic levels (the frequency of the "electrostatic field").

Obviously, spaces of the g-lepton level (we mean the internal spaces of nucleons) have another absolute value of the wave radius. The spherical space of a nucleon, like the spherical space of an atom, is also a system of wave shells, but its own whose relative size is defined by the *relative* radius $\rho = kr = z_{m,n}$. The internal proper shells of nucleons with its own nodes, where g-particles are localized, form the superfine discrete structure of atoms.

Thus, we stressed again that solutions of the wave equation (2) give only the *relative* radius ρ, and hence, the *relative* value of the corresponding wave radius $\lambda\!\!\!^{-}$. The a*bsolute* value of the latter one must seek from some conditions general for wave processes at different levels.

We will define $\lambda\!\!\!^{-}$ from the scale analogy which exists between wave processes at any levels and, in particular, which must exist between ones at the nucleon and g-lepton levels. The matter is that the fundamental relations existed between the main wave parameters in both scales must keep. One of the fundamental relations exists between the radius of the wave spherical shell of a proton r_p and the fundamental wave radius $\lambda\!\!\!^{-}_{e}$ of exchange of the proton with other particles and the surrounding field. The theoretical radius of the wave shell of the proton (proton's radius for short), obtained from the formula of mass at the condition $(k_e r_p)^2 << 1$ and $\varepsilon_r = 1$, is

$$r_p(th) = (m_p / 4\pi\varepsilon_0)^{1/3} = 0.510578616 \cdot 10^{-8}\, cm . \tag{67}$$

The fundamental wave radius is

$$\lambda\!\!\!^{-}_{e} = c / \omega_e = 1.603886538 \cdot 10^{-8}\, cm . \tag{68}$$

The ratio of both magnitudes is equal, with some accuracy, to the fundamental constant π,

$$\lambda\!\!\!^{-}_{e} / r_p(th) = 3.141311617 \approx \pi . \tag{69}$$

This ratio shows that the wave radius $\lambda\!\!\!^{-}_{e}$, in value, is a half of the length of the equatorial circumference of the wave spherical shell of a proton. Obviously, the same ratio must be

valid for the radius of the wave spherical shell of g-lepton, r_g, and the wave radius of the g-lepton level, $\lambda\!\!\!^{-}_g$, so that we have the right to assume that

$$\lambda\!\!\!^{-}_g / r_g(th) = \pi . \tag{70}$$

Hence, for

$$r_g(th) = (m_g / 4\pi\varepsilon_0)^{1/3} = 0.170370509 \cdot 10^{-8}\ cm \tag{71}$$

with $m_g = 6.214420763 \cdot 10^{-26}\ g$ (see (53)), the wave radius of the g-lepton level $\lambda\!\!\!^{-}_g$ is

$$\lambda\!\!\!^{-}_g = \pi r_g(th) = 0.534 \cdot 10^{-8}\ cm . \tag{72}$$

Note that the mass of g-lepton is close to a quarter of the fundamental period D (in units of the electron mass) [7, 8]:

$$m_g = \frac{1}{45}(2\pi \lg e) \cdot 10^2\ m_e \tag{73}$$

We see that the value of $\lambda\!\!\!^{-}_g$ obtained on the basis of a series of approximations is close to the Bohr radius $r_0 = 0.529 \cdot 10^{-8}\ cm$. It is quite possible that more accurate derivations will lead to the equality $\lambda\!\!\!^{-}_g = r_0$. Thus, we cannot exclude the equality of the above parameters: of the Bohr radius and the wave radius of g-lepton level $\lambda\!\!\!^{-}_g$, which both are the basic parameters of the wave sphere atomic space.

Hence, taking the root of Bessel functions, $z_{m,n} = y_{0,1} = 0.89357697$, as in the case of the helium atom, we arrive at the following distance r between two pairs of g-leptons (see Fig. 9) in coupling nucleons:

$$r = y_{0,1}\lambda\!\!\!^{-}_g = 0.477 \cdot 10^{-8}\ cm . \tag{74}$$

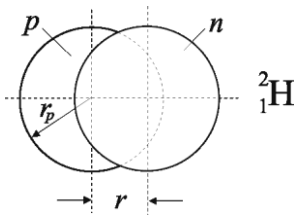

Fig. 10. The relative disposition of two nucleons in the deuterium atom ^2_1H; $r < r_0$.

It means that wave spherical shells of two H-atoms in the deuterium ^2_1H are partially overlapped as is shown in Fig. 10 (where $r_p = 0.51 \cdot 10^{-8}\ cm$ (67)). Centers of masses of two constituent H-atoms are at the distance $r = 0.477 \cdot 10^{-8}\ cm$, which is some less than the Bohr radius, $r < r_0$.

At such conditions (distance r of the value (74)), the binding energy of internodal g-leptons pairs (Fig. 9) is

$$E_g = \frac{q_g^2}{8\pi\varepsilon_0 r} = 0.070246848 \cdot 10^6 \, eV \,, \qquad (75)$$

where

$$q_g = m_g \omega_e = 1.161576228 \cdot 10^{-7} \, g \cdot s^{-1} \qquad (76)$$

is the exchange charge of the g-lepton, which is an elementary quantum of exchange at the g-lepton level.

According to the above definition (model), a proton has 28 g-leptons (14 nodes filled every with 2 coupled g-leptons). A neutron, in comparison with the proton, has one more g-lepton located in the central polar node (see Figs. 6 and 7). Thus, because of all g-leptons take part in the exchange (interaction), we have 28.5 pairs of interacting g-leptons in ${}_1^2H$. Hence, the resulting binding energy, related to the internodal exchange (interaction) of all g-leptons belonging to two interacting nucleons, is

$$E_{g,exch} = 28.5 \cdot E_g = 2.002 \, MeV \,. \qquad (77)$$

The obtained value is close to the known value of 2.224 *MeV* (12) for the binding energy of a deuteron. It is the main (1st) but not alone constituent of the total binding energy of ${}_1^2H$ (as in the case of helium and carbon atoms considered above). By accepted analogy between wave processes at two levels under consideration (nucleon and g-lepton), we must take also into account (2nd) the energy of coupling of two g-leptons in their nodes and (3rd) the binding energy of g-lepton nodes with the shells where these nodes are located.

However, we will not derive the rest (2nd and 3rd) constituents here. The derivation of the third one was carried out for helium and carbon atoms. A rough estimate of these constituents of the binding energy on the basis of the analogy between two-nodal structure of helium and two-nodal g-lepton helium structure (Fig. 9) will be quite sufficient here.

In this connection, let us assume that the ratio existed between the total binding energy of helium ${}_2^4He$, 28.3 *MeV*, and its second constituent, the binding energy of coupled nucleons in its nodes (*i.e.*, the binding energy of deuterium), 2.224 *MeV*, keeps the same and for the corresponding g-lepton helium structure shown in Fig. 9. In this case, because the total binding energy of all 28 g-lepton helium structures must be equal to 2.224 *MeV* (according to (12)), the binding energy of all g-lepton "deuterons" in all g-lepton nodes must be

$$E_{g(2)} = 0.175 \, MeV \,. \qquad (78)$$

And the binding energy of one g-lepton "deuteron" is

$$\varepsilon_{2g} = 6.25 keV. \quad (79)$$

Hence, finally, we arrive at the following binding energy of ${}^{2}_{1}H$:

$$E({}^{2}_{1}H) = E_{g,exch} + E_{g(2)} + E_{g(3)} = 2.177\, MeV + E_{g(3)}. \quad (80)$$

Obviously, the contribution of the third constituent $E_{g(3)}$, corresponding to the binding energy of all 28 g-nodes with their wave spherical shells will be less than the contribution of the second constituent estimated above. Therefore, we assume that after adding of $E_{g(3)}$ to the total energy we will closer approach to the value 2.224 *MeV*, which follows from the formula on mass defect (12).

In addition, let us proceed now to the derivation of the binding energy of tritium. The shell-nodal structure of three joined g-lepton nodes in tritium (belonging to three interacting nucleons), on the g-lepton level, recalls the nodal structure of helium isotope ${}^{6}_{2}He$ (Fig. 11). Appearance of two coupled g-leptons in the central polar node slightly changes (increases) the former equilibrium distance *r* existed between outmost pairs of g-leptons in the g-lepton helium structure shown in Fig. 9.

The nearest to the $r = 0.477 \cdot 10^{-8}\, cm$ equilibrium distance between g-lepton nodes, admitted by solutions of the wave equation (2), is the distance equal to the wave radius of the g-lepton level, $\lambda\!\!\!^{-}_{g} = 0.534 \cdot 10^{-8}\, cm$. Therefore, we accept this value of the distance between the outermost g-lepton nodes in tritium (Fig. 11) for further calculations, so that we have

$$r = \lambda\!\!\!^{-}_{g} = 0.534 \cdot 10^{-8}\, cm,$$

$$r_1 = r_2 = \lambda\!\!\!^{-}_{g} / 2 = 0.267 \cdot 10^{-8}\, cm. \quad (81)$$

We also assume that the exchange interaction in the presented structure exists between every two partially overlapped pairs as is shown conditionally by two arrows in Fig. 11.

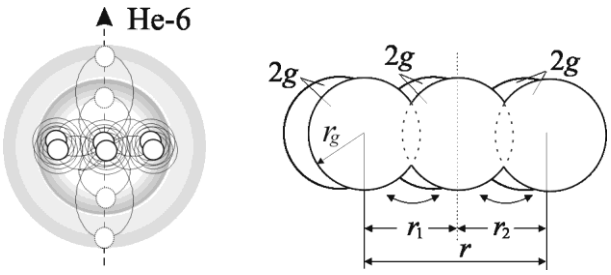

Fig. 11. The nodal structure of helium isotope ${}^{6}_{2}He$, and the local structure formed under the joining of three g-lepton nodes in tritium regarded as the *p-n-n* system.

The main constituent of the binding energy in this case, the energy of internodal exchange between two nearest nodes, is

$$E_g = \frac{q_g^2}{8\pi\varepsilon_0 r_1} = 0.140493696\,MeV\,. \qquad (82)$$

Hence, the total binding energy of internodal exchange, with allowance for all g-lepton bonds in tritium, is

$$E_{g,exch} = N_{g,bonds} \cdot E_g = 8.07838752\,MeV\,, \qquad (83)$$

where $N_{g,bonds} = 57.5$ is the number of internodal g-lepton bonds (*p*-*n* and *n*-*n*, 28.5+29) in tritium consisted of two neutron and one proton.

The second constituent, the total binding energy of all g-lepton "deuterons" in tritium, is (according to (79))

$$E_{g(2)} = N_{g-nodes} \cdot \varepsilon_{2g} = 0.2625\,MeV\,, \qquad (84)$$

where $N_{g-nodes} = 3 \cdot 14 = 42$ is the number of completed polar-azimuth g-lepton nodes (or the number of coupled g-leptons).

Without the smallest in value contribution of the third constituent $E_{g(3)}$ (related to the binding energy of g-lepton nodes with the shells of their localization), we obtain finally the following magnitude

$$E({}_1^3H) = E_{g,exch} + E_{g(2)} = 8.34088752\,MeV\,. \qquad (85)$$

For comparison, the binding energy of tritium, originated from the formula (10), is

$$\Delta E = c^2 \Delta m = 8.481821\,MeV\,. \qquad (86)$$

Thus, we have an approximate coincidence in the resulting data obtained by two ways different of principle.

8. Interatomic bindings

In accordance with the shell-nodal atomic model, we consider atoms as elementary quasi-spherical *multiplicative* molecules of the hydrogen atoms. The word "*multiplicative*" means that the particles (hydrogen atoms), constituents of these elementary molecules, are bound by the *strong force* (analogous in value to common "*nuclear*"). Accordingly, we call the intra-atomic internodal bindings by the word *multiplicative.*

Ordinary molecules with relatively weak (chemical) bonds (analogous to cohesive or adhesive bonds), we call *additive* molecules. They are related to the electron level of binding.

For example, if deuterium D ($^{2}_{1}H$), an isotope of the hydrogen atom containing two hydrogen atoms) is the *multiplicative* molecule then the hydrogen molecule ($^{1}_{1}H_{2}$) containing also two hydrogen atoms is the *additive* molecule. Accordingly, in the latter case we have relation with *additive bindings*.

Therefore we should distinguish *additive bindings* from *multiplicative bindings*. Thus, in the light of the shell-nodal atomic model, elementary molecules of the hydrogen atoms and common molecules formed on their basis differ in principle by the different character of bindings in these molecules: *intra-molecular* (*multiplicative*) in the elementary molecules and *intermolecular* (*additive*) in the common molecules.

Let us proceed now to estimating the *electron level* of the bindings, the level of *additive bindings*. The energy of electron binding is equal to

$$E_e = \omega_e^2 \frac{m_e^2}{8\pi\varepsilon_0 \lambda\!\!\!^{-}_e} \approx 4.49\ eV\,, \tag{87}$$

where $\lambda\!\!\!^{-}_e$ is the fundamental wave radius defining the *characteristic distances* in wave atomic spaces,

$$\lambda\!\!\!^{-}_e = \frac{c}{\omega_e} = 1.603886538 \cdot 10^{-8}\ cm\,, \tag{88}$$

ω_e is the fundamental frequency of the atomic and subatomic level, and

$$\omega_e m_e = e = 1.702691627 \cdot 10^{-9}\ g \cdot s^{-1} \tag{89}$$

is the *minimal quantum of the rate of mass exchange*, the electron exchange charge; $\varepsilon_0 = 1\ g \cdot cm^{-3}$ is the absolute unit density.

The energy obtained, 4.49 *eV*, predetermines the electron work function of solids. For instance, the electron work function of mono- and polycrystals of Al, B, Bi, W, Fe, Co, and Cu is within $4.25 \div 4.67\ eV$ [9, 10].

The energy (87) practically coincides with the dissociation energy of the molecules: H_2 (4.48 *eV*), HD (4.51 *eV*), HT (4.52 *eV*) and close to the dissociation energy of the molecules O_2 (5.1 *eV*) and OH (4.4 *eV*) [11] (p. 425), *etc*. The energy of electron binding (87) correlates with the break energy of bindings in molecules and radicals. For instance, it is equal to 5.0 *eV* in reactions $H_2O \rightarrow H + OH$ and $N_2O \rightarrow NO + N$; in $NaOH \rightarrow Na + OH$, it is 4.8 *eV*.

The binding energy (of the electron level) per mole of substance defines the characteristic break energy (dissociation) of chemical bonds,

$$E_e = \frac{e^2}{8\pi\varepsilon_0 \lambda\!\!\!^{-}_e} N_A = 433.1211762\ kJ \cdot mol^{-1} = 103.4492\ kcal \cdot mol^{-1} \tag{90}$$

where N_A is the Avogadro number.

A definite energy is spent upon tearing off the hydrogen atom from a node of the improper shell. In accordance with the experimental data [9, 12], this energy is equal to $101\,kcal\cdot mol^{-1}$ for CH_4 and $104\,kcal\cdot mol^{-1}$ for C_2H_4 that is consistent with the obtained value (90). Obviously, in a case of breaking of two bonds simultaneously, the break energy must be approximately twice as much. Actually, a breakdown of O_2 molecule with two similar bonds requires about $179\pm17\,kcal\cdot mol^{-1}$. The additive bindings (of the electron level) show its worth in the molar heat capacity of molecules and other phenomena considered in detail in [1].

9. Conclusion

Thus, the shell-nodal atomic model on the basis of a unified theoretical concept of the wave exchange interaction reveals the nature and mechanism of *multiplicative* (called in modern physics "*nuclear"*) and *additive* ("*chemical"*) bindings.

If we will assume that external and internal spaces of hydrogen atoms are delimited by the Bohr radius $r_0 = 5.291772083\cdot10^{-9}$ *cm*, so that the mass of the hydrogen atoms calculated from the formula of associated mass, $m = \dfrac{4\pi r_0^3 \varepsilon_0}{1+k_e^2 r_0^2}$, is equal to $m_{\text{H}} = 1843.524607\ m_e$.

The *rate of mass exchange* (or, in other words, *exchange charge* of the hydrogen atom) responsible for internodal bindings between atomic constituents, the hydrogen atoms, is equal to

$$q_H = \omega_e m_H = 3.138953779\cdot10^{-6}\ g\cdot s^{-1}. \qquad (91)$$

The rate of mass exchange of such a value determines the high stability of individual atoms. Actually, the energy of interchange (interaction) of two separate hydrogen atoms (situated in two conjugated nodes of the same atom) being apart at the distance $r = 1.40\cdot10^{-8}$ *cm* (that is the length of double bindings in graphite, see Figure 8 in L. 6), is equal to

$$E = \frac{q_H^2}{8\pi\varepsilon_0 r} = 17.478\ MeV\ . \qquad (92)$$

This value correlates with the experimental data for the binding energy of neutron in a carbon nucleus and with the threshold energy of (γ, n) reactions [11] equal to 18.7 *MeV*. If we shall take the length $r = 1.31\cdot10^{-8}$ *cm* quoted from [13], corresponding to the isolated double binding in $C=C=C$ and $CH_2=C=O$ structures, the obtained internodal energy of interaction of constituent hydrogen atoms of 18.679 *MeV* (following from Eq. 92), will practically coincide with the above threshold energy of (γ, n) reactions. Accepting $r = 1.15\cdot10^{-8}$ *cm* (indicated in brackets in Figure 8 of L. 6), we arrive at the energy E= 21.4 *MeV*

that is close to the threshold energy 20.3 *MeV* of (*n*, 2*n*) reactions in $^{12}_{6}C$ isotope [11] (p. 887), *etc*.

The energy of interchange (interaction) of two separate hydrogen atoms situated in two conjugate nodes of the same atom being apart at $r = 1.45 \cdot 10^{-8}$ *cm* is equal to 16.875 *MeV*. The taken distance *r* is the length of a single binding between the internal nodes 1 and 2 (see Figures 6 and 8a in L. 6). This distance is also equal to an averaged characteristic length of different bindings with participation of oxygen (S – O, C – O, N – O, B – O, *etc*. [13]). The obtained energy correlates with the experimental value for the binding energy of neutron in an oxygen nucleus and with the threshold energy of (γ, n) reactions in the nucleus, equal to 16.3 ± 0.4 *MeV* [11].

The shell-nodal atomic model allows understanding the physics of atomic reactions caused by an inelastic interaction with matter of high-energy particles. The *d*-, *p*-, and *n*-emanation occur when nodal hydrogen atoms are removed from their nodes for some reasons.

The main "structural" units of the shells are bound pairs of nearest potential nodes filled with coupled hydrogen atoms (representing by themselves deuterons) belonging to two outer shells. As outgoing important elementary parts of atomic shells, these two strongly bound nodes, completed each with two hydrogen atoms, form α-radiation.

A "splitting off" of external shells of heavy atoms with the formation of lighter elements takes place under powerful impact. "Elementary" splinters, such as *p*, *n*, and *t* ($^{3}_{1}H^{+}$), appear in such cases as well.

Thus, the obtained results justify in favor of the validity of conceptually a new basic physics theory developed as an alternative to the Standard Model. Concerning hierarchy of particles beginning from an electron up to a nucleon, considered in Lectures 11-13 of Vol. 3, we can add the following.

As was discussed earlier in Vol. 3, it is possible to suppose that electron at the g-level is a very miniature nucleon. Then g-lepton, judging from its reference mass $m_g = 68.22 m_e$, represents a composite atom-molecule of the electron level with the ordinal number $z \approx 32$ (if we shall rely on the wave equation in the g-lepton space). Indeed, an atom of the periodic table at the nucleon level with the mass number more than 68 ("more", because we must take into account the binding energy of g-leptons) corresponds rather to $_{32}Ge$, than $_{31}Ga$, with the mass numbers of the stable isotopes within 70-76. Moreover, the germanium atom is in the same 4th group of the periodic table as the silicon atom, which is an analogous of nucleons at the g-lepton level.

In that case, it is possible to say that all elementary particles consist finally of electrons. The relation of radii of the electron and g-lepton spheres makes it possible to give one more prediction: the spectrum of particles with measures beginning from the electron to g-quantum masses (the constituent of the vast variety of e-class particles) also exists in nature. The last is

the most probable. Therefore, as we already stated in Vol. 3, electrons as elementary particles are at the end of a hierarchical chain of e-class microobjects.

References

[1] L. Kreidik and G. Shpenkov, *Atomic Structure of Matter-Space*, Geo. S., Bydgoszcz, 2001, 584 p.

[2] L. Kreidik and G. Shpenkov, *Dynamic Model of Elementary Particles and the Nature of Mass and 'Electric' Charge*, "Revista Ciencias Exatas e Naturais", Vol. 3, No 2, 157-170, (2001); http://shpenkov.com/pdf/masscharge.pdf

[3] F.W.J. Olver, ed., *Royal Society Mathematical Tables*, Vol. 7, Bessel Functions, part. III, Zeros and Associated Values, Cambridge, 1960.

[4] G. P. Shpenkov, *The Role of Electrons in Chemical Bonds Formations* (*In the Light of Shell-Nodal Atomic Model*), Molecular Physics Reports **41**, 89-103, (2005).

[5] G. P. Shpenkov, *An Elucidation of the Nature of the Periodic Law*, Chapter 7 in "*The Mathematics of the Periodic Table*", edited by Rouvray D. H. and King R. B., Nova Science Publishers, NY, pp. 119-160, 2006.

[6] Fundamental Physical Constants from NIST; http://physics.nist.gov/cuu/Constants/

[7] L. Kreidik and G. Shpenkov, *Interrelation of Values of Base Units and Fundamental Constants with the Fundamental Quantum of Measures*, in *Foundations of Physics: 13.644…Collected Papers*, Geo. S., Bydgoszcz, 1998, 55-68 pp; http://shpenkov.com/pdf/Metrology.pdf

[8] L. Kreidik and G. Shpenkov, *Philosophy and the Language of Dialectics and the Algebra of Dialectical Judgments*, Proceedings of The Twentieth World Congress of Philosophy, Copley Place, Boston, Massachusetts, USA, 10-16 August, 1998; http://www.bu.edu/wcp/Papers/Logi/LogiShpe.htm

[9] A. P. Babichev, et al., *Physical Quantities*, Reference Book, Atomenergoizdat, Mosvow, 1991, Table 23.1, p. 568, in Russian.

[10] H. B. Michelson, *The Work Function of the Elements and Its Periodicity*, Journal of Applied Physics, Vol. 48, No 11, pp. 4729-4733, (1977).

[11] *Tables of Physical Quantities*, Reference Book (in Russian), edited by I. K. Kikoin, Moscow, Atomizdat, 1976, pp. 891-892.

[12] V. I. Vedeneev, et al., *The Chemical Bond Brake Energy* (in Russian), Moscow, 1962.

[13] A. J. Gordon and R. A. Ford, *The Chemist's Companion: A Handbook of Practical Data*, Techniques and References, A Wille-Interscience Publication, 1972.